LSD1-mediated Grob-like fragmentation as a novel drug resistance mechanism

HARVARD UNIVERSITY
Graduate School of Arts and Sciences

DISSERTATION ACCEPTANCE CERTIFICATE

The undersigned, appointed by the

Department of Chemistry & Chemical Biology

have examined a dissertation entitled:

LSD1-mediated Grob-like fragmentation as a novel drug resistance mechanism

presented by: Paloma Tuttle-Vasseur

candidate for the degree of Doctor of Philosophy and hereby certify that it is worthy of acceptance.

Signature _____
Typed name: Professor Brian Liau

Signature _____
Typed name: Professor Theodore Betley

Signature _____
Typed name: Professor Emily Balskus

Date: 12 July 2023

LSD1-mediated Grob-like fragmentation as a novel drug resistance mechanism

A dissertation presented by

Paloma Tuttle-Vasseur

to

The Department of Chemistry and Chemical Biology

in partial fulfillment of the requirements

for the degree of

Doctor of Philosophy

in the subject of

Chemistry

Harvard University

Cambridge, Massachusetts

July 2023

Dissertation Advisor: Brian B. Liau Paloma Tuttle-Vasseur

LSD1-mediated Grob-like fragmentation as a novel drug resistance mechanism

Abstract

Small molecules are powerful tools to illuminate biological functions and have played an instrumental role in making seminal discoveries in chromatin biology. Dysregulation of epigenetic states has been directly implicated in cancers such as acute myeloid leukemia (AML), highlighting the utility in developing therapies that target epigenetic regulators and in characterizing and mitigating resultant drug resistance mechanisms. Herein we present our strategy to elucidate a novel Grob-like fragmentation mechanism involving small molecule epigenetic inhibitors of lysine-specific demethylase 1 (LSD1), a chromatin modifier that regulates histone methylation and exerts dynamic control over numerous transcriptional programs. LSD1 plays a critical role in hematopoiesis through formation of a corepressor complex with growth factor independence 1(B) (GFI1(B)), and previous work from our group indicates that LSD1 complex formation with GFI1(B) is essential for AML proliferation, while its demethylase activity is dispensable. Our characterization of an unprecedented fragmentation mechanism illuminates the demethylase-specific activity of LSD1 inhibitors that rescue binding activity to GFI1(B), reversing inhibitor-related hematotoxicity and antiproliferative effects in AML. We interrogated the requirements for Grob-like fragmentation of covalent LSD1-inhibitor adducts through kinetic and structure-activity relationship studies on T-448, a lead compound for treatment of neuropsychiatric illnesses associated with epigenetic dysregulation. We observed that *N*-aryl benzamide substitution was essential in facilitating covalent LSD1-inhibitor adduct cleavage and that substitution *meta* to the tranylcypromine warhead directed Grob-like fragmentation in wild-type LSD1. We conversely identified an allosteric mutant of LSD1, called TTASdel, that disrupts distal αD helical hydrogen-bonding interactions to stimulate fragmentation of a *para*-substituted inhibitor adduct and confer

drug resistance in AML. Overall, our efforts elucidate new reactivity of LSD1 and detail the mechanism responsible for early clinical success of demethylase-specific inhibitors as therapeutics for neurological disease indications.

Table of Contents

Dedicated to my family, given and chosen, for all the snacks and sacrificial love.

I have written this out of abundance, not of leisure, but of love for you.

- Cicero

Acknowledgements

Frank Capra's "It's a Wonderful Life" played in my living room most Christmases, exerting significant influence on my life philosophy twenty-some years and as many viewings later. Now, the final days of my PhD seem to echo the film's arc: the loss, grief, and failure of my most devastating moments utterly eclipsed in an overflowing of love all around me. Like George Bailey in the final scene, I stand the "richest man in town," not in my own endeavors alone but in the community and relationships that defined my graduate career.

I must firstly express the deepest gratitude to my research advisor and lab *Boss*, Professor Brian Liau, whose encouragement and dedication have provided critical supports in the completion of my doctoral work. Most of us in the Liau lab cite the same initial impression of Brian as a brilliant scientist with a captivating enthusiasm and ambition for research. It has indeed been an honor to learn from Brian the joy and rigor of the scientific process and to mature as a chemist in the Liau lab. Thank you, Brian, for your unwavering kindness and genuine investment in my education and personal development.

I would like to thank my committee members, Professors Emily Balskus and Ted Betley, for their helpful discussions and support in the completion of my dissertation. I am grateful to Dr. Gregory Tucci, Dr. Catherine DuBreuil, Dr. Sheila Thomas, Dr. Daniel Kahne, and Dr. Josh Cox for their invaluable time and support in my graduate work. I am especially thankful for Dr. Amanda Waterbury and Dr. Jiaming Li for their patience, time, and mentorship in Brian's lab. I also thank Dr. Amanda Waterbury and Olivia Zhang, as well as Professor Andrea Mattevi and Jonatan Caroli for their incredibly rewarding collaboration on the T-448-TTASdel project. I am grateful to Dr. Shaw Huang, Dr. Dongtao Cui, and Anthony Lowe for assistance with NMR through the Laukien-Purcell Instrumentation Center, to Dr. Sunia Trager for assistance with LC-MS and GC-MS analysis through the Harvard Center for Mass Spectrometry, and to Dr. Grace Kenney and the Balskus lab for their generous assistance and QTOF run-time.

I am especially grateful to the scientists who first nurtured my nascent love of chemistry. I thank Zaida “Mama Z” Morales-Martinez for encouraging me to pursue research training at FIU, Dr. Sandra Stojanovic for introducing me to the enchanting world of organic chemistry, and Dr. Stanislaw Wnuk for inviting me to join his research lab and providing me with a welcoming and fruitful training environment. Thank you especially to Dr. Zhiwei Wen for his daily companionship and treasured mentorship and training during my time in the Wnuk lab. I also thank Professor Christina Woo and Dr. Hope Flaxman for hosting me as an undergraduate research intern and propelling me in my pursuit of a graduate education.

Above all, I extend my highest love and gratitude to my family. No words can encapsulate my thankfulness for the sacrifices and freely-given love of my parents, Rick and Mary—I love you Mama and Papa. To my sister Anna, the darling of my heart—I love you endlessly. Thank you, Abuelo and Abuela, Tia Liana and Hugh, my Tia Frances and Tia Grisel, and my cousins Joshua, Michelle, and Rebecca, for their enthusiastic support and love. Finally, I thank my chosen family for their dearly cherished companionship and love. Thank you, Arlinda, for your devotion and generosity over the last decade. Thank you, Ceejay, my first lab buddy, my baymate, and my best friend, for your compassion and fierce loyalty. Thank you, Alejandra, for your passion and steadfastness. Thank you, Clare, for your gentleness, kindness, and brilliance. Thank you, Bailey and Stephen, for your priceless humor and support in life and in science. Thank you, Samanta, for the comfort of your company and your delicious cooking. Thank you, Fred, for your biting wit and infallible spirit, and for the little piece of home you always shared with me. Thank you, Megan, for the fun and inspiration in and out of lab. Finally, this one goes out to Karis, my teammate in life and twin of our binary star, for giving me the pickle off your sandwich that first day and for your love all the days after; my heart is yours.

List of Abbreviations

AML	acute myeloid leukemia
Boc	*tert*-butyloxycarbonyl
BOX	bis(oxazoline) ligand
Bz	benzyl
°C	degrees Celsius
CNS	central nervous system
CoREST	co-repressor of repressor element1 silencing transcription factor
DIPEA	diisopropylethylamine
DMAP	dimethylaminopyridine
DMF	*N,N*-dimethylformamide
DMSO	dimethyl sulfoxide
DNA	deoxyribonucleic acid
DPPA	diphenylphosphoryl azide
ee	enantiomeric excess
eq	equivalent
ESI	electrospray ionization
Et	ethyl
FAD	flavin adenine dinucleotide
FP	fluorescence polarization
g	gram
GFI1(B)	growth factor independence 1 (B)
h	hour(s)
HDAC	histone deacetylase
HATU	1-[Bis(dimethylamino)methylene]-1H-1,2,3-triazolo [4,5-b]pyridinium 3-oxide hexafluorophosphate

HEK 293T	Human embryonic kidney 293 cells with mutant SV40 large T antigen
HMT	histone methyltransferase
HRMS	high resolution mass spectrometry
HWE	Horner-Wadsworth Emmons
Hz	hertz
IC_{50}	half maximal inhibitory concentration
J	coupling constant (in Hz)
JCC	Johnson-Corey-Chaykovsky
JmjC	Jumonji-C
K_i	inhibition constant
LSD1	lysine-specific demethylase 1 (also KDM1A)
M	molar (mols/liter)
m	multiplet
µ	micron
MAO	monoamine oxidase
Me	methyl
mg	milligram
MHz	megahertz
min	minute(s)
mL	milliliter
mmol	millimole
mol	mole
MS	mass spectrometry
m/z	mass-to-charge ratio
NMR	nuclear magnetic resonance
pH	hydrogen ion concentration

Ph	phenyl
PPI	protein-protein interaction
ppm	parts per million
q	quartet
R	general substituent
R_f	retention factor
RT	room temperature
s	second(s); singlet
SAR	structure activity relationship
SET-2	human megakaryoblastic cell line from essential thrombocythemia
SNAG	Snail/Gfi-1
t	triplet
t-BuOH	*tert*-butylalcohol
TCP	tranylcypromine
TF	transcription factor
TFA	trifluoroacetic acid
THF	tetrahydrofuran
TLC	thin layer chromatography
UV	ultraviolet
δ	chemical shift

List of Figures

Chapter 1: Chemical tools reveal epigenetic regulator protein function.

1.1. Chemical biology of chromatin regulation

The nucleus of the eukaryotic cell encapsulates a complete copy of its genome: the genetic material encoding the proteins that orchestrate nearly every essential function of cellular life. The nucleus organizes the vast amount of chromosomal DNA in the genome into a series of nucleosome subunits which coil the DNA strand around an octamer of histone proteins (Fig. **1.1**A). These subunits comprise the highly condensed and dynamic complex called chromatin and play a pivotal role in gene regulation through covalent chemical modifications to histones and DNA.[1-3] These modifications, or "epigenetic marks," control nuclear processes such as DNA transcription, replication, and repair, thereby commanding cellular processes and coordinating cell differentiation. Chromatin-regulating proteins mediate this epigenetic signaling by installing, removing, and "reading" epigenetic marks and by moderating chromatin conformation and binding of regulatory protein complexes (Fig. **1.1**B).[4] Characterizing chromatin-associated complexes and pathways has proven instrumental to our understanding of cell function and differentiation.

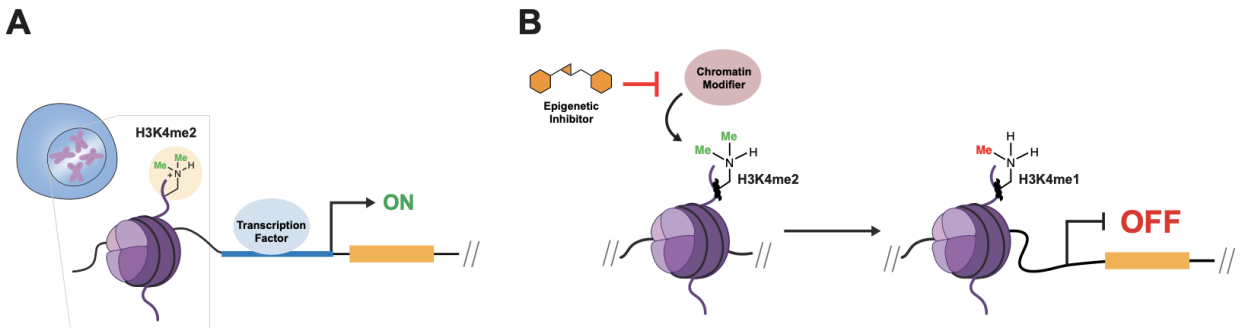

Figure 1.1. Small molecule modulation of epigenetic mechanisms.

A) The nucleus packages genetic material in the form of chromatin, in which DNA is wound around an octamer of histone proteins. DNA transcription is controlled in part through chemical modifications to chromatin, or "epigenetic marks." Methylation of lysine 4 of histone H3 (H3K4) marks active transcription. **B)** Chromatin modifiers function as readers, writers, and erasers to mediate epigenetic signaling. Small molecule inhibitors of chromatin modifiers can be used to reprogram epigenetic states.

Histone proteins play a key role in chromatin structure and function, binding to negatively charged DNA through electrostatic interactions with their high amount of positively charged lysine (K) and arginine (R) residues. In addition to this crucial role in DNA packaging, histones possess flexible N-terminal tails that can bind adjacent nucleosomes and recruit transcription

factors (TFs) to control DNA accessibility and mediate replication, repair, and transcription of corresponding genes. Modifications such as acetylation and phosphorylation remove positive charge and disrupt histone-DNA binding, serving to “open” the nucleosome and promote DNA access. In contrast, methylation maintains the positive charge of its recipient lysine and arginine residues, instead modulating binding behavior between DNA and chromatin-binding factors to perform a variety of functions associated with both transcriptional activation and repression.[5]

Methylation of histone lysines can mark both active and silenced chromatin states: for example, methylation of lysine 4 of histone H3 (H3K4) typically activates transcription whereas methylation of the neighboring H3K9 typically represses transcription.[6] Dysregulation of histone lysine methylation is implicated in numerous diseases: in cancers, methylation states are thought to promote oncogenesis through control of cell growth, migration, invasion, and angiogenesis, with certain methylation states correlating to disease prognosis.[7] Chromatin modifiers that control methylation and other epigenetic states have thus presented numerous attractive targets for development of anticancer therapeutics, particularly in acute myeloid leukemia (AML), a blood malignancy arising from hematopoietic precursor cells and characterized by enhanced proliferation and impaired differentiation. Development and application of small molecules to reprogram dysregulated epigenetic states have permitted the ability to therapeutically suppress oncogenes and reactivate tumor suppressor genes (TSGs) in AML, establishing these “epigenetic inhibitors” as powerful strategies for reversing disordered chromatin diseased states.[8]

1.2. Role of LSD1 in differentiation and disease pathology

While over 50 human histone lysine methyltransferases (HKMTs) across eight subgroups have been identified, only two classes of lysine demethylases have been more recently discovered: flavin- and iron-dependent demethylases.[9] Initial speculations considered histone methylation to be a permanent modification that could only be erased through removal of the histone tail or replacement of the entire histone subunit. The first discovery by Yang Shi of a histone demethylase, the flavin-dependent oxidase lysine-specific demethylase 1 (LSD1), overturned this notion and demonstrated that histone methylation is dynamic and enzymatically reversible. This discovery initiated rapid developments in the field of chromatin biology, including the subsequent discovery of the Jumonji-C (JmjC) family of lysine demethylases.[10] Like HMTs, histone demethylases (HDMs) exhibit specificity for their substrate amino acid residues and the degree of substrate methylation. The numerous histone demethylases within the non-heme iron(II) and α-ketoglutarate-dependent JmjC family can demethylate mono-, di-, and tri-methyl marks at H3K4/27/36 (Fig **1.2**A). In contrast, the flavin adenine dinucleotide (FAD)-dependent demethylases (LSD1 and its homolog LSD2) only remove mono- and di-methyl marks due to the requirement of flavin-containing amine oxidases to have a protonated substrate (Fig **1.2**B).[4,9,10] LSD1 thus demethylates the H3K4 substrate by accepting a hydride equivalent from the methylated lysine to generate an iminium intermediate which hydrolyzes to form the demethylated product and one equivalent of formaldehyde.

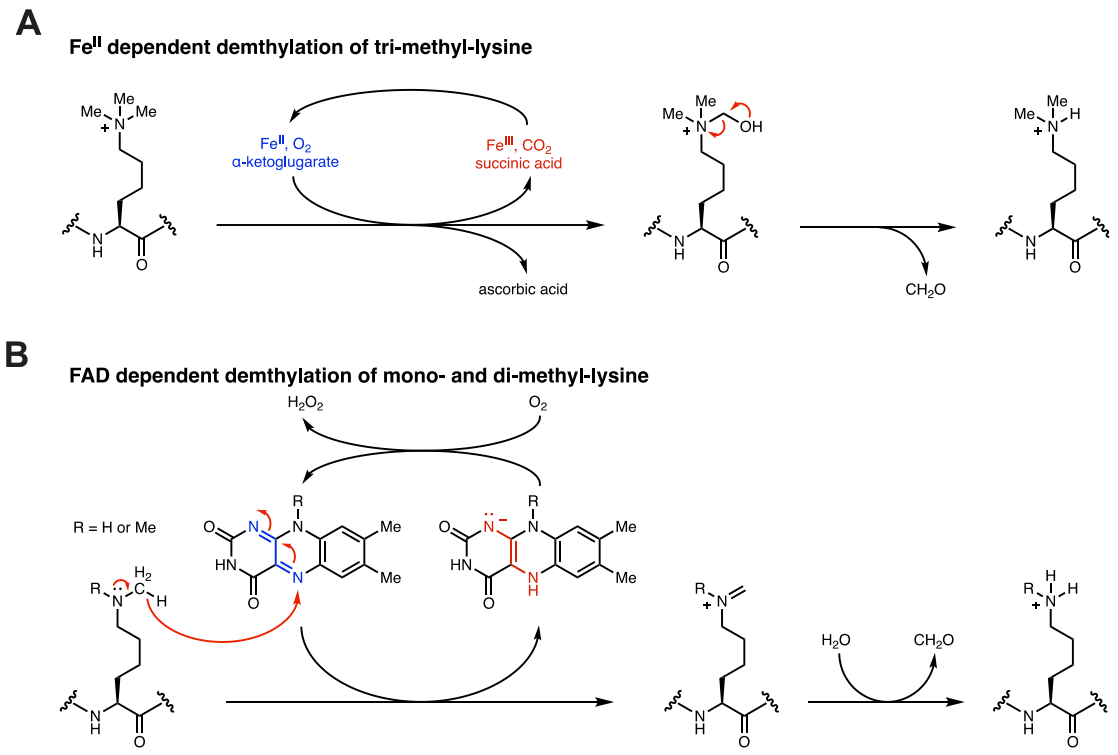

Figure 1.2. Demethylation catalysis by JmjC family and LSD1 enzymes.[9]

A) JmjC domain-containing demethylases use Fe(II) and α-ketoglutarate cofactors to remove mono-, di-, and tri-methyl marks from histone tail lysines. **B)** LSD1 demethylates H3K4me1/2 using a flavin cofactor. Following demethylation, the reduced flavin is reoxidized by molecular oxygen.

Since methylation at H3K4 is associated with active transcription, LSD1 exerts repressive action through demethylation of H3K4me1/2. LSD1 requires binding to CoREST (co-repressor of repressor element1 silencing transcription factor) for its enzymatic activity and additionally forms corepressor complexes with other chromatin regulators such as HDAC (histone deacetylase), CtBP (C-terminal binding protein 1), and the transcription factors GFI1/GFI1B (growth factor independence 1(/B).[11] Through its demethylase and scaffolding function, LSD1 performs numerous key functions as a central regulator in cell proliferation and division, embryonic development, hematopoietic differentiation, and stem cell pluripotency. When overexpressed, LSD1 also promotes cancer cell proliferation, migration, and invasion. Both genetic depletion and pharmacological inhibition experiments on LSD1 have demonstrated anticancer effects, identifying LSD1 as an oncogenic driver and a target for anticancer therapy.[12]

1.3. Pharmacology of LSD1 inhibitors

Epigenetic dysregulation in human diseases like cancer has motivated the development of small molecule inhibitors that target chromatin modifiers to alter the aberrant epigenetic states implicated in disease. Overexpression of LSD1 in cancers such as AML and small cell lung carcinoma (SLCL) motivated the search for demethylase inhibitors,[13,14] including the application of existing clinical monoamine oxidase (MAO) inhibitors as candidates for LSD1 inhibitors. Among these, the antidepressant tranylcypromine (TCP) exhibited the most potency for LSD1 and encouraged the derivatization of this scaffold towards improved potency and selectivity for LSD1.[15,16] These inhibitors deploy the TCP warhead as a substrate mimic to irreversibly bind the FAD cofactor through a single-electron mechanism and deposit a covalent inhibitor adduct to the enzyme active site.[17] Addition of amine headgroups to the TCP scaffold improves inhibitor potency and selectivity by participating in binding site electrostatic interactions. (Fig. **1.3**)

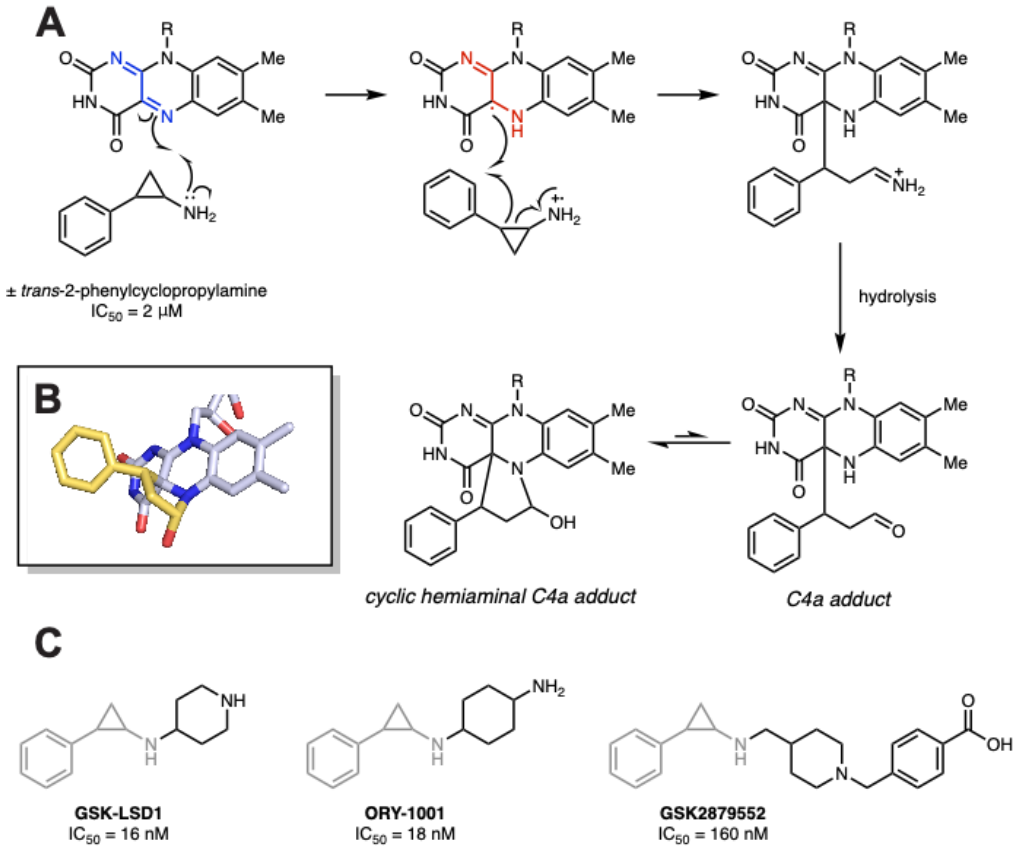

Figure 1.3. Mechanism-based inhibition of tranylcypromine compounds.

A) Tranylcypromine irreversibly reduces the FAD cofactor of LSD1 to deposit a C4a inhibitor adduct.[18] **B)** The cyclic hemiaminal C4a adduct is the major FAD-inhibitor adduct formed upon LSD1 inhibition (PDB: 2UXX). [17] **C)** Potent LSD1 inhibitors have been developed by attaching amine headgroups to the TCP warhead.[15,16]

Several potent and selective TCP inhibitors for LSD1 have been synthesized and profiled for anticancer therapies. ORY-1001 inhibited cell growth in AML, lung cancer, melanoma, GFI1-driven medulloblastoma, and solid tumors.[19–23] Notably, inhibition of LSD1 demethylase activity by ORY-1001 in Ewing Sarcoma and desmoplastic small round cell tumors (DSRCT) was insufficient to mitigate cell viability and invasion, suggesting demethylase-independent activity of LSD1 in these cancers.[24] Another small molecule, GSK2879552, inhibited H3K4 demethylation in AML and SCLC to facilitate tumor suppressor gene (TSG) expression and cell differentiation.[8] However, 28-day toxicology in animal models manifested severe toxicities including thrombocytopenia, neutropenia, and myelofibrosis, and three clinical trials for GSK2879552 in patients with AML, SCLC, and myelodysplastic syndromes (MDS) have been terminated due to unfavorable risk-benefit.[13,25]

1.4. Essential LSD1 protein-protein interactions on chromatin

Overexpression of LSD1 in acute myeloid leukemia (AML) and other hematologic malignancies marked the demethylase as a potential drug target, but early successes in identifying potent LSD1 enzymatic inhibitors for anticancer therapies have been tempered by discouraging toxicity profiles in animal models and in clinical trials.[13,15,16] Therapeutic deployment of TCP inhibitors induced severe hematological toxicities such as thrombocytopenia, possibly due to interference with demethylase-independent LSD1 functions.[24] In addition to its critical role in regulating methylation profiles (Fig. **1.4**A), LSD1 and its corepressor CoREST participate in many important regulatory complexes with epigenetic enzymes, transcription factors (TFs), and other chromatin modifiers. Of these, the paralogous transcription factors GFI1 and GFI1B recruit LSD1 to target gene promotors, and the resulting repressor complex blocks hematopoietic differentiation (Fig. **1.4**B).

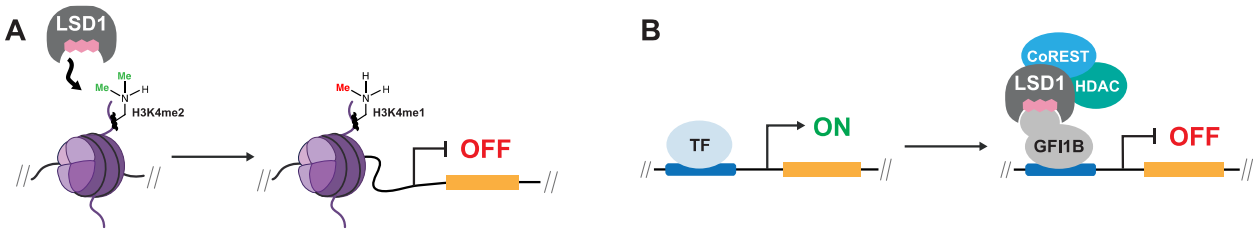

Figure 1.4. Transcriptional repression activity of LSD1.

A) LSD1 removes transcriptionally activating methyl marks from H3K4. **B)** LSD1 participates in regulatory complexes with other chromatin modifiers, including GFI1(B). LSD1-GFI1(B) binding represses enhancer activation.[26,27]

Recent work by the Liau group combined TCP inhibitor structure-activity relationship (SAR) analysis with mutational profiling to interrogate the biological mechanism of TCP toxicity in AML. The group synthetically derivatized GSK-LSD1, a potent and selective mechanism-based inhibitor which attenuates cancer cell line growth with an average EC_{50} < 5 nM, and employed a library of inhibitor analogs as selection tools to identify drug-resistant LSD1 mutations in AML. Intriguingly, mechanism based LSD1 inhibitors were initially designed to control histone post-translational modifications (PTMs); however, TCP inhibitors exert a second inhibitory

function by obstructing essential protein-protein interactions (PPIs) with binding partners such as the hematopoietic factor GFI1 and its paralogue GFI1B, which bind the LSD1 active site with an N-terminal SNAIL-GFI1 (SNAG) peptide (Fig. **1.5**B).

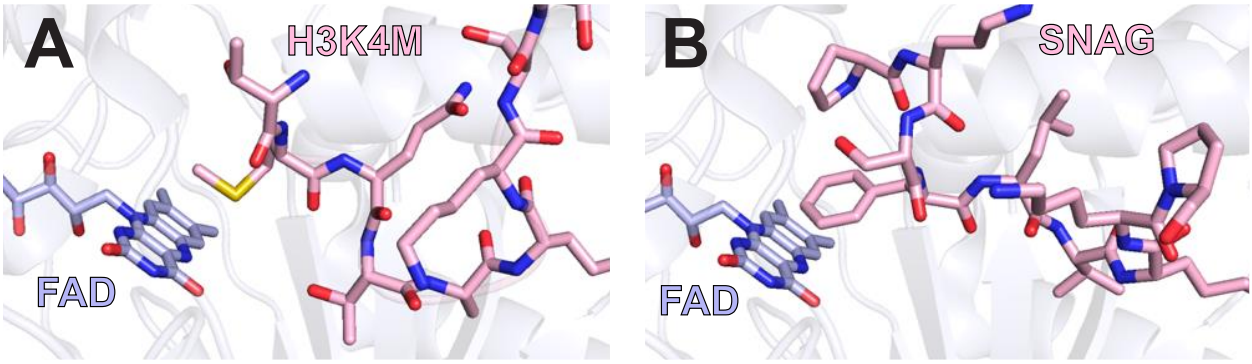

Figure 1.5. LSD1 active site bound to its substrates.

A) The H3 N-terminal tail extends into the LSD1 active site, positioning the H3K4 substrate above the FAD cofactor. Crystal structure of LSD1 is shown in complex with an H3K4M peptide mutant (PDB: 6VYP). **B)** The N-terminal SNAG peptide of GFI1(B) similarly binds the active site of LSD1 (PDB: 2Y48).

Discovery of viable LSD1 mutants that were catalytically inactive yet still tolerant of GFI1(B) binding suggested that drug-resistance in AML is conferred by LSD1 scaffolding function rather than by enzymatic activity, indicating that TCP inhibitors exert their anti-proliferative effects in AML by impeding the LSD1-GFI1(B) binding event. This mechanism is further supported by the design and characterization of a drug-compensatory F5A GFI1B allele that complements the LSD1 active site modified with the GSK-LSD1 inhibitor adduct (Fig. **1.6**A,B). The observed "bump-hole" rescue validated the essentiality of LSD1-GFI1(B) binding in AML, further indicating that binding of LSD1 to GFI1(B) was sufficient for AML proliferation even with loss of demethylase activity. While the pharmacologic disruption of the LSD1-GFI1(B) complex promotes on-target toxicity in AML, it is also responsible for hematotoxic side effects of LSD1 inhibitors in clinical trials.[13,26–30]

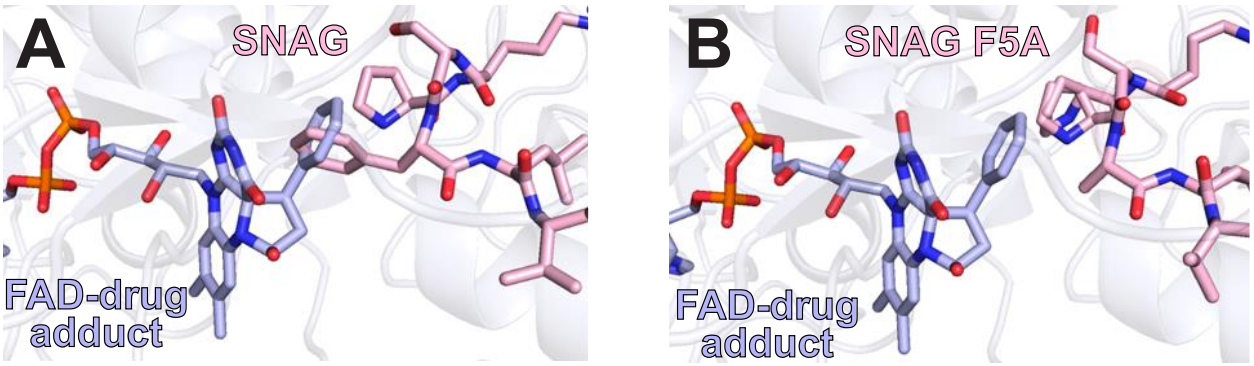

Figure 1.6. GSK-LSD1 inhibition evicts GFI1B.

A) The FAD-drug adduct of GSK-LSD1 inhibits SNAG binding and prevents LSD1-GFI1B complex formation. **B)** The FAD-drug adduct of GSK-LSD1 binds an F5A drug-complementary GFI1B allele.

Despite the discouraging toxicity profile of early mechanism-based LSD1 inhibitors, demethylase inhibition remains a noteworthy therapeutic target, particularly in the treatment of psychiatric disorders, where increased H3K4 methylation has been linked to improved cognitive function in Alzheimer's diseases and to alleviation of schizophrenia and mood disorders.[31–33] Development of safe and effective LSD1 inhibitors for neurological disease applications will require careful consideration to selectively target demethylation while minimally inhibiting essential LSD1-TF interactions.

1.5. Goals of this work

Recent discovery of demethylase-selective TCP inhibitors has uncovered novel transformations involving the LSD1 active site and opened exciting avenues towards safe and effective therapeutic application of demethylase inhibitors.[34–36] LC-MS and crystal analysis indicate that these inhibitors install a transient full inhibitor adduct to the LSD1 flavin cofactor and subsequently N-formylate the flavin via an undescribed mechanism (Fig. **1.7**). *In vitro* binding assays demonstrated that LSD1 pre-treatment with these compounds initially inhibits LSD1-GFI1B binding, then recovers binding in a time-dependent fashion, suggesting that catalytic deactivation by the compact formyl adduct rescues LSD1-GFI1B binding activity. The unique demethylase-selective behavior of these inhibitors highlights these compounds as attractive candidates for therapeutic treatment of neuropsychiatric disorders for their potential to restore H3K4 methylation levels without causing GFI1B-associated hematotoxicity.

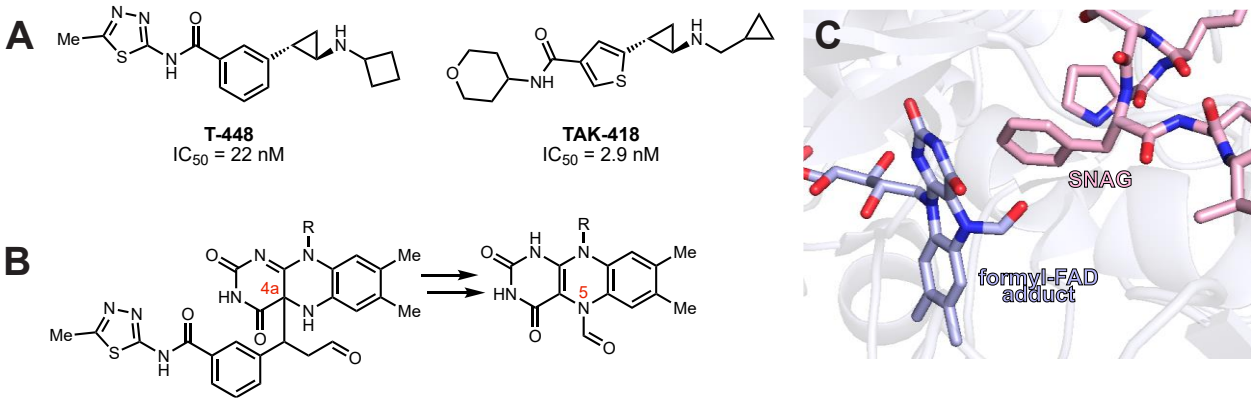

Figure 1.7. Demethylase-specific LSD1 inhibitors rescue GFI1B binding.

A) Two LSD1 inhibitors, T-448 and TAK-418, selectively inhibit demethylase activity without preventing LSD1-GFI1(B) binding. **B)** Demethylase-specific inhibitors formylate FAD through a transient full inhibitor adduct by an undefined mechanism. **C)** The compact formyl-FAD (PDB: 7E0G) adduct deactivates FAD and retains SNAG-binding ability.[35]

This dissertation details our collaborative effort to elucidate a novel mechanism for TCP-FAD fragmentation within the LSD1 active site. We present our findings supporting homolytic cleavage of the full-inhibitory adduct followed by C-C bond rupture to deposit a compact formyl adduct and rescue LSD1-GFI1B binding. We additionally report a distal mutation in LSD1 which

grants drug resistance to LSD1-GFI1B inhibitors by promoting an analogous mechanism within the active site. Together, our results identify Grob-like fragmentation of covalent inhibitor adducts as a drug-resistance mechanism and interrogate the chemical constraints of this reactivity.

Chapter 2: Distal drug-resistance mutations promote Grob-like fragmentation.

The following chapter summarizes the results of a manuscript in preparation. Paloma Tuttle-Vasseur (P.R.T.) and Jiaming Li (J. L.) designed and synthesized molecules. Amanda L. Waterbury (A.L.W.), Jonatan Caroli (J.C.), Olivia Zhang (O.Z.), and P.R.T. designed, performed, and analyzed protein purification and biochemical assays. A.L.W., O.Z., and P.R.T. designed, performed, and analyzed cell and molecular biology experiments. Brian B. Liau (B.B.L.) and Andrea Mattevi (A.M.) held primary responsibility for the study. Text and figures from section 2.5 have been reproduced with consent from a manuscript draft written by A.L.W.

2.1. LSD1 inhibition by T-448 and subsequent rescue of scaffolding function

Mechanism-based TCP inhibitors of LSD1 exhibit antiproliferative activity in AML by obstructing the binding of LSD1 to the transcription factor GFI1B. However, the disruption of this protein complex also causes hematotoxicity such as thrombocytopenia, which has presented a significant challenge in developing safe LSD1 inhibitor therapies. Previous work from our group identified drug-resistant LSD1 mutants in AML which were enzymatically dead yet retained GFI1B-binding activity, highlighting the potential to therapeutically restrict LSD1 demethylase activity without inducing GFI1B-related hematotoxicity. Towards this aim, Takeda identified a potent LSD1 inhibitor with an improved hematological safety profile; this inhibitor, T-448, deactivated LSD1 demethylase activity while minimally disturbing the LSD1-GFI1B complex through deposition of a compact formyl adduct to the flavin cofactor of the enzyme.

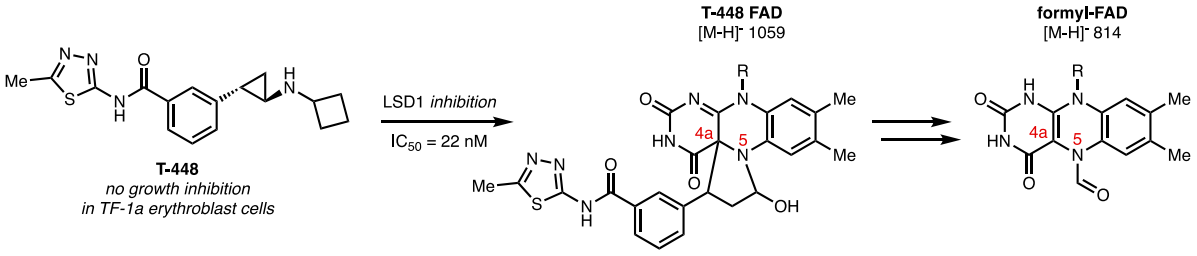

Figure 2.1. T-448 inactivation of LSD1 demethylase activity with a compact formyl-FAD.

Extraction and LC-MS analysis of FAD-inhibitor products revealed that T-448 installs a transient inhibitor adduct with *m/z* 1059 which converts to formyl-FAD (*m/z* 814) in a time-dependent manner.[34]

Fascinatingly, T-448 exhibited time-dependent recovery of LSD1-GFI1B binding; at 7.5 min, T-448 treatment disrupted LSD1-GFI1B binding, before rescuing binding to DMSO-control levels after 10 hours. Mass spectrometry analysis revealed two FAD-adduct peaks following T-448 treatment: *m/z* 1,059, corresponding to the full T-448-FAD adduct, as well as *m/z* 814, corresponding to formylated FAD. Over time, the peak count of the formylated-FAD trace increased while the count of the full adduct trace decreased—suggesting that initial inhibition of the LSD1 flavin in the canonical TCP fashion generates a transient full adduct which fragments to the final formyl-FAD adduct (Fig. **2.1**). In a mouse model of schizophrenia, T-448 increased

methylation of histones in the central nervous system (CNS) and improved learning function without inducing GFI1B-associated thrombocytopenia, opening an exciting avenue for demethylase-specific therapeutics for psychiatric disorders associated with epigenetic dysregulation.[34] The chemical mechanism by which T-448 fragments to rescue LSD1-GFI1B binding has not been reported, and characterizing this remarkable reactivity would illuminate nonenzymatic functions of LSD1 and support the therapeutic applications of demethylase-specific inhibitors.

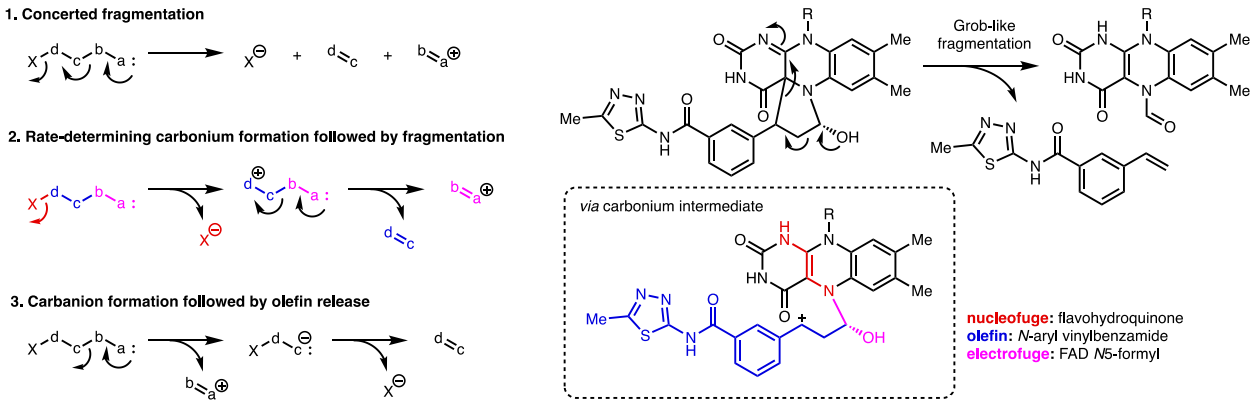

Figure 2.2. Grob fragmentation of an aliphatic chain into three components.

Grob-like fragmentation of FAD-inhibitor adducts yields an *N*5-formylated flavohydroquinone and a styrene byproduct.

We propose a Grob-like fragmentation mechanism for T-448 adduct fragmentation by which deprotonation of the cyclic hemiaminal hydroxyl induces a fragmentation to eject an olefin byproduct and fully reduce the flavin cofactor to the flavohydroquinone form, leaving an *N*5-formyl adduct (**Fig. 2.2**). Due to insufficient orbital alignment, the cyclic FAD-T-448 adduct fails to meet the stereoelectronic requirement for concerted fragmentation.[37,38] We instead propose two fragmentation steps, beginning with C-C bond cleavage between the adduct benzylic carbon and FAD C4a to reduce FAD and produce a reactive intermediate species. Grob-like fragmentation of the resulting intermediate liberates a styrene byproduct to deposit the remaining formyl group as a compact FAD inhibitor adduct. Our work illuminates the structural and electronic requirements for T-448 adduct fragmentation within the LSD1 active site and investigates whether the

isoalloxazine rings of FAD facilitate the reaction using one- or two-electron chemistry to generate a neutral radical or a carbonium intermediate, respectively.

2.2. Synthetic routes toward key compounds

We were interested in synthesizing derivatives of T-448 to characterize its FAD-formylating mechanism and to interrogate the structural components minimally necessary to facilitate Grob-like adduct fragmentation. We synthesized the trans-2-phenylcyclopropane-1 carboxylic acid (**T-21a**) via enantioselective copper (II) BOX cyclopropanation (>95% *ee* from 3-bromostyrene), and accessed the analogous racemate through successive Horner-Wadsworth-Emmons (HWE) olefination and diastereoselective Johnson-Corey-Chaykovsky (JCC) cyclopropanation (Figure **2.3**).[39–41] The TCP core is conveniently accessed from intermediate carboxylic acids through Curtius rearrangement to yield **T-22**, which can be further derivatized at this stage or after reductive amination and Boc protection (**T-23**) (Figure **2.4**).

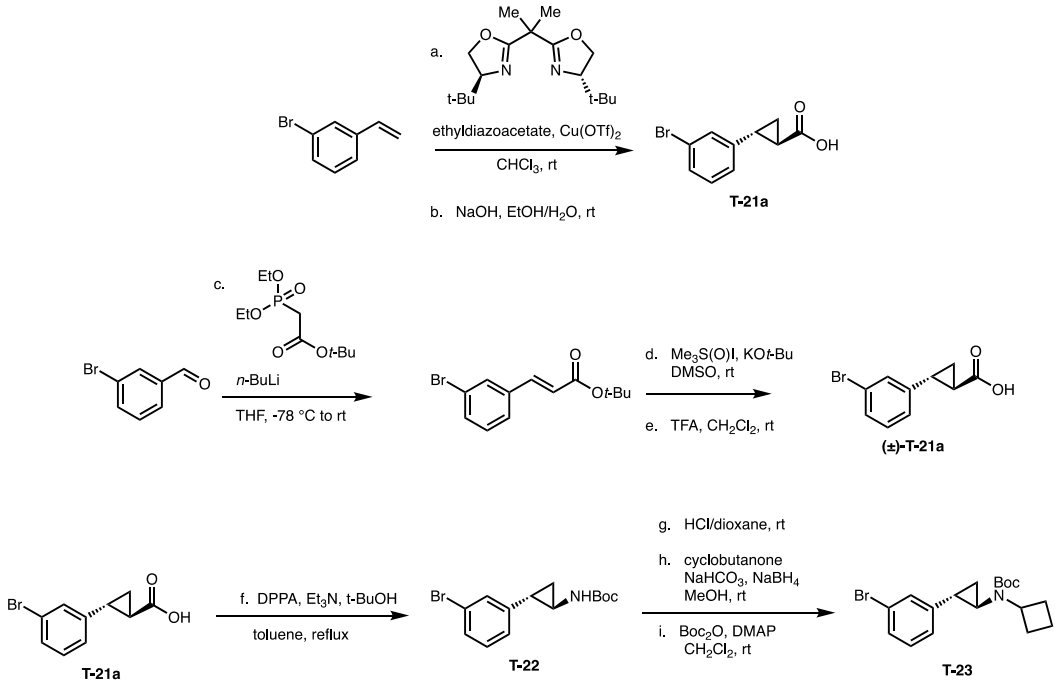

Figure 2.3. Representative synthesis of TCP inhibitor precursors.[39–41]

Reaction conditions: [a]$Cu(OTf)_2$, 2,2′-Isopropylidenebis[(4S)-4-tert-butyl-2-oxazoline], ethyldiazoacetate, $CHCl_3$, rt, 5 h (14%); [b]NaOH, $EtOH/H_2O$, reflux, overnight (90%); [c]tert-butyl diethylphosphonoacetate, *n*-BuLi, THF, -78 °C then rt, 2 h (95%); [d]trimethylsulfoxonium iodide, KO*t*-Bu, DMSO, rt, 3 h (60%); [e]TFA, CH_2Cl_2, rt, 2 h (90%); [f]DPPA, Et_3N, *t*-BuOH, toluene, reflux, overnight (60%); [g]HCl/dioxane, rt, 1-5 h (90%); [h]cyclobutanone or other carbonyl headgroup, $NaHCO_3$, MeOH, then $NaBH_4$, rt, overnight (40-60%); [i]Boc_2O, DMAP, CH_2Cl_2, rt, overnight (90%).

We synthesized enantiopure GSK-LSD1, T-448, and other tranylcypromine inhibitors, including **TCP-2**, a GSK-LSD1 analog which bore a cyclobutanamine headgroup identical to that of T-448. Consistent with literature characterization of T-448, we observed potent inhibition of LSD1 enzyme activity but not antiproliferative activity against SET-2 cells, a human megakaryoblastic cell line from essential thrombocythemia (Fig. **2.4**). Our data showed that enantiopure and racemic T-448 rescued SNAG binding with equal efficacy and demonstrated that **TCP-2** was not minimally sufficient to sustain cell viability at clinically relevant concentrations in SET-2 cells. We therefore decided to derivatize the aryl substituent of T-448 using the racemic HWE/JCC route due to improved scalability and substrate scope compared to the enantioselective route.

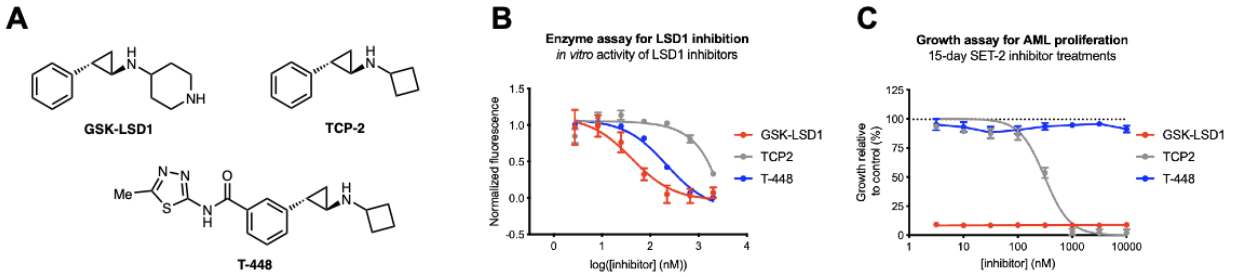

Figure 2.4. Preliminary characterization of T-448.

A,B) GSK-LSD1, TCP-2, and T-448 inhibit *in-vitro* demethylase activity of LSD1. **C)** GSK-LSD1 and TCP-2 exert antiproliferative effects in AML, while T-448 does not.

We synthesized aryl bromide and methyl benzoate intermediates **T-23** and **T-27** to derivatize the aryl substituents of TCP inhibitor analogs. From Boc-protected 3-bromo enantiomer **T-23**, we synthesized (1*S*,2*R*)-T-448 by lithium-halogen exchange followed by carboxylation, amide coupling, and amine deprotection. T-448 and aryl-substituted benzamide analogues were likewise accessed from Boc-protected reductive amination product **T-29** via ester hydrolysis, amide coupling, and amine deprotection. From the **T-23** racemate, we synthesized the T-448 reversed benzamide analog **T-18** through Buchwald–Hartwig amination and amide coupling. Finally, *N*-methyl and *N,N*-dimethyl benzamide analogues were synthesized by aluminum-mediated conversion of Boc-protected reductive amination product **T-29** (Fig. **2.5**).

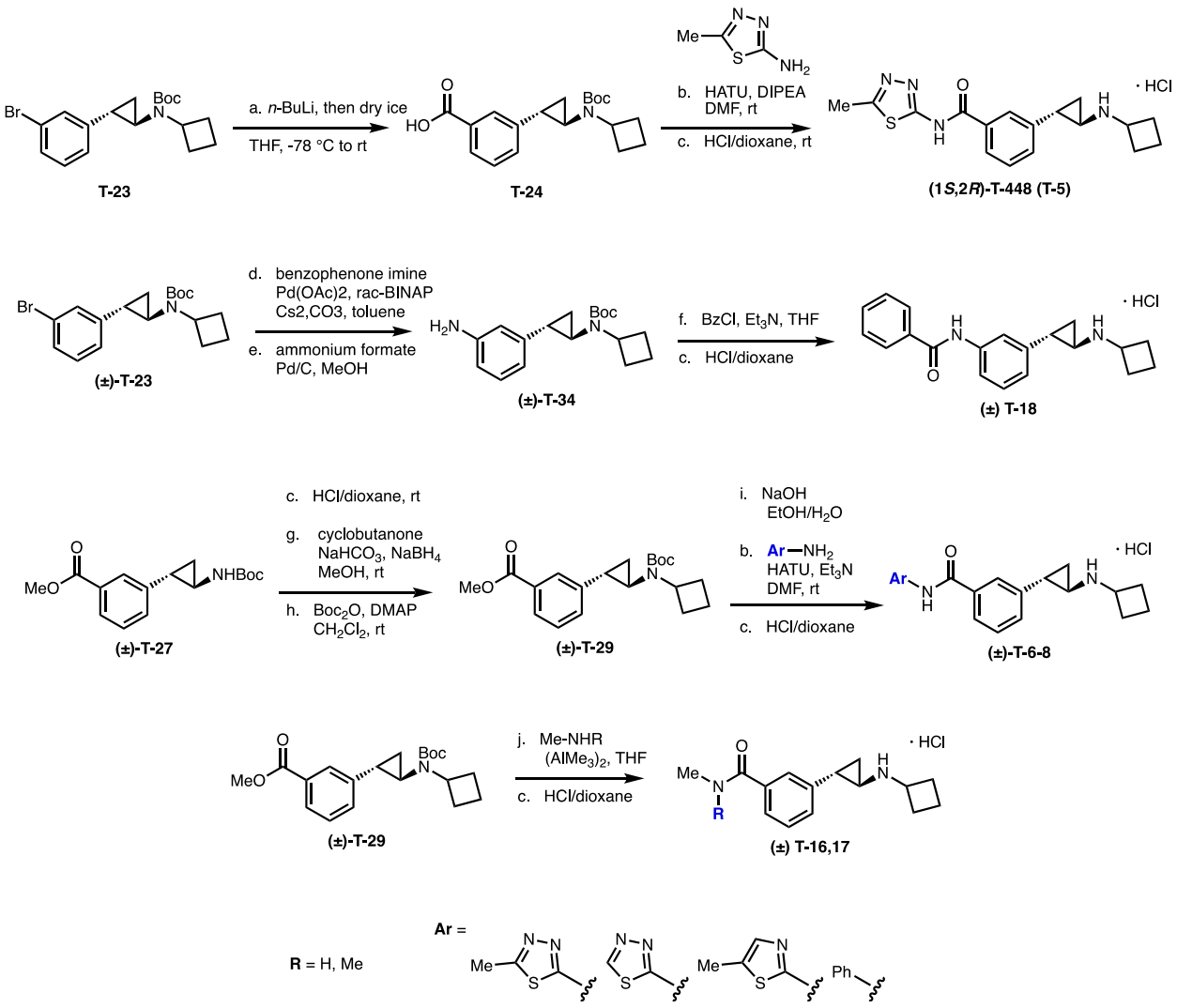

Figure 2.5. Functionalization of tranylcypromine intermediates.

Reaction conditions: [a]*n*-BuLi, THF, then CO_2, , -78 °C, 2 h (37%); [b]HATU, DIPEA, $ArNH_2$, DMF, rt, overnight (65%); [c]HCl-dioxane, rt, 1-5 h (90%); [d]benzophenone imine, $Pd(OAc)_2$, *rac*-BINAP, Cs_2CO_3, toluene, 100 °C, overnight (60%); [e]ammonium formate, Pd/C, MeOH, 60 °C, 1 h (70%); [f]BzCl, Et_3N, THF, 0 °C to rt, 1 h (50%); [g]cyclobutanone, $NaHCO_3$, MeOH, then $NaBH_4$, rt overnight (60%); [h]Boc_2O, DMAP, CH_2Cl_2, rt, overnight(90%); [i]NaOH, $EtOH/H_2O$, rt, overnight (80%); [j]NH_2Me or $NHMe_2$, $(AlMe_3)_2$, THF, -78 °C to rt, overnight (30%).

We synthesized isotopically labelled T-448 and tri-substituted aryl analogs for labelling and kinetic experiments according to the following procedures (Fig. **2.6**). Deuteration of tert-butyl diethylphosphonoacetate and application to the HWE olefination of methyl 3-formylbenzoate afforded us the isotopically labeled 3-(cyclopropyl-2-*d*)-benzamide precursor **2-*d*-T-25**. Conversely, we accessed the 3-(cyclopropyl-1-*d*)-benzamide precursor methyl 3-(formyl-*d*)

benzoate by reduction of monomethyl isophthalate with sodium borodeuteride and subsequent oxidization to the aldehyde. Finally, we synthesized a panel of three 2-X-substituted benzamide analogs with electron-donating and withdrawing groups installed *para* to the cyclopropylamine substituent. From commercially available 2-fluoro-5-formylbenzonitrile, we accessed the fluorinated benzaldehyde **T-35**. From **T-35**, we synthesized the brominated benzaldehyde **T-36** through a series of S_NAr, Staudinger, and Sandmeyer reactions. The 2-X substituted analogs **T12** and **T-19** were synthesized from the starting benzaldehydes according the previously described racemic route (Fig. **2.3**). We obtained the methylated analog **T-20** by subjecting the brominated JCC intermediate **T-41** to Suzuki coupling using trimethylboroxine and carrying the resulting product through the remainder of the synthetic route.

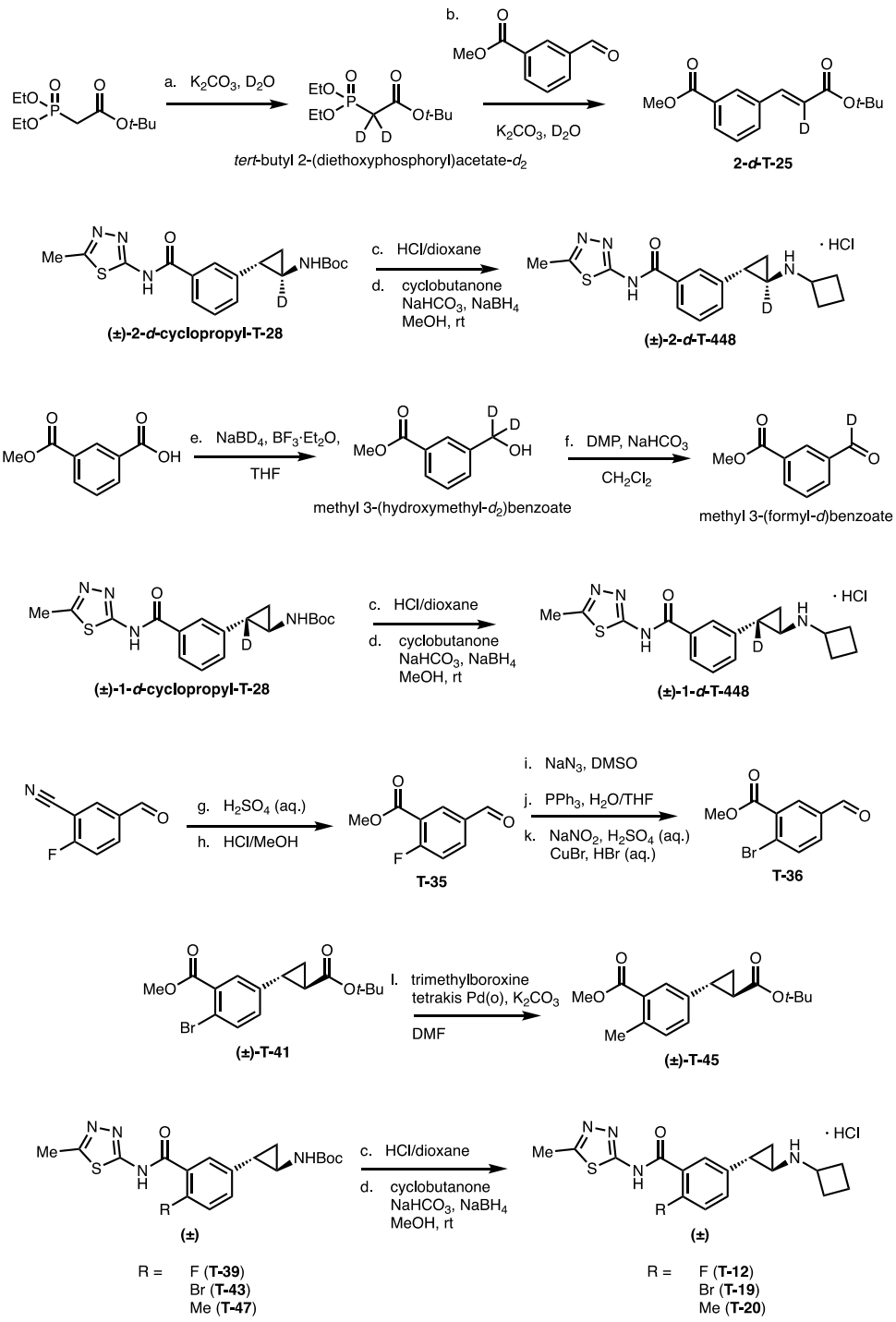

Figure 2.6. Synthesis of analog precursors for kinetic experiments.

Reaction conditions: [a]K_2CO_3, D_2O, rt, overnight (quant.); [b]methyl 3-formylbenzoate, K_2CO_3, D_2O, rt, overnight (50%); [c]HCl-dioxane, rt, 1-5 h (90%); [d]cyclobutanone, $NaHCO_3$, MeOH, then $NaBH_4$, rt overnight (60%); [e]$NaBD_4$, $BF_3{\cdot}Et_2O$, THF, reflux then rt, 2 h (95%); [f]DMP, $NaHCO_3$, CH_2Cl_2, rt, 5 h (67%); [g]aq. H_2SO_4, reflux, overnight (95%); [h]MeOH, HCl, reflux, overnight (80%); [i]NaN_3, DMSO, 70 °C, 2 h (quant.); [j]PPh_3, THF/H_2O, rt, 4 h (60-80%); [k]$NaNO_2$, aq. H_2SO_4, CuBr, HBr, 0 °C to rt to 60°C (30-70%); [l]trimethylboroxine, tetrakis(triphenylphosphine)palladium(0), K_2CO_3, DMF, 115 °C, overnight (70%).

Lastly, we hydrolyzed various methyl formylbenzoate precursors and subjected the resulting carboxylic acids to gentle Wittig conditions using potassium tert-butoxide and methyltriphenylphosphonium bromide. Amide coupling of the resultant vinylbenzoic acids to 5-methyl-1,3,4-thiadiazol-2-amine provided vinylbenzamide authentic standards of Grob-fragmentation byproducts to calibrate kinetic measurements of *in vitro* styrene generation as a proxy for Grob-like fragmentation (Fig. **2.7**).

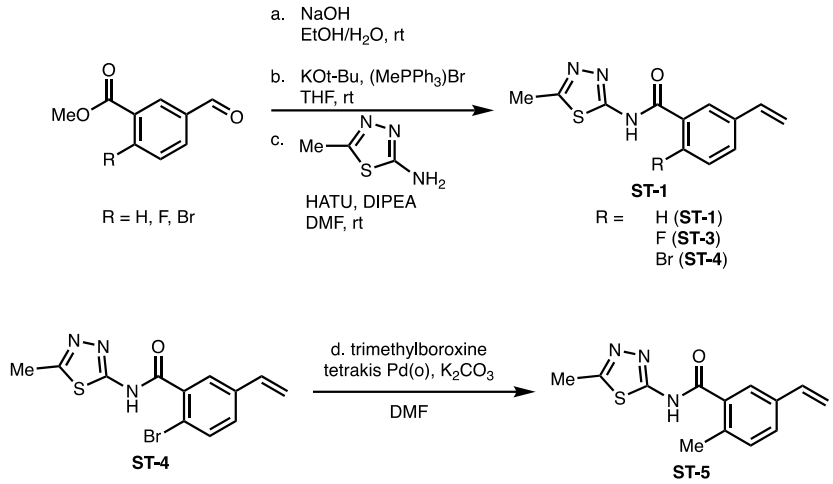

Figure 2.7. Synthesis of styrene authentic standards for calibration of kinetic experiments.

Reaction conditions: [a]NaOH, EtOH/H_2O, rt, overnight (90%); [b]KO*t*-Bu, ($MePPh_3$)Br, THF, 0 °C to rt, 2 h (60%); [c]HATU, DIPEA, 5-methyl-1,3,4-thiadiazol-2-amine, DMF, rt, overnight (65%); [d]trimethylboroxine, tetrakis(triphenylphosphine)palladium(0), K_2CO_3, DMF, 115 °C, overnight (20%).

2.3. Mechanistic and kinetic characterization with inhibitor derivatives

The mechanism of FAD-formylation by T-448 has not been reported, and we hypothesize that the T-448-FAD covalent inhibitor adduct enables a Grob-like fragmentation via a reactive intermediate species. Our first efforts towards characterizing the fragmentation mechanism sought to confirm that the initial inhibition of T-448 proceeded analogously to GSK-LSD1: through installation of a covalent adduct at C4a which equilibrates to a five membered cyclic hemiaminal at N5. By our proposed mechanism, the formyl carbon deposited by T-448 would originate from the C2 tranylcypromine carbon alpha to the amine (Fig. **2.8**). We therefore synthesized and treated LSD1 with cyclopropyl-2-*d* T-448 (**2-*d*-T-448**) to isotopically label the putative formyl carbon. Consistent with our proposed Grob-like fragmentation mechanism, LC-MS analysis of 2-*d*-T-448 incubation products yielded characteristic +1 m/z shifts of 1,060 and 815, corresponding to both the full 2-*d*-T-448-FAD adduct and the *d*-formyl adduct, respectively. Further analysis of the formyl-FAD sample revealed a peak with m/z 246, corresponding to the styrene byproduct expected from Grob-like fragmentation. Taken together, these results support an FAD formylation mechanism by which T-448 inhibits LSD1 by first deactivating the FAD cofactor through addition of a classic TCP suicide adduct, then subsequently fragmenting to eject a styrene byproduct and deposit a compact formyl adduct to the FAD cofactor.

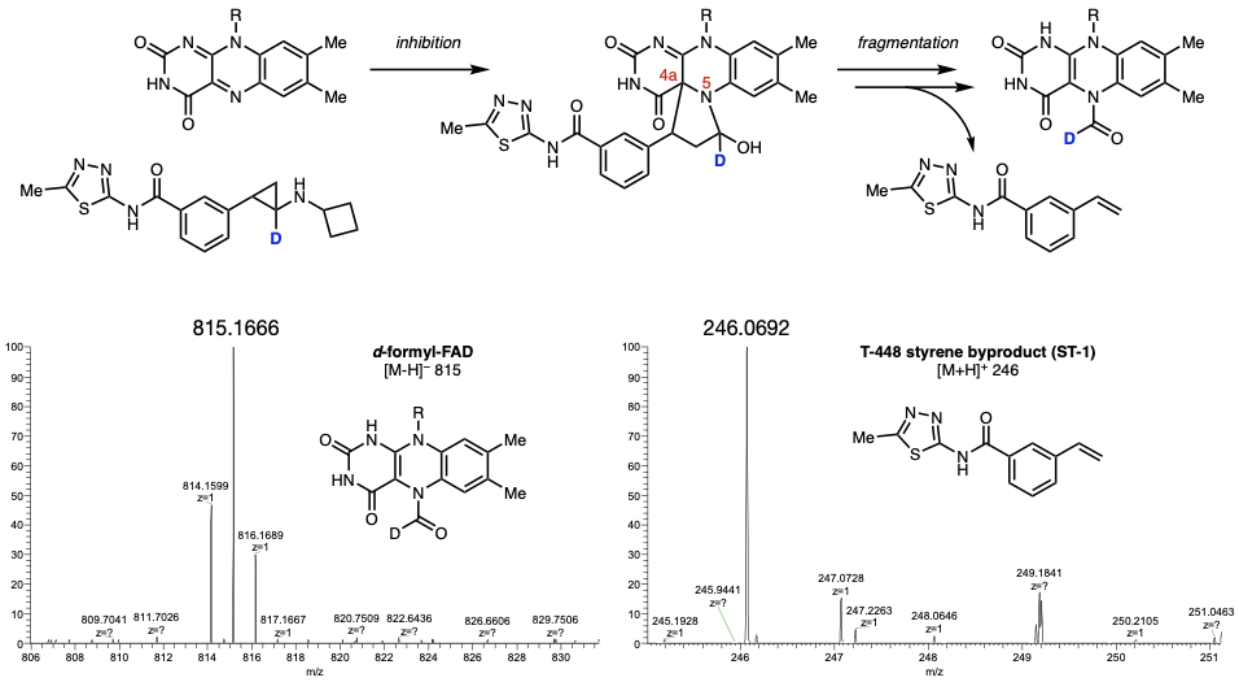

Figure 2.8. Formation of *N*5-formyl FAD and styrene ST-1 through Grob-like fragmentation.

After extracting recombinant LSD1 treated with 2-*d*-T-448 for 4 h, the full FAD-drug adduct, formyl-FAD adduct, and byproduct styrene were detected by LC-MS.

After observing formation of both Grob products, we next optimized the LC-MS method to quantify styrene byproduct formation as a proxy for T-448 adduct fragmentation. We synthesized T-448 styrene (**ST-1**) and calibrated its detection by LC-MS against caffeine as an internal standard. We incubated LSD1 with 8-fold excess T-448, monitored styrene formation over 8 hours, and assumed rapid, full inhibition of LSD1 to obtain a kinetic plot for adduct fragmentation by subtracting the detected concentration of styrene from the concentration of fully inhibited protein. The resulting first-order kinetic trend yielded an estimated rate constant $k \approx 0.10\ h^{-1}$ (Fig. **2.9**).

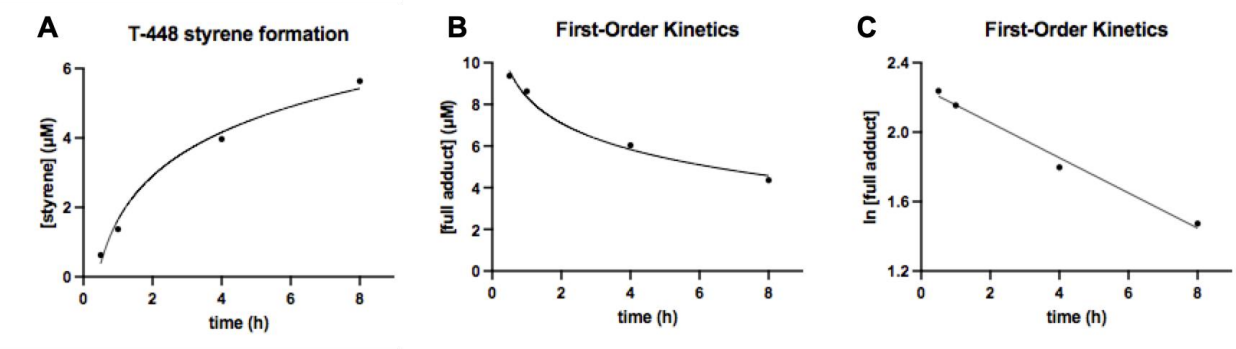

Figure 2.9. First-order reaction kinetics of T-448 adduct fragmentation.

A) Generation of styrene was monitored by LC-MS and quantified against an internal standard. **B)** A kinetic plot for styrene production was calculated by assuming rapid and complete LSD1 inhibition. **C)** The rate constant (k) was obtained from the linear first-order kinetic plot.

Canonically, stepwise cationic Grob fragmentation proceeds through rate-determining ionization, and we wondered whether we might observe a kinetic isotope effect (KIE) by absolute rates. We synthesized **1-*d*-T448** to label the benzylic position of the full inhibitory adduct and observed a secondary KIE ≈ 1.18 (Fig. **2.10**), indicative of a change in hybridization from sp^3 to sp^2 within the rate determining step (RDS).[42] The magnitude of this secondary isotope effect falls within the margin of error for our LC-MS method, and a definitive conclusion cannot be reached with the data we obtained. This result would support rate-limiting cleavage of the cyclic inhibitor adduct from the FAD C4a, consistent with our mechanism. Upon bond cleavage, the isoalloxazine rings of the FAD cofactor could accept one or two electrons to generate a carbonium or a radical at the benzylic position of the inhibitor adduct.

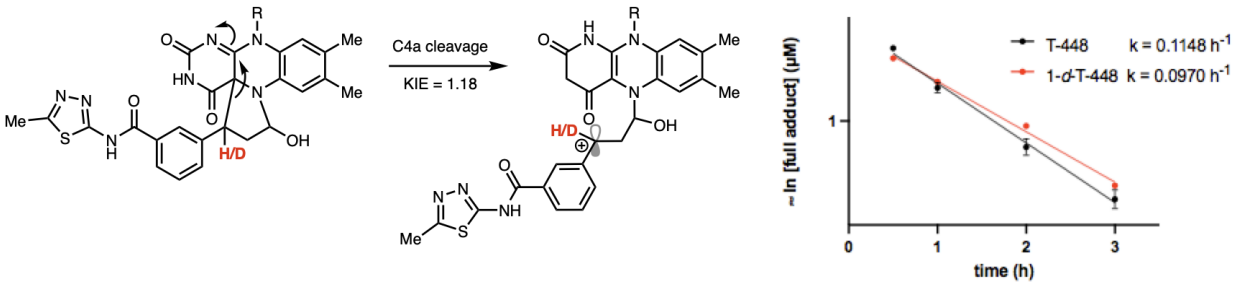

Figure 2.10. Secondary kinetic isotope effect indicative of a change in hybridization.

LSD1 was treated with a T-448 analog bearing a deuterium at the cyclopropyl C1. Putative benzylic carbonium formation yields a small secondary KIE, indicative of a change in hybridization from sp^3 to sp^2 consistent with both cationic and one-electron mechanisms.

The proposed mechanism for stepwise fragmentation would likely proceed first through a C-C bond cleavage step to generate a carbocation or a radical at the inhibitor adduct benzylic position. We chose to investigate the electronic character of the putative Grob-like intermediate through Hammett analysis. We synthesized a panel of 2-X-benzamide T-448 analogs in which we installed electron-donating and withdrawing groups at the *para* position relative to the benzylic cyclopropyl-C1 (Fig. **2.11**), aiming to illuminate the adduct fragmentation mechanism through a trend in substituent effects. We did not observe the linear trend indicative of substituent perturbations to the same overall mechanism but rather that every para-substitution we applied to T-448 slowed the fragmentation reaction. This result suggests that the inhibitor adducts might not fragment through a one-electron mechanism, since *para*-bromide and *para*-methyl substituents would in that case stabilize radical formation due to spin delocalization and increase rather than decrease reaction rates.[43] However, the observed substituent effects do not reflect identical mechanism of positive charge buildup within the transition state, which would be destabilized by the electron-withdrawing bromide and stabilized by the electron-donating methyl group.[44]

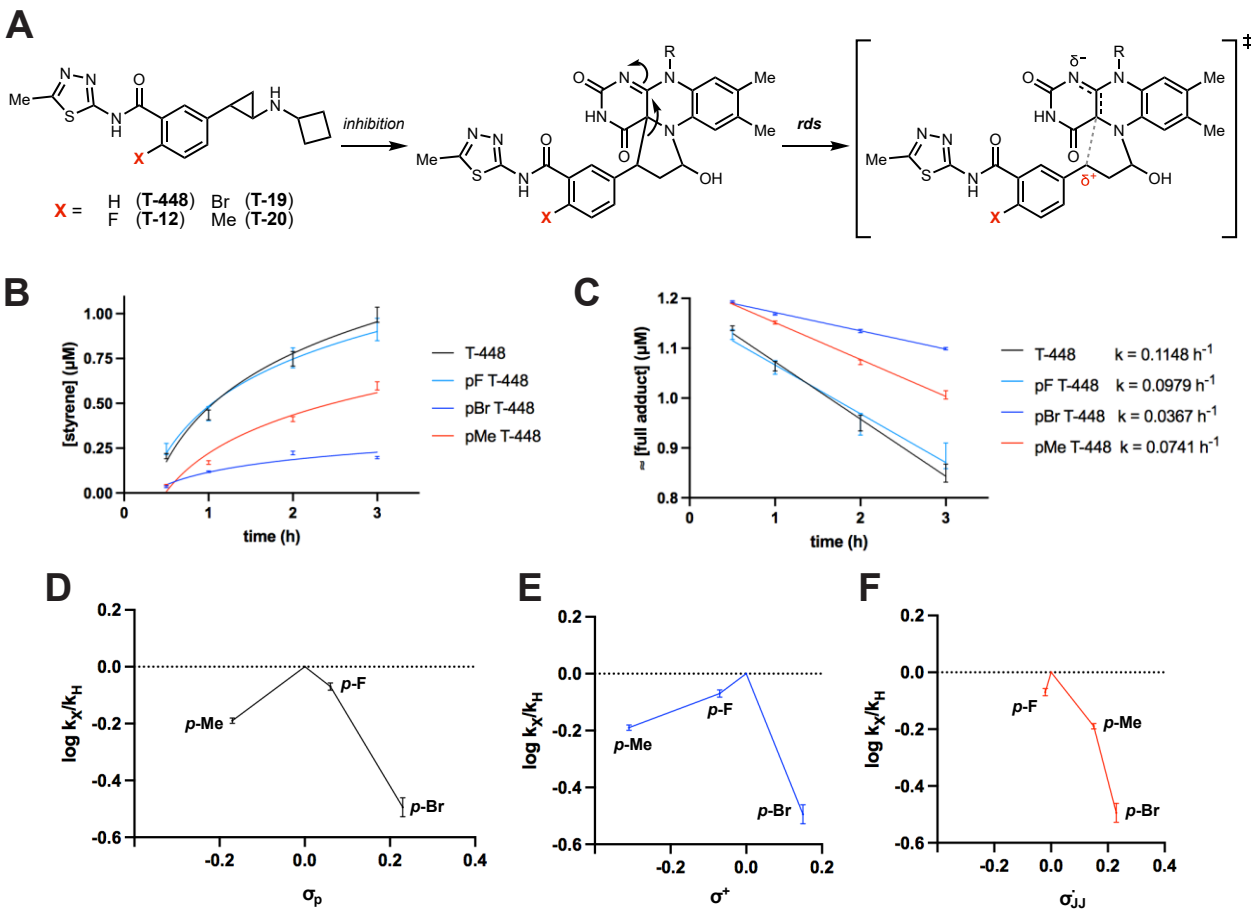

Figure 2.11. Hammett analysis of T-448 adduct fragmentation.

A) LSD1 was treated with 2-X substituted T-448 analogs in tandem to assess rate-determining substituent effects. **B)** Kinetic plots were obtained for styrene generation of each reaction. **C)** Rate constants were calculated for each reaction. All *para*-substituted inhibitors generated styrene more slowly than T-448, producing concave-down plots for **D)** σ_p, **E)** σ^+, and **F)** $\sigma_{JJ}^{\cdot}$ substituent constants.

We postulate that our result could reflect the signature "concave down" Hammett trend indicative of a change in rate-determining step.[45,46] This interpretation would support a dramatic change in slope between electron-donating and withdrawing substituent effects: while the *para*-bromide slows down rate-limiting carbonium formation, the *para*-methyl might stabilize the carbonium intermediate and increase the energetic barrier to Grob-like fragmentation sufficiently to make this second step rate-determining.

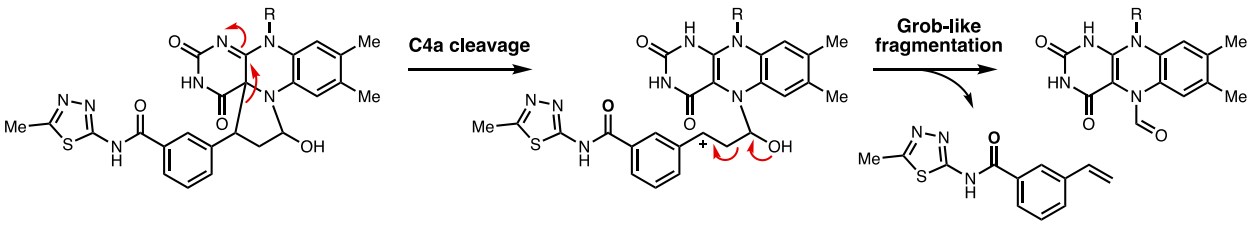

Figure 2. 12. Proposed mechanism for stepwise Grob-like fragmentation.

Initial C-C bond cleavage yields a benzylic carbonium intermediate, which subsequently fragments to product formyl-FAD and styrene byproduct.

We alternatively speculate that the LSD1 active site might simply not tolerate *para*-substituents to the T-448 adduct, causing the mechanism to diverge and compromising the integrity of the Hammett analysis. The four substituent effect data points we obtained are insufficient to confirm the linearity of both slopes of a concave Hammett plot, and 2-3 additional substituent rates would be required to confidently support our proposed mechanism for rate-determining heterolysis of the C-C bond between FAD C4a and the benzylic adduct carbon, followed by Grob-like fragmentation of a reactive carbonium intermediate to yield formyl-FAD and byproduct styrene (Fig. **2.12**).

2.4. Insights into structural requirements for fragmentation

Cursory examination of T-448 highlights its *N*-thiadiazole benzamide substituent as a notable structural feature which distinguishes T-448 from GSK-LSD1 and other tranylcypromine inhibitors. In addition to our kinetic measurements by LC-MS, we qualitatively monitored the progression of T-448 adduct fragmentation reaction using a fluorescence polarization (FP) binding assay in which light polarization of a fluorescently labelled SNAG peptide reports on binding of the peptide to LSD1 as a proxy for Grob-like fragmentation. Using our optimized protocol, we observed SNAG-LSD1 binding within 30 min after T-448 treatment and noted time-dependent recovery to DMSO control levels after 5 hours (Fig. **2.13**).

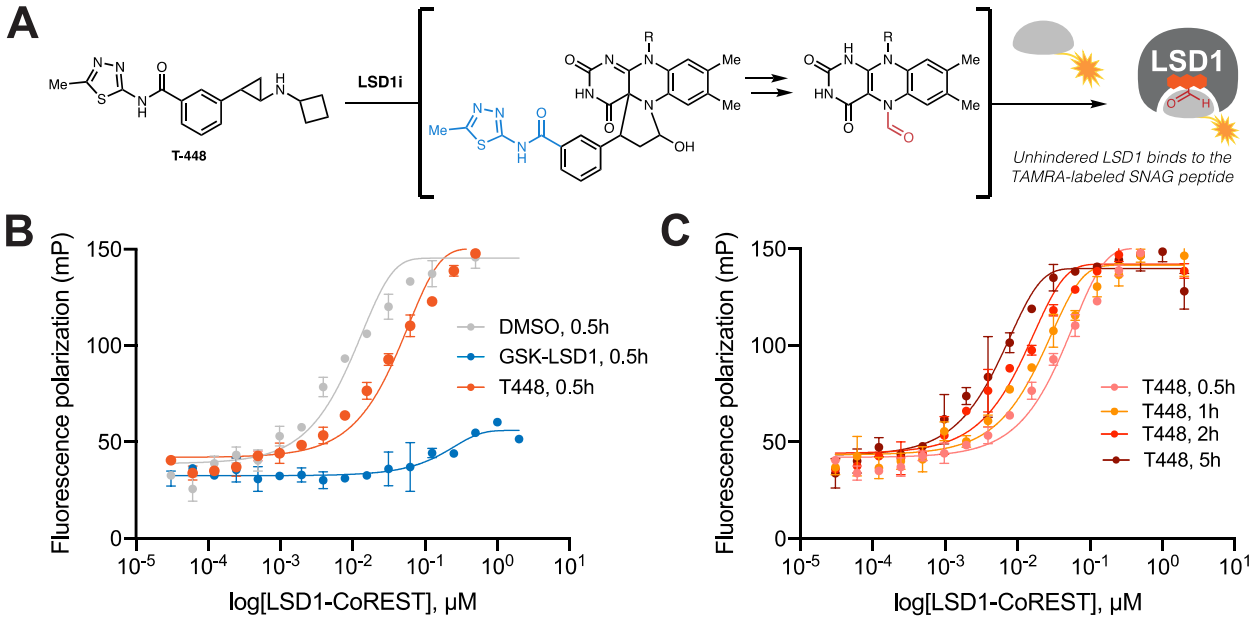

Figure 2.13. Fluorescence polarization reports on time-dependent adduct fragmentation.

A) Fluorescence polarization of a TAMRA-labeled SNAG peptide reports on LSD1-SNAG binding as a proxy for Grob-like fragmentation. **B)** T-448 pre-treated LSD1 partially binds SNAG peptide at 0.5 h. **C)** T-448 pre-treated LSD1 recovers SNAG binding activity in a time dependent fashion.

We applied the FP binding assay to profile structure-activity relationships (SAR) of T-448 inhibitor adducts and interrogate the minimal structural requirements for Grob-like fragmentation.[41,47] We hypothesized that the thiadiazole ring might be responsible for stereoelectronic interactions necessary for fragmentation and synthesized a panel of N-aryl

substituted T-448 analogs. Our goal in this aim was to investigate whether fragmentation could be attenuated by minimally altering the steric or electronic character of the T-448 inhibitor adduct (Fig. **2.14**A). By fluorescence polarization, we concluded that Grob-like adduct fragmentation tolerated the minor changes in N-substituent of **T-6** and **T-7**, but that the N-phenyl substituent of analog **T-8** partially inhibited SNAG binding (Fig. **2.14**B). Consistent with T-448 behavior, **T-8** did not inhibit proliferation in SET-2s or disrupt LSD1-GFI1B binding in HEK 293T cells (Fig. **2.14**C), and we detected **T-8** styrene from extracted SET-2 cell media following compound treatment. Taken together, these data support Grob-like fragmentation of **T-8** inhibitor-adducts in cells.

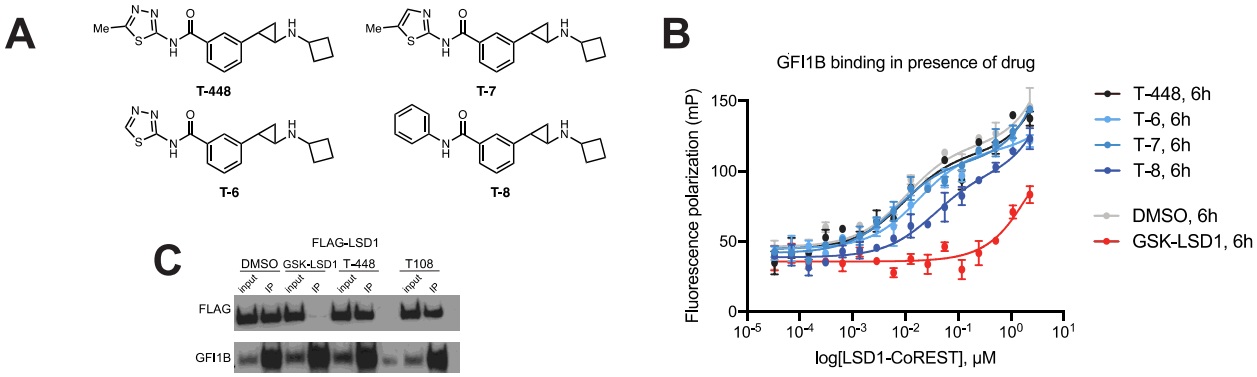

Figure 2.14. SAR on *N*-aryl benzamide substituent of T-448 inhibitors.

A) T-448 analogs **T-6-8** minimally modify the N-aryl benzamide substituent. **B)** LSD1 recovers SNAG binding after **T-6-8** inhibition. **C)** Co-IP of wild-type FLAG–LSD1 with GFI1B was performed after vehicle or inhibitor treatment (500 nM, 48 h) in transiently transfected HEK 293T cells. Co-IP was performed using an anti-GFI1B antibody. LSD1 was detected using an anti-FLAG antibody.

Quantification of FAD inhibition products by LC-MS (Fig. **2.15**) revealed that **T-8** indeed attenuated Grob fragmentation compared to T-448, producing only 16% formyl-FAD as the minor inhibitor product compared to T-448 (78% formyl-FAD). Given that the *N*-phenyl benzamide substituent of the **T-8** inhibitor adduct is insufficient to fully arrest fragmentation, we performed more drastic modifications to the inhibitor structure. Reversing the amide group of the **T-8** *N*-phenyl benzamide (**T-18**) further reduced formyl-FAD production to 6%, as did replacement of the *N*-aryl benzamide with a methyl benzoate (**T-15**, 4% formyl-FAD) and an *N*-methylbenzamide (**T-16**, 2% formyl-FAD). Finally, we observed full inhibition of fragmentation to formyl-FAD upon

replacement of the T-448 substituent with an *N,N*-dimethylbenzamide (**T-17**) and migration of the T-448 substituent *para* to the cyclopropylamine warhead (**T-14**).

Inhibitor	IC_{50}	Inhibition products	
		full adduct	formyl adduct
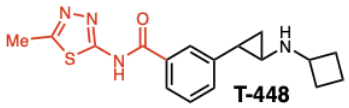 T-448	0.2 μM	22%	**78%**
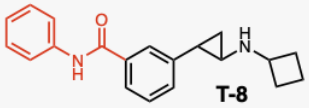 T-8	0.3 μM	**84%**	16%
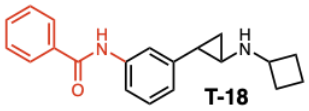 T-18	10 μM	**94%**	6%
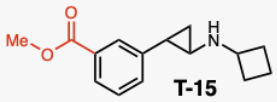 T-15	17 μM	**96%**	4%
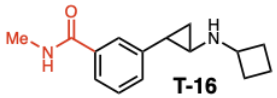 T-16	26 μM	**98%**	2%
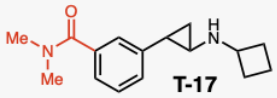 T-17	49 μM	**100%**	-
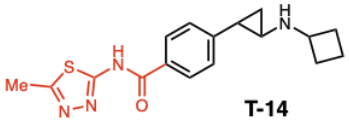 T-14	0.4 μM	**100%**	-

Figure 2.15. Covalent FAD-inhibitor products of T-448 analogs.

FAD adducts were detected by LC-MS and quantified by relative abundance after extracting recombinant LSD1 treated with inhibitor for 24 h.

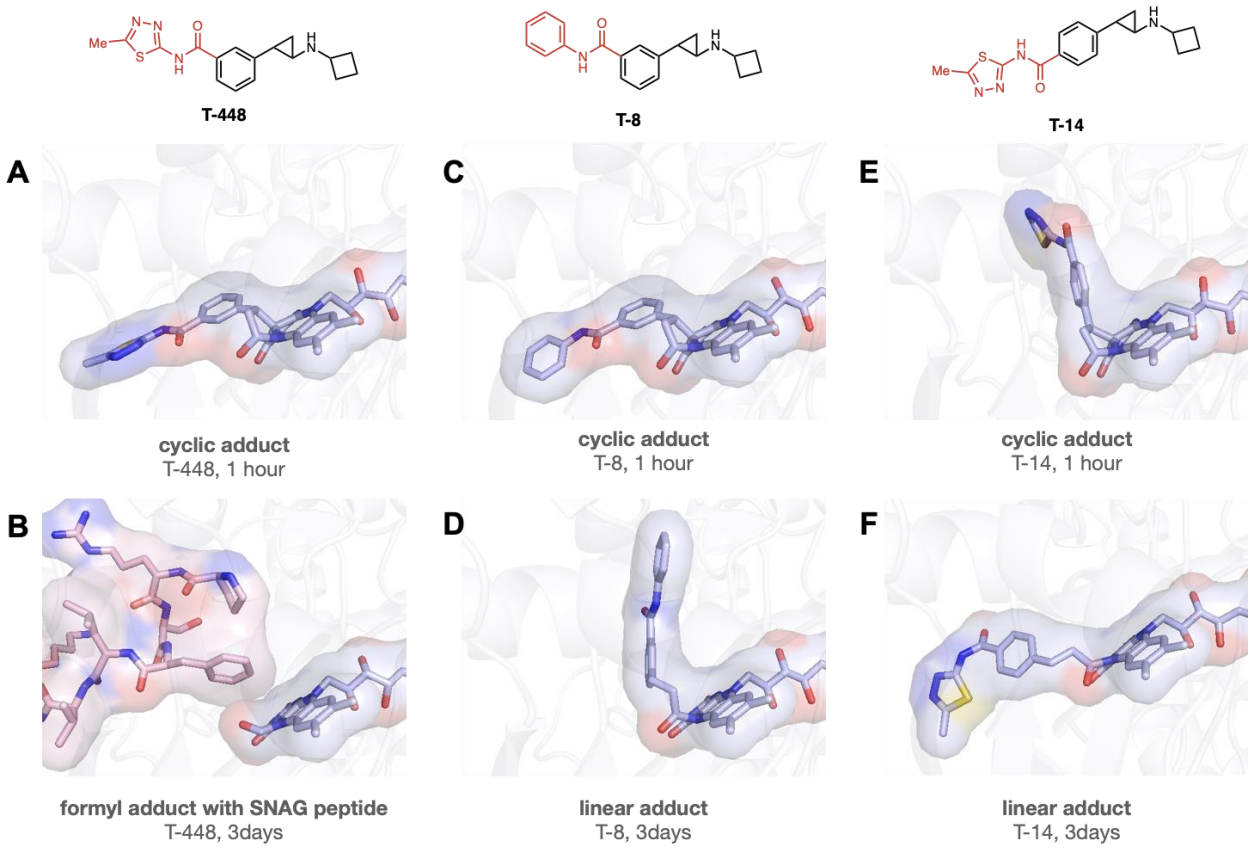

Figure 2.16. Crystal structures of major inhibitor adducts.

A,B) T-448 forms a cyclic hemiaminal adduct at 1 hour, subsequently fragmenting to a compact formyl adduct that rescues SNAG binding. **C,D) T-8** forms a cyclic hemiaminal adduct analogous to that of T-448, subsequently undergoing rearrangement to a linear N5 adduct. **E,F) T-14** forms a cyclic hemiaminal adduct with different stereochemistry to those of T-448 and **T-8**, subsequently fragmenting to a linear N5 adduct.

Intrigued by these results, we treated LSD1-CoREST crystals with T-448 and analogs to investigate structural features of FAD-inhibitor adducts within the LSD1 active site that might facilitate fragmentation (Fig. **2.16**). Following compound soaking, crystals were treated with 1 mM SNAG peptide prior to flash-freezing. Following T-448 treatment, we observed the full T-448 inhibitor adduct (analogous to GSK-LSD1) after one hour and the formyl adduct after 3 days. We further observed recovery of SNAG peptide binding to LSD1 with formyl-FAD. One-hour treatments with **T-8** and **T-14** yielded characteristic cyclic inhibitor adducts with an apparent change in **T-14** adduct stereochemistry at the benzylic position likely resulting from steric effects

of the *para*-substituent during enzyme inhibition. Notably, 3-day crystal soakings with **T-8** and **T-14** each yielded full N5 adducts that had been liberated from the FAD C4a. **T-8** and **T-14** exhibited similar LSD1 potency to T-448 and did not inhibit proliferation in SET-2s, indicating that the fragmentation activity of these compounds sufficiently rescues essential LSD1-SNAG binding.

The linear N5-adduct of **T-8** and **T-14** could result from the same C4a cleavage event that initiates the Grob-like fragmentation of the T-448 adduct, with a possible pathway divergence due to the differing conformation of the **T-14** inhibitor adduct within the active site and from the differing electronic or steric character of the **T-8** benzamide. We propose a possible mechanism for 1,3-hydride transfer as reported in some synthases[48–50] to generate the linear N5-FAD adduct via a tertiary N5-(1-hydroxy-3-phenylpropylidene) carbocation (Fig. **2.17**). While rearrangement of the **T-14** adduct would proceed solely through this mechanism, the *meta*-amide moiety of the T-448 and **T-8** adducts might facilitate Grob-like fragmentation to formyl-FAD by participating in a hydrogen-bond network with the adduct hemiaminal hydroxyl. While **T-8** produces both products, T-448 likely promotes the Grob-like fragmentation mechanism over the rearrangement mechanism due to the electron-deficiency of the *N*-thiadiazole benzamide substituent.

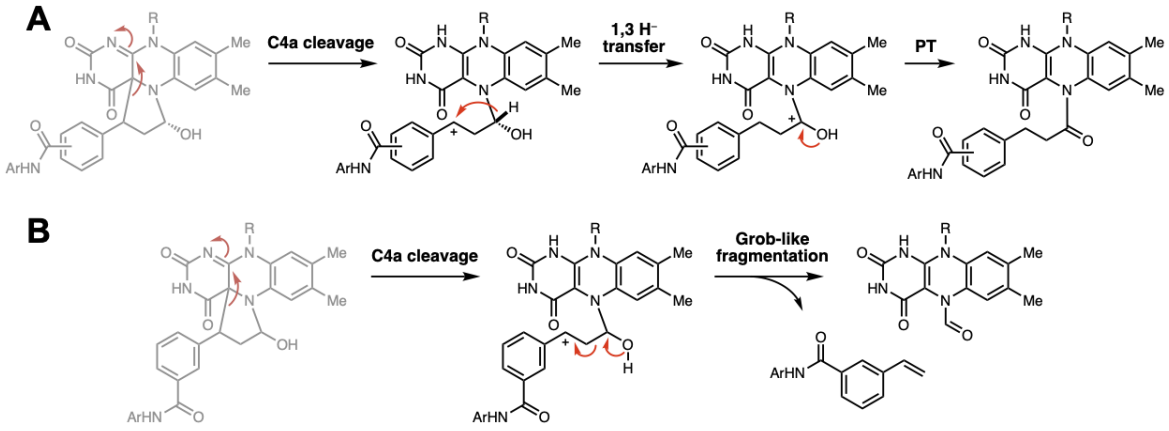

Figure 2.17. C-C cleavage of C4a cyclic hemiaminal inhibitor adducts yields *N*5-formyl and *N*5-full adducts via a divergent mechanism.

A) Inhibitor adducts of analogs **T-8** and **T-14** exhibit time-dependent conversion to a linear N5 major product. A proposed mechanism for adduct rearrangement is provided in which a 1,3-H- transfer occurs prior to carbonium quenching. **B)** The T-448 adduct favors Grob-like fragmentation, generating *N*5-formyl FAD as the major inhibitor product. Some inhibitors, like **T-8** and **T-18**, generate small amounts of *N*5-formyl in addition to their linear N5 products.

2.5. Grob-like fragmentation as a novel drug resistance mechanism in AML

Previous work from our lab used various demethylase inhibitors as selection tools to identify drug-resistance mutations in LSD1 through CRISPR-suppressor scanning to identify drug-resistance mutations selected by various inhibitors (Fig. **2.18**A). Most enriched mutations were within exon 15, consistent with drug-resistance mutations within the active site that prevent inhibitor binding. Notably, inhibitor analog AW4 selectively enriched distal deletion mutations in exon 16, the most prevalent being the 4-amino acid deletion T684_S687 (TTASdel) (Fig. **2.18**B). Biochemical characterization of TTASdel revealed that the mutant maintains enzymatic activity, and that AW4 irreversibly inhibits TTASdel enzyme activity. However, AW4-treated TTASdel exhibited time-dependent recovery of SNAG binding by FP (Fig. **2.18**C), and an LSD1 TTASdel clonal cell line exhibited selective resistance to AW4 compared to other inhibitors.

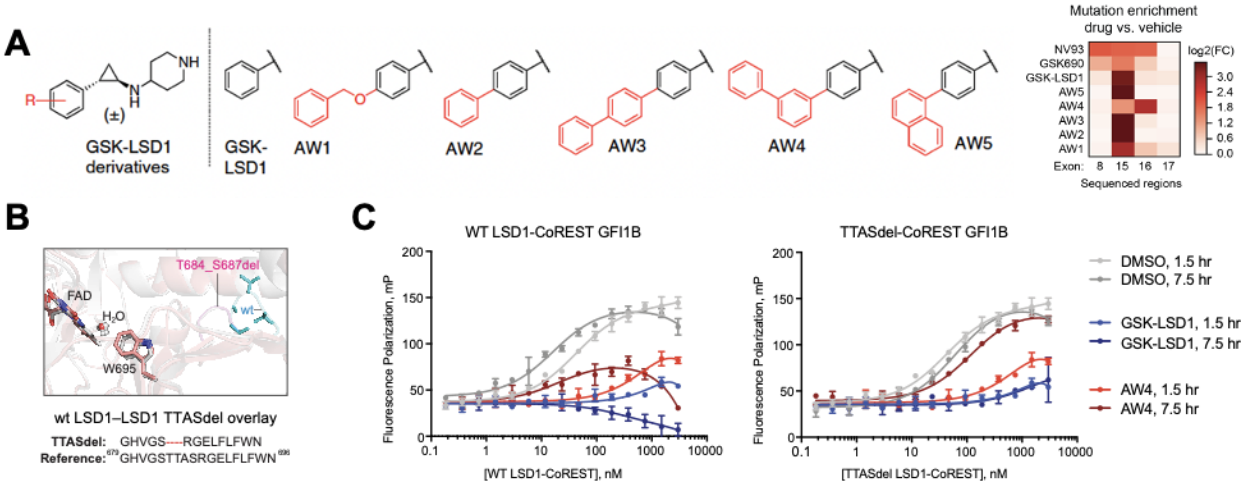

Figure 2.18. Rescue of GFI1B binding in LSD1 TTASdel upon AW treatment.

A) CRISPR-suppressor scanning identified drug-resistance mutations enriched across different drug treatment conditions. Heat map shows mutation enrichment in sequenced exons. **B)** Homology model of LSD1 TTASdel (salmon) overlaid with WT LSD1 (gray) is shown to highlight the deletion of the WT loop (cyan) compared to the truncated mutant loop (magenta). (PDB: 2HKO). **C)** Binding curves show fluorescence polarization (*y*-axis) for increasing concentrations of LSD1-CoREST (*x*-axis) in the presence of a fluorescently labeled GFI1B(1-9) peptide after treatment with DMSO, GSK-LSD1 or AW4.

Compound soaking of LSD1 crystals with AW4 revealed an initial C4a cyclic hemiaminal inhibitor adduct in a similar conformation to the **T-14** inhibitor adduct (Fig. **2.19**A,B). Moreover, 3-day AW4 soaking yielded an *N*5-full adduct as the major inhibitor product, similarly to **T-8** and

T-14. Overlay of the SNAG peptide revealed that the 3-day N5 adduct appeared to occupy the GFI1B binding cleft (Fig. **2.19**), and we wondered whether AW4-treatment of TTASdel rescues GFI1B binding due to flexibility of the liberated **T-14**-analogous linear adduct to accommodate the SNAG peptide or to **T-8**-analogous generation of small amounts of *N*5-formyl FAD as a minor product. Towards, this aim, we identified TTAS loop residues of wild-type LSD1 that we predicted might participate in H-bond interactions with the αD helix of the amine oxidase domain, theorizing that disruption of this network might activate the drug-resistance rearrangement mechanism of AW4 (Fig. **2.19**C).

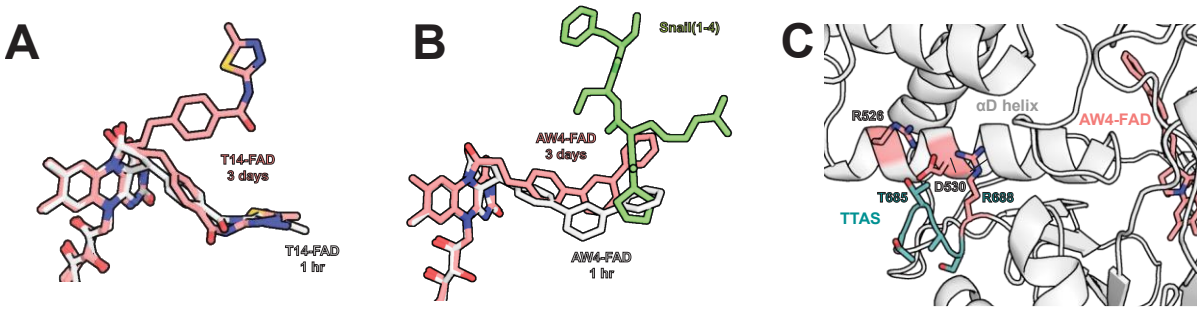

Figure 2.19. Facilitation of C4a AW4 inhibitor adduct rearrangement by the αD helix of LSD1 TTASdel.

A,B) T-14 and AW4 form structurally similar C4a hemiaminal inhibitor adduct before rearranging to their respected linear N5 adducts. **C)** The αD helix of the LSD1 amine oxidase domain makes potential H-bond interactions with TTASdel, potentially mediating crosstalk with the active site.

LC-MS analysis of AW4-treated LSD1 TTASdel covalent inhibitor products detected peaks of *m/z* 1070 and *m/z* 814, corresponding to the full AW4-FAD adduct and the formyl-FAD adduct, respectively (Fig. **2.20**A,B). Notably, no formyl-FAD was detected upon treatment of wild-type LSD1 with AW4 under the same conditions. Furthermore, formation of formyl-FAD by LC-MS accompanied time-dependent increase in detection of AW4 styrene by GC-MS, supporting fragmentation of the TTASdel-AW4 inhibitor adduct to Grob-like minor products during adduct rearrangement (Fig. **2.20**C,D).

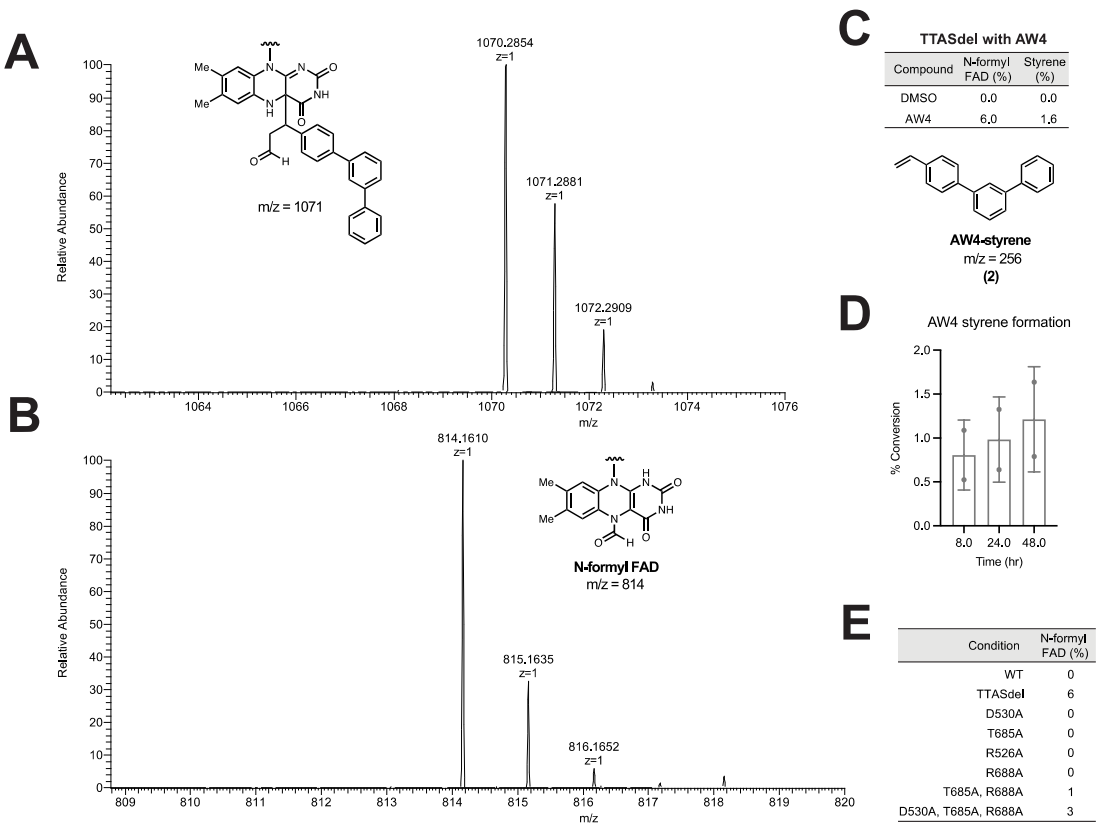

Figure 2.20. Grob-like fragmentation of AW4 inhibitor adducts to LSD1 TTASdel.

A,B,C) After extracting recombinant LSD1 TTASdel-CoREST treated with AW4 for 24 h, both the full FAD-drug adduct **(A)** and formyl-FAD adduct **(B)** were detected by LC-MS, and the AW4 styrene **(C)** was detected by GC-MS. **D)** Generation of AW4 styrene was quantified by GC-MS at the indicated time points. **E)** *N*-formyl FAD was detected by LC/MS after treating double and triple alanine mutants of LSD1-CoREST for 24 h with AW4.

Having detected Grob fragmentation products from AW4-inhibited LSD1 TTASdel, we revisited the proposed TTAS-αD helix contacts through mutational profiling of the identified TTAS-loop residues (T685A, R688A) and αD helix residues (R526A, D530A). We did not detect formyl-FAD upon AW-4 treatment of single-point alanine mutants; however, double (T685A, R688A) and triple (D530A, T685A, R688A) alanine mutants produced *N*-formyl-FAD, recapitulating the Grob-like fragmentation mechanism of TTASdel. These results support the hypothesis that TTASdel may facilitate AW4-FAD fragmentation by modulating αD helix-mediated crosstalk with the active site (Fig. **2.19**C, **2.20**E).

2.6. Conclusions and implications for LSD1 inhibitor therapies

Drug resistance presents a major limiting factor in developing treatments to cure cancers, mitigating initial therapeutic successes with discouraging patterns of cancer remission, resistance development, and disease relapse. Identification and characterization of resistance-conferring mutations can aid advances in therapeutic development by integrating new discoveries in target biochemistry with clearer understanding of drug pharmacology.[51] Previous work from the Liau lab has employed CRISPR-suppressor scanning to identify mutations in several chromatin-modifying enzymes that confer resistance to small molecule anticancer inhibitors.[27,52,53] While many prevalent resistance mechanisms block inhibitor binding, we report a novel drug-resistance mechanism against LSD1 inhibitors in AML in which a distal deletion mutation, TTASdel, facilitates Grob-like fragmentation of the covalent adduct of the demethylase inhibitor AW4. We report that TTASdel promotes ring opening of the cyclic C4a inhibitor adduct to produce an N5 adduct mixture consisting of a full adduct isomer major product and a Grob-like fragmentation minor product, *N*5-formyl-FAD. The latter reaction proceeds through a similar mechanism to the recently published demethylase-specific LSD1 inhibitors T-448 and TAK-418, which are being investigated for applications in psychiatry.[34–36] We characterized the mechanism of Grob-like inhibitor adduct fragmentation within the LSD1 active site using T-448 analogs to profile structure-activity relationships and fragmentation kinetics and applied our findings to elucidate the structural requirements for TTASdel-mediated fragmentation.

Isotopic labelling of the T-448 tranylcypromine warhead confirmed that FAD formylation occurred through an initial enzyme inhibition mechanism identical to GSK-LSD1, before subsequently proceeding through an unprecedented fragmentation mechanism. We later corroborated this result through crystallographic analysis of the covalent inhibitor products of T-448 and other tranylcypromine inhibitor analogs. SAR profiling of LSD1-inhibitor analog adducts suggested that *meta*-carbonyl substitution to the tranylcypromine warhead was essential for

Grob-like fragmentation both in directing the stereoselectivity of initial C4a inhibitor adduction and participating in a hydrogen-bond network within the LSD1 active site. Quantification of final inhibitor adducts by LC-MS indicated that electron-deficient *N*-heterocyclic benzamide substitution (T-448, **T-6**, **T-7**) promoted Grob-like fragmentation and produced *N*-formyl FAD as the major inhibitor product. In contrast, *N*-phenyl substitution (**T-8**) attenuated Grob-like fragmentation, producing *N*-formyl FAD as the minor inhibitor product, and instead favoring rearrangement of the full inhibitor adduct upon cleavage from the FAD C4a.

Our kinetic investigation of T-448 fragmentation suggested that C-C bond cleavage of the benzylic adduct carbon from FAD C4a was rate limiting, possibly proceeding through a carbonium intermediate. While our Hammett analysis of T-448-adduct fragmentation proved inconclusive, a concave-down Hammett plot would support our proposed cationic mechanism and could explain why the electron-deficient thiadiazole substituent of T-448 is privileged in its ability to promote Grob-like fragmentation within the active site.

We confirmed that TTASdel promoted Grob-like fragmentation of covalent AW4 adducts through detection of Grob products by LC-MS and GC-MS. Crystallographic analysis of AW4 covalent inhibitor adducts revealed time-dependent liberation of the initial cyclic hemiaminal product from the FAD C4a to generate a linear N5 adduct isomer, similarly to **T-8**. Mutational profiling of TTAS-loop interactions with the amine oxidase αD helix suggested that disruption of TTAS-αD helical H-bonding contacts might reposition the αD helix to subsequently trigger AW4 inhibitor adduct fragmentation upon C4a cleavage. This explanation indicates that LSD1 might mediate Grob-like fragmentation of inhibitor adducts through two possible mechanisms: firstly, through participation of meta-carbonyl TCP substituents in an active-site H-bond network and secondly, through disruption of αD helix-mediated crosstalk between the active site and distal loop deletions.

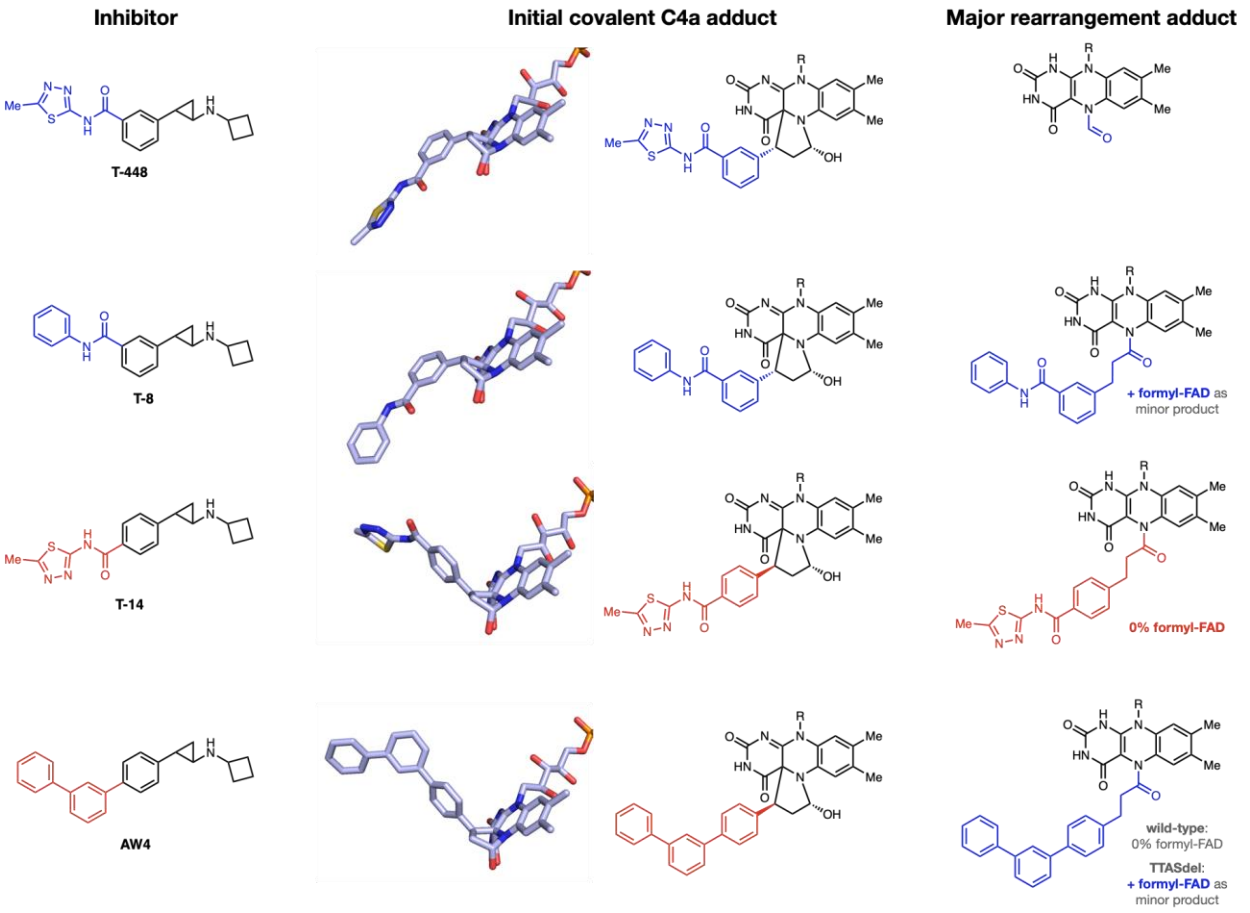

Figure 2.21. Summary of LSD1-mediated Grob-like fragmentation SAR.

Upon LSD1 inhibition, *meta*-substituted inhibitors T-448 and **T-8** form analogous cyclic hemiaminal adducts before undergoing Grob-like fragmentation. Upon LSD1 inhibition, *para*-substituted inhibitors **T-14** and AW4 form cyclic hemiaminal adducts with different stereochemistries compared to *meta*-substituted inhibitors. **T-14** and AW4 both form linear N5 rearrangement products with 0% conversion to formyl-FAD; however, TTASdel facilitates minor conversion of the AW4 inhibition adduct to formyl-FAD.

The identification of a Grob-like mechanism for LSD1-inhibitor adduct fragmentation holds exciting implications, both in uncovering a novel drug-resistance mechanism and in opening new avenues for therapeutic applications of demethylase inhibitors for neurological disease applications. T-448 marked the first of these compounds, revealing the potential of tranylcypromine derivatization to access demethylase-specific inhibitor therapies with improved safety profiles. Administration of T-448 in mice with *N*-methyl-D-aspartate receptor (NMDAR) hypofunction, a preclinical model of schizophrenia and autism spectrum disorder (ASD) enhanced H3K4me2 levels, increased mRNA expression of neural plasticity-related genes such as brain

derived neurotrophic factor (*Bdnf*), and rescued learning deficits, indicating therapeutic potential to treat NMDAR hypofunction-associated psychiatric illnesses such as schizophrenia and ASD.[34] Another recently identified demethylase-specific inhibitor, TAK-418 (Fig. **2.22**), similarly recovered gene expression homeostasis in the rodent brain and ameliorated ASD-like social and cognitive deficits in rodents.[35] TAK-418 is currently undergoing clinical trials as a potential therapy for central nervous system disorders such as Kabuki syndrome, exhibiting rapid brain-penetrance and dose-dependent formation of formyl-FAD. TAK-418 has performed well in phase 1 studies with no reported clinically significant adverse side effects.[36]

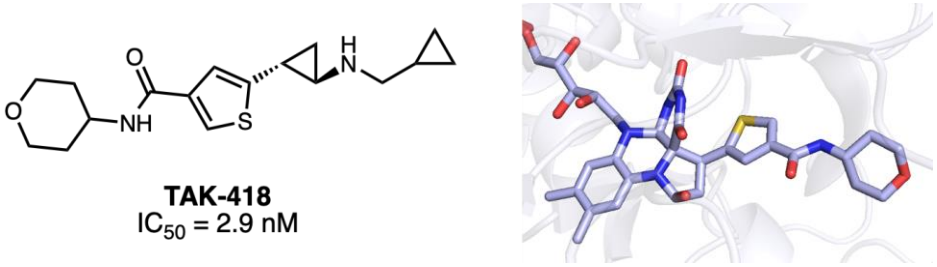

Figure 2.22. Molecular Operating Environment (MOE) computational model of TAK-418-FAD adduct.

In summary, we illuminated novel reactivity exhibited by the histone demethylase LSD1 and interrogated structural features within the active site and the allosteric TTAS loop that promote Grob-like fragmentation of covalent tranylcypromine suicide adducts and enable demethylase-specific inhibition by rescuing essential binding function to the transcription factor GFI1B. Future efforts will include further validation of LSD1 TTAS-loop deletions in SET-2 cellular model systems and completion of inhibitor analog adduct characterizations by fluorescence polarization binding assays and crystallographic analysis.

Experimental

Expression and Purification of Human LSD1 Protein

For bacterial constructs, the LSD1 (Δ1-150) gene was codon optimized and synthesized as two fragments from Integrated DNA Technologies and Quintara Biosciences. The fragments were cloned into pET28b containing an N-terminal His_6-tag using Gibson cloning. Mutations were introduced with Q5 Site-Directed Mutagenesis Kit. The constructs were expressed in NiCo21(DE3) competent *E. coli* (New England Biolabs) using a previously described protocol.[54] Protein fractions with > 95% purity as assessed by SDS PAGE were pooled and stored at –80 ºC in 25 mM sodium phosphate pH 7.4, 150 mM NaCl, 0.3 mM TCEP, and 5% glycerol (storage buffer). CoREST(305-482) was codon optimized for bacterial expression and assembled into pET28b containing an N-terminal GST-tag followed by a TEV cleavage site from a synthesized fragment purchased from GeneWiz. Recombinant CoREST expression and purification were carried out according to a modified literature procedure.[55] Recombinant protein was purified by GST affinity chromatography using a linear gradient of 0-50 mM reduced glutathione in lysis buffer and the buffer was exchanged to TEV protease cleavage buffer (50 mM Tris-HCl pH 8.0, 75 mM NaCl, 1 mM DTT, and 0.5 mM EDTA). The GST-tag was removed by incubation with TEV protease overnight at 4 °C. The cleaved protein was purified using a GSTrap column followed by Superdex 200 10/300 GL column (GE Healthcare) in storage buffer. Purified CoREST was incubated with LSD1 in a 2:1 molar ratio for 2 h and gel-filtered on a Superdex 200 10/300 GL column equilibrated in storage buffer. The purity of the complex was verified by SDS-PAGE and fractions with 90-95% purity were pooled and stored at -80 ºC.

In Vitro LSD1 Demethylase Assay

LSD1 enzymatic activity assays were performed in triplicate using Amplex Red Hydrogen Peroxide/Peroxidase Assay Kit (Invitrogen) with recombinant LSD1 and a synthetic peptide

corresponding to the first 21 amino acids of H3K4me2 (Anaspec). LSD1 (500 ng/well) was incubated with 20 μM peptide at rt for 30 min. The endpoint fluorescence was measured on a microplate reader (excitation: 530 nm; emission: 590 nm) after 60 min following the addition of the Amplex Red/HRP mixture. Inhibition assays were performed as described above. Briefly, LSD1 (75 ng/well) and inhibitors at the appropriate concentration were incubated at rt for 10 min in reaction buffer with 0.01% BRIJ35 (ThermoFisher Scientific) prior to the addition of peptide. K_i values were determined in GraphPad Prism v.7 by nonlinear regression analysis (log(inhibitor) vs. response—variable response) of the concentration/inhibition data.

Fluorescence Polarization Binding Assay

Binding assays were performed in two independent experiments with three technical replicates. The change in fluorescence polarization of fluorescently labeled GFI1B peptide upon binding to LSD1-CoREST was monitored using a previously described protocol.[56] LSD1-CoREST (2 μM) was incubated with the labeled peptide (2 nM) for 1 h on ice. After incubation, the samples were prepared by a 2-fold serial dilution in the assay buffer (15 mM KH_2PO_4, pH 7.2, 5% glycerol, and 1 mg/mL BSA) containing 2 nM labeled peptide. For assays in the presence of 10 μM inhibitor, the protein complex was incubated with the inhibitor for 1 h on ice and then with the labeled peptides for 1 h. Fluorescence polarization was measured using a microplate reader in 384-well black microplates at 25 °C. The G-factor on the microplate reader was adjusted to 35 mP for the reference well containing labeled peptide. The binding curves were fit by nonlinear regression analysis in GraphPad Prism v.7 as described previously.

SET-2 Cell Culture and Growth Assays

SET-2 cells were gifted from Matthew Shair and were cultured at 37 °C in RPMI-1640 (Life Technologies) containing 20% fetal bovine serum (FBS, Peak Serum). Cell viability was assessed by CellTiter-Glo™ Luminescent Cell Viability Assay (Promega, #G7570) according to the

manufacturer's instructions. SET-2 were seeded in 96-well plates with 2,000 cells per well in triplicate with drug or vehicle treatments. Cell viability was monitored at day 7 by measuring end point luminescence using CellTiter-Glo on a SpectraMax i3x plate reader. ATP standard curve was prepared using known concentrations of ATP and used to calculate the ATP content of cells. Dose-response curves were determined through interpolation using GraphPad Prism v.7 nonlinear regression fit ([inhibitor] vs normalized response -- variable slope). All growth assays were performed at least twice.

FAD-adduct and styrene detection by LC/Q-TOF MS. Analysis of FAD-adducts after LSD1 protein treatment with inhibitor was adopted from Matsuda *et al*.[34] Briefly, 100 μM of LSD1 was treated with 800 μM inhibitor at room temperature for indicated time points in 50 mM Tris-HCl (pH 8.0) and then subjected to 8 M urea to a final concentration of 6.4 M for 1 hr at 4 ºC to denature the sample. The compound-FAD adducts were then extracted at 4 ºC with acetonitrile for 15 min. The precipitates were removed by centrifugation at 10,000 *x* g for 10 min, and the supernatant was supplemented with 500 mM ammonium acetate to a final concentration of 5 mM and filtered before sample injection. Samples were then injected onto a Phenomenex Kinetix C18 column (2.1 mm, 2.6 micron particle size, 150 mm length) with Orbitrap (Thermo q-Exactive Plus). Water with 0.1% formic acid and acetonitrile were used as mobile phases A and B, respectively. The mobile phase composition was changed to 100% B over 20 minutes.

Styrene quantitation by LC/Q-TOF MS

For WT LSD1, 80 μM of LSD1 was treated with 640 μM inhibitor at room temperature for indicated time points in 50 mM Tris-HCl (pH 8.0) and then subjected to 8 M urea to a final concentration of 6.4 M for 1 hr at 4 ºC to denature the sample. The compound-FAD adducts were then extracted at 4 ºC with 240 μL acetonitrile with 3.3 μM caffeine as an internal standard for 15 min. The precipitates were removed by centrifugation at 10,000 *x* g for 10 min. The supernatant was

supplemented with 500 mM ammonium acetate to a final concentration of 5 mM and filtered before sample injection. Samples were then injected onto a C18 Zorbax RR StableBond column (4.6 x 50 mm, 3.5 µm, Agilent) coupled to a high resolution QTOF mass spectrometer (Bruker, Impact II). Water and acetonitrile each with 0.1% formic acid were used as mobile phases A and B, respectively. The mobile phase composition was changed to 100% B over 40 min. MassHunter software was used for data acquisition and processing. Product quantitation was calculated from integration of extracted ion chromatogram peaks against the calibrated internal standard.

For TTASdel LSD1-CoREST, 50 µM of LSD1 was treated with 400 µM inhibitor and 100 µM GFI1b peptide at room temperature for indicated time points in 50 mM Tris-HCl, pH 8.0. Styrene was extracted with 200 µL DCM with 100 µM tridecane as an internal standard. The DCM was subsequently removed and the extract was resuspended in 200 µL of ACN and analyzed with Waters Quattro micro GC/MS/MS.

Styrene detection from cell media

5 million SET-2 cells were resuspended in 1 mL of R-20 and treated with 1 µM of inhibitor for 24 hr. The cells were spun down and the media was filtered through a 0.22 µm filter and then extracted 2x with 300 µL dichloromethane. Dichloromethane was subsequently removed and the extract was resuspended in 100 µL of acetonitrile and analyzed by high-resolution mass-spectrometry.

Molecular mass determination of FAD inhibition products

The inhibition was realized on samples of > 100 µM LSD1-CoREST complex in 25 mM KH_2PO_4, pH 7.2 and 5% glycerol. Inhibitors was added for a final concentration of 400 µM and the incubation was at 20°C room for 24 hours. Inhibited LSD1-CoREST is unfolded by adding a proper volume of 8 M urea solution to have a final concentration of 6.4 M urea. After one hour on ice,

acetonitrile (final concentration 30%) was added to percipitate protein debris. After centrifugation, supernatant is stored at -20°C untill spectrometric analysis. The sample solution was diluted 1:1 with 5 mM ammonium acetate and was injected to a high resolution QTOF mass spectrometer UHPLC-HRMS/MS- AB Sciex X500B. Chromatographic separation was achieved using a C18 Zorbax extend analytical column (2.1 x 50 mm, 1.8 µm, Agilent). The mobile phase consisted of (A) 5 mM ammonium acetate in water and (B) methanol. The compositions of gradient elution (the mixture of (A) and (B) were as follows designated in percentage of (B), v/v); 5-10% at 0–1 min, 10–80% at 1–10 min, 80% at 10–15 min, 5% at 15–25 min. The flow rate was set at 0.3 mL/min. The mass spectrometer was operated in the negative ionization mode. SCIEX software was used for data acquisition and processing. The percentage of products represent the percentage of total area of all extracted ion current peaks. FAD-adducts were usually distributed in different peaks comprising [M-H]-, [M-H-H2O]- (dehydrated adduct), [M-2H+Na]-and [M-H+CH3]- (methylester).

General Synthetic Procedures

Unless otherwise noted, all reactions were performed in dry glassware under N_2 atmosphere. Flash column chromatography was conducted on a Biotage Isolera automated chromatography system or manually in a glass column unless otherwise specified. Celite filtration was performed using Celite. 545 (EMD Millipore). Preparatory and analytical thin-layer chromatography (TLC) was performed on Silica Gel 60 F_{254} plates (EMD Millipore). TLC plates were visualized by exposure to ultraviolet light (UV) and exposure to an aqueous solution of ceric ammonium molybdate (CAM), ninhydrin, *p*-anisaldehyde, or potassium permanganate stain followed by heating on a hot plate. Organic solvents were concentrated under reduced pressure on a Büchi rotary evaporator.

Commercial reagents and solvents were used as received with the following exceptions: tetrahydrofuran (THF), dichloromethane (CH_2Cl_2), toluene, and *N,N*-dimethylformamide (DMF)

were degassed with argon and passed through a solvent purification system (designed by Pure Process Technology) utilizing alumina columns. *n*-Butyllithium was purchased as a 2.5 M solution in hexanes (Sigma-Aldrich). The molarities of *n*-butyllithium solutions were determined by titration using 1,10-phenanthroline as an indicator (average of three determinations). Deuterated solvents $CDCl_3$, CD_3OD, and DMSO-d_6 (Cambridge Isotope Laboratories) were used as purchased. Extraction and chromatography solvents were reagent grade and used without purification (VWR or Fisher Scientific). Celite® 545 (EMD Millipore) was used.

NMR spectra were recorded with a Varian INOVA-400 spectrometer, are reported in parts per million (δ), and were calibrated using residual undeuterated solvent as an internal reference ($CDCl_3$: δ 7.26 for ^{1}H NMR and δ 77.00 for ^{13}C NMR; CD_3OD: δ 3.31 for ^{1}H NMR and δ 49.00 for ^{13}C NMR). Data for ^{1}H NMR spectra are reported as follows: chemical shift (δ ppm) (multiplicity, coupling constant (Hz), integration). Multiplicities are reported as follows: s = singlet, d = doublet, t = triplet, q = quartet, m = multiplet, br = broad, or combinations thereof. High-resolution mass spectra (HRMS) were recorded using electrospray ionization (ESI) mass spectroscopy experiments on an Agilent 1220 Infinity II TOF LC-MS.

Inhibitor Synthesis and Characterization of Novel Compounds.[34,39–41,57–61]

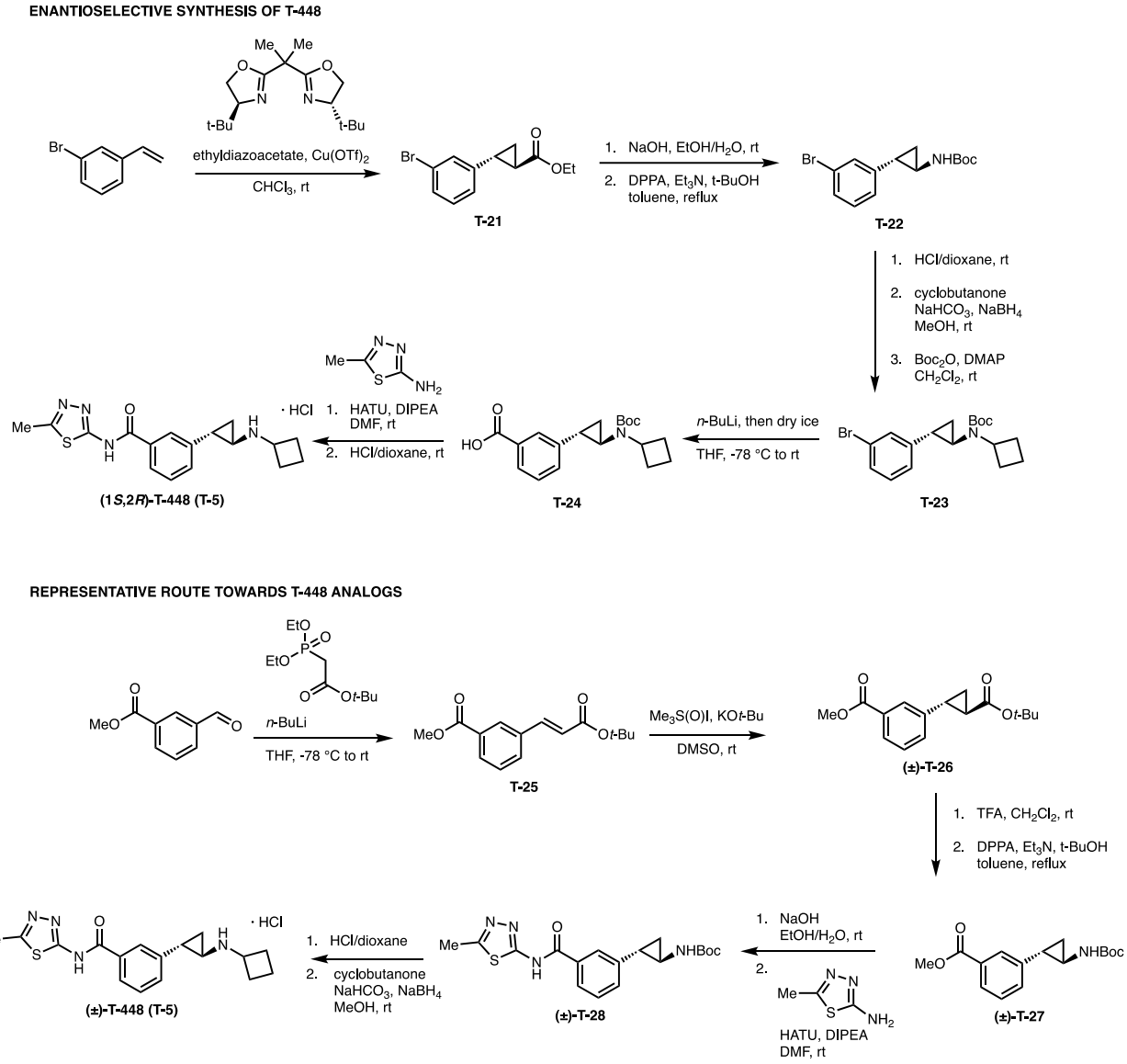

ROUTES TOWARDS T-448 DERIVATIVES

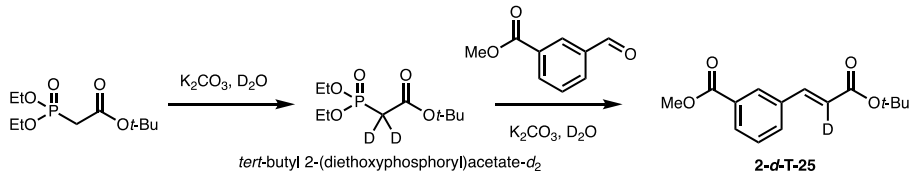

tert-butyl 2-(diethoxyphosphoryl)acetate-d_2 **2-*d*-T-25**

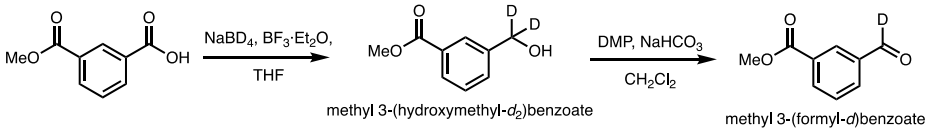

methyl 3-(hydroxymethyl-d_2)benzoate

methyl 3-(formyl-*d*)benzoate

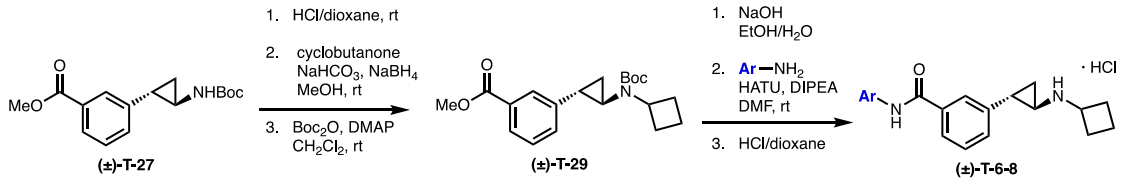

(±)-T-27 **(±)-T-29** **(±)-T-6-8**

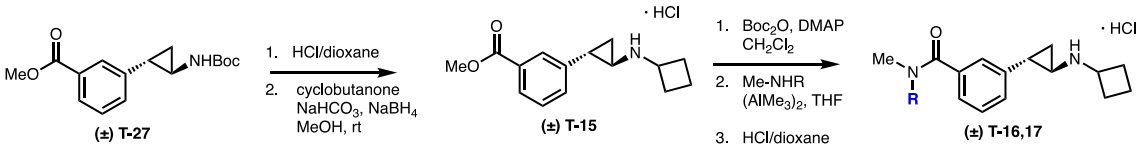

(±) T-27 **(±) T-15** **(±) T-16,17**

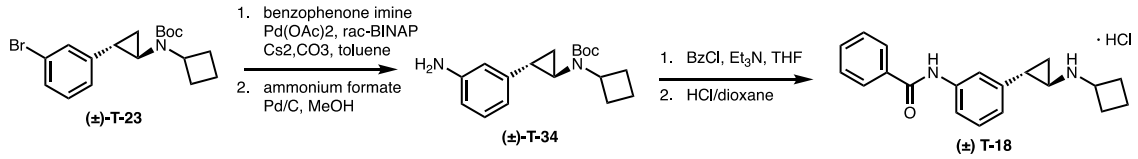

(±)-T-23 **(±)-T-34** **(±) T-18**

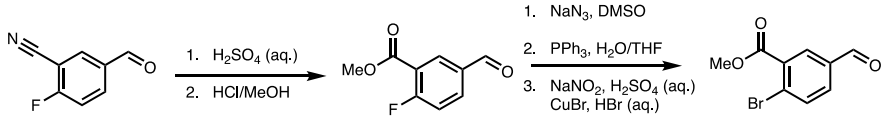

T-35 **T-36**

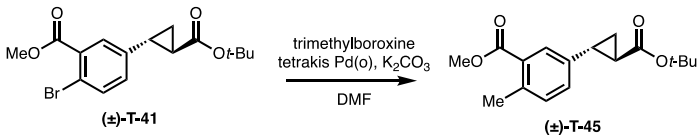

(±)-T-41 **(±)-T-45**

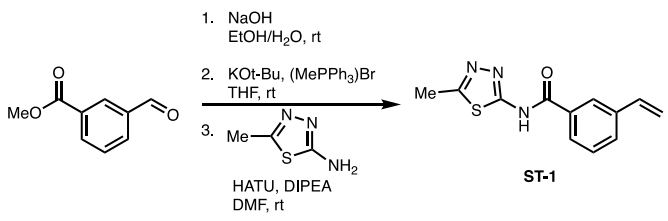

ST-1

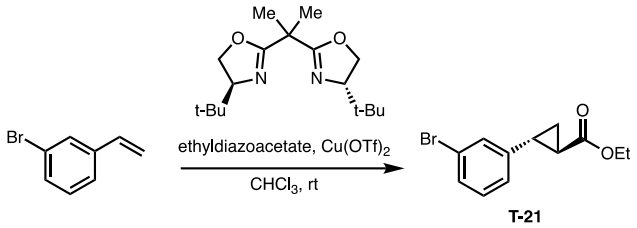

T-21

ethyl (1*R*,2*R*)-2-(3-bromophenyl)cyclopropane-1-carboxylate (T-21).

According to a literature procedure,[39,40] copper(II) triflate (8 mg, 0.02 mmol) was added to a stirred solution of (S,S)-2,2′-isopropylidene-bis(4-tert-butyl-2-oxazoline) ligand (6 mg, 0.02 mmol) in CH_2Cl_2 at rt. The reaction was stirred under N_2 atmosphere at rt for 1 h, after which 3-bromostyrene (1.4 mL, 11 mmol) and a 15% solution of ethyl diazoacetate (2.0 mL, 2.2 mmol) in toluene were added under N_2 atmosphere. The reaction was stirred for 5 h at rt. The reaction mixture was concentrated under reduced pressure and purified by column chromatography (silica gel, eluent: 0 to 20% CH_2Cl_2 /hexanes, v/v) to recover excess styrene and afford **(±)-T-21** (96% *ee*, 72% yield).

^{1}H NMR (400 MHz, $CDCl_3$) δ 7.36 (ddt, *J* = 0.9, 2.0, 8.0 Hz, 1H), 7.25-7.26 (m, 1H), 7.16 (td, *J* = 1.4, 7.8 Hz, 1H), 7.05 (dt, *J* = 1.6, 7.8 Hz, 1H), 4.20 (qd, *J* = 1.4, 7.2 Hz, 2H), 2.5 (ddt, *J* = 2.8, 6.0, 10.7 Hz, 1H), 1.92 (m, 1H), 1.62 (m, 1H), 1.31 (m, 1H).

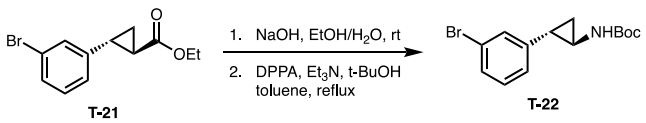

T-21 T-22

***tert*-butyl ((1*R*,2*S*)-2-(3-bromophenyl)cyclopropyl)carbamate (T-22)**.

According to a literature procedure,[40] **T-21** (250 mg, 0.93 mmol) was added to a solution of 30 mg of NaOH (0.74 mmol) dissolved in 75% aqueous EtOH (1.3 mL). The solution was refluxed overnight, then cooled and diluted with water and washed with EtOAc. The aqueous phase was acidified with conc. HCl to pH = 1, and the precipitated product was collected and recrystallized. The resulting colorless solid was dried and taken up in anhydrous toluene (3.6 mL) in a round-

bottom flask. Diphenyl phosphoryl azide (240 μL, 1.11 mmol) and triethylamine (260 μL, 1.85 mmol) were added under a nitrogen atmosphere and stirred for 30 min at rt. The reaction mixture was then heated and refluxed for 1.5 h before *t*-BuOH (1.1 mL, 0.87 mmol) was added, and the resulting solution was refluxed overnight. The reaction mixture was cooled to room temperature and was concentrated under reduced pressure. The crude residue was purified by column chromatography (silica gel, eluent: 0 to 30% EtOAc/hexanes, v/v) to afford carbamate **(±)-T-22** (24% yield over two steps).

^{1}H NMR (400 MHz, $CDCl_3$) δ 7.31 (dt, *J* = 1.6, 7.7 Hz, 1H), 7.26-7.28 (m, 1H), 7.14 (t, *J* = 7.7 Hz, 1H), 7.09 (d, *J* = 7.8 Hz, 1H), 4.84 (s, 1H), 2.73 (s, 1H), 2.03 (m, 1H), 1.47 (s, 9H), 1.20-1.15 (m, 2H).

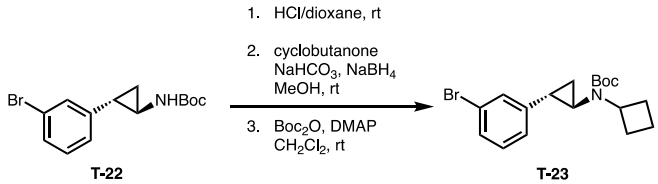

T-22 **T-23**

General Procedure for tert-butyl ((1R,2S)-2-(3-bromophenyl)cyclopropyl)(cyclobutyl) carbamate (T-23).

According to literature procedures,[57] carbamate **(±)-T-22** (50 mg, 0.16 mmol) was taken up in 1,4-dioxane (80 μL) and 4.0 M HCl in 1,4-dioxane was added (160 μL). The reaction mixture was stirred at room temperature until completion as monitored by TLC (4 h) before being concentrated under reduced pressure. The residue was taken up in water, diluted with saturated aqueous $NaHCO_3$ solution, and the aqueous layer was extracted with CH_2Cl_2. The combined organic fractions were dried over anhydrous sodium sulfate, filtered, and concentrated under reduced pressure. The deprotection product was suspended in methanol, and cyclobutanone (14 μL, 0.19 mmol) and sodium hydrogen carbonate (40 mg, 0.47 mmol) were added to the mixture before

being stirred overnight at rt. Sodium borohydride (7 mg, 0.19 mmol) was added to the reaction mixture under ice-cooling, and the mixture was stirred at 0 °C for 1 h. Saturated aqueous sodium bicarbonate solution was added under ice-cooling and the mixture was extracted with ethyl acetate (2x). The combined organic layers were washed successively with water and brine, dried over anhydrous Na_2SO_4, filtered, and concentrated under reduced pressure. The crude product was taken up in CH_2Cl_2 and treated overnight with Boc_2O (80 mg, 0.4 mmol) and 4-DMAP (4 mg, 0.4 mmol). The mixture was then concentrated under reduced pressure and purified by column chromatography (silica gel, eluent: 0 to 30% EtOAc/hexanes, v/v) to afford carbamate **T-23** (45% yield over 3 steps).

^{1}H NMR (400 MHz, $CDCl_3$) δ 7.30 (d, *J* = 7.9 Hz, H), 7.22 (s, 1H), 7.13 (t, *J* = 7.8 Hz, 1H), 7.03 (d, *J* = 7.7 Hz, 1H), 4.08 (p, *J* = 8.6 Hz, 1H), 2.61 (dt, *J* = 8.6 Hz, 1H), 2.28-2.11 (m, 4H), 1.99 (ddd, *J* = 3.3, 6.5, 9.7 Hz, 1H), 1.68-1.53 (m, 2H), 1.43 (s, 9H), 1.31 (dt, *J* = 5.3, 10.3 Hz, 1H), 1.24 (p, *J* = 6.6 Hz, 1H). ^{13}C NMR (126 MHz, $CDCl_3$) δ 155.87, 143.75, 129.83, 128.99, 128.96, 124.81, 122.49, 79.72, 52.85, 37.08, 29.48, 29.45, 28.54, 25.94, 18.93, 15.06. HR ESI-MS *m/z*: 266.0643 ([M+H]$^+$ calc'd for $C_{13}H_{17}BrN^+$: 266.0539).

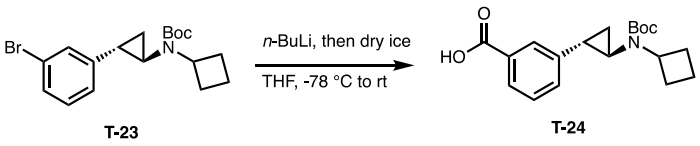

T-23 **T-24**

3-((1S,2R)-2-((tert-butoxycarbonyl)(cyclobutyl)amino)cyclopropyl)benzoic acid (T-24).

A 2.5 M solution of *n*-butyllithium in hexanes (72 µL, 0.18 mmol, 1.15 eq.) was added dropwise via syringe to a stirred solution of **(±)-T-23** (60 mg, 0.16 mmol) in 1 mL THF at -78 °C. The reaction was stirred at -78 °C until disappearance of starting material was observed by TLC, after which crushed dry-ice was added in a single portion at -78 °C, and the reaction was stirred for 10 min

before being warmed to rt for 2h. The reaction mixture was concentrated under reduced pressure, and the residue was diluted with water (5 mL) and washed with EtOAc (3 x 5 mL). Saturated $NaHCO_3$ solution was added to the aqueous layer and extracted with EtOAc (3x). The combined organic layers were washed successively with water and brine, dried over anhydrous Na_2SO_4, filtered, and concentrated under reduced pressure. The crude product **T-24** (37% yield) was used directly in the next step.

^{1}H NMR (400 MHz, $CDCl_3$) δ 7.91 (ddd, *J* = 1.7, 4.0, 5.3 Hz, 1H), 7.82-7.77 (m, 1H), 7.41-7.34 (m, 2H), 4.15-4.05 (m, 1H), 2.68 (ddd, *J* = 3.3, 4.7, 7.0 Hz, 1H), 2.26-2.16 (m, 4H), 2.12-2.08 (m, 1H), 1.68-1.55 (m, 2H), 1.43 (s, 9H), 1.37-1.30 (m, 2H).^{13}C NMR (126 MHz, $CDCl_3$) δ 170.70, 155.94, 131.65, 128.50, 127.77, 127.35, 79.74, 52.86, 37.17, 29.51, 28.55, 26.06, 18.95, 15.07. HR ESI-MS *m/z*: 232.1258 ([M+H]$^+$ calc'd for $C_{14}H_{18}NO_2^+$: 232.1332).

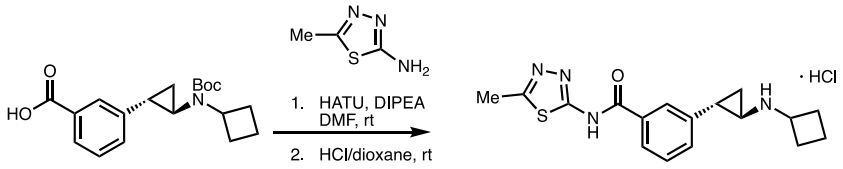

T-24 (1*S*,2*R*)-T-448 (T-5)

3-((1*S*,2*R*)-2-(cyclobutylamino)cyclopropyl)-*N*-(5-methyl-1,3,4-thiadiazol-2-yl)benzamide hydrochloride (T-448).

According to a literature procedure,[34] carboxylic acid **T-24** (20 mg, 0.06 mmol) and O-(7-azabenzotriazol-1-yl)-N,N,N',N'-tetramethyluronium hexafluoro-phosphate (27 mg, 0.08 mmol) were dissolved in N,N-dimethylformamide (1 mL), and N,N-diisopropylethylamine (42 µL, 0.24 mmol) was added at 0 °C. The mixture was stirred at room temperature for 30 min, 5-methyl-1,3,4-thiadiazol-2-amine (8 mg, 0.07 mmol) was added, and the reaction stirred overnight at rt. Upon completion, the reaction mixture was poured into water and the mixture was extracted with

ethyl acetate. The extract was washed successively with saturated aqueous sodium hydrogen carbonate solution and saturated brine, dried over anhydrous sodium sulfate, and concentrated under reduced pressure. The residue was purified by silica gel column chromatography (ethyl acetate) and concentrated under reduced pressure. The product was taken up in 1,4-dioxane (50 μL) and 4.0 M HCl in 1,4-dioxane was added (100 μL). The reaction mixture was stirred at room temperature until completion as monitored by TLC and then concentrated under reduced pressure. The residue was dissolved in water/MeOH (1 mL) and subsequently washed with 1:1 hexanes/DCM before being concentrated under reduced pressure to give the title compound (40% yield).

^{1}H NMR (400 MHz, CD_3OD) δ 7.98-7.92 (m, 1H), 7.88 (s, 1H), 7.55 (d, *J* = 4.6 Hz, 2H), 3.99 (p, *J* = 8.1, 8.2 Hz, 1H), 3.01 (dt, *J* = 3.7, 7.8 Hz, 1H), 2.89 (s, 3H), 2.63 (ddd, *J* = x Hz, 1H), 2.44-2.36 (m, 2H), 2.31 (td, *J* = 5.9, 12.1 Hz, 2H), 1.97 (dtd, *J* = 2.6, 6.4, 7.3, 12.0 Hz, 2H), 1.61 (ddd, *J* = 4.1, 6.6, 10.6 Hz, 1H), 1.5 (q, *J* = 7.0 Hz, 1H). ^{13}C NMR (126 MHz, CD_3OD) δ 166.34, 139.33, 131.64, 131.41, 129.11, 126.61, 125.95, 52.43, 35.68, 26.23, 26.21, 20.38, 14.67, 11.82. HR ESI-MS *m/z*: 329.1429 ([M+H]$^+$ calc'd for $C_{15}H_{20}NO_2^+$: 329.1431).

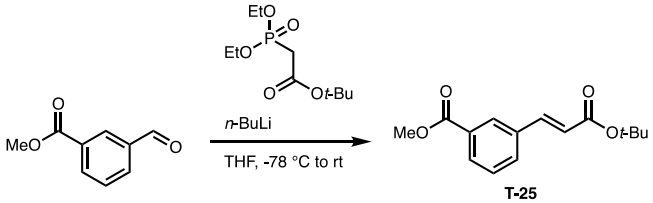

T-25

General Procedure for (methyl (*E*)-3-(3-(*tert*-butoxy)-3-oxoprop-1-en-1-yl)benzoate (T-25). According to a literature procedure,[57] a 2.5 M solution of *n*-butyllithium in hexanes (6.1 mL, 14.6 mmol) was added dropwise at -78 °C to a stirred solution of *tert*-butyl diethylphosphonoacetate (3.3 mL, 14.6 mmol) in THF (26 mL). After stirring for 30 min at –78 °C, a solution of methyl 3-formylbenzaldehyde (2.1 g, 13.3 mmol) in THF (27 mL) was also cooled to –78 °C and transferred

via cannula. The resulting solution was stirred at –78 °C for 30 min before being allowed to warm to room temperature and stirred until disappearance of the starting material was observed by TLC analysis. Upon cooling back to -78 °C, the solution was quenched with saturated aqueous NH_4Cl solution (50 mL). The aqueous layer was extracted with CH_2Cl_2 (3 × 50 mL), and the combined organic fractions were dried over anhydrous sodium sulfate, filtered, and concentrated under reduced pressure. The crude residue was purified by column chromatography (silica gel, eluent: 0 to 30% EtOAc/hexanes, v/v) to afford **(±)-T-25** in high diastereoselectivity (94% yield; >90% *E:Z*).

^{1}H NMR (400 MHz, CDCl3) δ 8.19 (t, *J* = 1.7 Hz, 1H), 8.02 (dt, *J* = 1.5, 7.8 Hz, 1H), 7.67 (dt, *J* = 1.6, 7.7 Hz, 1H), 7.60 (d, *J* = 16.0 Hz, 1H), 7.45 (t, *J* = 7.7 Hz, 1H), 6.44 (d, *J* = 16.0 Hz, 1H), 3.93 (s, 1H), 1.54 (s, 1H).

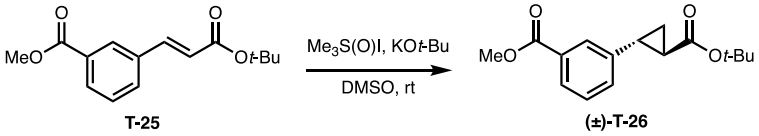

T-25 (±)-T-26

General Procedure for (±)-methyl 3-((1*R*,2*R*)-2-(*tert*-butoxycarbonyl)cyclopropyl)benzoate (T-26)

According to a literature procedure,[57] an anhydrous DMSO solution (15 mL) of **T-25** (3.3 g, 12.5 mmol) was added in one portion to a mixture of $Me_3S(O)I$/KO*t*-Bu (1:1 mixture, 3.3 g/1.7 g, 15 mmol) in a round-bottomed flask. The resulting solution was stirred for 30-60 min at 50-60 °C until disappearance of the starting material was observed by TLC analysis. The mixture was then treated with brine and extracted with EtOAc 3x. The combined organic extracts were washed with water 2x and brine, dried over anhydrous sodium sulfate, filtered, and concentrated under reduced pressure. The crude residue was purified by column chromatography (silica gel, eluent: 0 to 25% EtOAc/hexanes, v/v) to yield **(±)-T-26** as a single diastereomer (22% yield, two steps).

^{1}H NMR (400 MHz, CDCl3) δ 7.86 (dt, *J* = 1.6, 7.4 Hz, 1H), 7.74 (t, *J* = 1.8 Hz, 1H), 7.32 (m, 2H), 3.91 (s, 3H), 2.48 (ddd, *J* = 4.2, 6.4, 9.2 Hz, 1H), 1.87 (ddd, *J* = 4.2, 5.4, 8,4 Hz, 1H), 1.57 (m, 1H), 1.47 (s, 9H), 1.27 (ddd, *J* = 4.6, 6.4, 8.5 Hz, 1H).

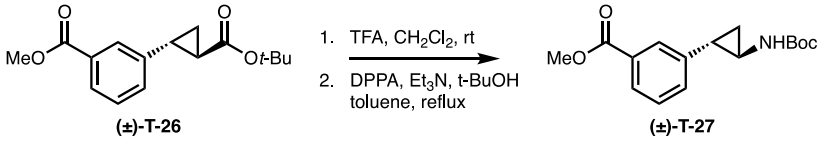

(±)-T-26 **(±)-T-27**

General Procedure for (±)-methyl 3-((1*S*,2*R*)-2-((*tert*-butoxycarbonyl)amino)cyclopropyl) benzoate (T-27).

TFA (1 mL) was added to a solution of **(±)-T-26** (300 mg, 1.11 mmol) in CH_2Cl_2 (3 mL). After stirring for 1 to 3 h, TFA was removed by a stream of nitrogen in a well-ventilated hood, and any remaining solvent was removed under reduced pressure. The crude material was passed through a silica plug (silica gel, eluent: 50% EtOAc/hexanes, v/v) and concentrated under reduced pressure. The resulting colorless solid was dried and taken up in anhydrous toluene (3.8 mL) in a round-bottom flask. Diphenyl phosphoryl azide (250 µL, 1.2 mmol) and triethylamine (275 µL, 1.9 mmol) were added under a nitrogen atmosphere and stirred for 30 min at rt. The reaction mixture was then heated and refluxed for 1.5 h before *t*-BuOH (1.1 mL, 0.87 mmol) was added, and the resulting solution was refluxed overnight. The reaction mixture was cooled to room temperature and was concentrated under reduced pressure. The crude residue was purified by column chromatography (silica gel, eluent: 0 to 30% EtOAc/hexanes, v/v) to afford carbamate **(±)-T-27** (40% yield over two steps).

^{1}H NMR (400 MHz, CDCl3) δ 7.87-7.81 (m, 1H), 7.76 (s, 1H), 7.39-7.31 (m, 2H), 4.85 (s, 1H), 3.90 (s, 3H), 2.76 (s, 1H), 2.13-2.06 (m, 1H), 1.45 (s, 9H), 1.25-1.20 (m, 2H).

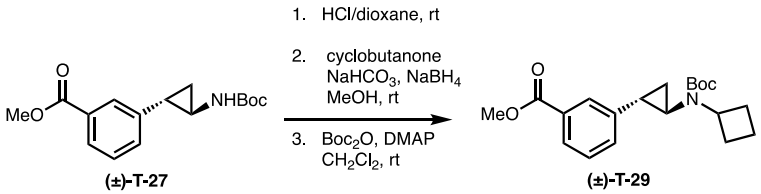

(±)-methyl 3-((1*S*,2*R*)-2-((*tert*-butoxycarbonyl)(cyclobutyl)amino)cyclopropyl)benzoate (T-29)

(±)-T-29 was prepared according to the general procedure for **(±)-T-23**. **(±)-T-29** was isolated as a yellow oil (38% yield over 3 steps).

^{1}H NMR (400 MHz, CDCl3) δ 7.85 (dt, *J* = 1.9, 7.0 Hz, 1H), 7.73 (d, *J* = 1.9 Hz, H), 7.36-7.31 (m, 2H), 4.13-4.09 (m, 1H), 3.91 (s, 3H), 2.66 (ddd, *J* = 3.3, 4.7, 7.7 Hz, 1H), 2.24-2.13 (m, 4H), 2.07 (td, *J* = 3.3, 6.6, 6.6 Hz, 1H), 1.58 (td, *J* = 1.5, 3.7, 4.3 Hz, 2H), 1.43 (s, 9H), 1.35-1.32 (m, 1H), 1.28-1.25 (m, 1H). ^{13}C NMR δ (126 MHz, $CDCl_3$) δ 167.17, 155.93, 141.76, 130.85, 128.36, 127.15, 126.74, 79.70, 52.86, 52.13, 37.14, 29.47, 28.54, 26.07, 18.98, 15.06. HR ESI-MS *m/z*: 246.2032 ([M+H]$^+$ calc'd for $C_{15}H_{20}NO_2^+$: 246.1489).

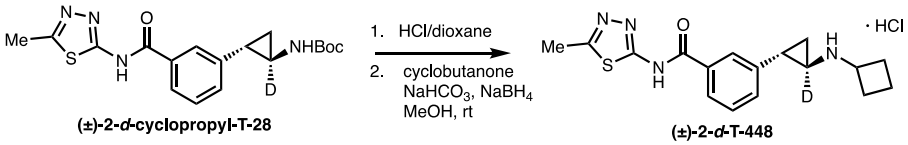

General Procedure for (±)-3-(*trans*-2-(cyclobutylamino)cyclopropyl-2-*d*)-*N*-(5-methyl-1,3,4-thiadiazol-2-yl) benzamide hydrochloride (2-*d*-T-448)

According to modified literature procedure,[34] *tert*-butyl ((1*R*,2*S*)-2-(3-((5-methyl-1,3,4-thiadiazol-2-yl)carbamoyl)phenyl)cyclopropyl-1-*d*)carbamate (10 mg, 0.04 mmol) was taken up in 1,4-dioxane (50 µL) and 4.0 M HCl in 1,4-dioxane was added (50 µL). The reaction mixture was stirred at room temperature until completion as monitored by TLC (4 h) before being concentrated under reduced pressure. The residue was taken up in water, diluted with saturated aqueous $NaHCO_3$ solution, and the aqueous layer was extracted with CH_2Cl_2 3x. The combined organic fractions

were dried over anhydrous sodium sulfate, filtered, and concentrated under reduced pressure. The deprotection product was suspended in methanol (100 µL), and cyclobutanone (2 µL, 0.03 mmol) and sodium hydrogen carbonate (7 mg, 0.1 mmol) were added to the mixture before being stirred overnight at rt. Sodium borohydride (2 mg, 0.03 mmol) was added to the reaction mixture under ice-cooling, and the mixture was stirred at 0 °C for 1 h. Saturated aqueous sodium bicarbonate solution was added under ice-cooling and the mixture was extracted with ethyl acetate (2x). The combined organic layers were washed successively with water and brine, dried over anhydrous Na_2SO_4, filtered, and concentrated under reduced pressure. The residue was acidified with 1 M HCl in MeOH and concentrated under reduced pressure to give the title compound (59% yield over 2 steps).

^{1}H NMR (400 MHz, DMSO-d_6) δ 9.36 (bs, 1H), 7.95-7.84 (m, 1H), 7.79 (s, 1H), 7.54-7.39 (m, 2H), 3.86-3.79 (m, 1H), 2.64-2.62 (m, 1H), 2.61 (s, 3H), 2.25-2.12 (m, 4H), 1.83-1.71 (m, 2H), 1.47 (dd, *J* = 6.2, 10.0 Hz, 2H), 1.41-1.37 (m, 1H). HR ESI-MS *m/z*: 330.1489 ([M+H]$^+$ calc'd for $C_{17}H_{20}DN_4OS^+$: 330.1493).

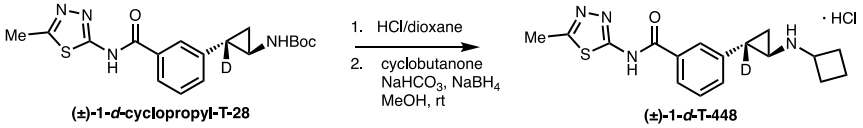

(±)-3-(*trans*-2-(cyclobutylamino)cyclopropyl-2-*d*)-*N*-(5-methyl-1,3,4-thiadiazol-2-yl) benzamide hydrochloride (1-*d*-T-448)

(±)-1-*d*-T-448 (49% yield over two steps). was prepared according to the general procedure for **(±)-2-*d*-T-448**.

^{1}H NMR (400 MHz, CD_3OD) δ 7.98-7.88 (m, 1H), 7.88-7.76 (m, 1H), 7.58-7.46 (m, 2H), 3.99 (p, *J* = 8.1, 8.2 Hz, 1H), 3.01-2.98 (m, 1H), 2.74 (s, 3H), 2.45-2.37 (m, 2H), 2.33-2.17 (m, 2H),

2.02-1.92 (m, 2H), 1.54-1.45 (m, 2H). HR ESI-MS *m/z*: 330.1496 ([M+H]$^+$ calc'd for $C_{17}H_{20}DN_4OS+$: 330.1493).

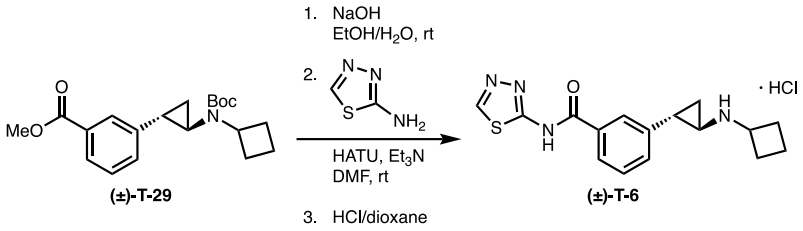

General Procedure for (±)-3-(*trans*-2-(cyclobutylamino)cyclopropyl)-*N*-(1,3,4-thiadiazol-2-yl)benzamide hydrochloride (T-6)

According to a literature procedure,[34] an 8 M aqueous sodium hydroxide solution (1 mL) was added to **(±)-T-29** (100 mg, 0.3 mmol) dissolved in ethanol (1 mL), and the mixture was stirred at room temperature overnight. The reaction mixture was neutralized with 1 M hydrochloric acid at 0 °C, and extracted with ethyl acetate (3x). The extract was washed successively with water and saturated brine, dried over anhydrous sodium sulfate, filtered, and concentrated under reduced pressure. Of the isolated product, 19 mg (0.06 mmol) was dissolved in N,N-dimethylformamide (1 mL), and O-(7-azabenzotriazol-1-yl)-N,N,N',N'-tetramethyluronium hexafluoro-phosphate (27 mg, 0.07 mmol) and N,N-diisopropylethylamine (42 µL, 0.24 mmol) was added at 0 °C. The mixture was stirred at room temperature for 30 min, 1,3,4-thiadiazol-2-amine (7 g, 0.07 mmol) was added, and the reaction stirred overnight at rt. Upon completion, the reaction mixture was poured into water and the mixture was extracted with ethyl acetate 2x. The extract was washed successively with saturated aqueous sodium hydrogen carbonate solution and saturated brine, dried over anhydrous sodium sulfate, and concentrated under reduced pressure. The residue was purified by silica gel column chromatography (ethyl acetate) and concentrated under reduced pressure. The intermediate was subsequently dissolved in 1,4-dioxane (21 µL) and 4.0 M HCl solution in 1,4-dioxane was added (43 µL). The reaction mixture was stirred at room temperature until completion as monitored by TLC and then concentrated under reduced pressure. The

residue was dissolved in water/MeOH and subsequently washed with 1:1 hexanes/DCM (2 × 1 mL) before being concentrated under reduced pressure to give the title compound (19% yield over 3 steps).

^{1}H NMR (400 MHz, CD_3OD) δ 9.49 (s, 1H), 7.96 (td, *J* = 1.7, 4.2, 3.9 Hz, 1H), 7.87 (s, 1H), 7.57-7.51 (m, 2H), 3.99 (p, *J* = 8.1 Hz, 1H), 3.01 (dt, *J* = 4.0, 7.9 Hz, 1H), 2.63 (ddd, *J* = 3.5, 6.6, 10.2 Hz, 1H), 2.45-2.24 (M, 4H), 2.06-1.89 (M, 2H), 1.60 (ddd, *J* = 4.5, 6.9, 10.3 Hz, 1H), 1.51 (q, *J* = 7.0 Hz, 1H). ^{13}C NMR (126 MHz, CD_3OD) δ 166.09, 139.23, 131.81, 131.43, 129.05, 126.57, 125.86, 52.41, 35.55, 26.22, 26.19, 20.39, 14.65, 11.89. HR ESI-MS *m/z*: 315.1283 ([M+H]$^+$ calc'd for $C_{16}H_{19}N_4OS^+$: 315.1274).

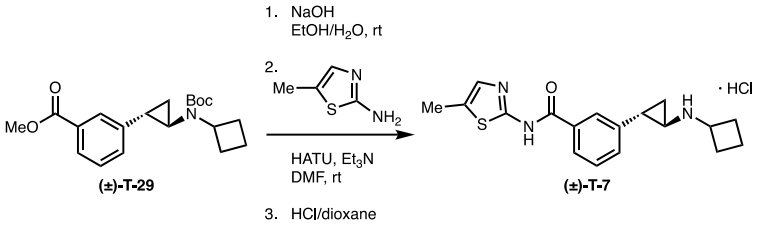

(±)-3-(*trans*-2-(cyclobutylamino)cyclopropyl)-*N*-(5-methylthiazol-2-yl)benzamide hydrochloride (T-7)

(±)-T-7 (24% yield, two steps). was prepared according to the general procedure for **(±)-T-6**.

^{1}H NMR (400 MHz, CD_3OD) δ 8.00-7.92 (m, 2H), 7.60-7.52 (m, 2H), 7.49 (s, 1H), 4.01 (p, *J* = 8.0 Hz, 1H), 3.01 (p, *J* = 3.9 Hz, 1H), 2.63 (ddd, *J* = 3.1, 6.4, 10.0 Hz, 1H), 2.50, (s, 3H), 2.45-2.22 (m, 4H), 2.05-1.89 (m, 2H), 1.60 (ddd, *J* = 3.9, 6.5, 10.5 Hz, 1H), 1.52 (q, *J* = 7.0 Hz, 1H). ^{13}C NMR (126 MHz, CD_3OD) δ 165.06, 139.58, 132.21, 130.84, 129.28, 126.86, 125.94, 124.19, 52.47, 35.75, 26.27, 26.24, 20.42, 14.69, 10.33. HR ESI-MS *m/z*: 328.1490 ([M+H]$^+$ calc'd for $C_{18}H_{22}N_3OS^+$: 328.1478).

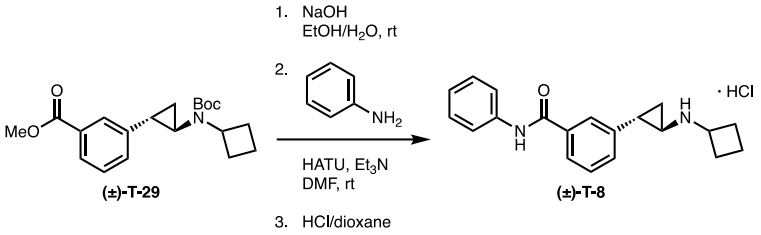

(±)-3-(*trans*-2-(cyclobutylamino)cyclopropyl)-*N*-phenylbenzamide hydrochloride (T-8)

(±)-T-8 (31% yield, two steps) was prepared according to the general procedure for **(±)-T-6**.

^{1}H NMR (400 MHz, CD_3OD) δ 7.82 (dt, *J* = 1.4, 7.5 Hz, 1H), 7.57-7.66 (m, 3H), 7.50-7.40 (m, 2H), 7.36 (t, *J* = 8.0 Hz, 2H), 7.16 (td, *J* = 1.1, 7.4 Hz, 1H), 3.98 (p, *J* = 8.1 Hz, 1H), 2.98 (dt, *J* = 4.0, 8.0 Hz, 1H), 2.58 (ddd, *J* = 3.4, 6.5, 10.2 Hz, 1H), 2.44-2.35 (M, 2H), 2.35-2.22 (M, 2H), 2.04-1.88 (M, 2H), 1.56 (ddd, *J* = 4.4, 6.8, 10.6 Hz, 1H), 1.48 (q, *J* = 7.0 Hz, 1H). HR ESI-MS *m/z*: 307.2356 ($[M+H]^+$ calc'd for $C_{20}H_{23}N_2O^+$: 307.1805).

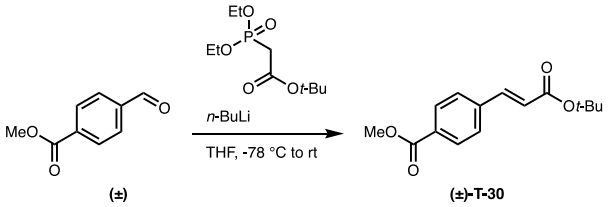

(±)-methyl 4-(2-(*tert*-butoxycarbonyl)cyclopropyl)benzoate (T-30)

(±)-T-30 (97% yield) was prepared according to the general procedure for **(±)-T-25**.

^{1}H NMR (400 MHz, CDCl3) δ 8.06-8.01 (m, 2H), 7.62-7.55 (m, 3H), 6.45 (d, *J* = 16.0 Hz, 1H), 3.93 (s, 3H), 1.54 (s, 9H).

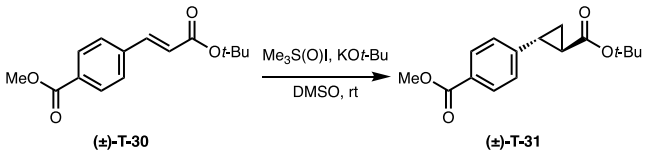

(±)-methyl 4-(*trans*-2-(*tert*-butoxycarbonyl)cyclopropyl)benzoate (T-31)

(±)-T-31 (60% yield, two steps) was prepared according to the general procedure for **(±)-T-26**.

^{1}H NMR (400 MHz, CDCl3) δ 7.97-7.90 (m, 2H), 7.17-7.06 (m, 2H), 3.90 (s, 3H), 2.47 (ddd, *J* = 4.2, 6.3, 9.2 Hz, 1H), 1.89 (ddd, *J* = 4.1, 5.4, 8.5 Hz, 1H), 1.62-1.57 (m, 1H), 1.47 (s, 9H), 1.28 (m, 1H).

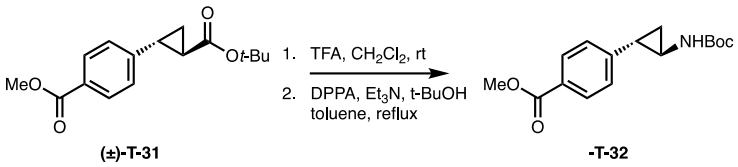

(±)-methyl 4-(*trans*-2-((*tert*-butoxycarbonyl)amino)cyclopropyl)benzoate (T-32)

(±)-T-32 (28% yield, two steps) was prepared according to the general procedure for **(±)-T-27**.

^{1}H NMR (400 MHz, CDCl3) δ 7.97-7.78 (m, 2H), 7.20-7.12 (m, 2H), 3.94 (s, 3H), 2.78 (s, 1H), 2.11-2.05 (m, 1H), 1.44 (s, 9H), 1.23 (m, 1H).

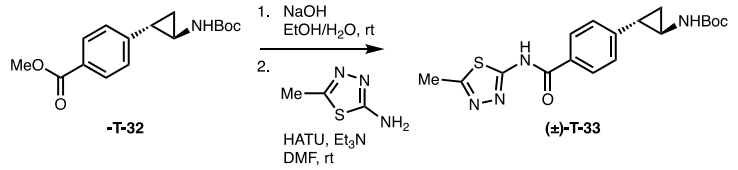

(±)-tert-butyl(*trans*-2-(4-((5-methyl-1,3,4-thiadiazol-2-yl)carbamoyl)phenyl)cyclopropyl) carbamate (T-33)

According to a literature procedure,[34] **an** 8 M aqueous sodium hydroxide solution (140 µL) was added to **(±)-T-32** (170 mg, 0.6 mmol) dissolved in ethanol (2 mL), and the mixture was stirred at room temperature overnight. The reaction mixture was neutralized with 1 M hydrochloric acid at 0 °C, and extracted with ethyl acetate (3 x 10 mL). The extract was washed successively with

water and saturated brine, dried over anhydrous sodium sulfate, filtered, and concentrated under reduced pressure. The product was dissolved in N,N-dimethylformamide (1.5 mL), and O-(7-azabenzotriazol-1-yl)-N,N,N',N'-tetramethyluronium hexafluoro-phosphate (246 mg, 0.7 mmol) and N,N-diisopropylethylamine (380 µL, 2 mmol) was added at 0 °C. The mixture was stirred at room temperature for 30 min, 5-methyl-1,3,4-thiadiazol-2-amine (70 mg, 0.5 mmol) was added, and the reaction stirred overnight at rt. Upon completion, the reaction mixture was poured into water and the mixture was extracted with ethyl acetate (2 x 5 mL). The extract was washed successively with saturated aqueous sodium hydrogen carbonate solution and saturated brine, dried over anhydrous sodium sulfate, and concentrated under reduced pressure. The residue was purified by silica gel column chromatography (ethyl acetate) and concentrated under reduced pressure to give **T-33** (44% yield over 2 steps).

^{1}H NMR (400 MHz, $CDCl_3$) δ 11.84, (s, 1H) 8.08 (d, *J* = 8.1 Hz, 2H), 7.24 (d, *J* = 8.2 Hz, 2H), 2.80 (s, 1H), 2.73 (s, 3H), 2.12 (m, 1H), 1.45 (s, 9H), 1.29-1.21 (m, 2H). ^{13}C NMR (126 MHz, $CDCl_3$) δ 164.78, 160.68, 160.14, 147.02, 128.81, 128.46, 126.64, 79.96, 60.42, 28.41, 21.07, 17.10, 15.36, 14.21. HR ESI-MS *m/z*: 375.1587 ([M+H]$^+$ calc'd for $C_{18}H_{23}N_4O_3S^+$: 375.1485).

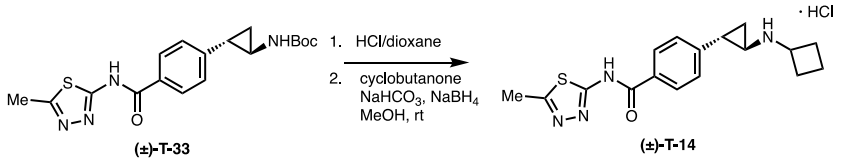

(±)-4-(*trans*-2-(cyclobutylamino)cyclopropyl)-*N*-(5-methyl-1,3,4-thiadiazol-2-yl)benzamide hydrochloride (T-14)

(±)-T-14 (67% yield over two steps). was prepared according to the general procedure for **(±)-2-*d*-T-448**.

^{1}H NMR (400 MHz, CD_3OD) δ 8.01 (d, *J* = 8.3 Hz, 2H), 7.38 (d, *J* = 8.3 Hz, 2H), 3.98 (t, *J* = 8.0 Hz, 1H), 3.01 (dt, *J* = 3.9, 7.8 Hz, 1H), 2.75 (s, 3H), 2.57-2.49 (m, 1H), 2.43-2.34 (m, 2H), 2.34-2.21 (m, 2H), 2.03-1.90 (m, 2H), 1.62-1.55 (m, 1H), 1.53-1.48 (m, 1H). HR ESI-MS *m/z*: 365.1197 ($[M+H]^+$ calc'd for $C_{17}H_{21}N_4OS^+$: 365.1406).

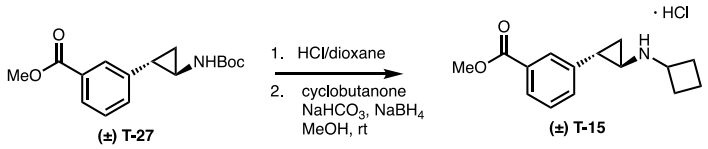

(±)-methyl 3-(*trans*-2-(cyclobutylamino)cyclopropyl)benzoate hydrochloride (T-15)

(±)-T-15 (52% yield, two steps) was prepared according to the general procedure for **(±)-2-*d*-T-448**.

^{1}H NMR (400 MHz, CD_3OD) δ 7.85 (td, *J* = 1.7, 4.6 Hz, 1H), 7.78 (s, 1H), 7.40 (d, *J* = 5.25, 2H), 3.92 (p, *J* = 8.1 Hz, 1H), 3.86 (s, 3H), 2.88 (p, *J* = 4.2 Hz, 1H), 2.55 (ddd, *J* = 3.6, 6.6, 10.3 Hz, 1H), 2.37-2.23 (m, 4H), 1.92 (dtd, *J* = 2.4, 7.5, 7.4, 10.0 Hz, 2H), 1.54 (ddd, *J* = 4.5, 6.9, 10.3 Hz, 1H), 1.38 (q, *J* = 6.9 Hz, 1H). ^{13}C NMR (126 MHz, CD_3OD) δ 166.81, 138.74, 130.90, 130.43, 128.70, 127.67, 127.07, 66.74, 51.34, 35.62, 26.17, 20.30, 14.66, 11.71. HR ESI-MS *m/z*: 246.2042 ($[M+H]^+$ calc'd for $C_{15}H_{20}NO_2^+$: 246.1418).

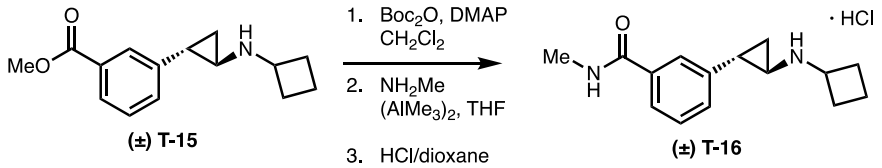

General Procedure for (±)-3-(*trans*-2-(cyclobutylamino)cyclopropyl)-*N*-methylbenzamide hydrochloride (T-16)

According to literature procedures,[59] a 2M solution of methylamine in THF (180 µL, 0.4 mmol) was added to **(±)-T-29** (25 mg, 0.07 mmol) in dry THF (200 µL). The reaction mixture was cooled to -78 °C under nitrogen and a 2M solution of trimethylaluminium in toluene (90 µL, 0.2 mmol) was added dropwise over 5 mins. The reaction mixture was allowed to warm slowly to room temperature and stirred overnight at rt. The reaction mixture was quenched with a 20% w/v solution of potassium sodium tartrate in water, then was extracted with ethyl acetate (2x) and washed with water and brine, dried over sodium sulfate, and evaporated under reduced pressure. The crude residue was purified by column chromatography (silica gel, eluent: 0 to 10% EtOAc/hexanes, v/v). The intermediate was subsequently dissolved in 1,4-dioxane (21 µL) and 4.0 M HCl solution in 1,4-dioxane was added (43 µL). The reaction mixture was stirred at room temperature until completion as monitored by TLC and then concentrated under reduced pressure. The residue was dissolved in water/MeOH (1 mL) and subsequently washed with 1:1 hexanes/DCM (2 × 1 mL) before being concentrated under reduced pressure to give the title compound (32% yield over 2 steps).

^{1}H NMR (400 MHz, CD_3OD) δ 7.67 (dt, *J* = 1.6, 7.6 Hz, 1H), 7.60 (t, *J* = 1.9 Hz, 1H), 7.42 (t, *J* = 7.6, 1H), 7.37 (dt, *J* = 1.7, 7.7 Hz, 1H), 3.98 (p, *J* = 8.3 Hz, 1H), 2.94 (p, *J* = 4.0 Hz, 1H), 2.92 (s, 3H), 2.51 (ddd, *J* = 3.6, 6.7, 10.3 Hz, 1H), 2.43-2.34 (m, 2H), 2.32-2.21 (m, 2H) , 2.01-1.92 (m, 2H), 1.52 (ddd, *J* = 4.5, 6.9, 10.3 Hz, 1H), 1.44 (q, *J* = 7.0 Hz, 1H). ^{13}C NMR (126 MHz, CD_3OD) δ 168.91, 138.53, 134.66, 129.40, 128.61, 125.24, 124.85, 66.74, 35.55, 26.20, 25.52, 20.46, 14.60, 11.72. HR ESI-MS *m/z*: 245.1845 ([M+H]$^+$ calc'd for $C_{15}H_{21}N_2O^+$: 245.1648).

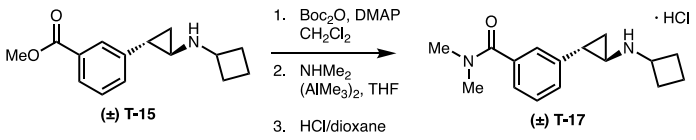

(±)-3-(*trans*-2-(cyclobutylamino)cyclopropyl)-*N*,*N*-dimethylbenzamide hydrochloride (T-17)

(±)-T-17 (28% yield, two steps) was prepared according to the general procedure for **(±)-T-16**.

^{1}H NMR (400 MHz, CD_3OD) δ 7.39 (t, *J* = 7.5 Hz, 1H), 7.28 (dd, *J* = 1.8, 7.4 Hz, 2H), 7.22 (s, 1H), 3.93 (p, *J* = 8.1 Hz, 1H), 3.09 (s, 3H), 2.96 (s, 3H), 2.88 (p, *J* = 4.2 Hz, 1H), 2.52 (ddd, *J* = 3.6, 6.6, 10.3 Hz, 1H), 2.39-2.19 (m, 4H) , 1.99-1.86 (m, 2H), 1.52 (ddd, *J* = 4.4, 6.8, 10.3 Hz, 1H), 1.38 (q, *J* = 7.1 Hz, 1H). ^{13}C NMR (126 MHz, CD_3OD) δ 172.12, 138.89, 135.71, 128.68, 127.87, 125.14, 124.79, 66.74, 38.77, 35.61, 34.48, 26.18, 20.37, 14.64, 14.64, 11.75. HR ESI-MS *m/z*: 259.2302 ([M+H]$^+$ calc'd for $C_{16}H_{23}N_2O^+$: 259.1805).

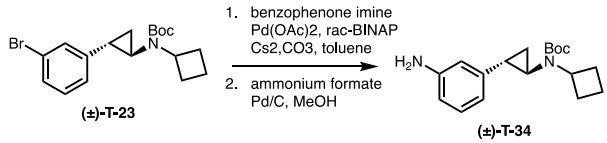

(±)-*tert*-butyl ((1*R*,2*S*)-2-(3-bromophenyl)cyclopropyl)(cyclobutyl)carbamate (T-34)

According a literature procedure,[58] **(±)-T-23** (40 mg, 0.08 mmol), benzophenone imine (19 mg, 0.10 mmol), palladium acetate (0.9 mg, 0.004 mmol), rac-BINAP (5 mg, 0.008 mmol), and cesium carbonate (36 mg, 0.11 mmol) were dissolved in 0.5 mL toluene and heated to 100°C overnight. The crude residue was diluted with EtOAc, filtered through celite, and purified by column chromatography (silica gel, eluent: 0 to 10% EtOAc/hexanes, v/v). The ketaimine product was taken up into 0.3 mL MeOH, subjected to ammonium formate (56 mg, 0.88 mmol) and Pd/C (6 mg, 0.006), and heated to 60°C for 1 h. The solution was cooled to rt, diluted with CH_2Cl_2, passed through celite, and washed with 1 M NaOH. The organic layer was washed with brine, dried over sodium sulfate, and condensed under reduced pressure. The residue was purified by column chromatography (silica gel, eluent: 0 to 50% EtOAc/hexanes, v/v) to give **T-34** (15 mg, 0.06 mmol, 46% yield).

^{1}H NMR (400 MHz, CDCl3) δ 7.05 (t, *J* = 7.8 Hz, H), 6.53-6.46 (m, 2H), 6.46-6.35 (m, 1H), 4.09 (p, *J* = 8.3, 8.5 Hz, H), 2.61-2.56 (m, 1H), 2.27-2.12 (m, 4H), 1.92 (ddd, *J* = 3.3, 6.7, 9.8 Hz, 1H), 1.66-1.62 (m, 2H), 1.44 (s, 9H), 0.91-0.81 (m, 2H). HR ESI-MS *m/z*: 203.1543 ([M+H]$^+$ calc'd for $C_{13}H_{19}N_2^+$: 203.1543).

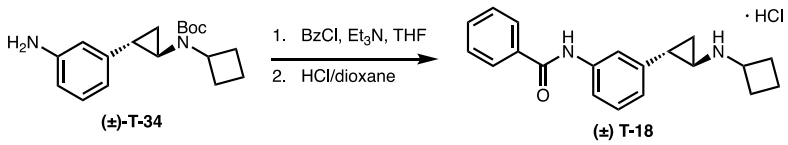

(±)-*N*-(3-(*trans*-2-(cyclobutylamino)cyclopropyl)phenyl)benzamide hydrochloride (T-18)

According to literature procedures,[60] aniline **(±)-T-31** (15 mg, 0.05 mmol) and triethylamine (0.06 mmol, 10 µL) were taken up in 200 µL anhydrous THF, and benzoyl chloride (6 µL, 0.05 mmol) was added dropwise at 0 °C. The reaction was allowed to return to rt and stirred overnight. The resulting mixture was filtered, and the solvent was evaporated. The residue was purified by column chromatography (silica gel, eluent: 0 to 50% EtOAc/hexanes, v/v), and the isolated intermediate was subsequently dissolved in 1,4-dioxane (20 µL) and 4.0 M HCl solution in 1,4-dioxane was added (40 µL). The reaction mixture was stirred at room temperature until completion as monitored by TLC and then concentrated under reduced pressure. The residue was dissolved in water/MeOH (1 mL) and subsequently washed with 1:1 hexanes/DCM (2 × 1 mL) before being concentrated under reduced pressure to give the title compound (49% yield over 2 steps).

^{1}H NMR (400 MHz, CD_3OD) δ 7.90 (m, 2H), 7.60 (t, *J* = 2.0 Hz, 1H), 7.55 (tt,*J* = 1.3, 7.3 Hz, 1H), 7.51-7.44 (m, 3H), 7.28 (t, *J* = 7.9 Hz, 1H), 6.94 (dt, *J* = 1.6, 7.7 Hz, 1H), 3.94 (p, *J* = 8.2 Hz,1H), 2.84 (qu, *J* = 3.9 Hz,1H), 2.47 (ddd, *J* = 3.6, 6.6, 10.3 Hz,1H), 2.41-2.32 (m, 2H), 2.31-2.18 (m, 2H) , 1.99-1.87 (m, 2H), 1.48 (ddd, *J* = 4.5, 6.9, 10.3 Hz, 1H), 1.36 (q, *J* = 7.0 Hz, 1H). ^{13}C NMR (126 MHz, CD_3OD) δ 167.56, 138.91, 138.66, 134.74, 131.61, 128.84, 128.28, 127.23, 122.29,

119.43, 118.88, 66.74, 35.58, 26.19, 20.64, 14.65, 11.51. HR ESI-MS *m/z*: 307.2396 ($[M+H]^+$ calc'd for $C_{20}H_{23}N_2O^+$: 307.1805).

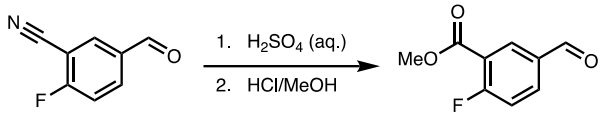

methyl 2-fluoro-5-formylbenzoate

2-fluoro-5-formylbenzonitrile (5 g, 33.5 mmol) was added to a solution of sulfuric acid (2 mL) in water (20 mL), and the reaction was heated at reflux overnight. The product solid was filtered from the reaction mixture, taken up in MeOH (20 mL), treated with hydrochloric acid (2 mL), and heated at reflux overnight. Upon completion, the reaction mixture was washed with $NaHCO_3$, water, and brine, dried over sodium sulfate, and concentrated under reduced pressure to give methyl 2-fluoro-5-formylbenzoate (5.1 g, 84% yield).

^{1}H NMR (400 MHz, CDCl3) δ 10.06 (s, 1H), 8.49 (dd, *J* = 2.2, 6.9 Hz, 1H), 8.09 (ddd, *J* = 2.2, 4.6, 8.5 Hz, 1H), 7.32 (dd, *J* = 8.5, 10.0 Hz, H), 3.98 (s, 3H).

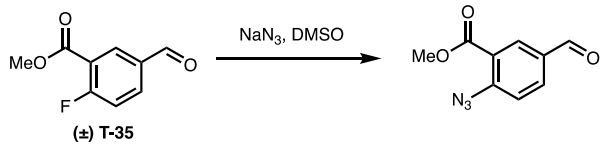

methyl 2-azido-5-formylbenzoate

T-35 (2.5 g, 13.7 mmol) and sodium azide (1 g, 16.5 mmol) were taken up in 15 mL DMSO and heated to 70 °C for 2 h. The reaction mixture was cooled to rt and the product solid was diluted with cold water, filtered, and dried to yield methyl 2-azido-5-formylbenzoate in quantitative yield.

^{1}H NMR (400 MHz, CDCl3) δ 9.98 (s, 1H), 8.38 (d, *J* = 2.0 Hz, 1H), 8.05 (dd, *J* = 2.0, 8.4 Hz, 1H), 7.39 (d, *J* = 8.4 Hz, 1H), 3.95 (s, 3H).

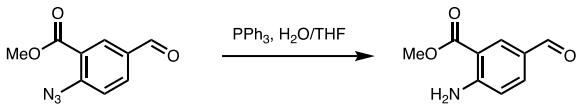

methyl 2-amino-5-formylbenzoate

Methyl 2-azido-5-formylbenzoate (2.8 g, 13.6 mmol) was dissolved in 20 mL THF and treated with triphenylphosphine (3.6 g, 13.6 mmol) and 3 mL water. The reaction was stirred for 4 h until reaction completion as monitored by TLC and then concentrated under reduced pressure. The residue was purified by column chromatography (silica gel, eluent: 0 to 30% EtOAc/hexanes, v/v), and pure product fractions were pooled and concentrated to give methyl 2-azido-5-formylbenzoate (1.6 g, 65% yield).

^{1}H NMR (400 MHz, CDCl3) δ 9.75 (s, 1H), 8.38 (d, *J* = 2.0 Hz, 1H), 7.81 (dd, *J* = 2.0, 8.6 Hz, 1H), 6.71 (d, *J* = 8.6 Hz, 1H), 6.40 (bs, 2H), 3.92 (s, 3H).

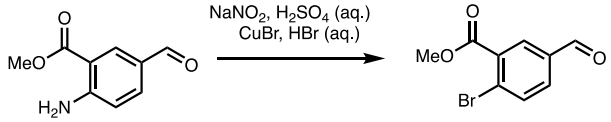

methyl 2-bromo-5-formylbenzoate

According to a modified literature procedure,[61] a suspension of methyl 2-amino-5-formylbenzoate (570 mg, 3.2 mmol) in 5 mL water was brough to 0 °C and treated with 1 mL sulfuric acid. After ten minutes, 1 mL of an aqueous solution of sodium nitrite (526 mg, 7.6 mmol) was added at 0 °C and the reaction was stirred for 20 mins. The resulting diazonium salt solution was kept at 0 °C and added in portions over 20 min to a stirred suspension of copper(I) bromide (821 mg, 5.71 mmol) in 40% hydrobromic acid (10 mL) at rt. The reaction was stirred for 1 h at 60 °C, then brought to rt and extracted 3x with EtOAc. The organic layers were pooled, washed with $NaHCO_3$, water, and brine, dried over sodium sulfate, filtered, and evaporated in vacuo. The residue was

purified by column chromatography (silica gel, eluent: 0 to 20% EtOAc/hexanes, v/v), to give methyl 2-bromo-5-formylbenzoate (180 g, 25% yield).

^{1}H NMR (400 MHz, CDCl3) δ 10.01 (s, 1H), 8.29 (d, *J* = 1.9 Hz, 1H), 7.95-7.75 (m, 2H), 3.98 (s, 3H).

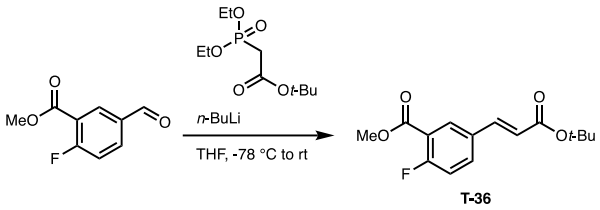

T-36

methyl (*E*)-5-(3-(*tert*-butoxy)-3-oxoprop-1-en-1-yl)-2-fluorobenzoate (T-36)

T-36 (99% yield) was prepared according to the general procedure for **T-25**.

^{1}H NMR (400 MHz, CDCl3) δ 8.09 (dd, *J* = 2.4, 6.9 Hz, 1H), 7.65 (ddd, *J* = 2.4, 4.5, 8.6 Hz, 1H), 7.54 (d, *J* = 16.0 Hz, 1H), 7.15 (dd, *J* = 8.6, 10.3 Hz, 1H), 6.36 (d, *J* = 16.0 Hz, 1H), 3.95 (s, 3H), 1.53 (s, 9H). ^{13}C NMR (126 MHz, CD_3OD) δ 165.85, 164.02, 141.14, 133.57, 133.30, 131.71, 130.91, 121.29, 117.60, 80.86, 52.55, 28.18.

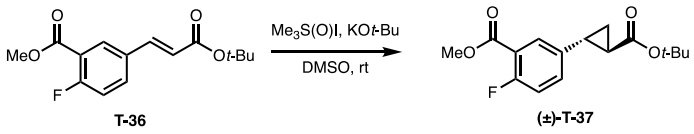

T-36 (±)-T-37

(±)-methyl 5-*trans*-2-(*tert*-butoxycarbonyl)cyclopropyl)-2-fluorobenzoate (T-37)

(±)-T-37 (72% yield) was prepared according to the general procedure for **(±)-T-26**.

^{1}H NMR (400 MHz, $CDCl_3$) δ 7.64 (dd, *J* = 2.5, 6.7 Hz, 1H), 7.28-7.23 (m, 1H), 7.05 (dd, *J* = 8.5, 10.4 Hz, 1H), 3.93 (s, 3H), 2.45 (ddd, *J* = 4.2, 6.4, 9.2 Hz, 1H), 1.81 (ddd, *J* = 4.2, 5.3, 8.5 Hz, 1H),

1.55-1.51 (m, 1H), 1.44 (s, 9H), 1.23-1.19 (m, 1H). ^{13}C NMR (126 MHz, $CDCl_3$) δ 172.17, 159.26, 136.31, 132.15, 129.52, 117.09, 116.86, 80.88, 55.32, 28.15, 25.10, 24.55, 16.84.

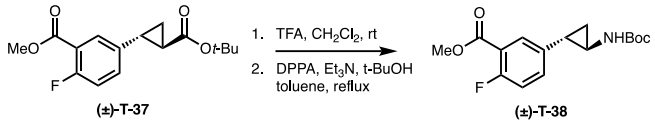

(±)-methyl 5-(*trans*-2-((*tert*-butoxycarbonyl)amino)cyclopropyl)-2-fluorobenzoate (T-38)

(±)-T-38 (38% yield, two steps) was prepared according to the general procedure for **(±)-T-27**.

^{1}H NMR (400 MHz, CDCl3) δ 7.66 (dd, *J* = 2.5, 6.8 Hz, 1H), 7.39-7.30 (m, 1H), 7.04 (dd, *J* = 8.5, 10.6 Hz, H), 4.82 (s, 1H), 3.92 (s, 3H), 2.71-2.65 (m, 1H), 2.10-2.01 (m, 1H), 1.45 (s, 9H), 1.19-1.13 (m, 1H). ^{13}C NMR (126 MHz, CD_3OD) δ 164.85, 158.53, 150.44, 145.47, 132.93, 131.11, 131.01, 129.44, 117.20, 83.77, 52.04, 25.20, 23.80, 22.71, 16.78. HR ESI-MS *m/z*: 310.2389 ([M+H]$^+$ calc'd for $C_{16}H_{21}FNO_4^+$: 310.1449).

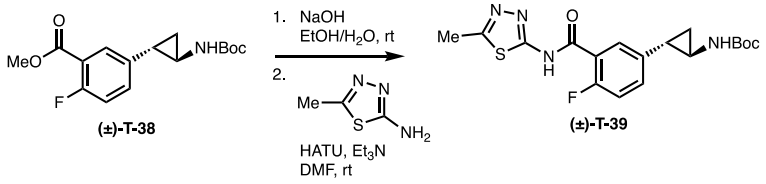

(±)-*tert*-butyl (*trans*-2-(4-fluoro-3-((5-methyl-1,3,4-thiadiazol-2-yl)carbamoyl)phenyl) cyclopropyl)carbamate (T-39)

(±)-T-39 (30% yield, two steps) was prepared according to the general procedure for **(±)-T-33**.

^{1}H NMR (400 MHz, $CDCl_3$) δ 9.94 (s, 1H), 7.90 (dd, *J* = 2.5, 7.3 Hz, 1H), 7.53-7.42 (m, 1H), 7.15 (dd, *J* = 8.5, 11.9 Hz, 1H), 4.85 (s, 1H), 2.74 (s, 3H), 2.70 (q, *J* = 2.1, 2.3 Hz, 1H), 2.14-2.08 (m, 1H), 1.45 (s, 1H), 1.30-1.24 (m, 1H), 1.24-1.20 (m, 1H). ^{13}C NMR (126 MHz, $CDCl_3$) δ 164.41, 160.50, 158.25, 156.27, 138.36, 134.27, 129.79, 117.83, 116.44, 79.44, 29.71, 24.79, 22.72, 16.74, 15.36. HR ESI-MS *m/z*: 393.1406 ([M+H]$^+$ calc'd for $C_{18}H_{22}FN_4O_3S^+$: 393.1391).

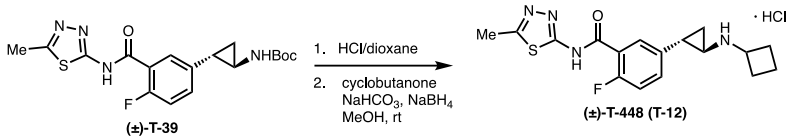

(±)-5-(*trans*-2-(cyclobutylamino)cyclopropyl)-2-fluoro-*N*-(5-methyl-1,3,4-thiadiazol-2-yl) benzamide hydrochloride (T-12)

(±)-T-12 (22% yield, two steps) was prepared according to the general procedure for **(±)-2-*d*-T-448**.

^{1}H NMR (400 MHz, CD_3OD) δ 12.87 (s, 1H), 9.75 (t, *J* = 5.7 Hz, 1H), 7.5 (ddd, *J* = 2.4, 5.4, 10.1 Hz, 1H), 7.31 (dd, *J* = 8.4, 10.2 Hz, 1H), 4.06-3.99 (m, 1H), 2.94-2.86 (m, 1H), 2.65 (s, 3H), 2.57 (ddd, *J* = 3.6, 6.3, 10.1 Hz, 1H), 2.34-2.22 (m, 2H), 2.22-2.13 (m, 2H), 1.87-1.72 (m, 2H), 1.54 (ddd, *J* = 4.5, 6.3, 10.4 Hz, 1H), 1.35 (dt, *J* = 6.3, 7.9 Hz, 1H). HR ESI-MS *m/z*: 347.1830 ($[M+H]^+$ calc'd for $C_{17}H_{20}FN_4OS^+$: 347.1336).

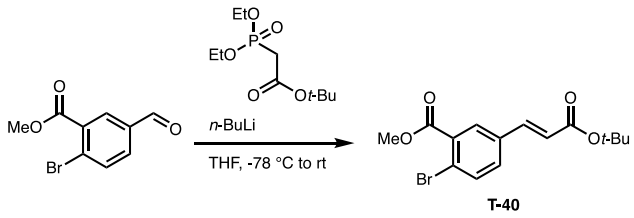

methyl (*E*)-5-(3-(*tert*-butoxy)-3-oxoprop-1-en-1-yl)-2-bromobenzoate (T-40)

T-40 (91% yield) was prepared according to the general procedure for **T-25**.

^{1}H NMR (400 MHz, CDCl3) δ 7.92 (d, *J* = 2.3 Hz, 1H), 7.66 (d, *J* = 8.3 Hz, 1H), 7.51 (d, *J* = 16.0 Hz, 1H), 7.44 (dd, *J* = 2.3, 8.3 Hz, 1H), 6.41 (d, *J* = 16.0 Hz, 1H), 3.95 (s, 3H), 1.53 (s, 9H). ^{13}C NMR (126 MHz, $CDCl_3$) δ 166.08, 165.68, 141.03, 134.97, 134.01, 131.28, 130.56, 123.09, 122.17, 80.97, 52.65, 28.16.

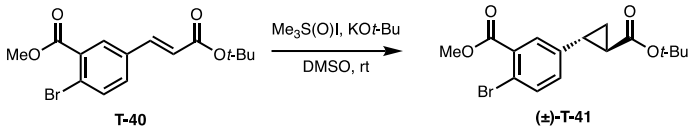

(±)-methyl 5-(*trans*-2-(*tert*-butoxycarbonyl)cyclopropyl)-2- bromobenzoate (T-41)

(±)-T-41 (30% yield, two steps) was prepared according to the general procedure for **(±)-T-26**.

^{1}H NMR (400 MHz, CDCl3) δ 7.55 (dt, *J* = 2.0, 4.1 Hz, 1H), 7.51 (t, *J* = 2.5 Hz, 1H), 7.06 (dq, *J* = 2.1, 2.2, 8.4 Hz, 1H), 3.94 (s, 3H), 2.47-2.39 (m, 1H), 1.87-1.81 (m, 1H), 1.59-1.54 (m, 1H), 1.48 (s, 9H), 1.24-1.20 (m, 1H). ^{13}C NMR (126 MHz, $CDCl_3$) δ 171.93, 166.53, 141.63, ,140.13, 134.28, 132.08, 130.40, 129.02, 119.07, 80.94, 52.50, 28.14, 25.27, 24.76, 16.97.

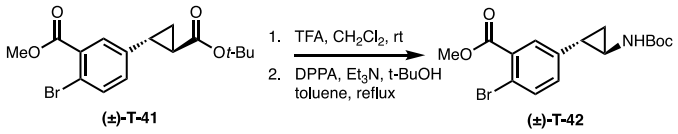

(±)-methyl 5-((1*S*,2*R*)-2-((*tert*-butoxycarbonyl)amino)cyclopropyl)-2- bromobenzoate (T-42)

(±)-T-42 (46% yield, two steps) was prepared according to the general procedure for **(±)-T-27**.

^{1}H NMR (400 MHz, CDCl3) δ 7.55-7.49 (m, 2H), 7.13 (d, *J* = 7.13 Hz, 1H), 4.85 (s, 1H), 3.91 (s, 3H), 2.71 (s, 1H), 2.06-2.00 (m, 1H), 1.44 (s, 9H), 1.19-1.15 (m, 2H). ^{13}C NMR (126 MHz, $CDCl_3$) δ 166.64, 156.25, 140.36, 134.20, 131.89, 131.05, 129.33, 118.83, 79.85, 52.44, 28.39, 24.69, 22.70, 16.24. HR ESI-MS *m/z*: 370.2785 ([M+H]$^{+}$ calc'd for $C_{16}H_{21}BrNO_4^{+}$: 370.0648).

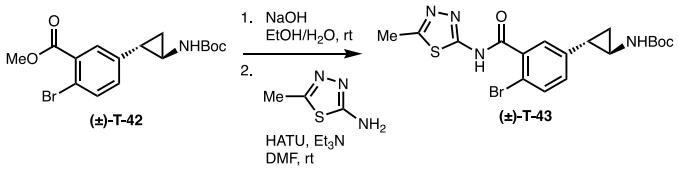

(±)-methyl 5-(*trans*-2-((tert-butoxycarbonyl)amino)cyclopropyl)-2-bromobenzoate (T-43)

(±)-T-43 (39% yield, two steps) was prepared according to the general procedure for **(±)-T-33**.

^{1}H NMR (400 MHz, CDCl3) δ 11.75 (s, 1H), 7.53 (d, *J* = 8.2 Hz, 1H), 7.47 (s, 1H), 7.18 (d, *J* = 8.50 Hz, 1H), 4.93 (s, 1H), 2.72 (s, 1H), 2.67 (s, 3H), 2.08 (t, *J* = 7.5 Hz, 1H), 1.41 (s, 9H), 1.22-1.16 (m, 2H). ^{13}C NMR (126 MHz, $CDCl_3$) δ 165.08, 160.39, 159.47, 156.27, 140.99, 134.32, 133.79, 130.98, 128.61, 117.31, 79.91, 28.38, 24.69, 22.66, 15.99, 15.31. HR ESI-MS *m/z*: 453.0617 ([M+H]$^+$ calc'd for $C_{18}H_{22}BrN_4O_3S^+$: 453.0591).

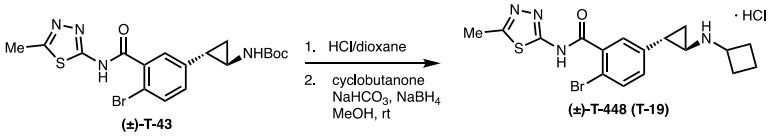

(±)-5-(*trans*-2-(cyclobutylamino)cyclopropyl)-2-bromo-*N*-(5-methyl-1,3,4-thiadiazol-2-yl) benzamide hydrochloride (T-19)

(±)-T-19 (59% yield, two steps) was prepared according to the general procedure for **(±)-2-*d*-T-448**.

^{1}H NMR (400 MHz, CD_3OD) δ 7.68 (d, *J* = 8.4 Hz, 1H), 7.44 (t, *J* = 2.6 Hz, 1H), 7.32 (dt, *J* = 2.4, 8.4 Hz, 1H), 3.96 (p, *J* = 8.1 Hz, 1H), 2.97 (p, *J* = 4.2 Hz, 1H), 2.83 (s, 3H), 2.54 (m, 1H), 2.41-2.33 (m, 2H), 2.32-2.21 (m, 2H), 2.00-1.92 (m, 2H), 1.57 (ddd, *J* = 3.0, 7.3, 10.7 Hz, 1H), 1.46 (q, *J* = 7.0 Hz, 1H). ^{13}C NMR (126 MHz, CD_3OD) δ 170.31, 147.63, 138.44, 133.50, 130.39, 127.02, 117.50, 52.43, 35.68, 26.23, 26.21, 20.38, 14.67, 11.82. HR ESI-MS *m/z*: 407.0634 ([M+H]$^+$ calc'd for $C_{17}H_{20}BrN_4OS^+$: 407.0536).

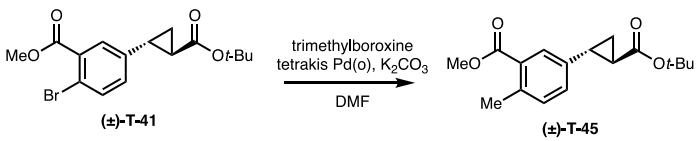

(±)-methyl 5-(*trans*-2-(*tert*-butoxycarbonyl)cyclopropyl)-2-methylbenzoate (T-45)

Tetrakis(triphenylphosphine)palladium (27 mg, 0.02 mmol), trimethylboroxine (10 uL, 0.24 mmol, 50% in THF), and K_2CO_3 (99 mg, 0.7 mmol) were added to a solution of the aryl bromide **(±)-T-41** (85 mg, 0.2 mmol) in anhydrous DMF (1 mL). The reaction mixture was heated to 115 °C overnight. After cooling to room temperature, the mixture was diluted with EtOAc, filtered through a plug of celite and concentrated under reduced pressure. The residue was purified by column chromatography (silica gel, eluent: 0 to 35% EtOAc/hexanes, v/v) to give **(±)-T-45** (71% yield).

^{1}H NMR (400 MHz, CDCl3) δ 7.62 (s, 1H), 7.16-7.07 (m, 1H), 3.89 (s, 3H), 2.54 (s, 3H), 2.44 (ddd, *J* = 4.0, 6.4, 9.9 Hz, 1H), 1.82 (dt, *J* = 4.7, 9.4 Hz, 1H), 1.75 (dd, *J* = 6.2, 8.6 Hz, 1H), 1.52 (d, *J* = 4.4 Hz, 1H), 1.47 (s, 9H). ^{13}C NMR (126 MHz, $CDCl_3$) δ 172.45, 167.76, 138.06, 131.79, 129.78, 129.59, 129.40, 128.27, 128.19, 80.69, 51.86, 28.17, 25.13, 21.28, 19.36, 16.87.

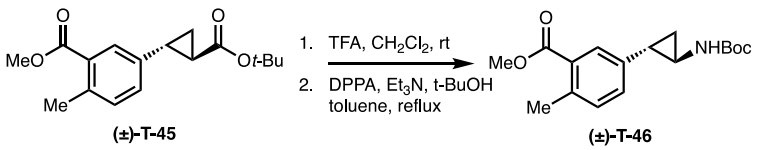

(±)-methyl 5-((1*S*,2*R*)-2-((*tert*-butoxycarbonyl)amino)cyclopropyl)-2-fluorobenzoate (T-46)

(±)-T-46 (53% yield, two steps) was prepared according to the general procedure for **(±)-T-27**.

^{1}H NMR (400 MHz, $CDCl_3$) δ 7.66-7.61 (m, 1H), 7.43-7.36 (m, 2H), 4.88-4.82 (m, 1H), 3.88 (s, 3H), 2.04 (s, 3H), 1.75-1.72 (m, 1H), 1.59 (s, 9H), 1.02-0.96 (m, 1H), 0.90-0.85 (m, 1H). ^{13}C NMR (126 MHz, $CDCl_3$) δ 168.07, 157.21, 138.25, 137.29, 131.87, 130.44, 128.58, 115.29, 77.23, 51.86, 32.45, 28.40, 24.49, 21.28, 15.71. HR ESI-MS *m/z*: 306.1884 ($[M+H]^+$ calc'd for $C_{17}H_{24}NO_4^+$: 306.1700).

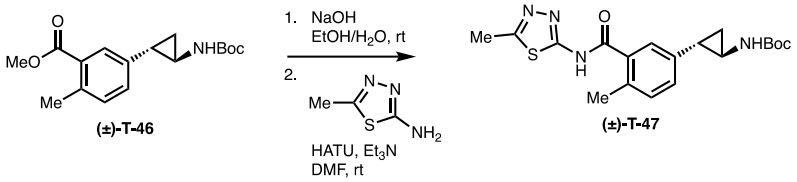

(±)-methyl 5-(*trans*-2-((tert-butoxycarbonyl)amino)cyclopropyl)-2-fluorobenzoate (T-47)

(±)-T-47 (35% yield, two steps) was prepared according to the general procedure for **(±)-T-33**.

^{1}H NMR (400 MHz, $CDCl_3$) δ 7.24-7.22 (m, 1H), 7.22-7.20 (m, 2H), 4.92-4.87 (m, 1H), 2.70 (s, 3H), 2.04 (s, 3H), 1.78-1.72 (m, 1H), 1.44 (s, 9H), 1.17-1.13 (m, 1H), 1.00-0.97 (m, 1H). ^{13}C NMR (126 MHz, $CDCl_3$) δ 171.20, 166.70, 160.16, 159.74, 136.11, 132.18, 129.85, 129.59, 120.46, 77.24, 60.42, 28.40, 21.07, 20.00, 15.27, 14.62. HR ESI-MS *m/z*: 389.1889 ([M+H]$^+$ calc'd for $C_{19}H_{25}N_4O_3S^+$: 389.1642).

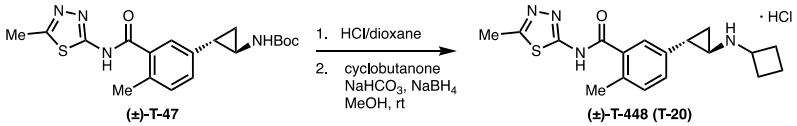

(±)-5-(*trans*-2-(cyclobutylamino)cyclopropyl)-2-fluoro-*N*-(5-methyl-1,3,4-thiadiazol-2-yl) benzamide hydrochloride (T-20)

(±)-T-20 (11% yield, two steps) was prepared according to the general procedure for **(±)-2-*d*-T-448**.

^{1}H NMR (400 MHz, CD_3OD) δ 7.39-7.29 (m, 3H), 3.98 (q, *J* = 8.1 Hz, 1H), 2.93 (dd, *J* = 4.0, 7.7 Hz, 1H), 2.74 (s, 3H), 2.50-2.45 (m, 1H), 2.44 (s, 3H), 2.42-2.34 (m, 2H), 2.28-2.18 (m, 2H), 2.02-1.92 (m, 2H), 1.47-1.43 (m, 1H), 0.91-0.85 (m, 1H). HR ESI-MS *m/z*: 347.1360 ([M+H]$^+$ calc'd for $C_{17}H_{20}FN_4OS^+$: 347.1336).

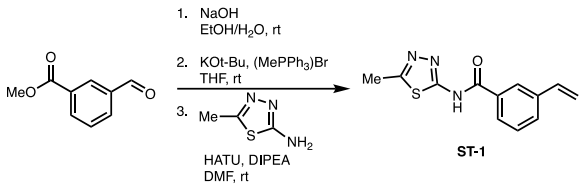

General Procedure for *N*-(5-methyl-1,3,4-thiadiazol-2-yl)-3-vinylbenzamide (ST-1)

An 8 M aqueous sodium hydroxide solution (1 mL) was added to methyl 3-formylbenzoate (70 mg, 0.42 mmol) dissolved in ethanol (1.5 mL), and the mixture was stirred at room temperature overnight. The reaction mixture was neutralized with 1 M hydrochloric acid at 0 °C, and extracted with ethyl acetate (3x). The extract was washed successively with water and saturated brine, dried over anhydrous sodium sulfate, filtered, and concentrated under reduced pressure. The product was dried under vacuum and directly taken up in anhydrous THF (2 mL) and treated with KO*t*-Bu (179 mg) for 15 min at at 0 °C. Trimethylphosphonium bromide (214 mg) was added in one portion at 0 °C, after which the reaction mixture was allowed to return to rt and stirred for 2 h. The reaction mixture was neutralized with 1 M hydrochloric acid at 0 °C, and extracted with ethyl acetate (3 x 10 mL). The extract was washed successively with water and saturated brine, dried over anhydrous sodium sulfate, filtered, and concentrated under reduced pressure. The product was dissolved in N,N-dimethylformamide (1 mL), and O-(7-azabenzotriazol-1-yl)-N,N,N',N'-tetramethyluronium hexafluoro-phosphate (152 mg, 0.37 mmol) and N,N-diisopropylethylamine (233 µL, 1.3 mmol) was added at 0 °C. The mixture was stirred at room temperature for 30 min, 5-methyl-1,3,4-thiadiazol-2-amine (42 mg, 0.4 mmol) was added, and the reaction stirred overnight at rt. Upon completion, the reaction mixture was poured into water and the mixture was extracted with ethyl acetate (2x). The extract was washed successively with saturated aqueous sodium hydrogen carbonate solution and saturated brine, dried over anhydrous sodium sulfate, and concentrated under reduced pressure. The residue was purified by silica gel column chromatography (ethyl acetate) and concentrated under reduced pressure to give **ST-1** (46% yield over two steps).

^{1}H NMR (400 MHz, $CDCl_3$) δ 11.42 (bs, 1H), 8.12 (s, 1H), 7.98 (d, *J* = 7.9 Hz, 1H), 7.67 (d, *J* = 7.9 Hz, 1H), 7.50 (t, *J* = 7.8 Hz, 1H), 6.81 (dd, *J* = 10.9, 17.6 Hz, 1H), 5.85 (d, *J* = 17.5 Hz, 1H), 5.37 (d, *J* = 11.0 Hz, 1H), 2.72 (s, 3H). ^{13}C NMR (126 MHz, $CDCl_3$) δ 166.26, 138.33, 135.87, 131.63, 130.57, 129.10, 127.84, 126.43, 115.39, 15.29. HR ESI-MS *m/z*: 246.0721 ([M+H]$^+$ calc'd for $C_{12}H_{12}N_3OS^+$: 246.0696).

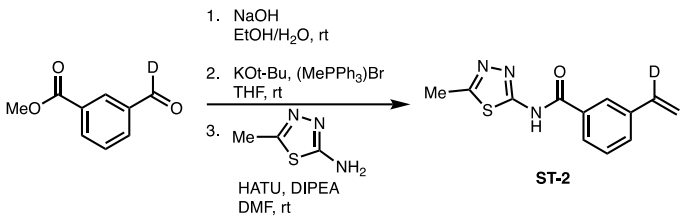

***N*-(5-methyl-1,3,4-thiadiazol-2-yl)-3-(vinyl-1-*d*)benzamide (ST-2)**

ST-2 (41% yield, two steps) was prepared according to the general procedure for **ST-1**.

^{1}H NMR (400 MHz, $CDCl_3$) δ 11.73 (bs, 1H), 8.15 (t, *J* = 1.8 Hz, 1H), 8.03 (d, *J* = 7.8 Hz, 1H), 7.72-7.64 (m, 1H), 7.50 (td, *J* = 4.6, 7.8 Hz, 1H), 5.83 (s, 1H), 5.36 (s, 1H), 2.71 (s, 3H). HR ESI-MS *m/z*: 247.0758 ([M+H]$^+$ calc'd for $C_{12}H_{11}DN_3OS^+$: 247.0758).

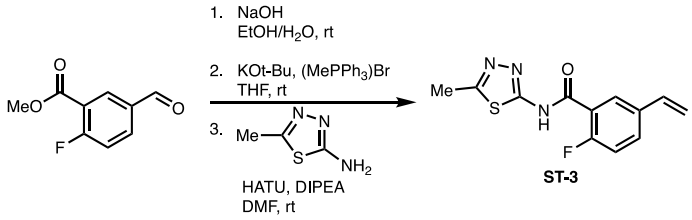

2-fluoro-*N*-(5-methyl-1,3,4-thiadiazol-2-yl)-5-vinylbenzamide (ST-3)

ST-3 (28% yield, two steps) was prepared according to the general procedure for **ST-1**.

^{1}H NMR (400 MHz, $CDCl_3$) δ 8.22 (dd, *J* = 2.4, 7.5 Hz, 1H), 7.64 (ddd, *J* = 2.5, 5.0, 8.6 Hz, 1H), 7.24-7.16 (m, 1H), 6.73 (dd, *J* = 10.9, 17.6 Hz, 1H), 5.81 (d, *J* = 17.6 Hz, 1H), 5.37 (d, *J* = 10.9 Hz,

1H), 2.75 (s, 3H). ^{13}C NMR (126 MHz, $CDCl_3$) δ 161.00, 135.20, 134.42, 132.66, 132.56, 129.87, 118.55, 116.97, 116.72, 115.92, 15.35. HR ESI-MS *m/z*: 264.0626 ($[M+H]^+$ calc'd for $^+$: 264.0601).

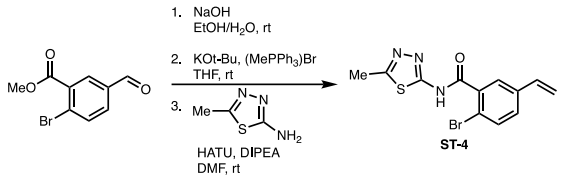

2-bromo-*N*-(5-methyl-1,3,4-thiadiazol-2-yl)-5-vinylbenzamide (ST-4)

ST-4 (18% yield, two steps) was prepared according to the general procedure for **ST-1**.

^{1}H NMR (400 MHz, $CDCl_3$) δ 7.80 (d, *J* = 2.2 Hz, 1H), 7.64 (d, *J* = 8.3 Hz, 1H), 7.44 (dd, *J* = 2.2, 8.3 Hz, 1H), 6.70 (dd, *J* = 10.9, 17.6 Hz, 1H), 5.85 (d, *J* = 17.6 Hz, 1H), 5.41 (d, *J* = 10.9 Hz, 1H), 2.73 (s, 3H). ^{13}C NMR (126 MHz, $CDCl_3$) δ 165.12, 137.33, 134.95, 134.48, 134.12, 132.08, 129.77, 128.34, 119.30, 116.01, 15.30. HR ESI-MS *m/z*: 323.9808 ($[M+H]^+$ calc'd for $C_{12}H_{11}BrN_3OS^+$: 323.9801).

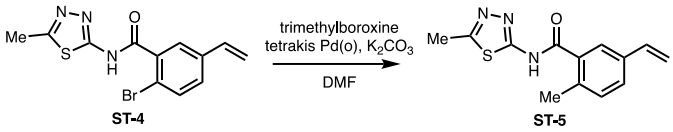

2-methyl-*N*-(5-methyl-1,3,4-thiadiazol-2-yl)-5-vinylbenzamide (ST-5)

ST-5 (20% yield) was prepared according to the general procedure for **(±)-T-45**.

^{1}H NMR (400 MHz, $CDCl_3$) δ 7.71-7.65 (m, 1H), 7.49-7.44 (m, 2H), 6.72 (dd, *J* = 10.9, 17.6 Hz, 1H), 5.74 (d, *J* = 17.6 Hz, 1H), 5.28 (d, *J* = 10.9 Hz, 1H), 2.68 (s, 3H), 2.53 (s, 3H). HR ESI-MS *m/z*: 260.0852 ($[M+H]^+$ calc'd for $C_{13}H_{14}N_3OS^+$: 260.0852).

References

1. Arrowsmith, C. H., Bountra, C., Fish, P. V., Lee, K. & Schapira, M. Epigenetic protein families: a new frontier for drug discovery. *Nat Rev Drug Discov* **11**, 384–400 (2012).

2. Allis, C. D. & Jenuwein, T. The molecular hallmarks of epigenetic control. *Nat Rev Genet* **17**, 487–500 (2016).

3. Zhang, Y. & Kutateladze, T. G. Exploring epigenetics with chemical tools. *Nat Chem* **12**, 506–508 (2020).

4. Zhang, P., Torres, K., Liu, X., Liu, C. & E. Pollock, R. An Overview of Chromatin-Regulating Proteins in Cells. *Curr Protein Pept Sci* **17**, 401–410 (2016).

5. Jenuwein, T. & Allis, C. D. Translating the Histone Code. *Science (1979)* **293**, 1074–1080 (2001).

6. Black, J. C., Van Rechem, C. & Whetstine, J. R. Histone Lysine Methylation Dynamics: Establishment, Regulation, and Biological Impact. *Mol Cell* **48**, 491–507 (2012).

7. Deb, M. *et al.* Chromatin dynamics: H3K4 methylation and H3 variant replacement during development and in cancer. *Cellular and Molecular Life Sciences* **71**, 3439–3463 (2014).

8. Sun, Y., Chen, B.-R. & Deshpande, A. Epigenetic Regulators in the Development, Maintenance, and Therapeutic Targeting of Acute Myeloid Leukemia. *Front Oncol* **8**, (2018).

9. Culhane, J. C. & Cole, P. A. LSD1 and The Chemistry of Histone Demethylation. *Curr Opin Chem Bio* **162**, 214–220 (2007).

10. Shi, Y. *et al.* Histone demethylation mediated by the nuclear amine oxidase homolog LSD1. *Cell* **119**, 941–953 (2004).

11. Shi, Y. J. *et al.* Regulation of LSD1 histone demethylase activity by its associated factors. *Mol Cell* (2005) doi:10.1016/j.molcel.2005.08.027.

12. Kozub, M. M., Carr, R. M., Lomberk, G. L. & Fernandez-Zapico, M. E. LSD1, a double-edged sword, confers dynamic chromatin regulation but commonly promotes aberrant cell growth. *F1000Res* **6**, 2016 (2017).

13. Mohammad, H. P. *et al.* A DNA Hypomethylation Signature Predicts Antitumor Activity of LSD1 Inhibitors in SCLC. *Cancer Cell* **28**, 57–69 (2015).

14. Magliulo, D., Bernardi, R. & Messina, S. Lysine-Specific Demethylase 1A as a Promising Target in Acute Myeloid Leukemia. *Front Oncol* **8**, (2018).

15. C. Zheng, Y. *et al.* Irreversible LSD1 Inhibitors: Application of Tranylcypromine and Its Derivatives in Cancer Treatment. *Curr Top Med Chem* **16**, 2179–2188 (2016).

16. Fang, Y., Liao, G. & Yu, B. LSD1/KDM1A inhibitors in clinical trials: advances and prospects. *J Hematol Oncol* **12**, 129 (2019).

17. Yang, M. *et al.* Structural basis for the inhibition of the LSD1 histone demethylase by the antidepressant trans-2-phenylcyclopropylamine. *Biochemistry* **46**, 8058–8065 (2007).

18. Szewczuk, L. M. *et al.* Mechanistic Analysis of a Suicide Inactivator of Histone Demethylase LSD1 †. *Biochemistry* **46**, 6892–6902 (2007).

19. Northcott, P. A. *et al.* Enhancer hijacking activates GFI1 family oncogenes in medulloblastoma. *Nature* **511**, 428–434 (2014).

20. Somervaille, T. *et al.* Safety, Phamacokinetics (PK), Pharmacodynamics (PD) and Preliminary Activity in Acute Leukemia of Ory-1001, a First-in-Class Inhibitor of Lysine-Specific Histone Demethylase 1A (LSD1/KDM1A): Initial Results from a First-in-Human Phase 1 Study. *Blood* **128**, 4060–4060 (2016).

21. Lu, Z. *et al.* ORY-1001 Suppresses Cell Growth and Induces Apoptosis in Lung Cancer Through Triggering HK2 Mediated Warburg Effect. *Front Pharmacol* **9**, (2018).

22. Fiskus, W. *et al.* Synergistic Pre-Clinical Activity of Targeted Inhibition of KDM1A and BET Proteins Against Human AML Blast Progenitor Cells. *Blood* **132**, 3930–3930 (2018).

23. Maes, T., Mascaró, C., Sacilotto, N., Lufino, M. M. & Ciceri, F. Targeting KDM1A with iadademstat in combination with immunotherapy in an *in vivo* model of melanoma. *Journal of Clinical Oncology* **37**, e14248–e14248 (2019).

24. Romo-Morales, A., Aladowicz, E., Blagg, J., Gatz, S. A. & Shipley, J. M. Catalytic inhibition of KDM1A in Ewing sarcoma is insufficient as a therapeutic strategy. *Pediatr Blood Cancer* **66**, (2019).

25. Mohammad, H. P. & Kruger, R. G. Antitumor activity of LSD1 inhibitors in lung cancer. *Mol Cell Oncol* **3**, e1117700 (2016).

26. Barth, J. *et al.* LSD1 inhibition by tranylcypromine derivatives interferes with GFI1-mediated repression of PU.1 target genes and induces differentiation in AML. *Leukemia* **33**, 1411–1426 (2019).

27. Vinyard, M. E. *et al.* CRISPR-suppressor scanning reveals a nonenzymatic role of LSD1 in AML. *Nat Chem Biol* **15**, 529–539 (2019).

28. Alsaqer, S. F. *et al.* Inhibition of LSD1 epigenetically attenuates oral cancer growth and metastasis. *Oncotarget* **8**, 73372–73386 (2017).

29. Cusan, M. *et al.* LSD1 inhibition exerts its antileukemic effect by recommissioning PU.1- and C/EBPa-dependent enhancers in AML. *Blood* **131**, 1730–1742 (2018).

30. Maiques-Diaz, A. *et al.* Enhancer Activation by Pharmacologic Displacement of LSD1 from GFI1 Induces Differentiation in Acute Myeloid Leukemia. *Cell Rep* **22**, 3641–3659 (2018).

31. Collins, B. E., Greer, C. B., Coleman, B. C. & Sweatt, J. D. Histone H3 lysine K4 methylation and its role in learning and memory. *Epigenetics Chromatin* **12**, 7 (2019).

32. Li, Y. *et al.* Biological and therapeutic role of LSD1 in Alzheimer's diseases. *Front Pharmacol* **13**, (2022).

33. Rapanelli, M. *et al.* Targeting histone demethylase LSD1 for treatment of deficits in autism mouse models. *Mol Psychiatry* **27**, 3355–3366 (2022).

34. Matsuda, S. *et al.* T-448, a specific inhibitor of LSD1 enzyme activity, improves learning function without causing thrombocytopenia in mice. *Neuropsychopharmacology* **44**, 1505–1512 (2019).

35. Baba, R. *et al.* LSD1 enzyme inhibitor TAK-418 unlocks aberrant epigenetic machinery and improves autism symptoms in neurodevelopmental disorder models. *Sci Adv* **7**, (2021).

36. Yin, W. *et al.* Safety, pharmacokinetics and pharmacodynamics of TAK-418, a novel inhibitor of the epigenetic modulator lysine-specific demethylase 1A. *Br J Clin Pharmacol* **87**, 4756–4768 (2021).

37. Grob, C. A. & Baumann, W. Die 1,4-Eliminierung unter Fragmentierung. *Helv Chim Acta* **38**, 594–610 (1955).

38. Grob, C. A. Mechanisms and Stereochemistry of Heterolytic Fragmentation. *Angewandte Chemie International Edition in English* **8**, 535–546 (1969).

39. Evans, D. A., Woerpel, K. A., Hinman, M. M. & Faul, M. M. Bis(oxazolines) as chiral ligands in metal-catalyzed asymmetric reactions. Catalytic, asymmetric cyclopropanation of olefins. *J Am Chem Soc* **113**, 726–728 (1991).

40. Benelkebir, H. *et al.* Enantioselective synthesis of tranylcypromine analogues as lysine demethylase (LSD1) inhibitors. *Bioorg Med Chem* **19**, 3709–3716 (2011).

41. Vianello, P. *et al.* Synthesis, biological activity and mechanistic insights of 1-substituted cyclopropylamine derivatives: A novel class of irreversible inhibitors of histone demethylase KDM1A. *Eur J Med Chem* **86**, 352–363 (2014).

42. Streitwieser, A., Jagow, R. H., Fahey, R. C. & Suzuki, S. Kinetic Isotope Effects in the Acetolyses of Deuterated Cyclopentyl Tosylates [1,2]. *J Am Chem Soc* **80**, 2326–2332 (1958).

43. Jiang, X.-K. Establishment and Successful Application of the $\sigma_{JJ}^{\bullet}$ Scale of Spin-Delocalization Substituent Constants. *Acc Chem Res* **30**, 283–289 (1997).

44. Hammett, L. P. Some Relations between Reaction Rates and Equilibrium Constants. *Chem Rev* **17**, 125–136 (1935).

45. Santerre, G. M., Hansrote, C. J. & Crowell, T. I. The Reaction of Aromatic Aldehydes with n-Butylamine. Acid Catalysis and Substituent Effects [1]. *J Am Chem Soc* **80**, 1254–1257 (1958).

46. Crowell, T. I., Bell, C. E. & O'Brien, D. H. Extrathermodynamic Relationships in Schiff Base Formation. *J Am Chem Soc* **86**, 4973–4976 (1964).

47. Niwa, H. & Umehara, T. Structural insight into inhibitors of flavin adenine dinucleotide-dependent lysine demethylases. *Epigenetics* (2017) doi:10.1080/15592294.2017.1290032.

48. Rinkel, J., Rabe, P., Garbeva, P. & Dickschat, J. S. Lessons from 1,3-Hydride Shifts in Sesquiterpene Cyclizations. *Angewandte Chemie International Edition* **55**, 13593–13596 (2016).

49. Xu, H., Goldfuss, B. & Dickschat, J. S. 1,2- or 1,3-Hydride Shifts: What Controls Guaiane Biosynthesis? *Chemistry – A European Journal* **27**, 9758–9762 (2021).

50. Lou, T. *et al.* Structural Insights into Three Sesquiterpene Synthases for the Biosynthesis of Tricyclic Sesquiterpenes and Chemical Space Expansion by Structure-Based Mutagenesis. *J Am Chem Soc* (2023) doi:10.1021/jacs.3c00278.

51. Vasan, N., Baselga, J. & Hyman, D. M. A view on drug resistance in cancer. *Nature* **575**, 299–309 (2019).

52. Kwok, H. S. *et al.* Drug addiction unveils a repressive methylation ceiling in EZH2-mutant lymphoma. *Nat Chem Biol* (2023) doi:10.1038/s41589-023-01299-1.

53. Ngan, K. C.-H. *et al.* Activity-based CRISPR scanning uncovers allostery in DNA methylation maintenance machinery. *Elife* **12**, (2023).

54. Burg, J. M., Gonzalez, J. J., Maksimchuk, K. R. & McCafferty, D. G. Lysine-Specific Demethylase 1A (KDM1A/LSD1): Product Recognition and Kinetic Analysis of Full-Length Histones. *Biochemistry* **55**, 1652–1662 (2016).

55. Forneris, F., Binda, C., Adamo, A., Battaglioli, E. & Mattevi, A. Structural Basis of LSD1-CoREST Selectivity in Histone H3 Recognition. *Journal of Biological Chemistry* **282**, 20070–20074 (2007).

56. Pilotto, S. *et al.* Interplay among nucleosomal DNA, histone tails, and corepressor CoREST underlies LSD1-mediated H3 demethylation. *Proceedings of the National Academy of Sciences* **112**, 2752–2757 (2015).

57. Gooden, D. M., Schmidt, D. M. Z., Pollock, J. A., Kabadi, A. M. & McCafferty, D. G. Facile synthesis of substituted trans-2-arylcyclopropylamine inhibitors of the human histone demethylase LSD1 and monoamine oxidases A and B. *Bioorg Med Chem Lett* **18**, 3047–3051 (2008).

58. Wolfe, J. P. & Buchwald, S. L. Scope and Limitations of the Pd/BINAP-Catalyzed Amination of Aryl Bromides. *J Org Chem* **65**, 1144–1157 (2000).

59. Levin, J. I., Turos, E. & Weinreb, S. M. An Alternative Procedure for the Aluminum-Mediated Conversion of Esters to Amides. *Synth Commun* **12**, 989–993 (1982).

60. Caiuby, C. A. D., de Jesus, M. P. & Burtoloso, A. C. B. α-Imino Iridium Carbenes from Imidoyl Sulfoxonium Ylides: Application in the One-Step Synthesis of Indoles. *J Org Chem* **85**, 7433–7445 (2020).

61. Pospíšil, J., Müller, C. & Fürstner, A. Total Synthesis of the Aspercyclides. *Chemistry - A European Journal* **15**, 5956–5968 (2009).

Appendix: Catalog of Spectra

T-21

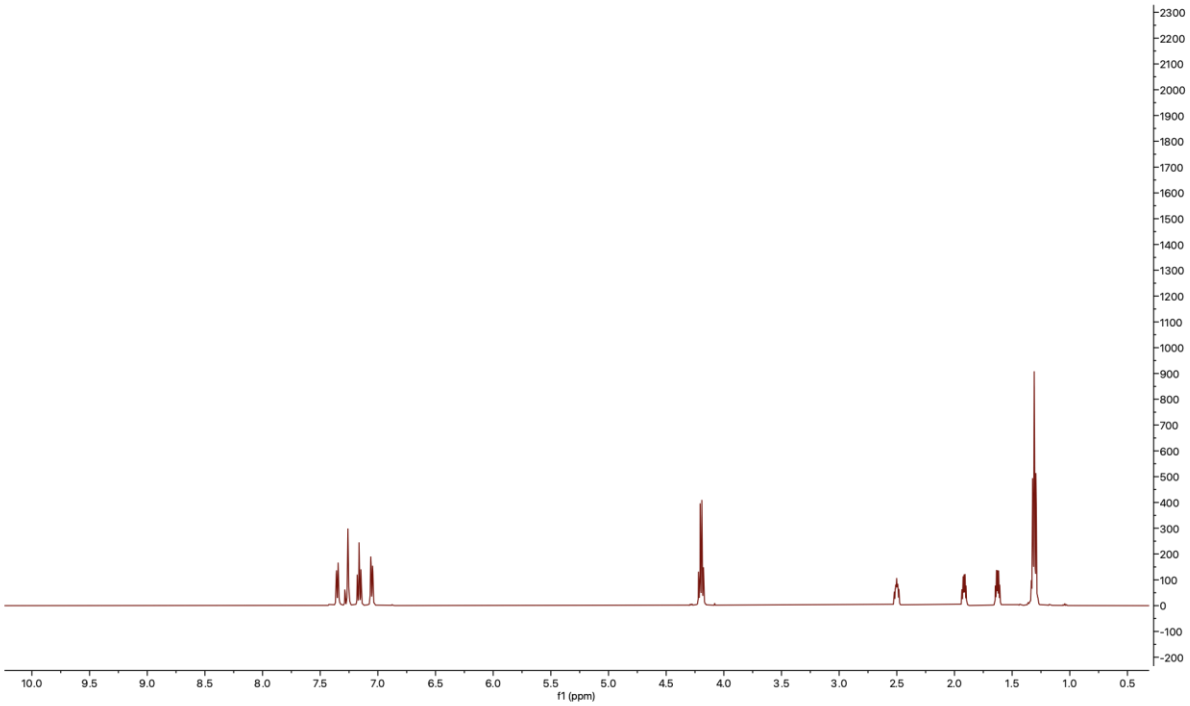

T-22

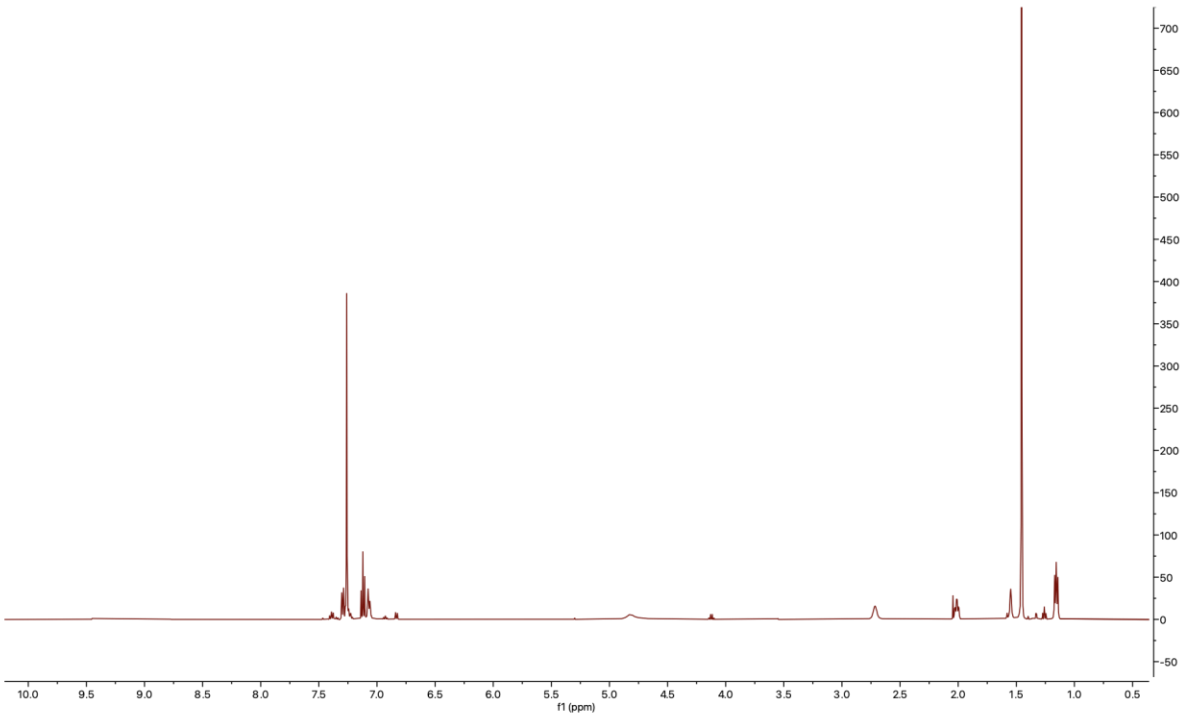

T-23

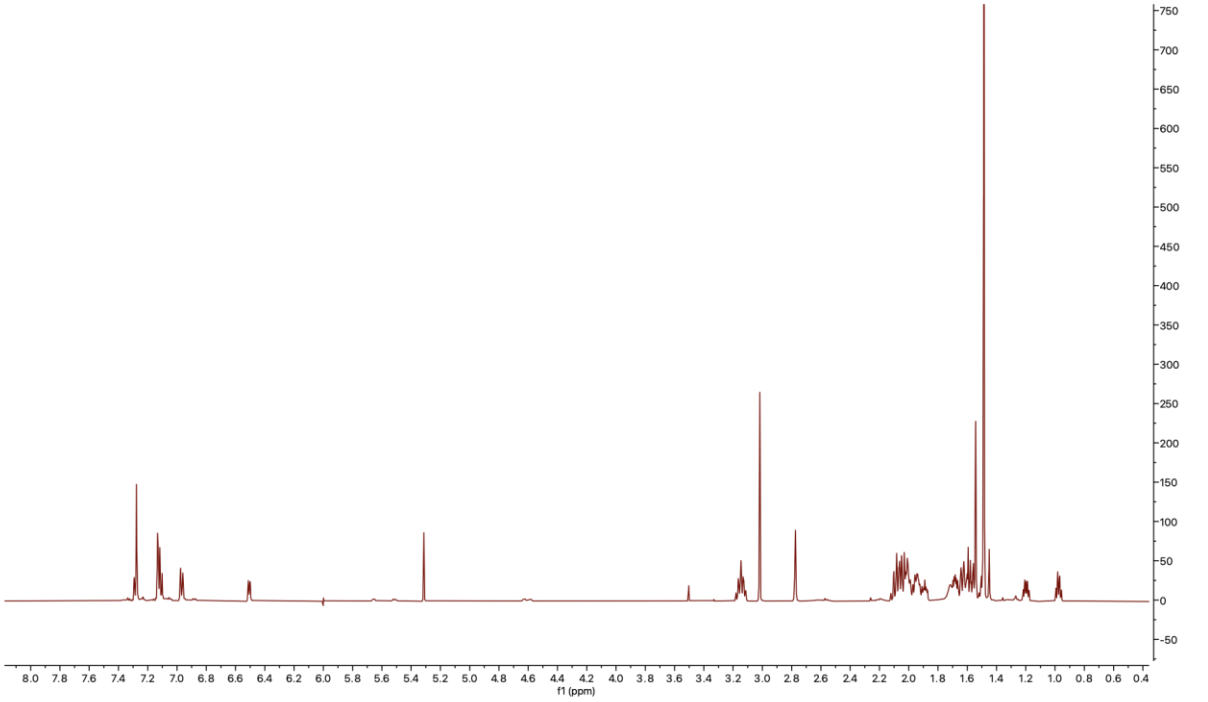
750
700
650
600
550
500
450
400
350
300
250
200
150
100
50
0
-50
8.0 7.8 7.6 7.4 7.2 7.0 6.8 6.6 6.4 6.2 6.0 5.8 5.6 5.4 5.2 5.0 4.8 4.6 4.4 4.2 4.0 3.8 3.6 3.4 3.2 3.0 2.8 2.6 2.4 2.2 2.0 1.8 1.6 1.4 1.2 1.0 0.8 0.6 0.4
f1 (ppm)

T-23

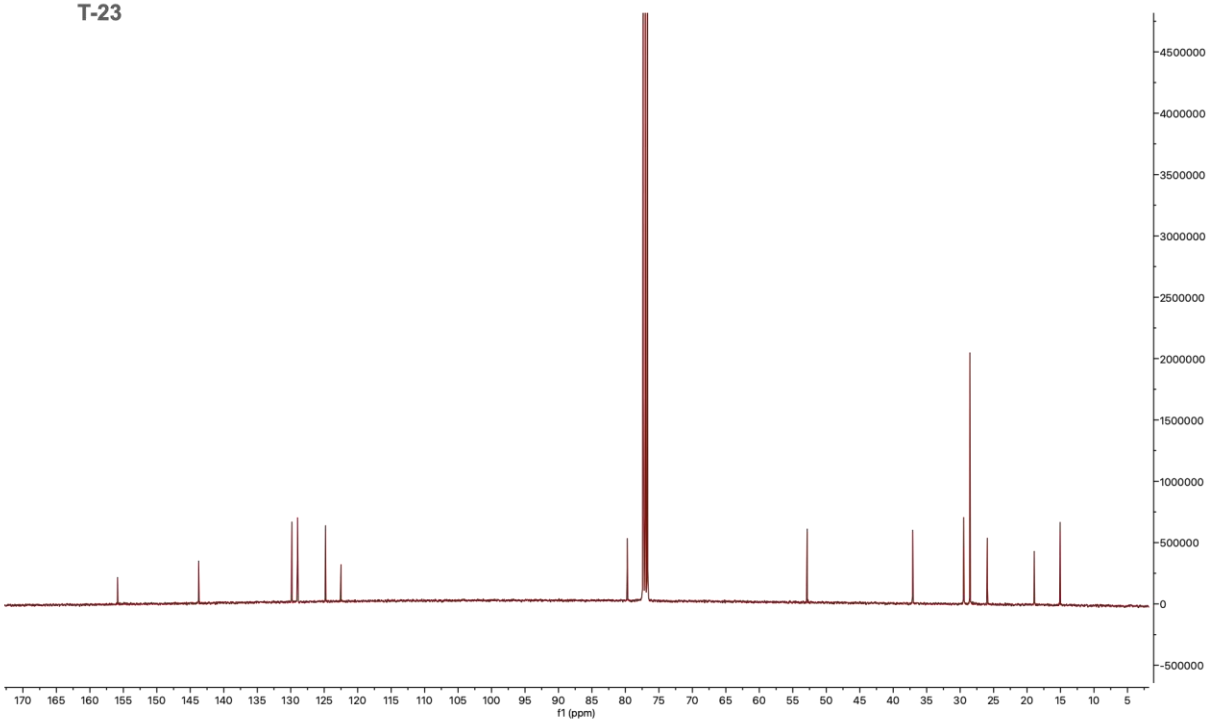
4500000
4000000
3500000
3000000
2500000
2000000
1500000
1000000
500000
0
-500000
170 165 160 155 150 145 140 135 130 125 120 115 110 105 100 95 90 85 80 75 70 65 60 55 50 45 40 35 30 25 20 15 10 5
f1 (ppm)

T-24

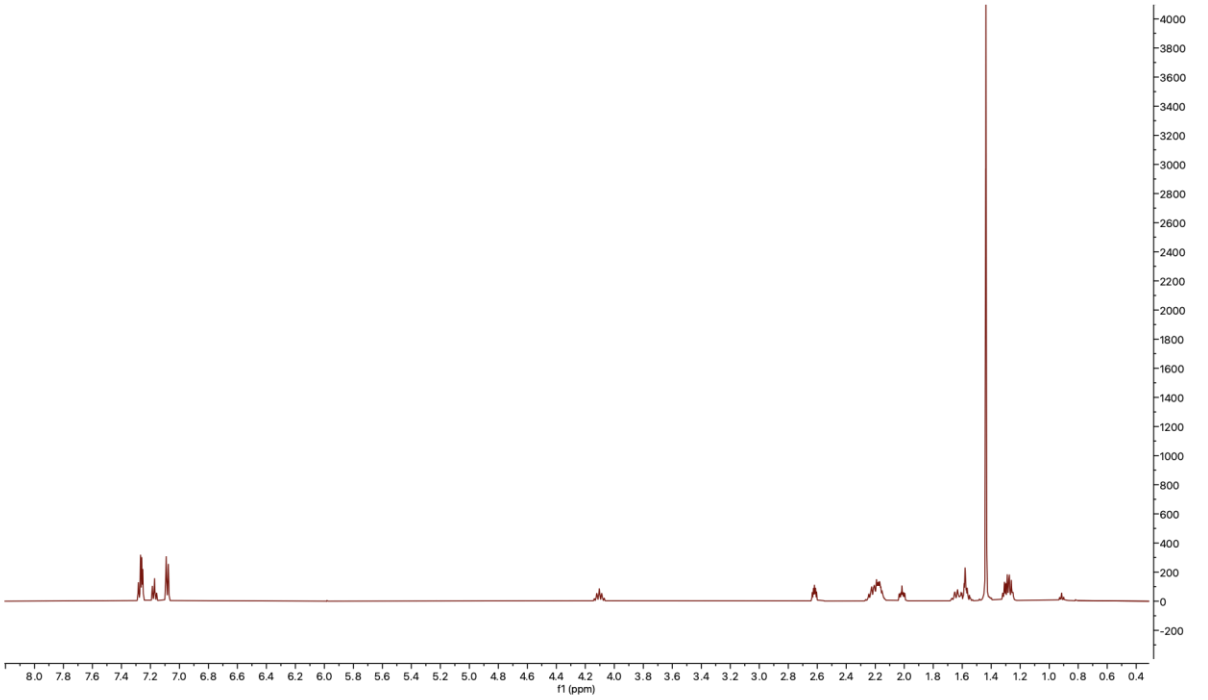
4000
3800
3600
3400
3200
3000
2800
2600
2400
2200
2000
1800
1600
1400
1200
1000
800
600
400
200
0
-200
8.0 7.8 7.6 7.4 7.2 7.0 6.8 6.6 6.4 6.2 6.0 5.8 5.6 5.4 5.2 5.0 4.8 4.6 4.4 4.2 4.0 3.8 3.6 3.4 3.2 3.0 2.8 2.6 2.4 2.2 2.0 1.8 1.6 1.4 1.2 1.0 0.8 0.6 0.4
f1 (ppm)

T-24

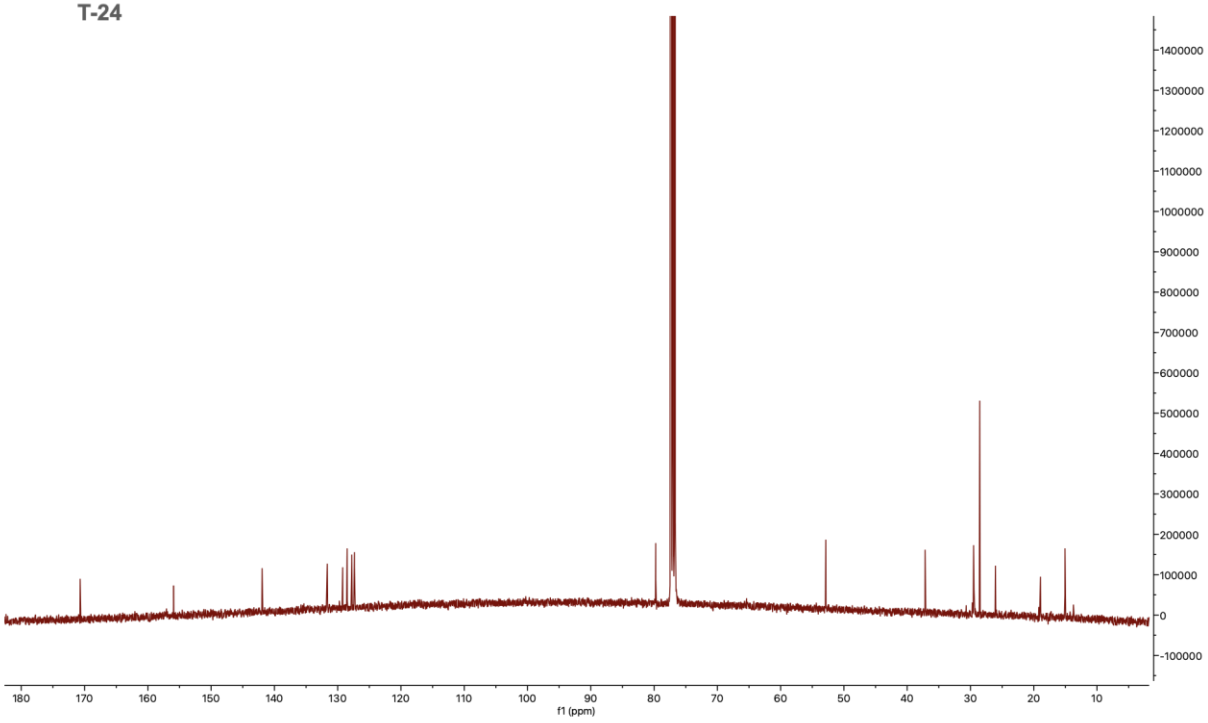
1400000
1300000
1200000
1100000
1000000
900000
800000
700000
600000
500000
400000
300000
200000
100000
0
-100000
180 170 160 150 140 130 120 110 100 90 80 70 60 50 40 30 20 10
f1 (ppm)

T-5

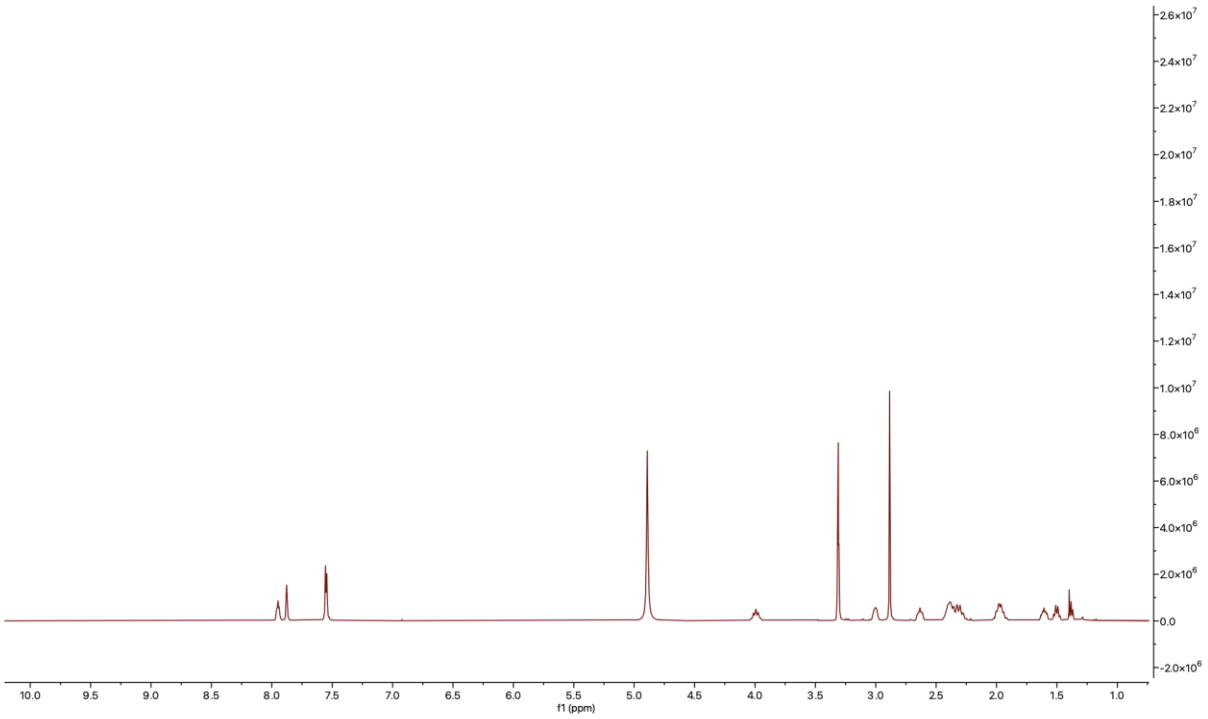
2.6×10^7
2.4×10^7
2.2×10^7
2.0×10^7
1.8×10^7
1.6×10^7
1.4×10^7
1.2×10^7
1.0×10^7
8.0×10^6
6.0×10^6
4.0×10^6
2.0×10^6
0.0
-2.0×10^6
10.0 9.5 9.0 8.5 8.0 7.5 7.0 6.5 6.0 5.5 5.0 4.5 4.0 3.5 3.0 2.5 2.0 1.5 1.0
f1 (ppm)

T-5

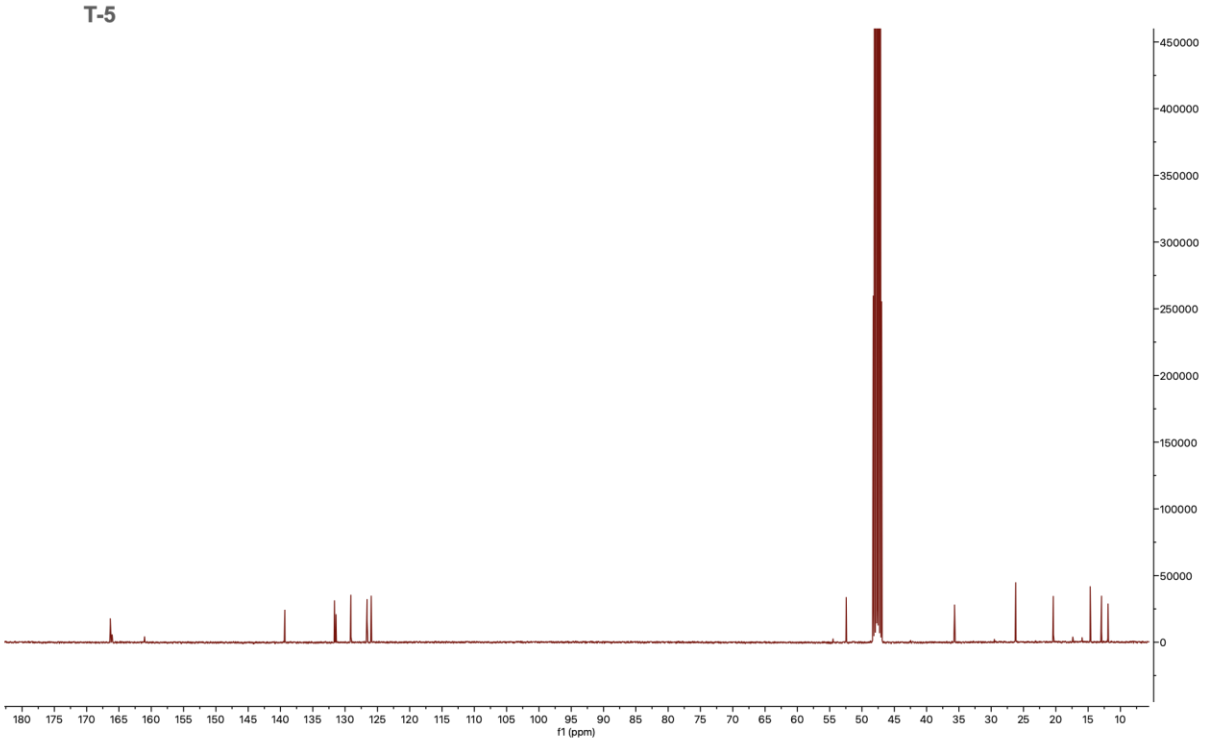
450000
400000
350000
300000
250000
200000
150000
100000
50000
0
180 175 170 165 160 155 150 145 140 135 130 125 120 115 110 105 100 95 90 85 80 75 70 65 60 55 50 45 40 35 30 25 20 15 10
f1 (ppm)

T-25

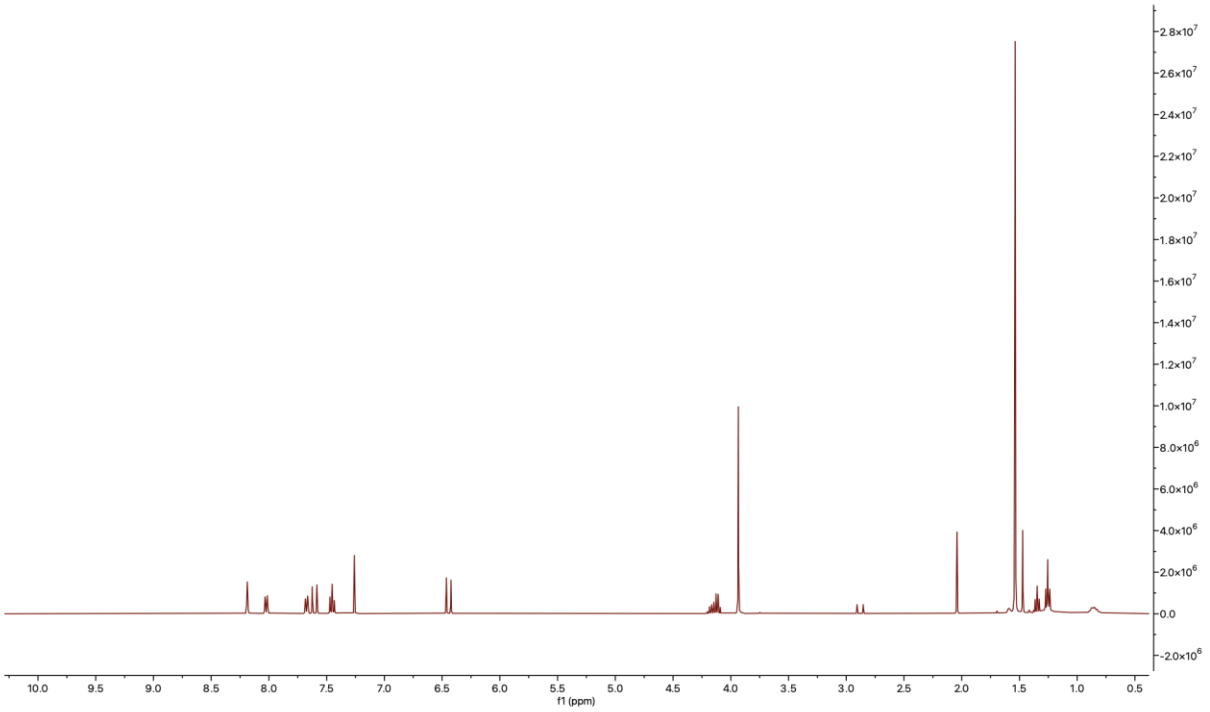
2.8x10^7
2.6x10^7
2.4x10^7
2.2x10^7
2.0x10^7
1.8x10^7
1.6x10^7
1.4x10^7
1.2x10^7
1.0x10^7
8.0x10^6
6.0x10^6
4.0x10^6
2.0x10^6
0.0
-2.0x10^6
10.0 9.5 9.0 8.5 8.0 7.5 7.0 6.5 6.0 5.5 5.0 4.5 4.0 3.5 3.0 2.5 2.0 1.5 1.0 0.5
f1 (ppm)

T-26

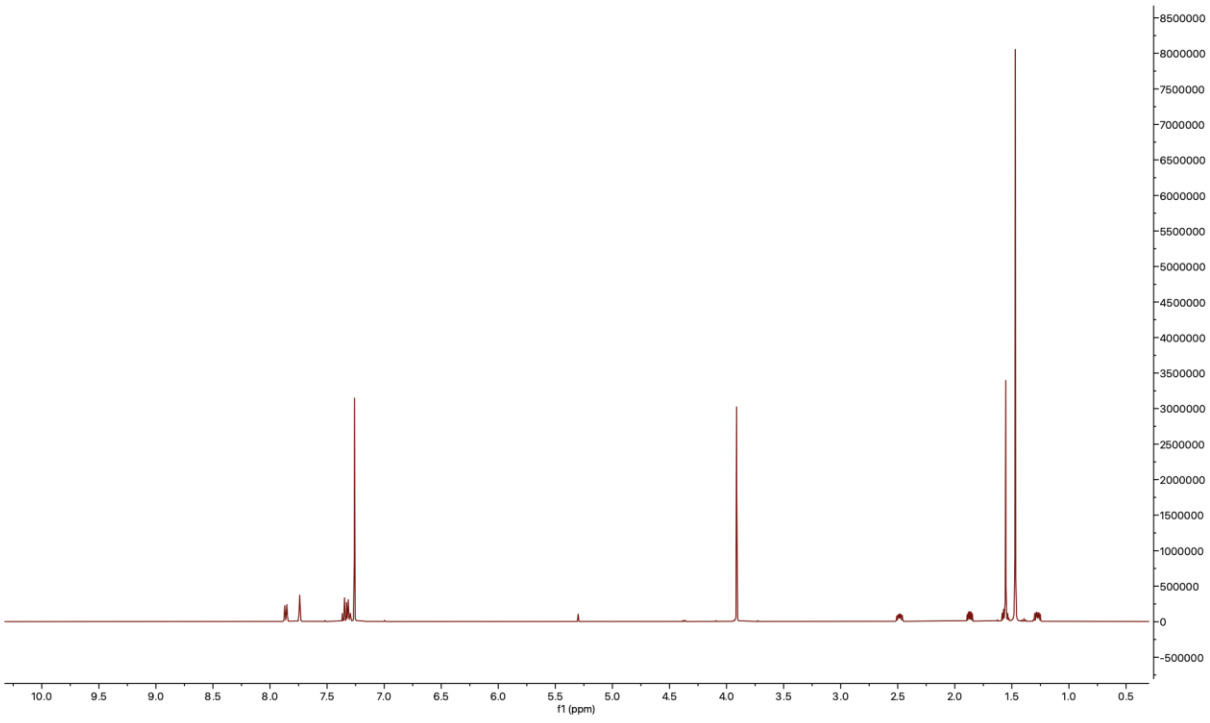
8500000
8000000
7500000
7000000
6500000
6000000
5500000
5000000
4500000
4000000
3500000
3000000
2500000
2000000
1500000
1000000
500000
0
-500000
10.0 9.5 9.0 8.5 8.0 7.5 7.0 6.5 6.0 5.5 5.0 4.5 4.0 3.5 3.0 2.5 2.0 1.5 1.0 0.5
f1 (ppm)

T-27

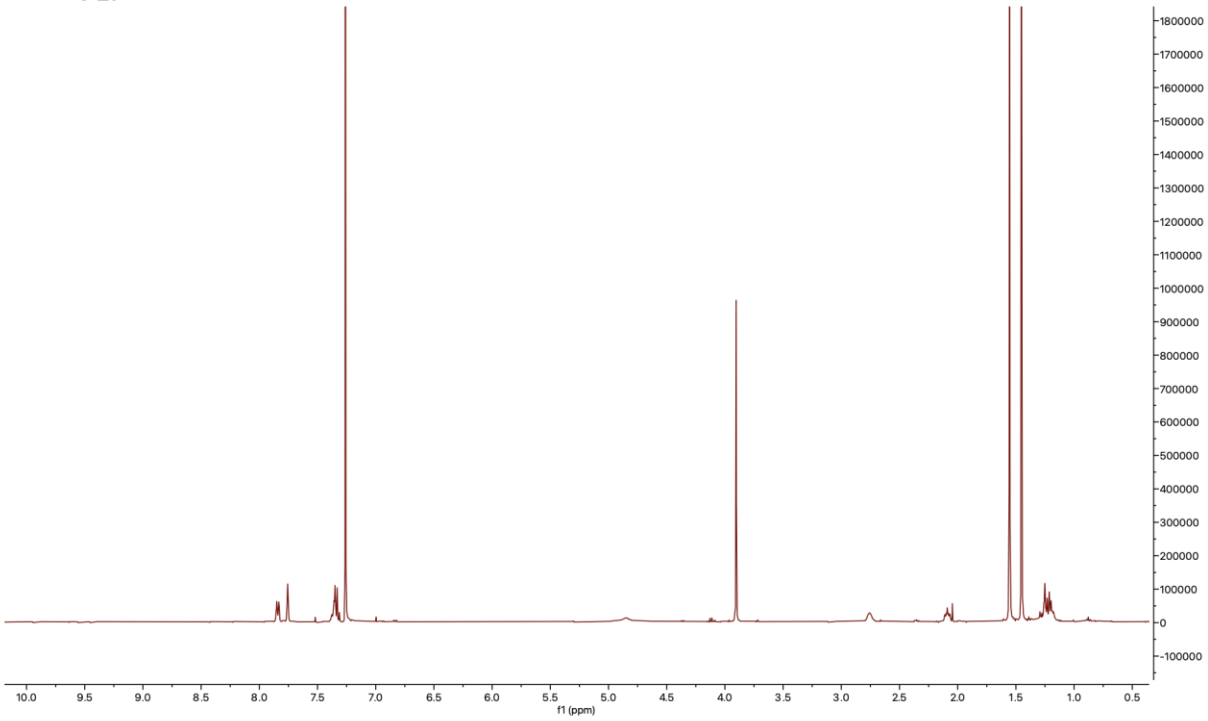
1800000
1700000
1600000
1500000
1400000
1300000
1200000
1100000
1000000
900000
800000
700000
600000
500000
400000
300000
200000
100000
0
-100000
10.0 9.5 9.0 8.5 8.0 7.5 7.0 6.5 6.0 5.5 5.0 4.5 4.0 3.5 3.0 2.5 2.0 1.5 1.0 0.5
f1 (ppm)

T-28

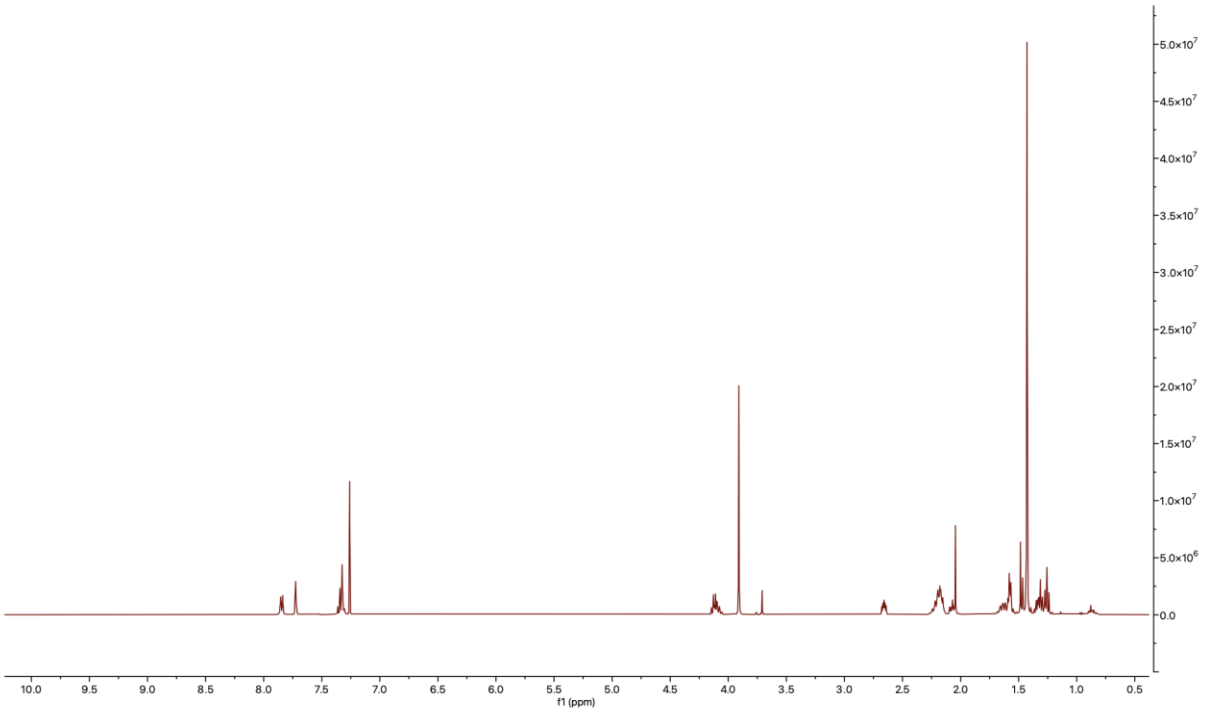
5.0×10^7
4.5×10^7
4.0×10^7
3.5×10^7
3.0×10^7
2.5×10^7
2.0×10^7
1.5×10^7
1.0×10^7
5.0×10^6
0.0
10.0 9.5 9.0 8.5 8.0 7.5 7.0 6.5 6.0 5.5 5.0 4.5 4.0 3.5 3.0 2.5 2.0 1.5 1.0 0.5
f1 (ppm)

T-29

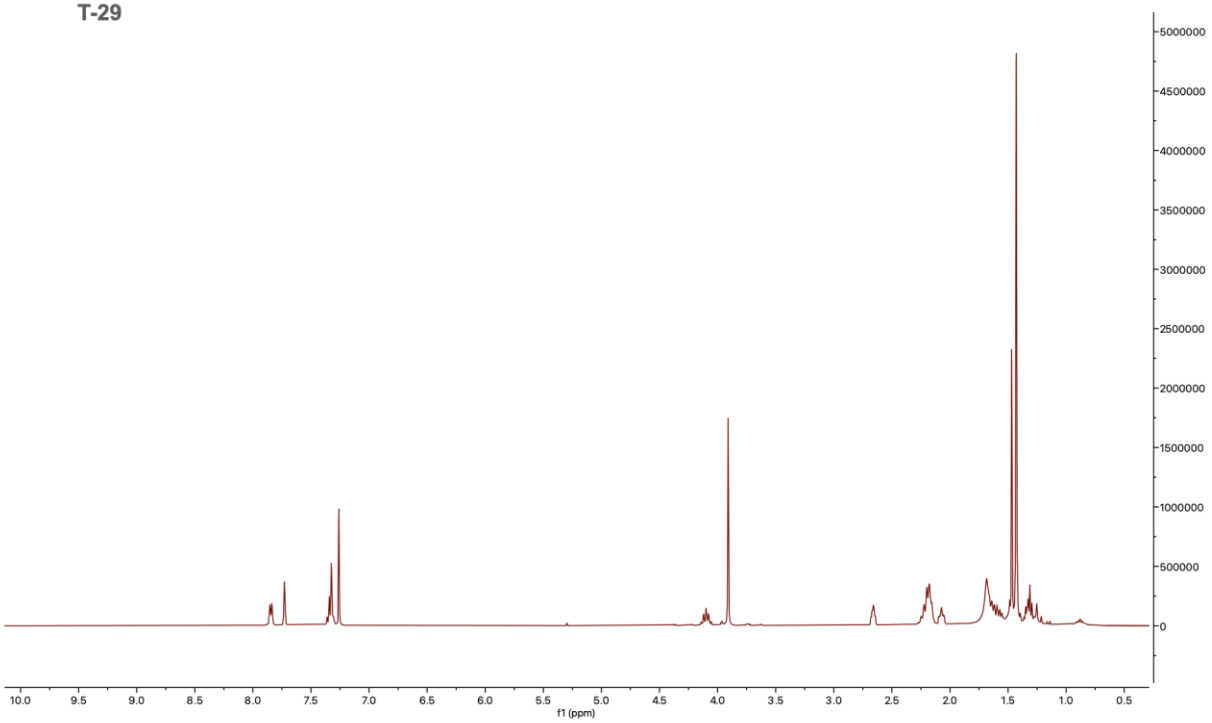
5000000
4500000
4000000
3500000
3000000
2500000
2000000
1500000
1000000
500000
0
10.0 9.5 9.0 8.5 8.0 7.5 7.0 6.5 6.0 5.5 5.0 4.5 4.0 3.5 3.0 2.5 2.0 1.5 1.0 0.5
f1 (ppm)

T-29

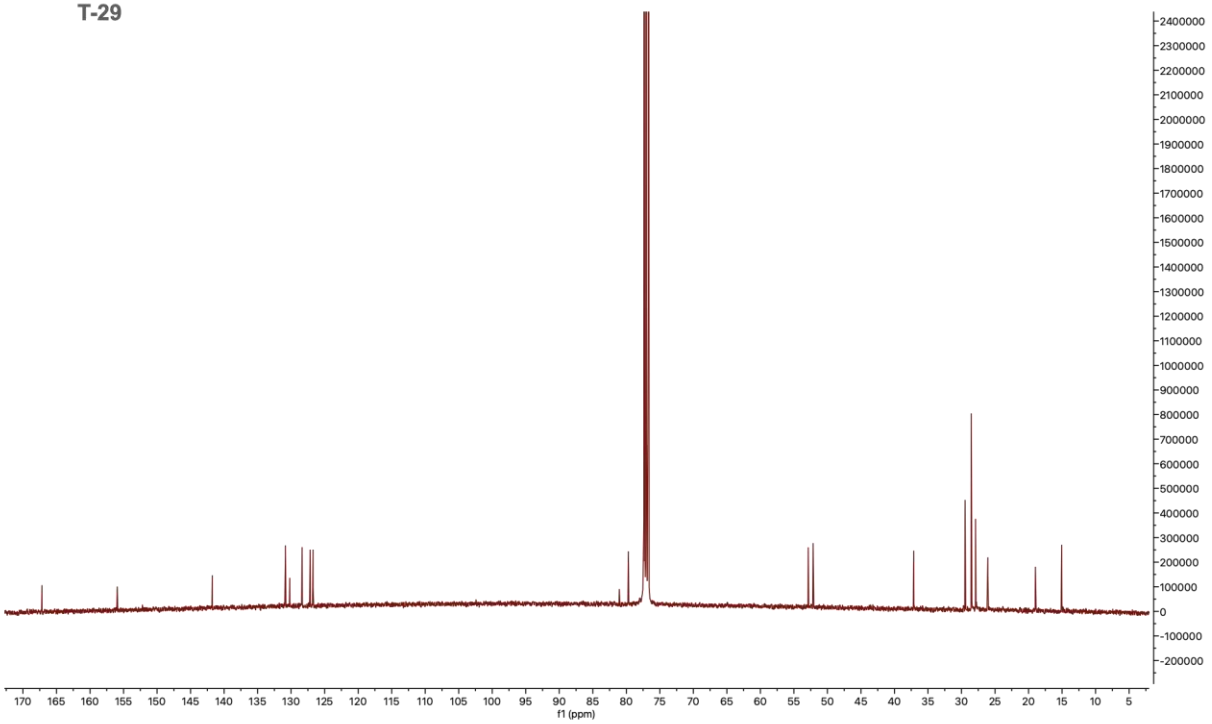
2400000
2300000
2200000
2100000
2000000
1900000
1800000
1700000
1600000
1500000
1400000
1300000
1200000
1100000
1000000
900000
800000
700000
600000
500000
400000
300000
200000
100000
0
-100000
-200000
170 165 160 155 150 145 140 135 130 125 120 115 110 105 100 95 90 85 80 75 70 65 60 55 50 45 40 35 30 25 20 15 10 5
f1 (ppm)

2-*d*-T-448

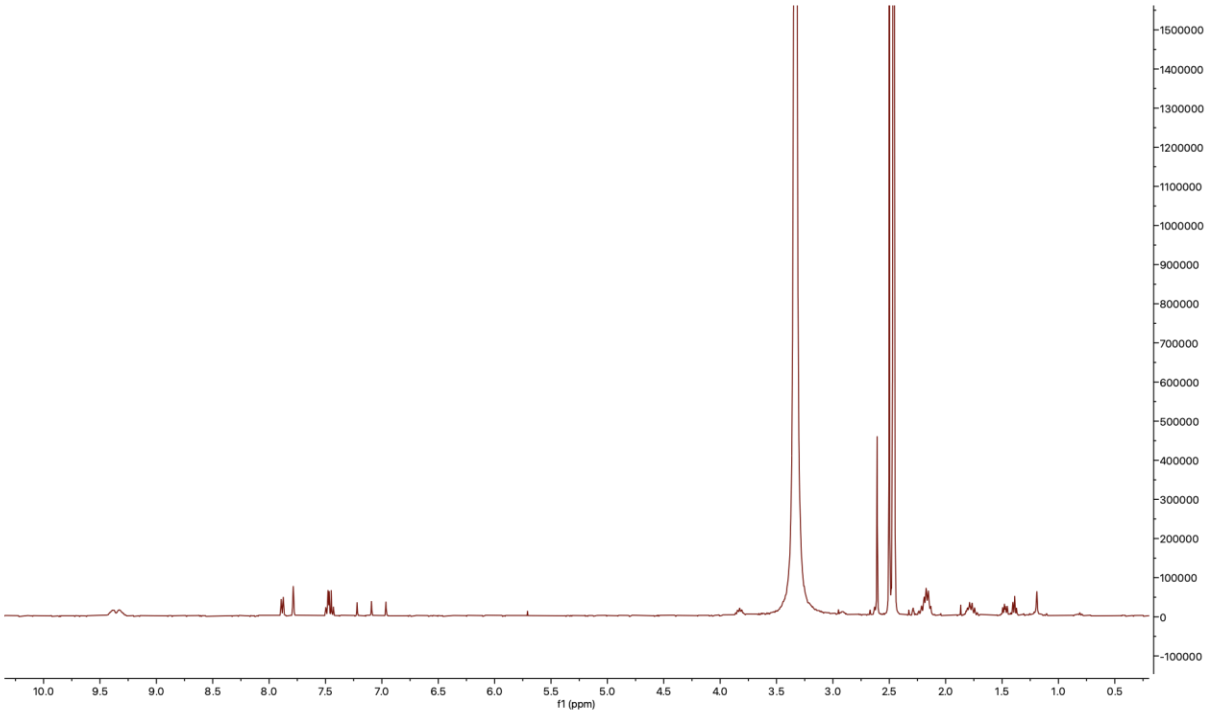

1-*d*-T-448

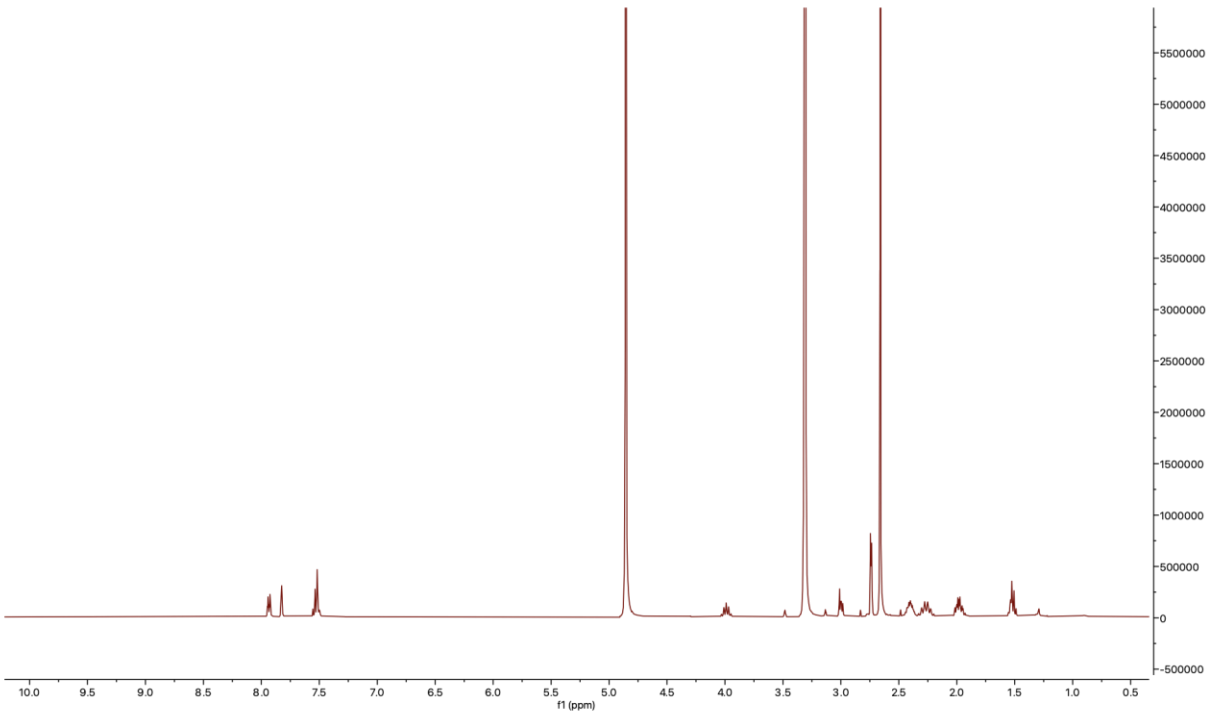

T-6

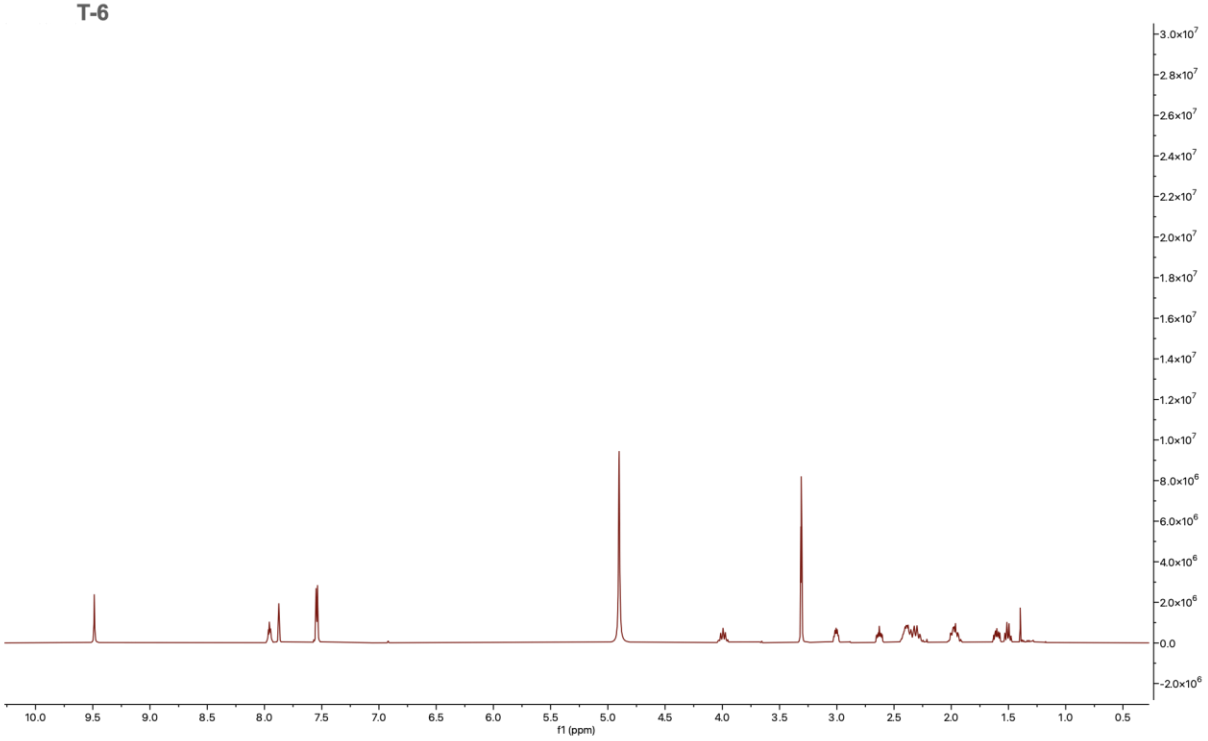
3.0×10^7
2.8×10^7
2.6×10^7
2.4×10^7
2.2×10^7
2.0×10^7
1.8×10^7
1.6×10^7
1.4×10^7
1.2×10^7
1.0×10^7
8.0×10^6
6.0×10^6
4.0×10^6
2.0×10^6
0.0
-2.0×10^6
10.0 9.5 9.0 8.5 8.0 7.5 7.0 6.5 6.0 5.5 5.0 4.5 4.0 3.5 3.0 2.5 2.0 1.5 1.0 0.5
f1 (ppm)

T-6

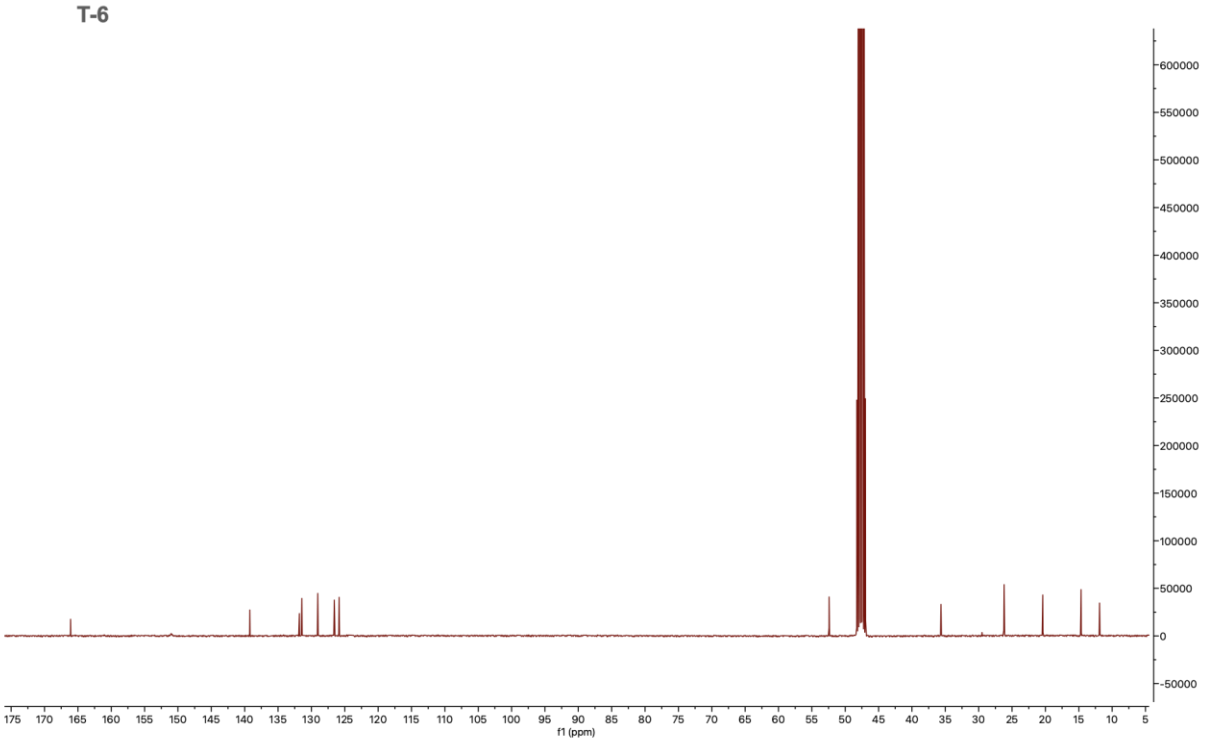
600000
550000
500000
450000
400000
350000
300000
250000
200000
150000
100000
50000
0
-50000
175 170 165 160 155 150 145 140 135 130 125 120 115 110 105 100 95 90 85 80 75 70 65 60 55 50 45 40 35 30 25 20 15 10 5
f1 (ppm)

T-7

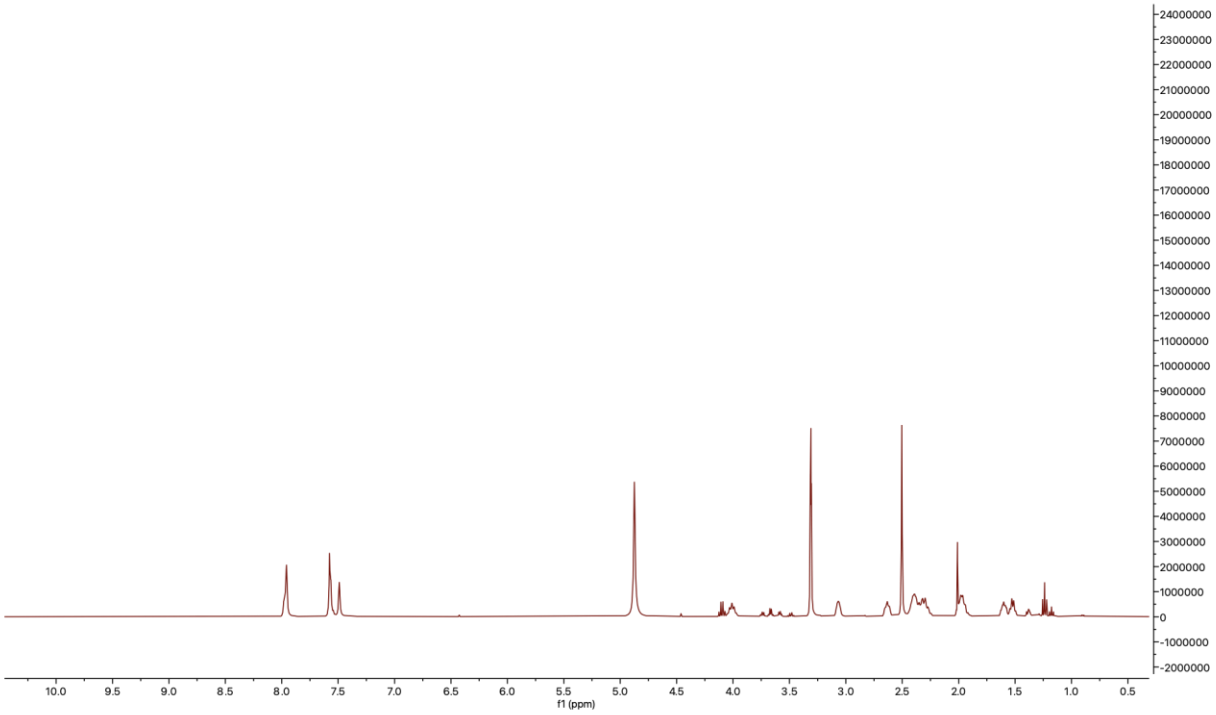
24000000
23000000
22000000
21000000
20000000
19000000
18000000
17000000
16000000
15000000
14000000
13000000
12000000
11000000
10000000
9000000
8000000
7000000
6000000
5000000
4000000
3000000
2000000
1000000
0
-1000000
-2000000
10.0 9.5 9.0 8.5 8.0 7.5 7.0 6.5 6.0 5.5 5.0 4.5 4.0 3.5 3.0 2.5 2.0 1.5 1.0 0.5
f1 (ppm)

T-7

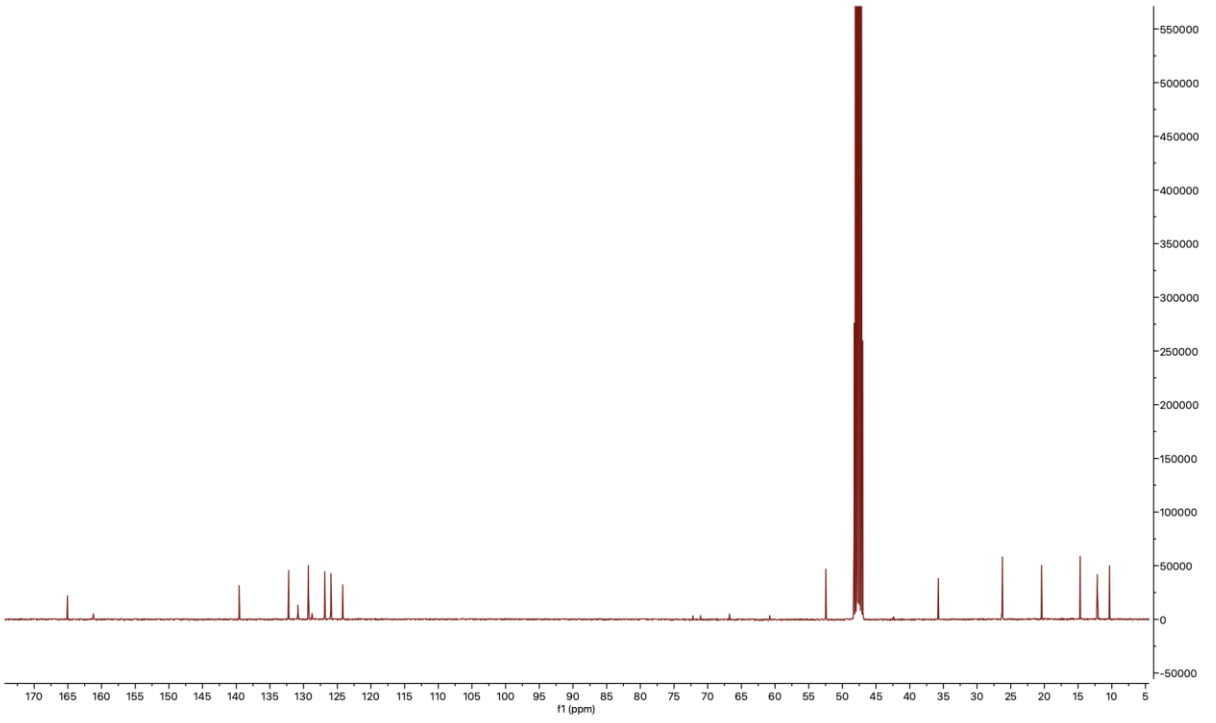
550000
500000
450000
400000
350000
300000
250000
200000
150000
100000
50000
0
-50000
170 165 160 155 150 145 140 135 130 125 120 115 110 105 100 95 90 85 80 75 70 65 60 55 50 45 40 35 30 25 20 15 10 5
f1 (ppm)

T-8

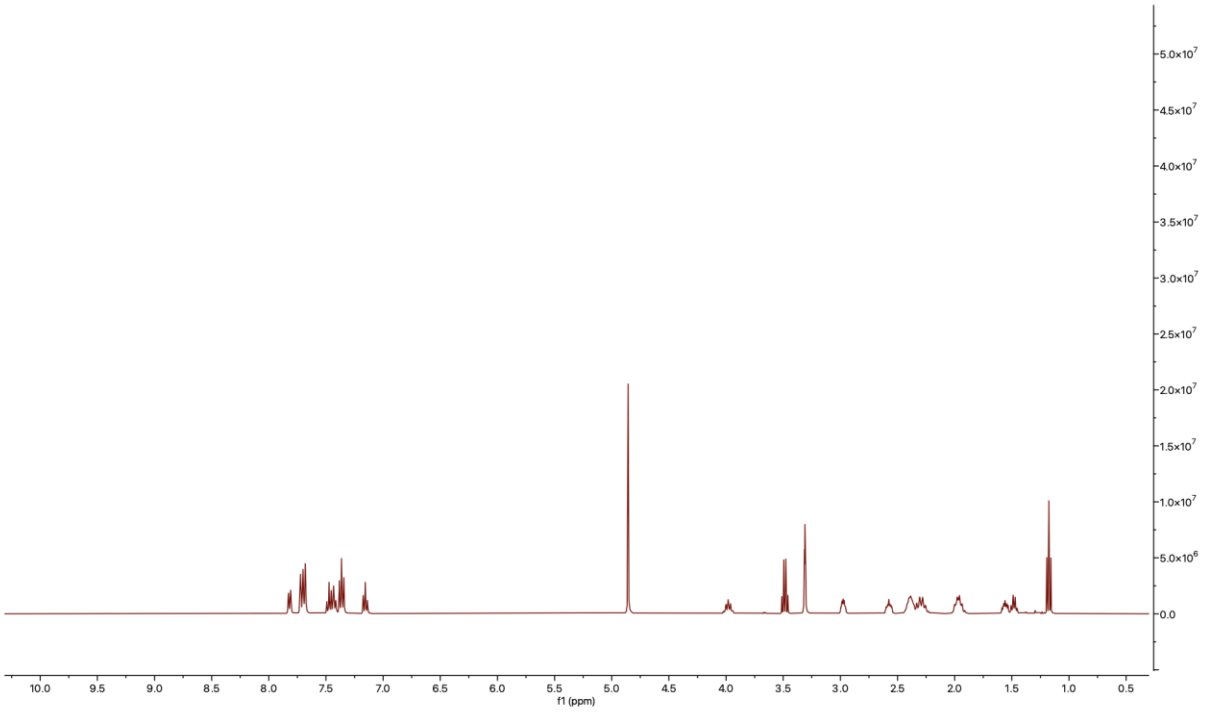
5.0×10^7
4.5×10^7
4.0×10^7
3.5×10^7
3.0×10^7
2.5×10^7
2.0×10^7
1.5×10^7
1.0×10^7
5.0×10^6
0.0
10.0 9.5 9.0 8.5 8.0 7.5 7.0 6.5 6.0 5.5 5.0 4.5 4.0 3.5 3.0 2.5 2.0 1.5 1.0 0.5
f1 (ppm)

T-30

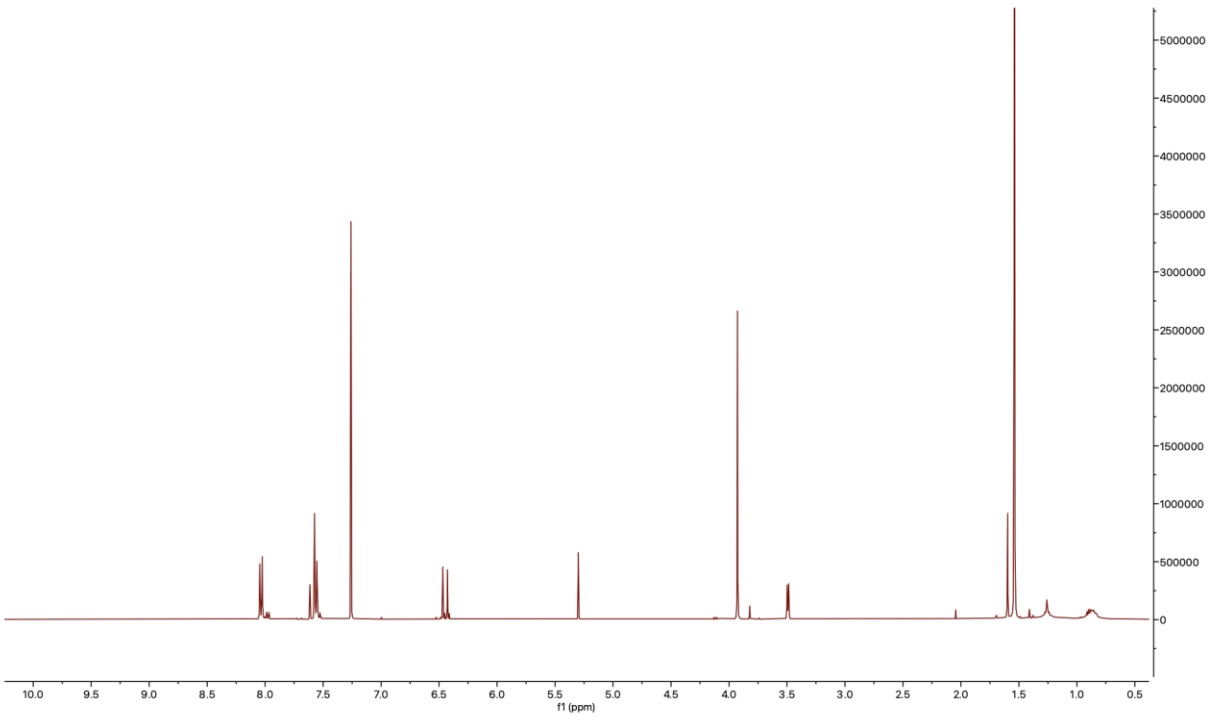
5000000
4500000
4000000
3500000
3000000
2500000
2000000
1500000
1000000
500000
0
10.0 9.5 9.0 8.5 8.0 7.5 7.0 6.5 6.0 5.5 5.0 4.5 4.0 3.5 3.0 2.5 2.0 1.5 1.0 0.5
f1 (ppm)

T-31

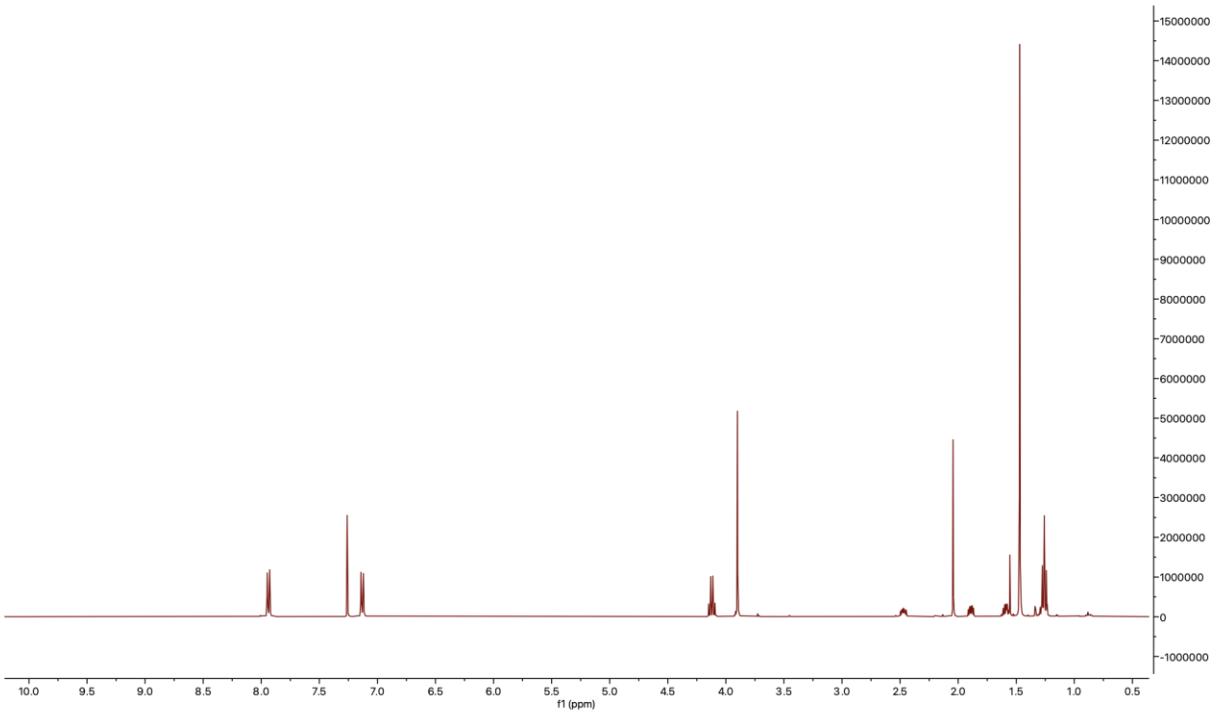
15000000
14000000
13000000
12000000
11000000
10000000
9000000
8000000
7000000
6000000
5000000
4000000
3000000
2000000
1000000
0
-1000000
10.0 9.5 9.0 8.5 8.0 7.5 7.0 6.5 6.0 5.5 5.0 4.5 4.0 3.5 3.0 2.5 2.0 1.5 1.0 0.5
f1 (ppm)

T-32

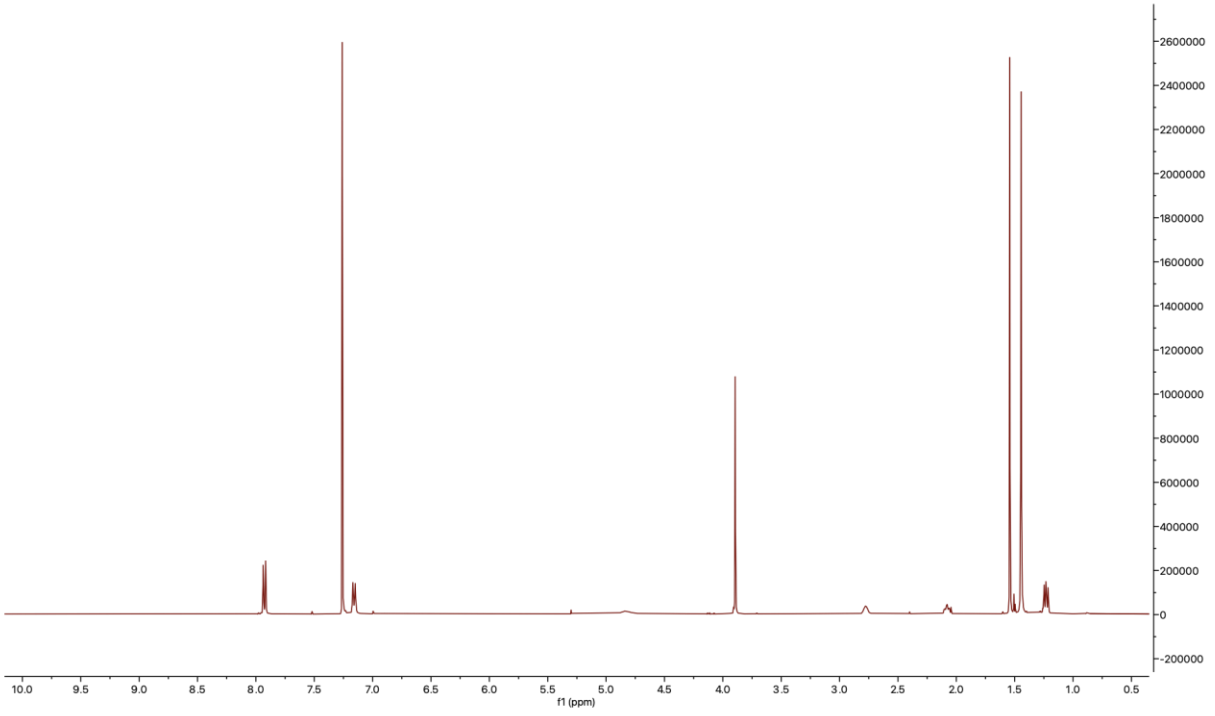
2600000
2400000
2200000
2000000
1800000
1600000
1400000
1200000
1000000
800000
600000
400000
200000
0
-200000
10.0 9.5 9.0 8.5 8.0 7.5 7.0 6.5 6.0 5.5 5.0 4.5 4.0 3.5 3.0 2.5 2.0 1.5 1.0 0.5
f1 (ppm)

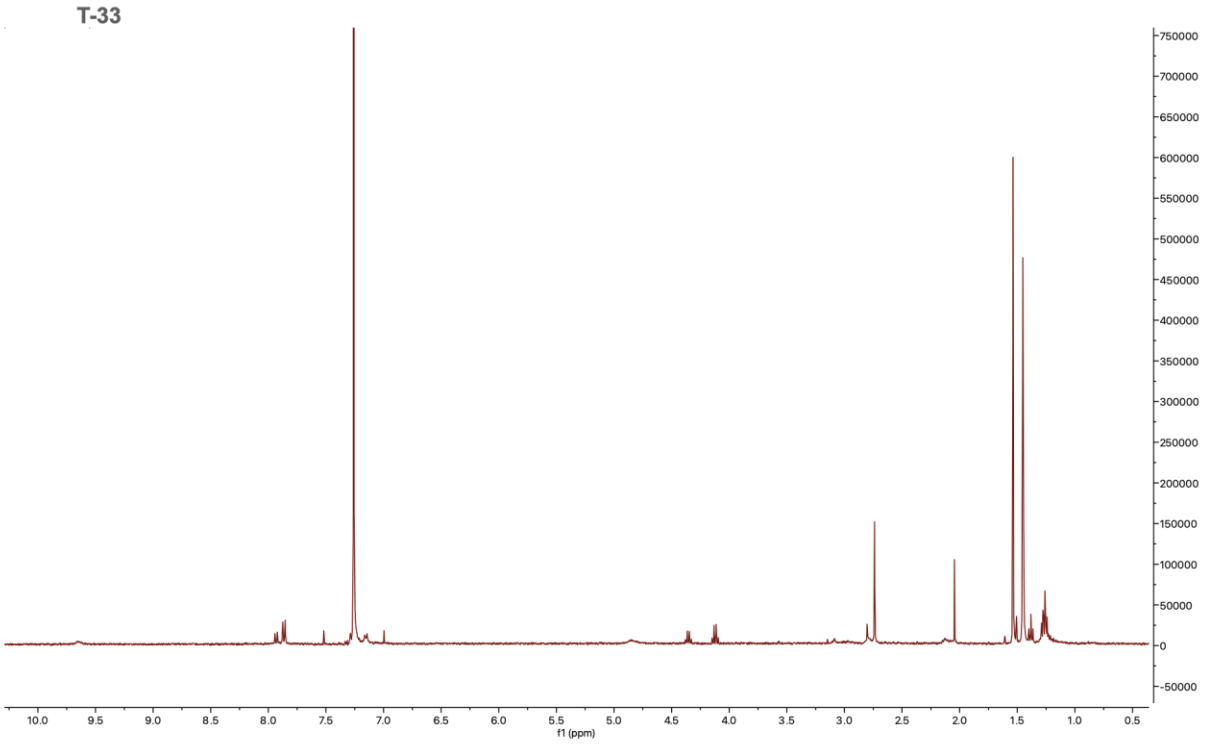
T-33
750000
700000
650000
600000
550000
500000
450000
400000
350000
300000
250000
200000
150000
100000
50000
0
-50000
10.0 9.5 9.0 8.5 8.0 7.5 7.0 6.5 6.0 5.5 5.0 4.5 4.0 3.5 3.0 2.5 2.0 1.5 1.0 0.5
f1 (ppm)

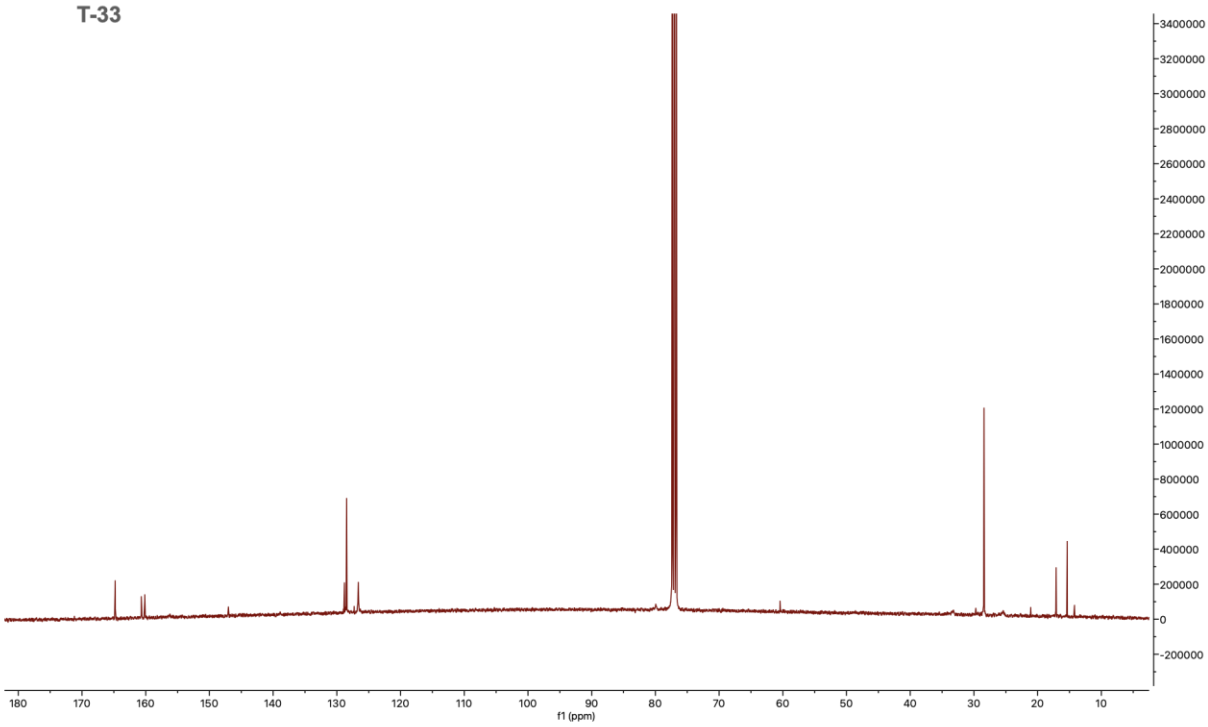
T-33
3400000
3200000
3000000
2800000
2600000
2400000
2200000
2000000
1800000
1600000
1400000
1200000
1000000
800000
600000
400000
200000
0
-200000
180 170 160 150 140 130 120 110 100 90 80 70 60 50 40 30 20 10
f1 (ppm)

T-14

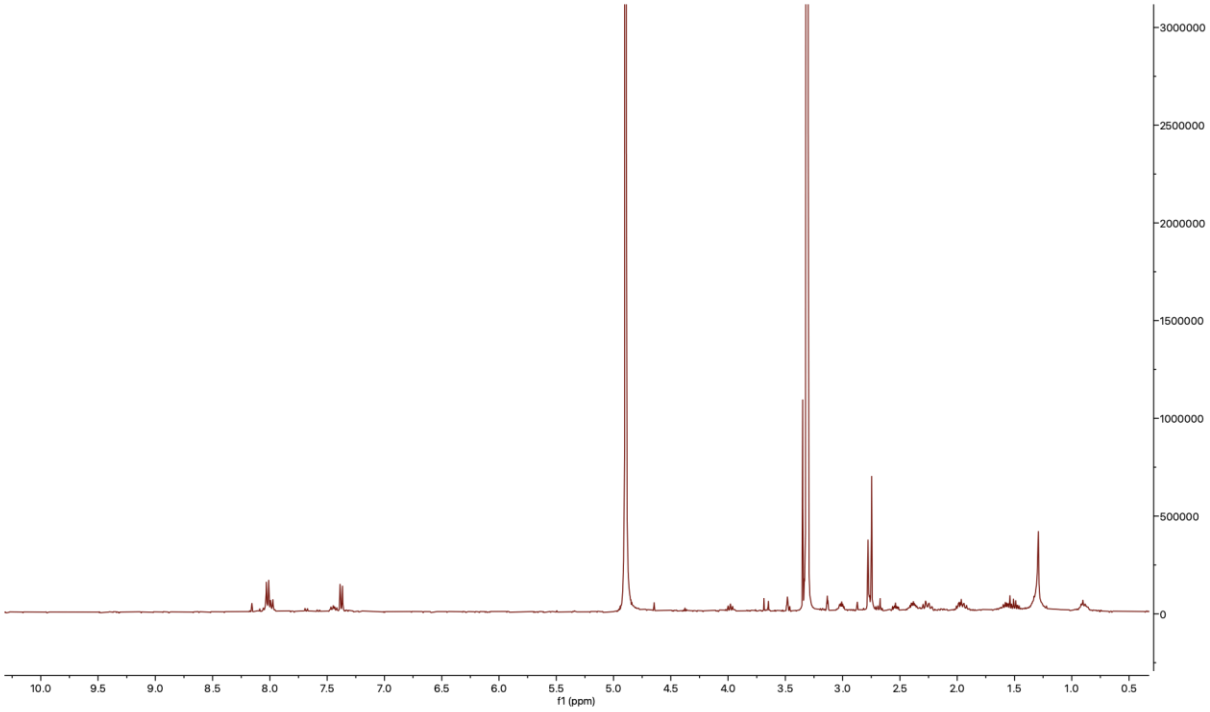
3000000
2500000
2000000
1500000
1000000
500000
0
10.0 9.5 9.0 8.5 8.0 7.5 7.0 6.5 6.0 5.5 5.0 4.5 4.0 3.5 3.0 2.5 2.0 1.5 1.0 0.5
f1 (ppm)

T-15

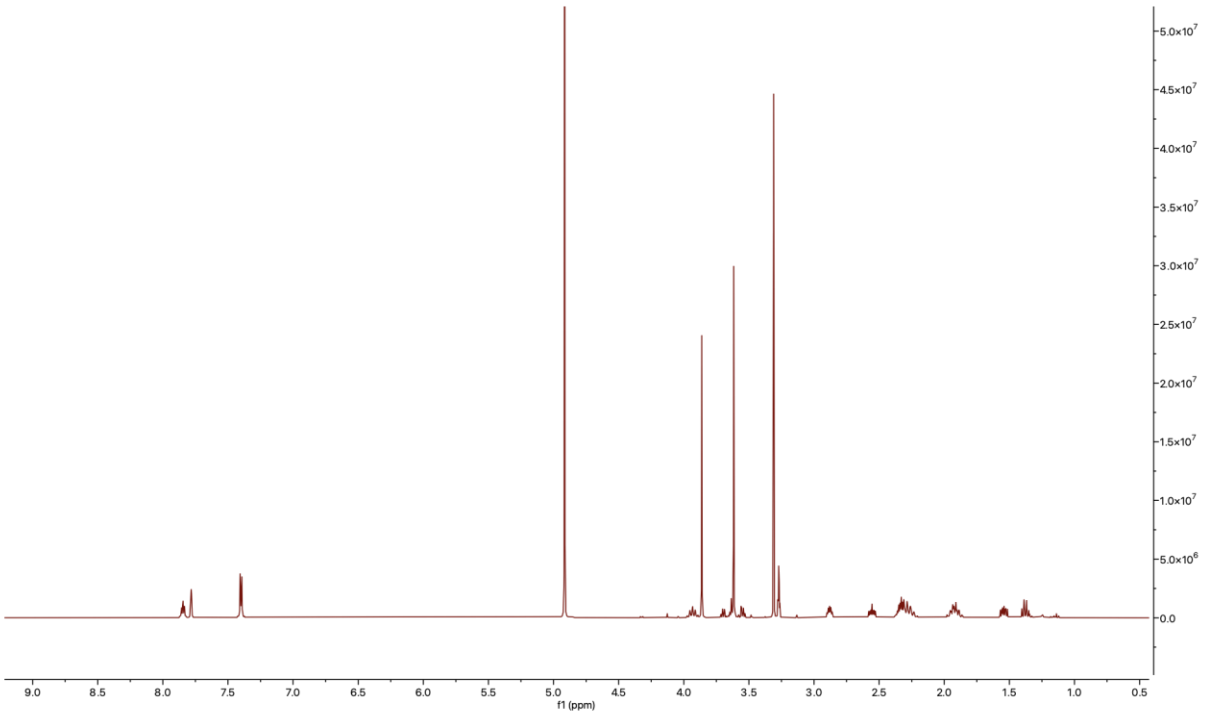
5.0×10^7
4.5×10^7
4.0×10^7
3.5×10^7
3.0×10^7
2.5×10^7
2.0×10^7
1.5×10^7
1.0×10^7
5.0×10^6
0.0
9.0 8.5 8.0 7.5 7.0 6.5 6.0 5.5 5.0 4.5 4.0 3.5 3.0 2.5 2.0 1.5 1.0 0.5
f1 (ppm)

T-15

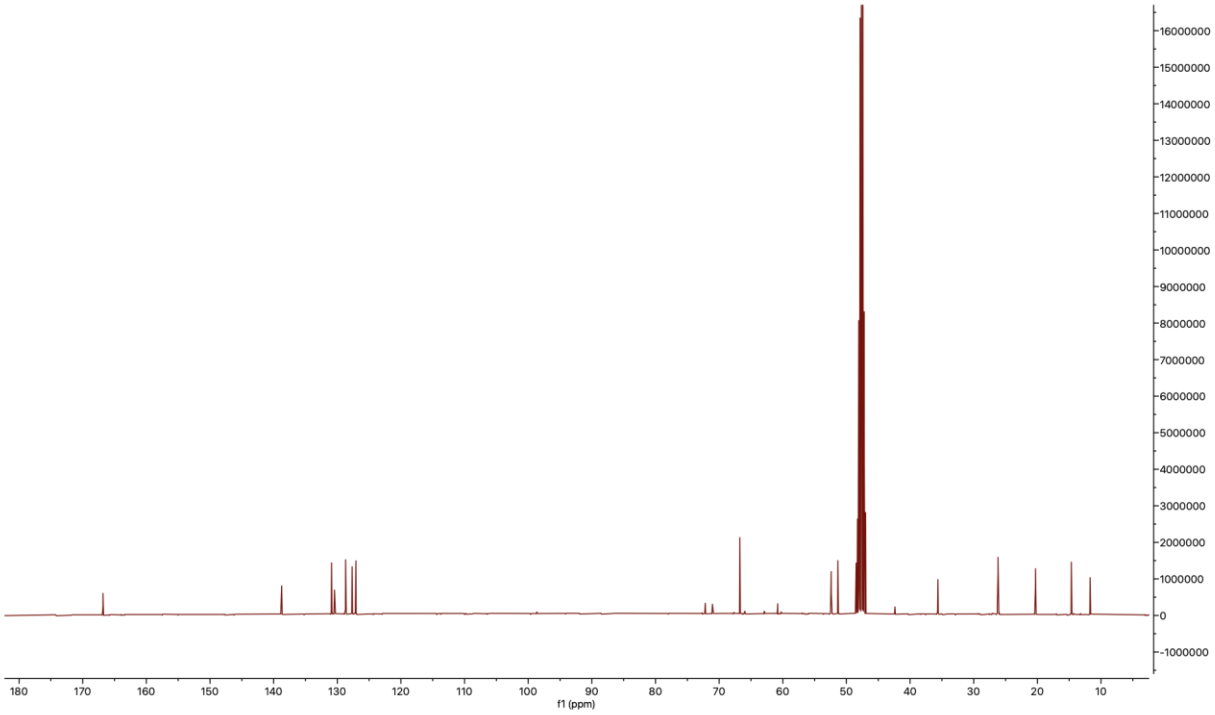
16000000
15000000
14000000
13000000
12000000
11000000
10000000
9000000
8000000
7000000
6000000
5000000
4000000
3000000
2000000
1000000
0
-1000000
180 170 160 150 140 130 120 110 100 90 80 70 60 50 40 30 20 10
f1 (ppm)

T-16

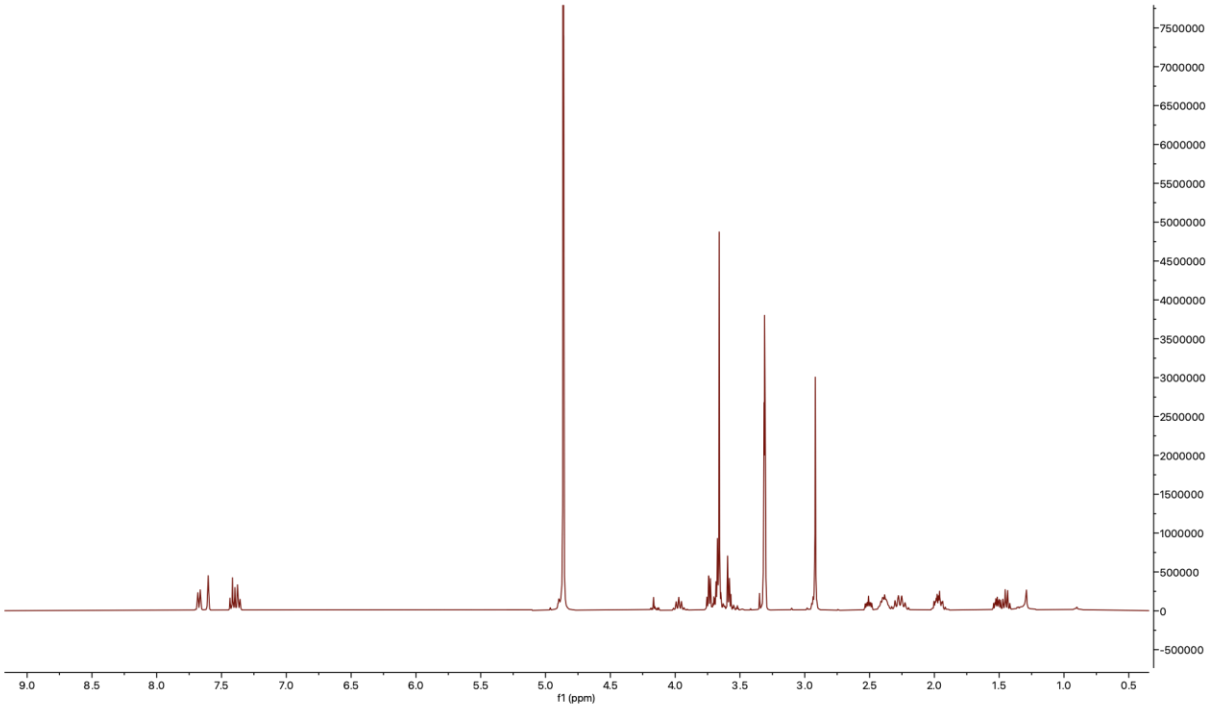
7500000
7000000
6500000
6000000
5500000
5000000
4500000
4000000
3500000
3000000
2500000
2000000
1500000
1000000
500000
0
-500000
9.0 8.5 8.0 7.5 7.0 6.5 6.0 5.5 5.0 4.5 4.0 3.5 3.0 2.5 2.0 1.5 1.0 0.5
f1 (ppm)

T-16

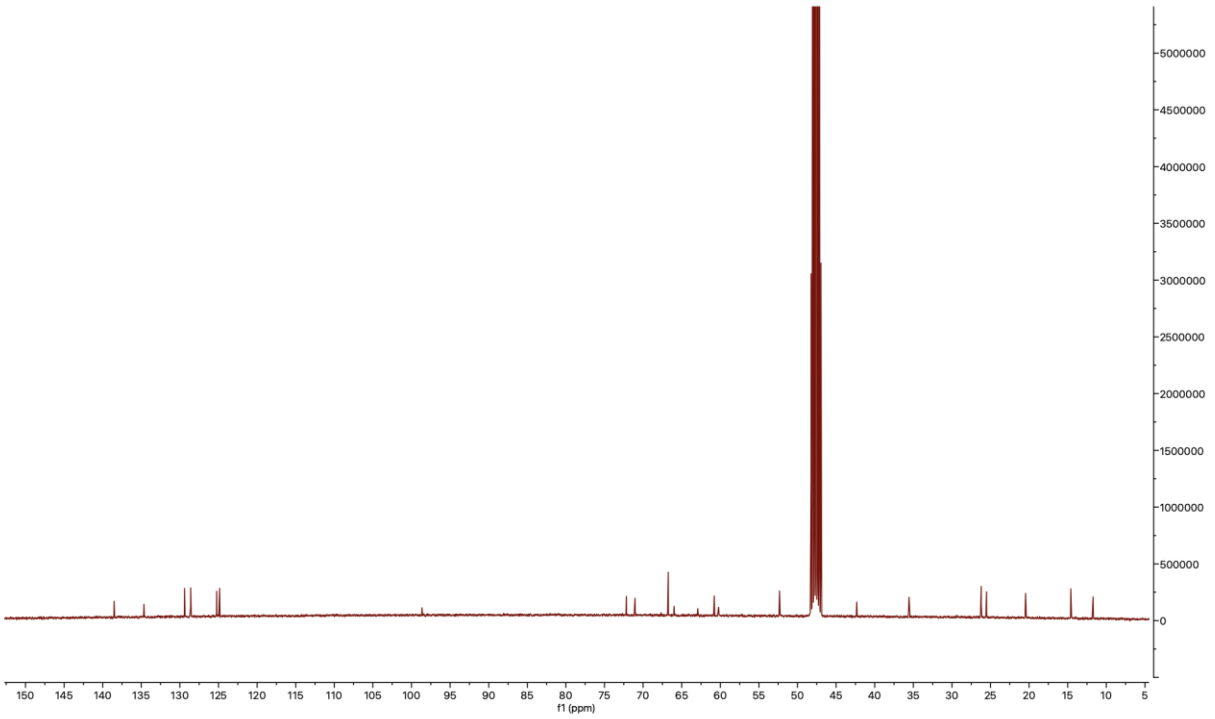
5000000
4500000
4000000
3500000
3000000
2500000
2000000
1500000
1000000
500000
0
150 145 140 135 130 125 120 115 110 105 100 95 90 85 80 75 70 65 60 55 50 45 40 35 30 25 20 15 10 5
f1 (ppm)

T-17

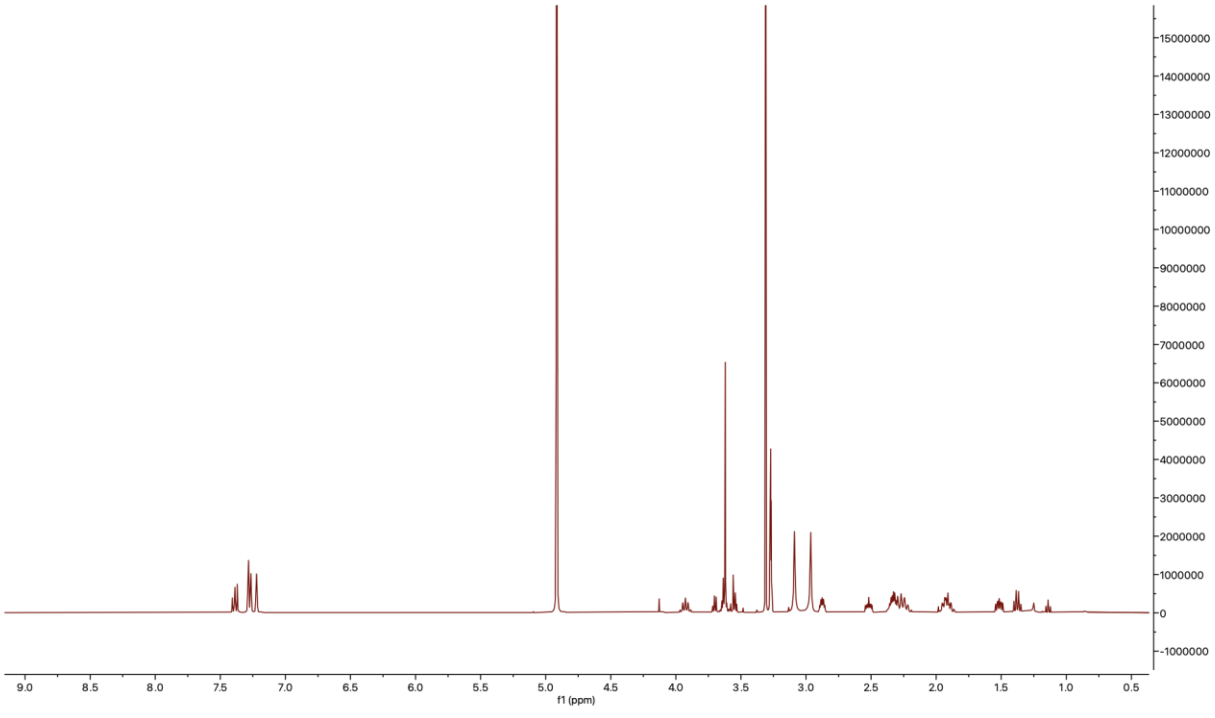
15000000
14000000
13000000
12000000
11000000
10000000
9000000
8000000
7000000
6000000
5000000
4000000
3000000
2000000
1000000
0
-1000000
9.0 8.5 8.0 7.5 7.0 6.5 6.0 5.5 5.0 4.5 4.0 3.5 3.0 2.5 2.0 1.5 1.0 0.5
f1 (ppm)

T-17

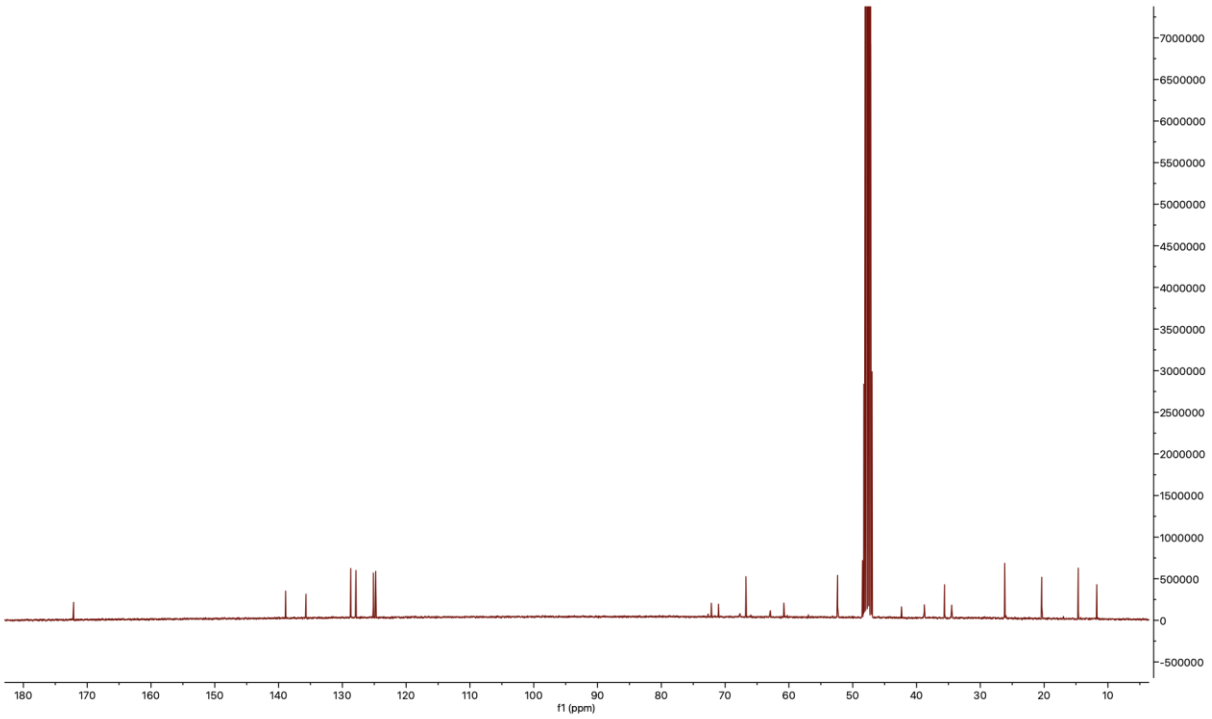
7000000
6500000
6000000
5500000
5000000
4500000
4000000
3500000
3000000
2500000
2000000
1500000
1000000
500000
0
-500000
180
170
160
150
140
130
120
110
100
90
80
70
60
50
40
30
20
10
f1 (ppm)

T-34

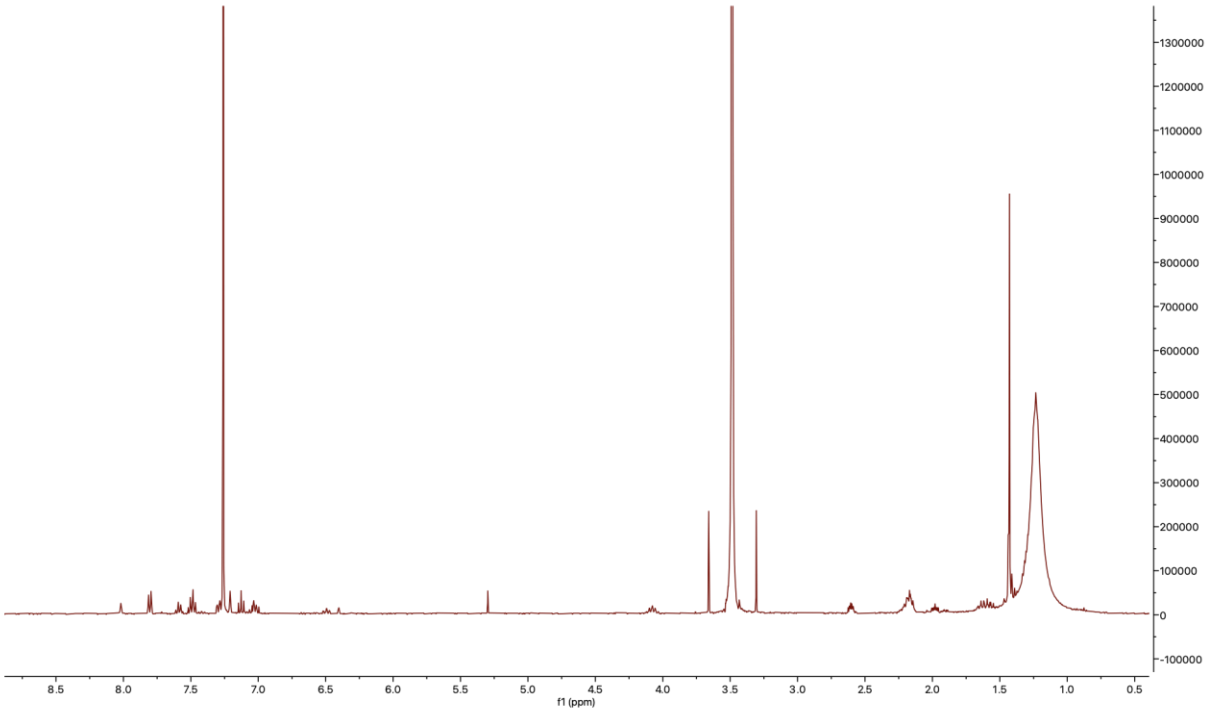
1300000
1200000
1100000
1000000
900000
800000
700000
600000
500000
400000
300000
200000
100000
0
-100000
8.5
8.0
7.5
7.0
6.5
6.0
5.5
5.0
4.5
4.0
3.5
3.0
2.5
2.0
1.5
1.0
0.5
f1 (ppm)

T-18

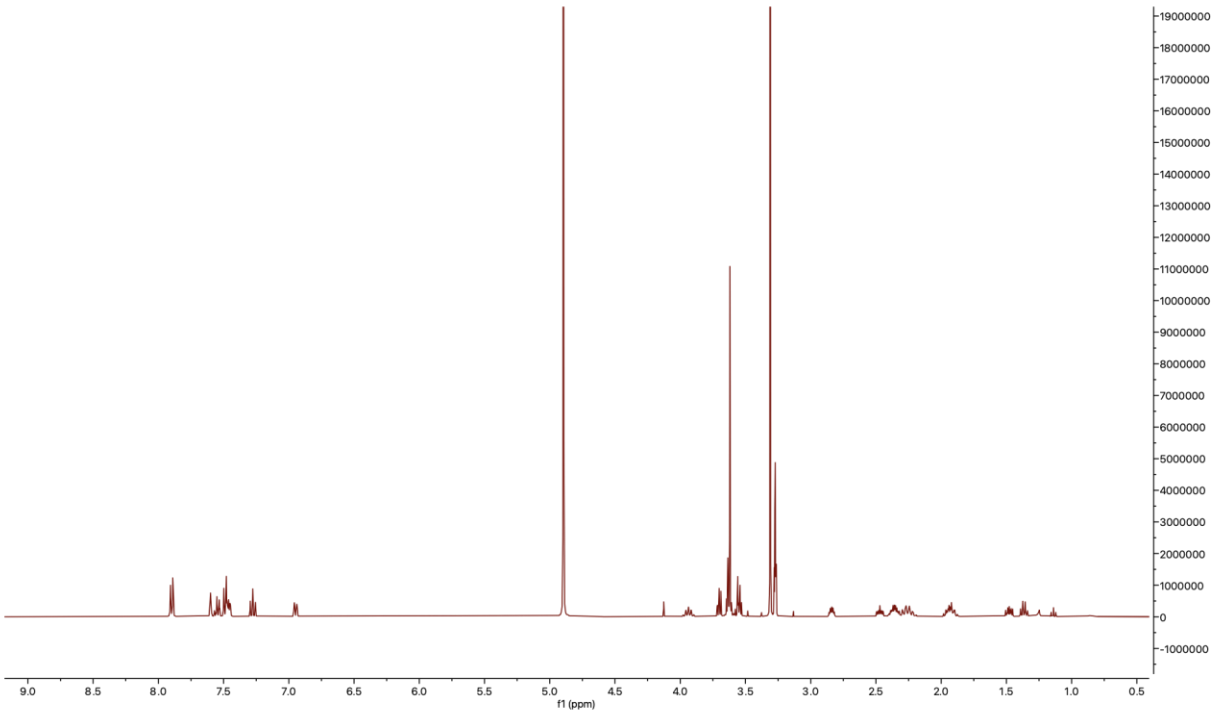
19000000
18000000
17000000
16000000
15000000
14000000
13000000
12000000
11000000
10000000
9000000
8000000
7000000
6000000
5000000
4000000
3000000
2000000
1000000
0
-1000000
9.0 8.5 8.0 7.5 7.0 6.5 6.0 5.5 5.0 4.5 4.0 3.5 3.0 2.5 2.0 1.5 1.0 0.5
f1 (ppm)

T-18

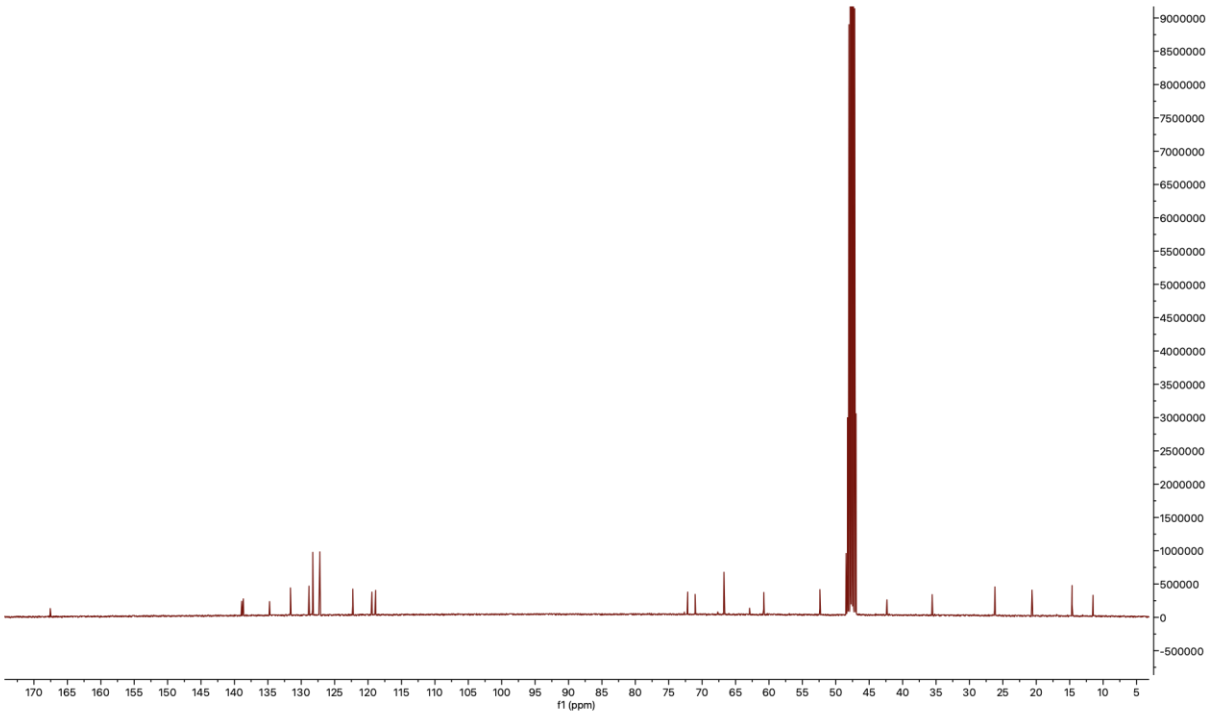
9000000
8500000
8000000
7500000
7000000
6500000
6000000
5500000
5000000
4500000
4000000
3500000
3000000
2500000
2000000
1500000
1000000
500000
0
-500000
170 165 160 155 150 145 140 135 130 125 120 115 110 105 100 95 90 85 80 75 70 65 60 55 50 45 40 35 30 25 20 15 10 5
f1 (ppm)

T-36

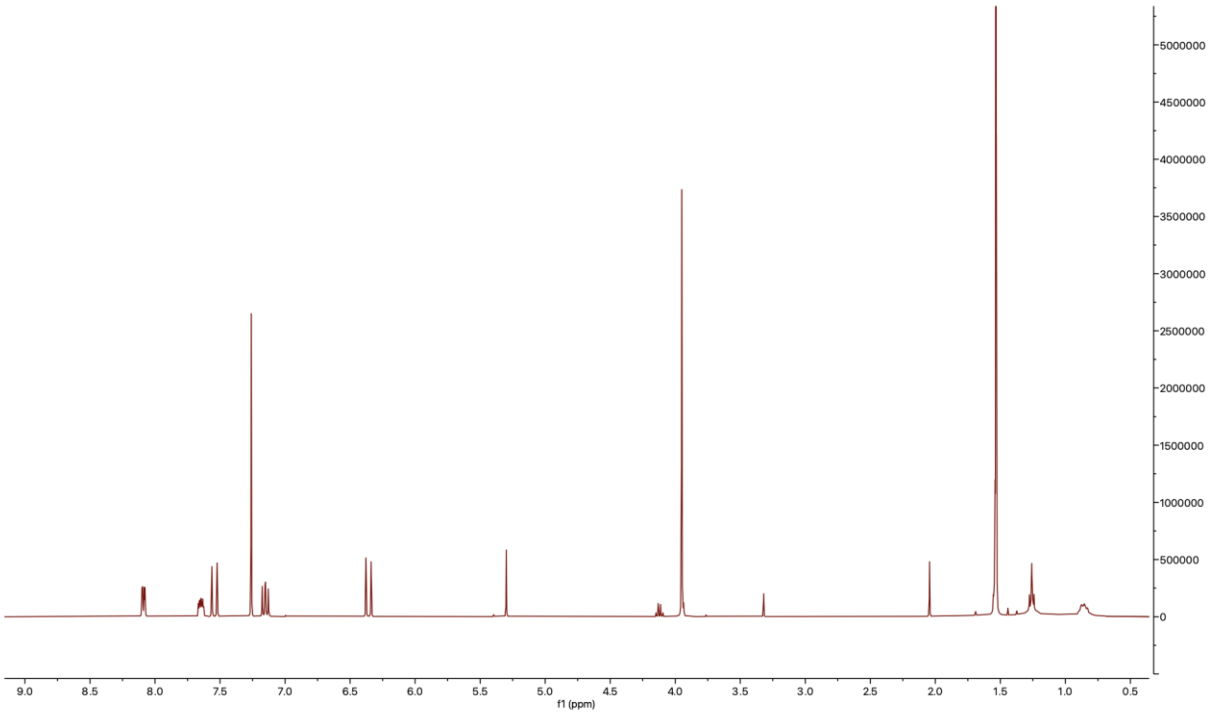
5000000
4500000
4000000
3500000
3000000
2500000
2000000
1500000
1000000
500000
0
9.0
8.5
8.0
7.5
7.0
6.5
6.0
5.5
5.0
4.5
4.0
3.5
3.0
2.5
2.0
1.5
1.0
0.5
f1 (ppm)

T-36

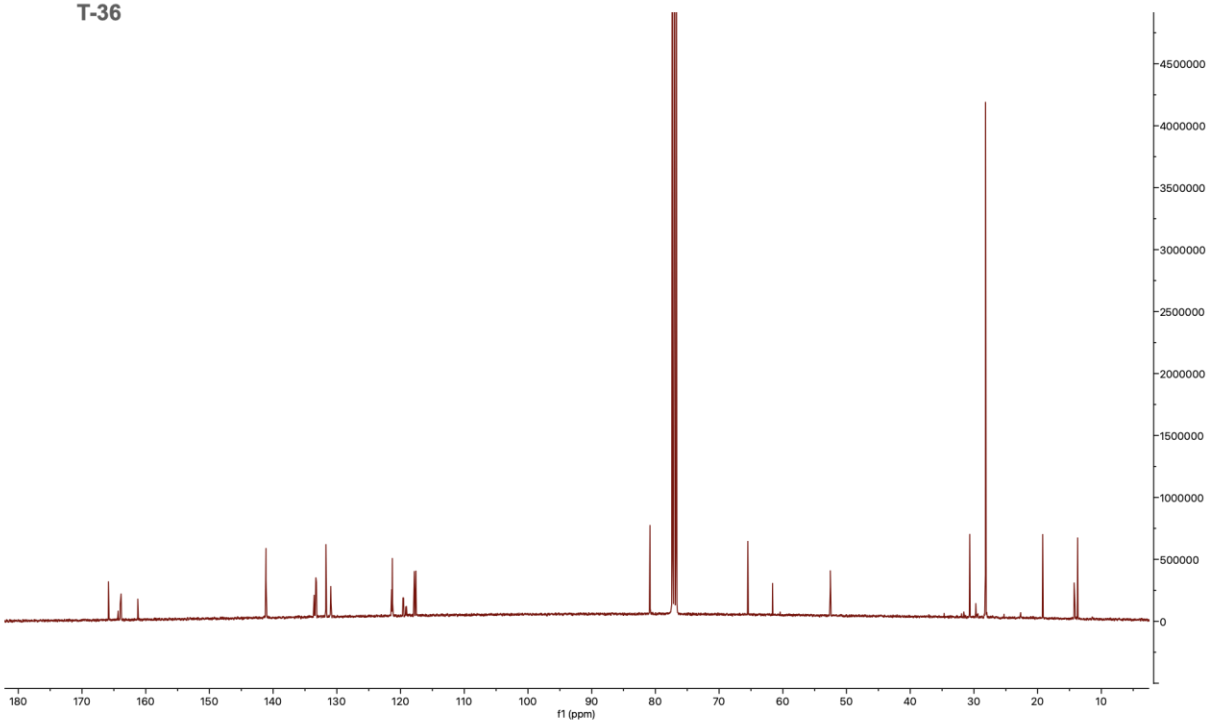
4500000
4000000
3500000
3000000
2500000
2000000
1500000
1000000
500000
0
180
170
160
150
140
130
120
110
100
90
80
70
60
50
40
30
20
10
f1 (ppm)

T-37

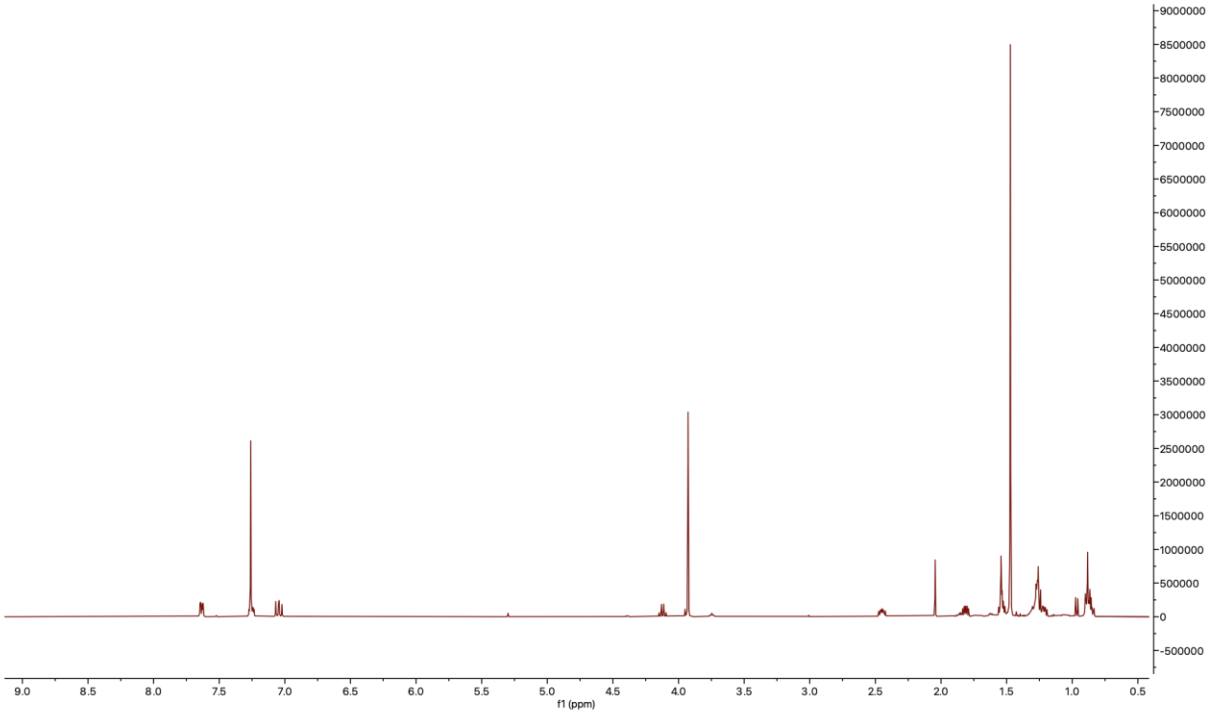
9000000
8500000
8000000
7500000
7000000
6500000
6000000
5500000
5000000
4500000
4000000
3500000
3000000
2500000
2000000
1500000
1000000
500000
0
-500000
9.0
8.5
8.0
7.5
7.0
6.5
6.0
5.5
5.0
4.5
4.0
3.5
3.0
2.5
2.0
1.5
1.0
0.5
f1 (ppm)

T-37

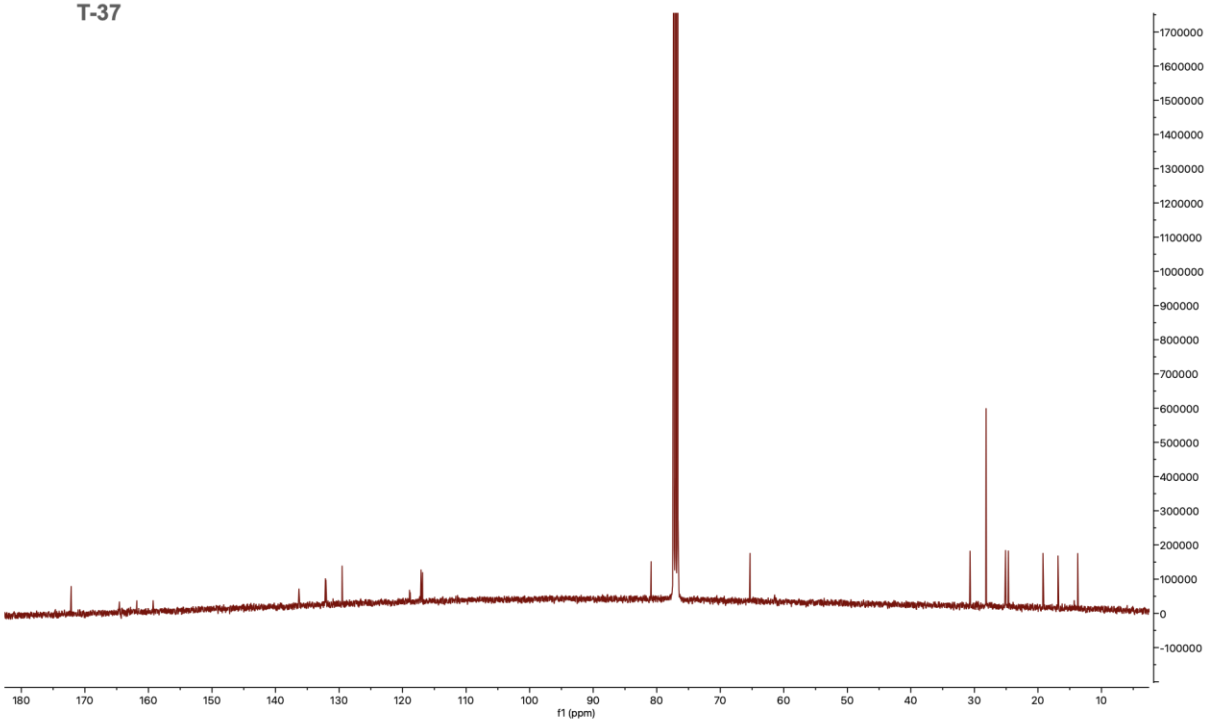
1700000
1600000
1500000
1400000
1300000
1200000
1100000
1000000
900000
800000
700000
600000
500000
400000
300000
200000
100000
0
-100000
180
170
160
150
140
130
120
110
100
90
80
70
60
50
40
30
20
10
f1 (ppm)

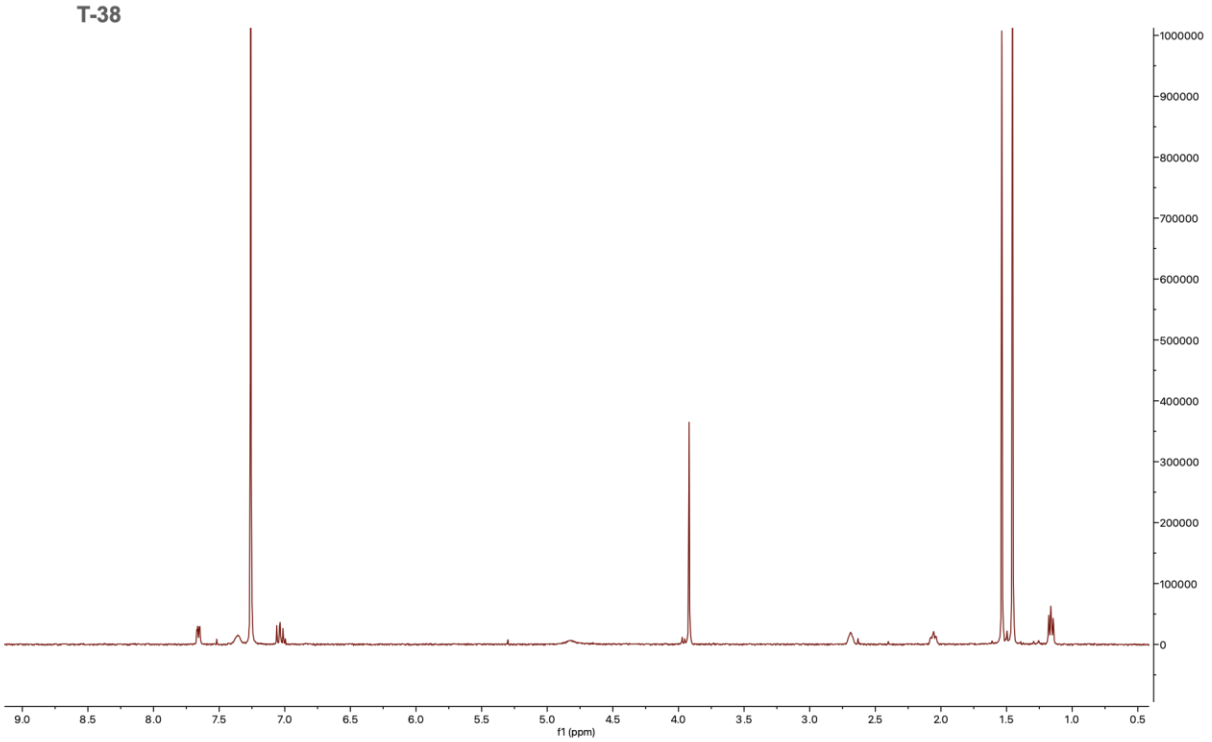
T-38
1000000
900000
800000
700000
600000
500000
400000
300000
200000
100000
0
9.0
8.5
8.0
7.5
7.0
6.5
6.0
5.5
5.0
4.5
4.0
3.5
3.0
2.5
2.0
1.5
1.0
0.5
f1 (ppm)

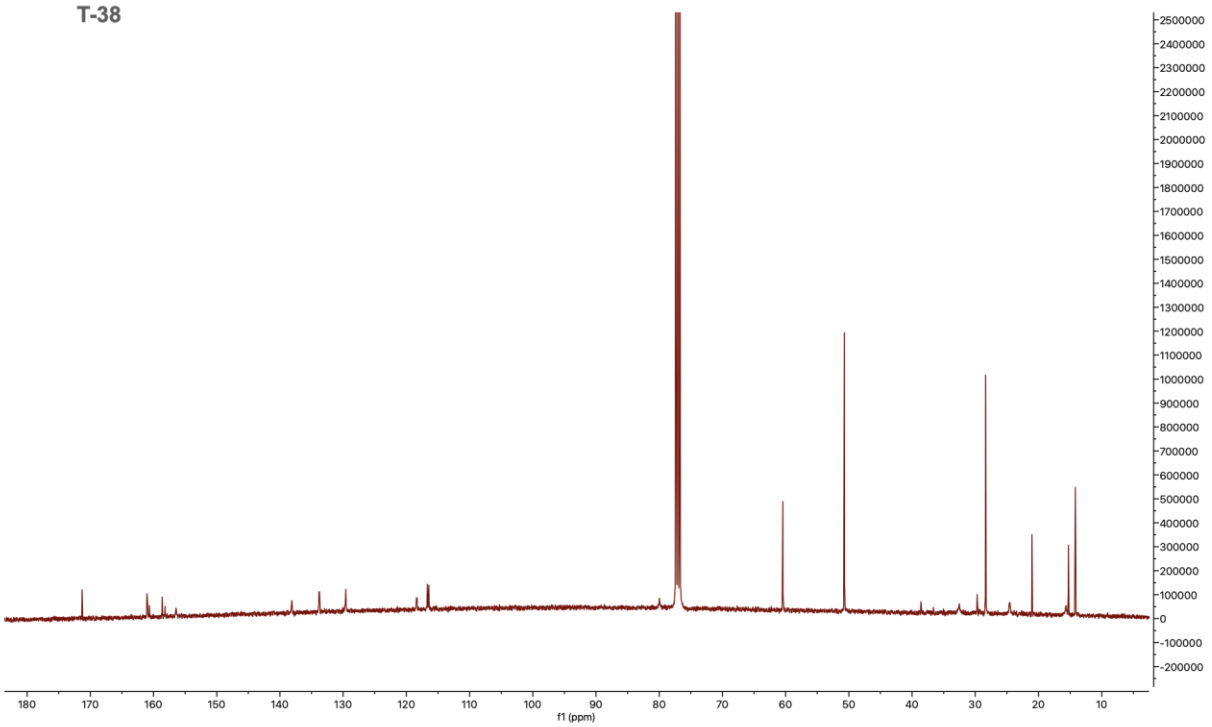
T-38
2500000
2400000
2300000
2200000
2100000
2000000
1900000
1800000
1700000
1600000
1500000
1400000
1300000
1200000
1100000
1000000
900000
800000
700000
600000
500000
400000
300000
200000
100000
0
-100000
-200000
180
170
160
150
140
130
120
110
100
90
80
70
60
50
40
30
20
10
f1 (ppm)

T-39

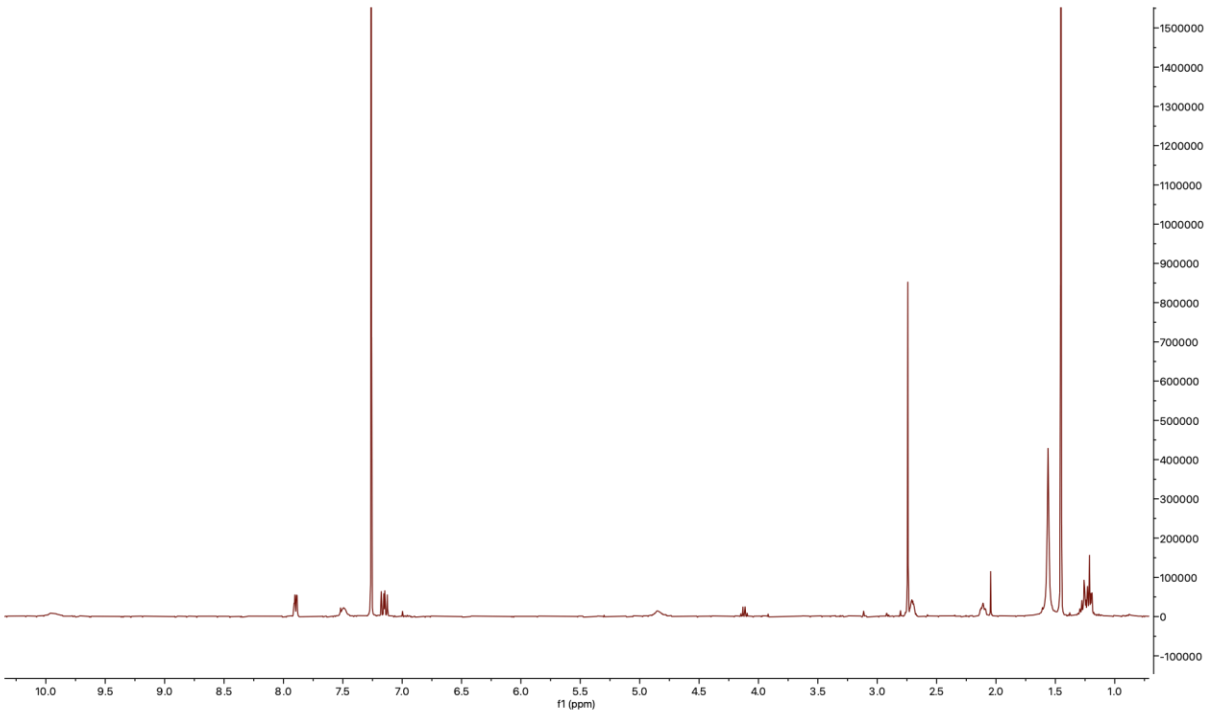
1500000
1400000
1300000
1200000
1100000
1000000
900000
800000
700000
600000
500000
400000
300000
200000
100000
0
-100000
10.0
9.5
9.0
8.5
8.0
7.5
7.0
6.5
6.0
5.5
5.0
4.5
4.0
3.5
3.0
2.5
2.0
1.5
1.0
f1 (ppm)

T-39

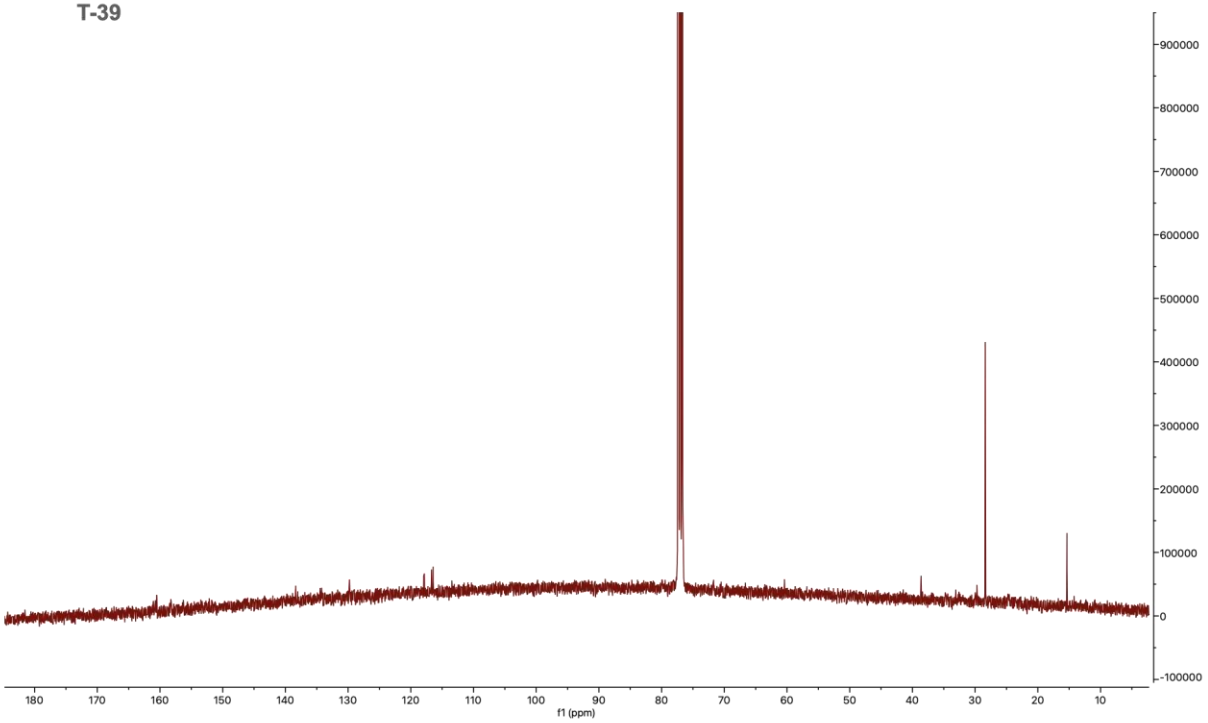
900000
800000
700000
600000
500000
400000
300000
200000
100000
0
-100000
180
170
160
150
140
130
120
110
100
90
80
70
60
50
40
30
20
10
f1 (ppm)

T-12

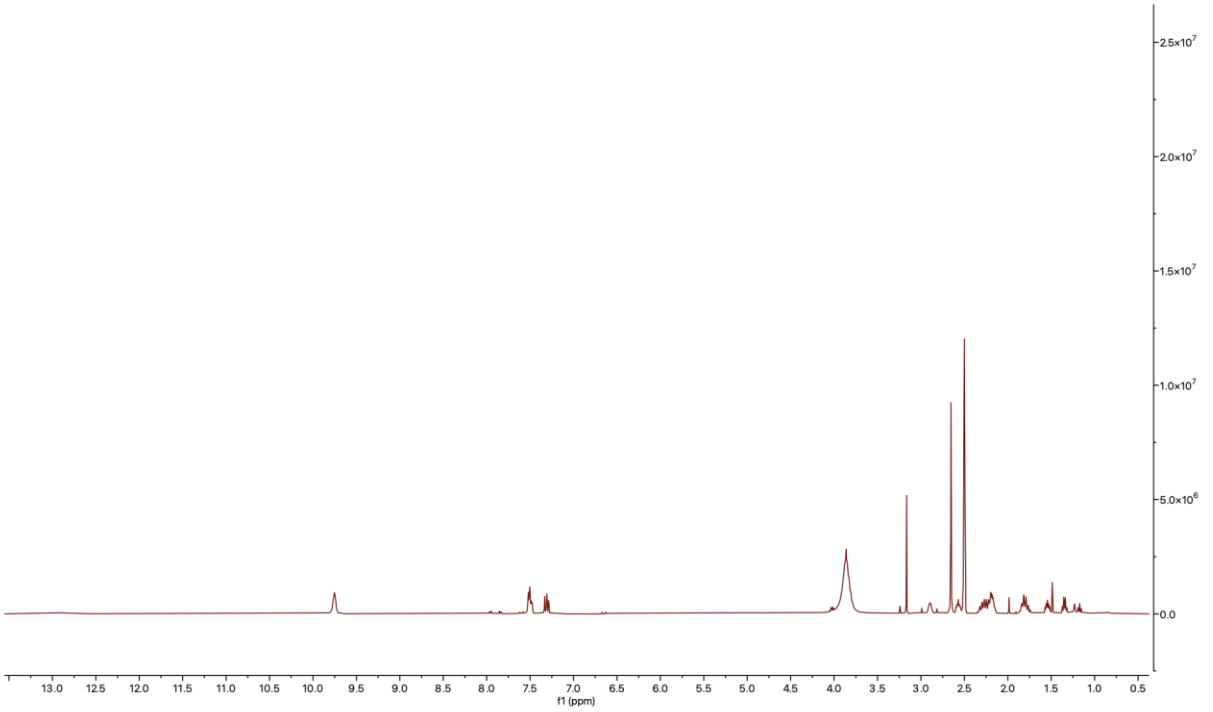
2.5×10^7
2.0×10^7
1.5×10^7
1.0×10^7
5.0×10^6
0.0
13.0 12.5 12.0 11.5 11.0 10.5 10.0 9.5 9.0 8.5 8.0 7.5 7.0 6.5 6.0 5.5 5.0 4.5 4.0 3.5 3.0 2.5 2.0 1.5 1.0 0.5
f1 (ppm)

T-40

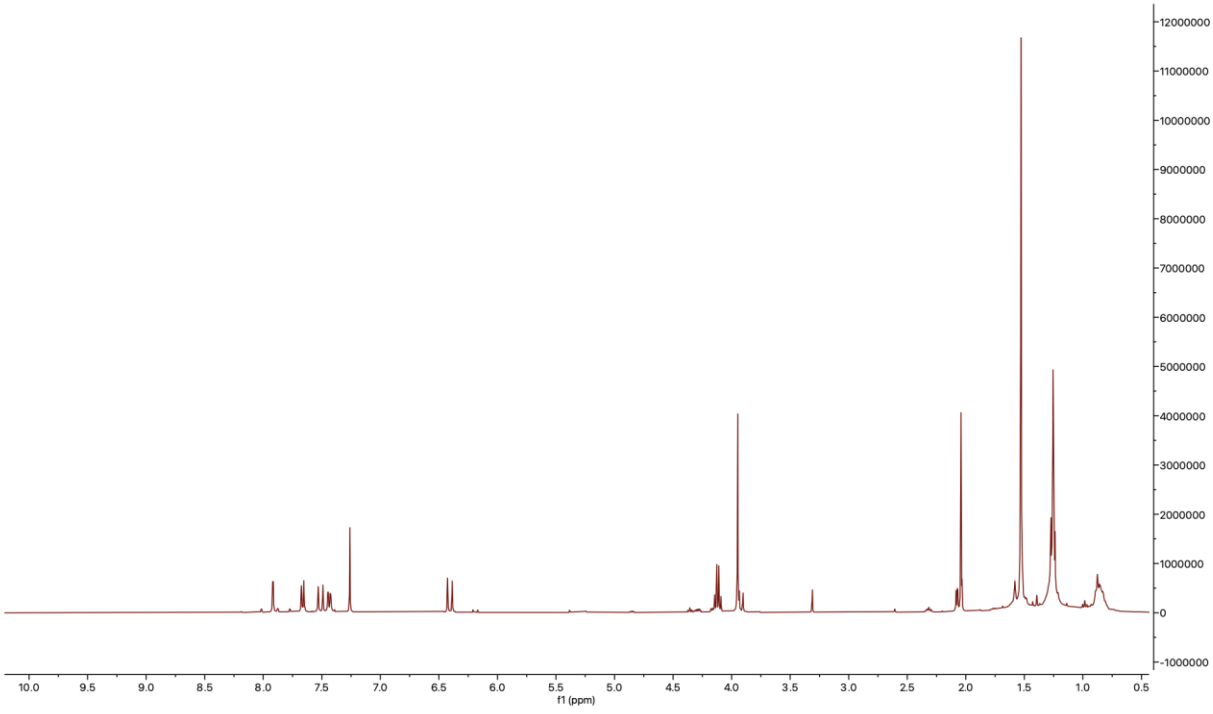
12000000
11000000
10000000
9000000
8000000
7000000
6000000
5000000
4000000
3000000
2000000
1000000
0
-1000000
10.0 9.5 9.0 8.5 8.0 7.5 7.0 6.5 6.0 5.5 5.0 4.5 4.0 3.5 3.0 2.5 2.0 1.5 1.0 0.5
f1 (ppm)

T-40

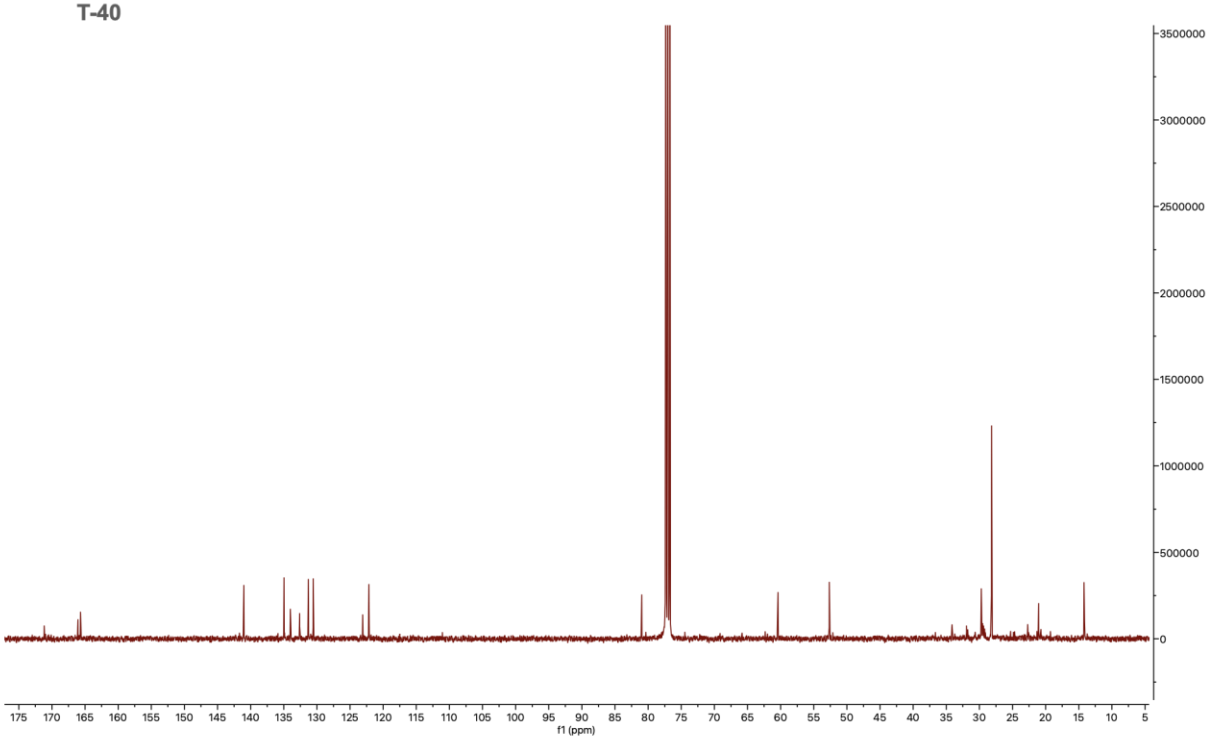
3500000
3000000
2500000
2000000
1500000
1000000
500000
0
175 170 165 160 155 150 145 140 135 130 125 120 115 110 105 100 95 90 85 80 75 70 65 60 55 50 45 40 35 30 25 20 15 10 5
f1 (ppm)

T-41

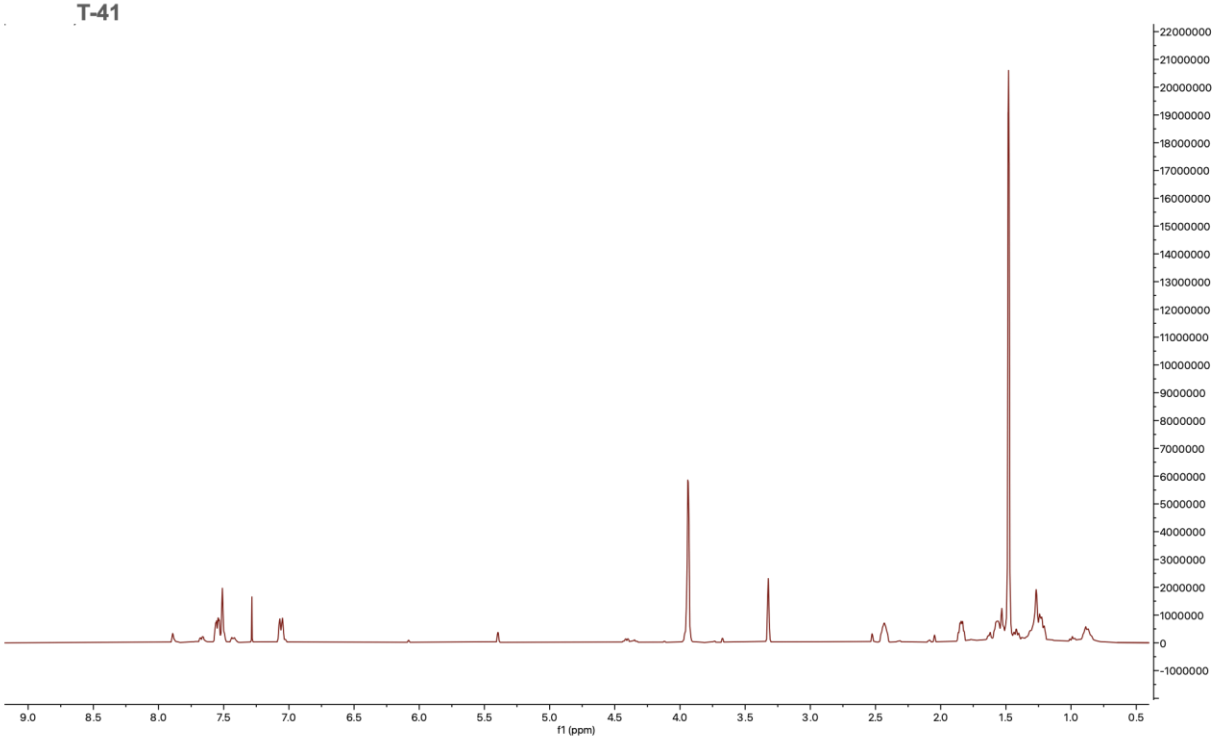
22000000
21000000
20000000
19000000
18000000
17000000
16000000
15000000
14000000
13000000
12000000
11000000
10000000
9000000
8000000
7000000
6000000
5000000
4000000
3000000
2000000
1000000
0
-1000000
9.0 8.5 8.0 7.5 7.0 6.5 6.0 5.5 5.0 4.5 4.0 3.5 3.0 2.5 2.0 1.5 1.0 0.5
f1 (ppm)

T-41

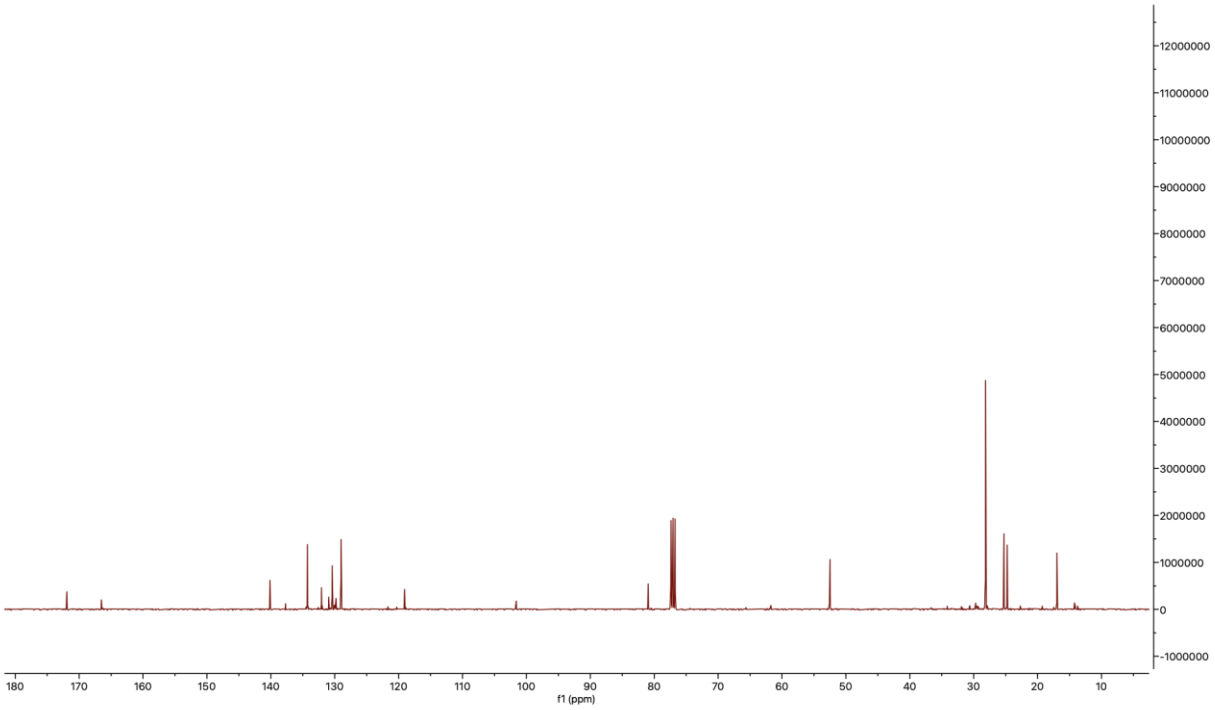
12000000
11000000
10000000
9000000
8000000
7000000
6000000
5000000
4000000
3000000
2000000
1000000
0
-1000000
180 170 160 150 140 130 120 110 100 90 80 70 60 50 40 30 20 10
f1 (ppm)

T-42

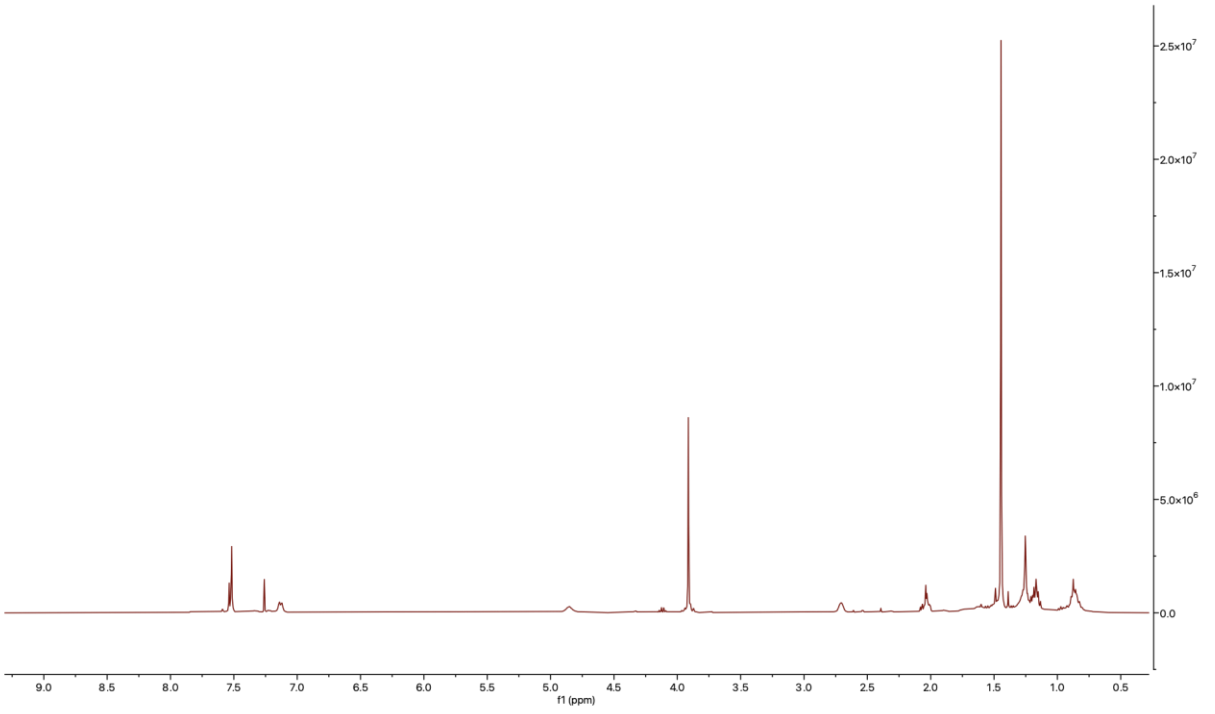
2.5×10^7
2.0×10^7
1.5×10^7
1.0×10^7
5.0×10^6
0.0
9.0 8.5 8.0 7.5 7.0 6.5 6.0 5.5 5.0 4.5 4.0 3.5 3.0 2.5 2.0 1.5 1.0 0.5
f1 (ppm)

T-42

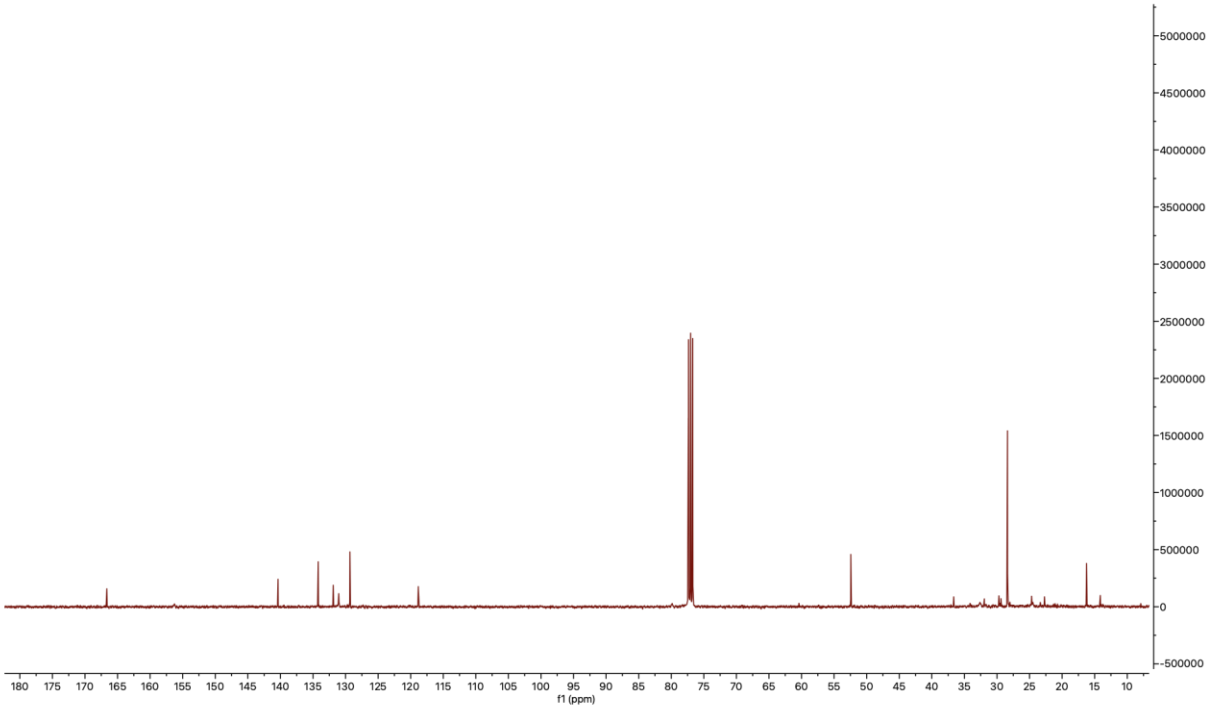
5000000
4500000
4000000
3500000
3000000
2500000
2000000
1500000
1000000
500000
0
-500000
180 175 170 165 160 155 150 145 140 135 130 125 120 115 110 105 100 95 90 85 80 75 70 65 60 55 50 45 40 35 30 25 20 15 10
f1 (ppm)

T-43

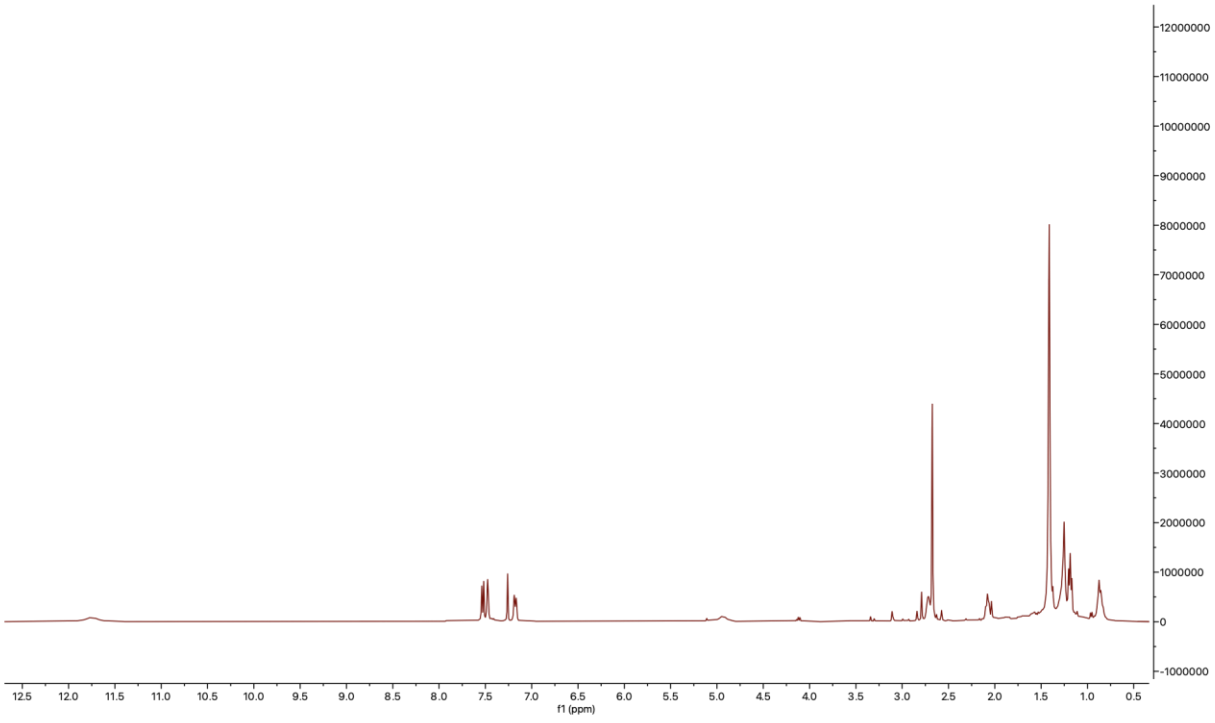
12000000
11000000
10000000
9000000
8000000
7000000
6000000
5000000
4000000
3000000
2000000
1000000
0
-1000000
12.5 12.0 11.5 11.0 10.5 10.0 9.5 9.0 8.5 8.0 7.5 7.0 6.5 6.0 5.5 5.0 4.5 4.0 3.5 3.0 2.5 2.0 1.5 1.0 0.5
f1 (ppm)

T-43

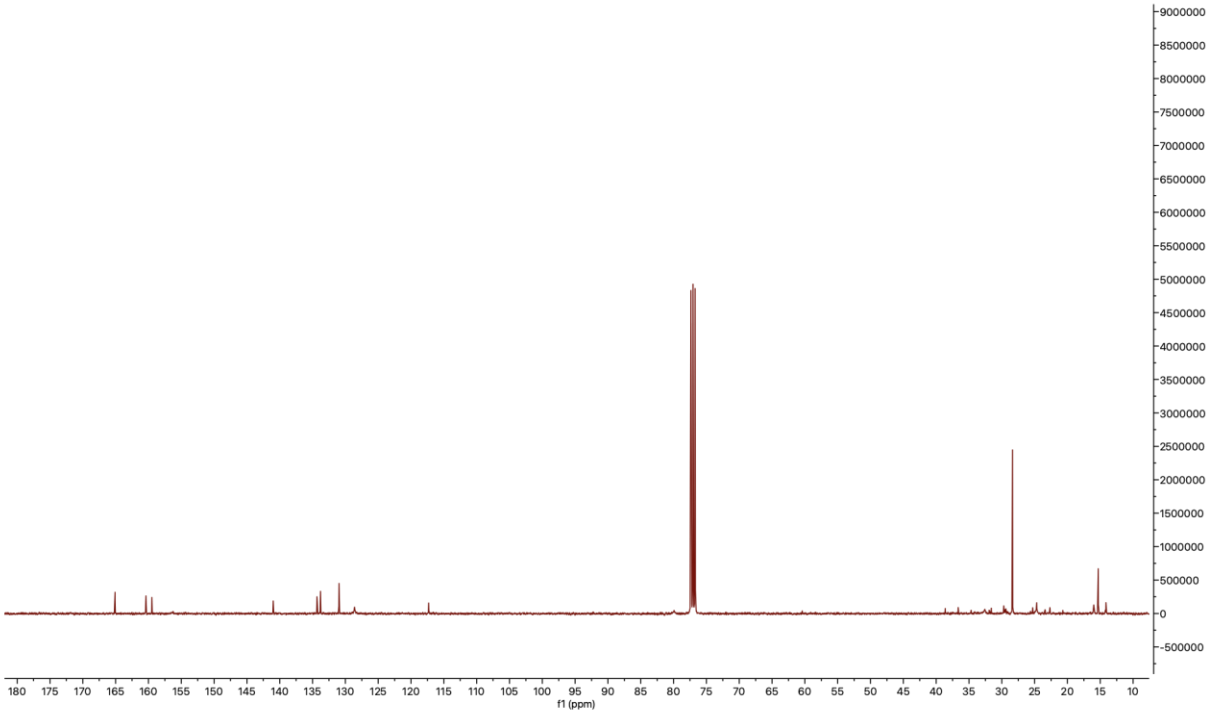
9000000
8500000
8000000
7500000
7000000
6500000
6000000
5500000
5000000
4500000
4000000
3500000
3000000
2500000
2000000
1500000
1000000
500000
0
-500000
180 175 170 165 160 155 150 145 140 135 130 125 120 115 110 105 100 95 90 85 80 75 70 65 60 55 50 45 40 35 30 25 20 15 10
f1 (ppm)

T-19

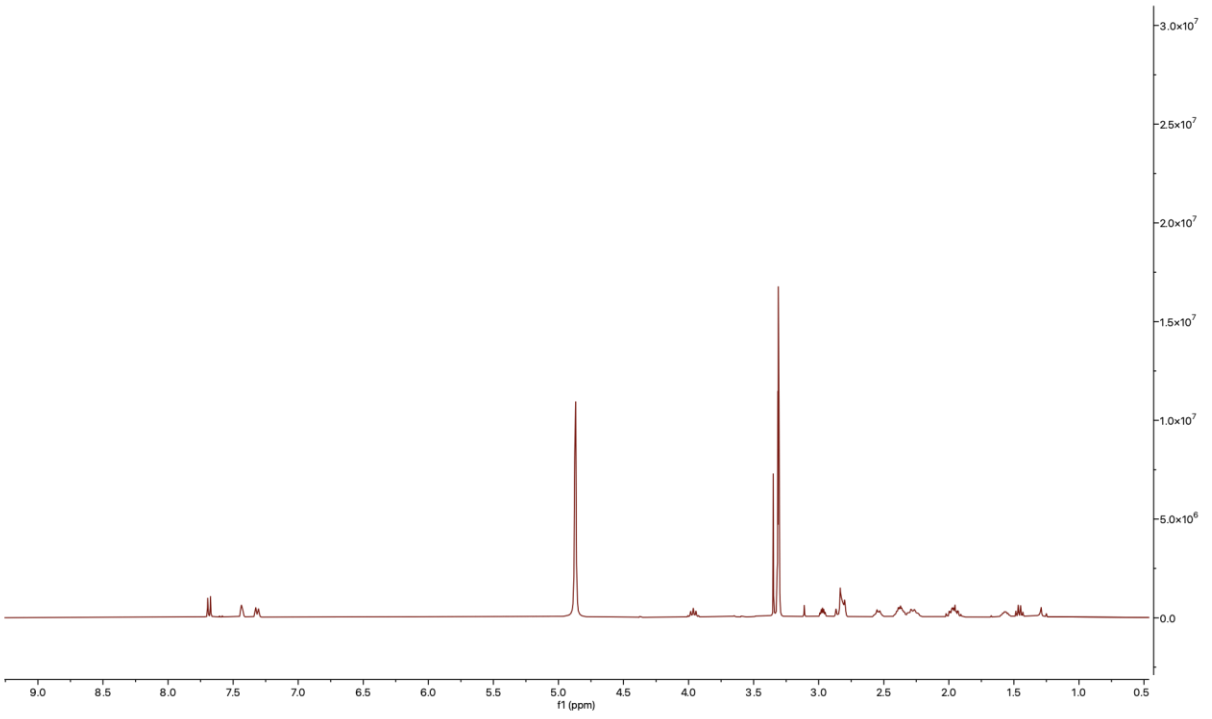
3.0×10^7
2.5×10^7
2.0×10^7
1.5×10^7
1.0×10^7
5.0×10^6
0.0
9.0 8.5 8.0 7.5 7.0 6.5 6.0 5.5 5.0 4.5 4.0 3.5 3.0 2.5 2.0 1.5 1.0 0.5
f1 (ppm)

T-45

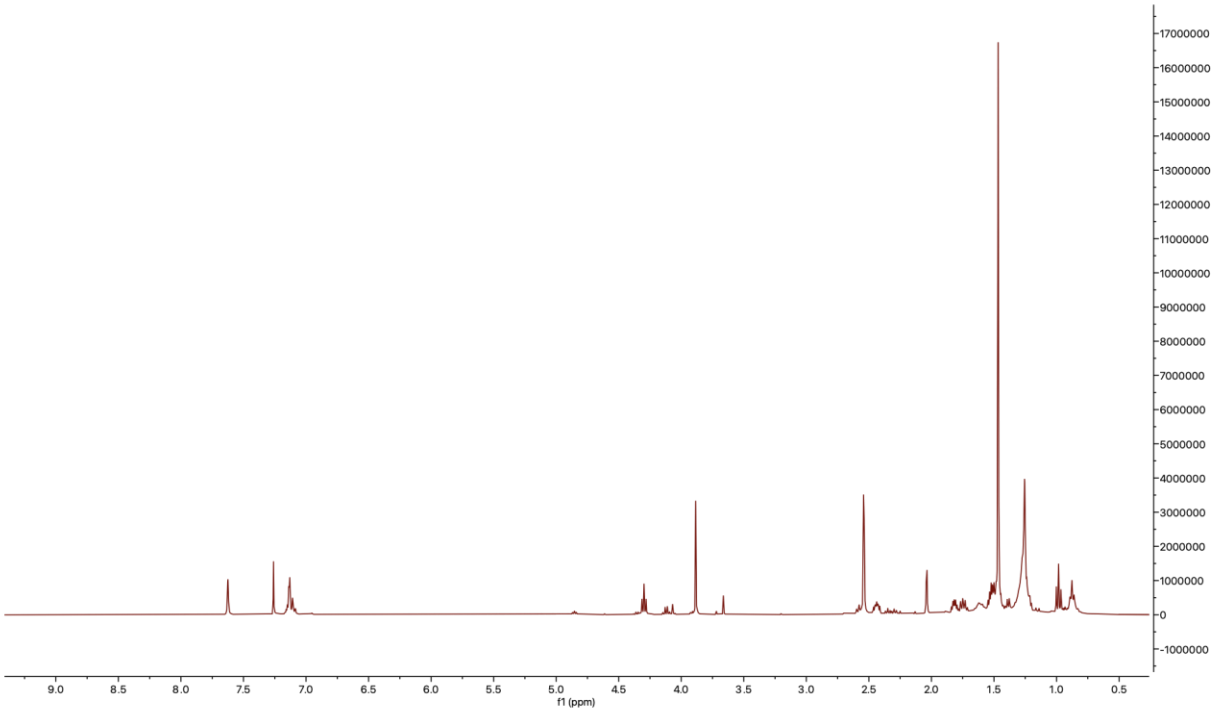
17000000
16000000
15000000
14000000
13000000
12000000
11000000
10000000
9000000
8000000
7000000
6000000
5000000
4000000
3000000
2000000
1000000
0
-1000000
9.0
8.5
8.0
7.5
7.0
6.5
6.0
5.5
5.0
4.5
4.0
3.5
3.0
2.5
2.0
1.5
1.0
0.5
f1 (ppm)

T-45

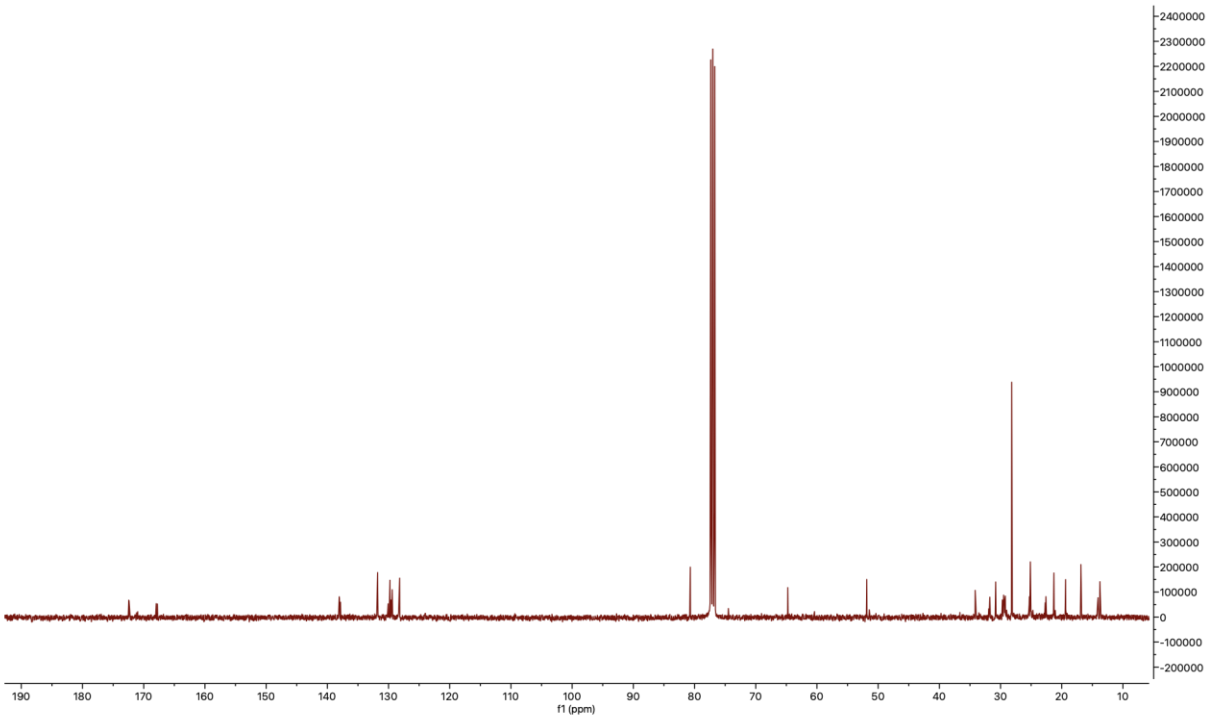
2400000
2300000
2200000
2100000
2000000
1900000
1800000
1700000
1600000
1500000
1400000
1300000
1200000
1100000
1000000
900000
800000
700000
600000
500000
400000
300000
200000
100000
0
-100000
-200000
190
180
170
160
150
140
130
120
110
100
90
80
70
60
50
40
30
20
10
f1 (ppm)

T-46

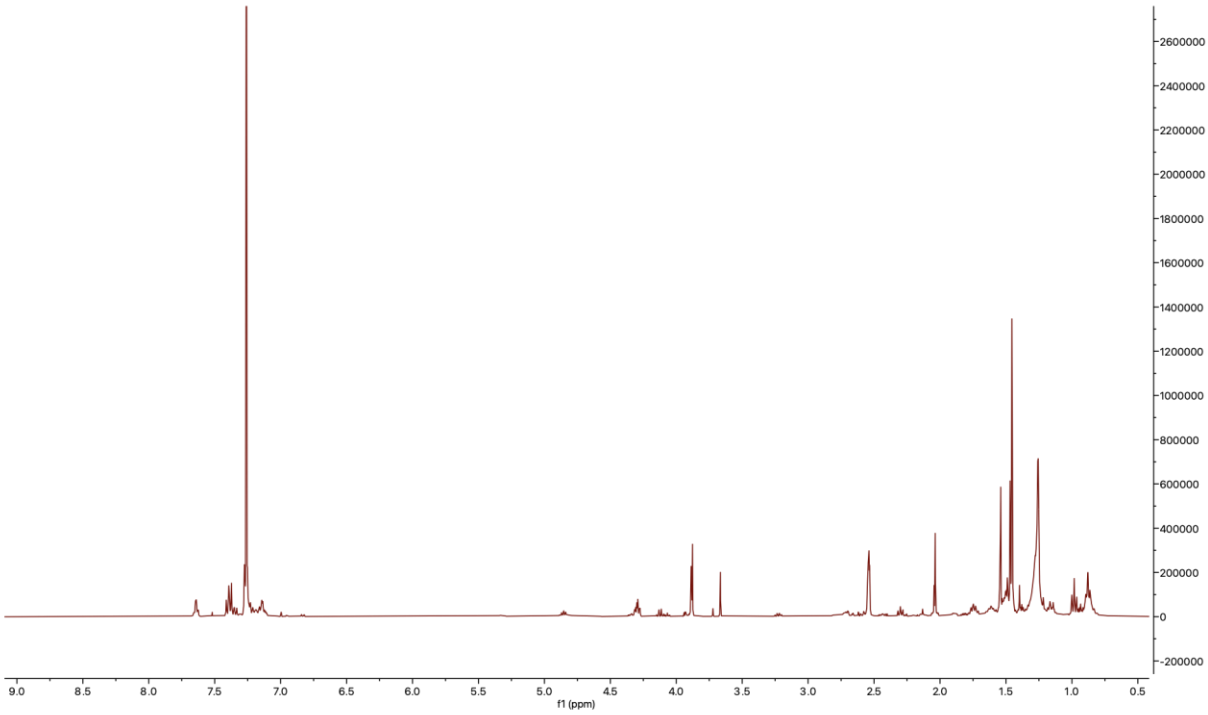
2600000
2400000
2200000
2000000
1800000
1600000
1400000
1200000
1000000
800000
600000
400000
200000
0
-200000
9.0
8.5
8.0
7.5
7.0
6.5
6.0
5.5
5.0
4.5
4.0
3.5
3.0
2.5
2.0
1.5
1.0
0.5
f1 (ppm)

T-46

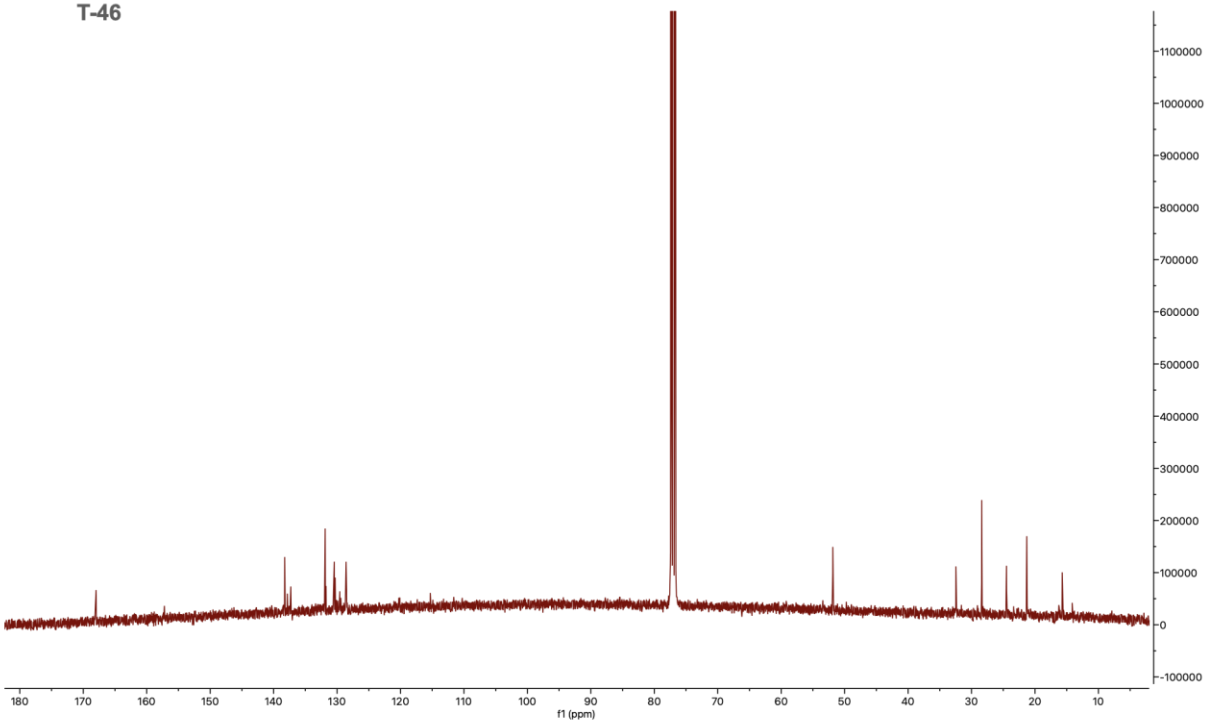
1100000
1000000
900000
800000
700000
600000
500000
400000
300000
200000
100000
0
-100000
180
170
160
150
140
130
120
110
100
90
80
70
60
50
40
30
20
10
f1 (ppm)

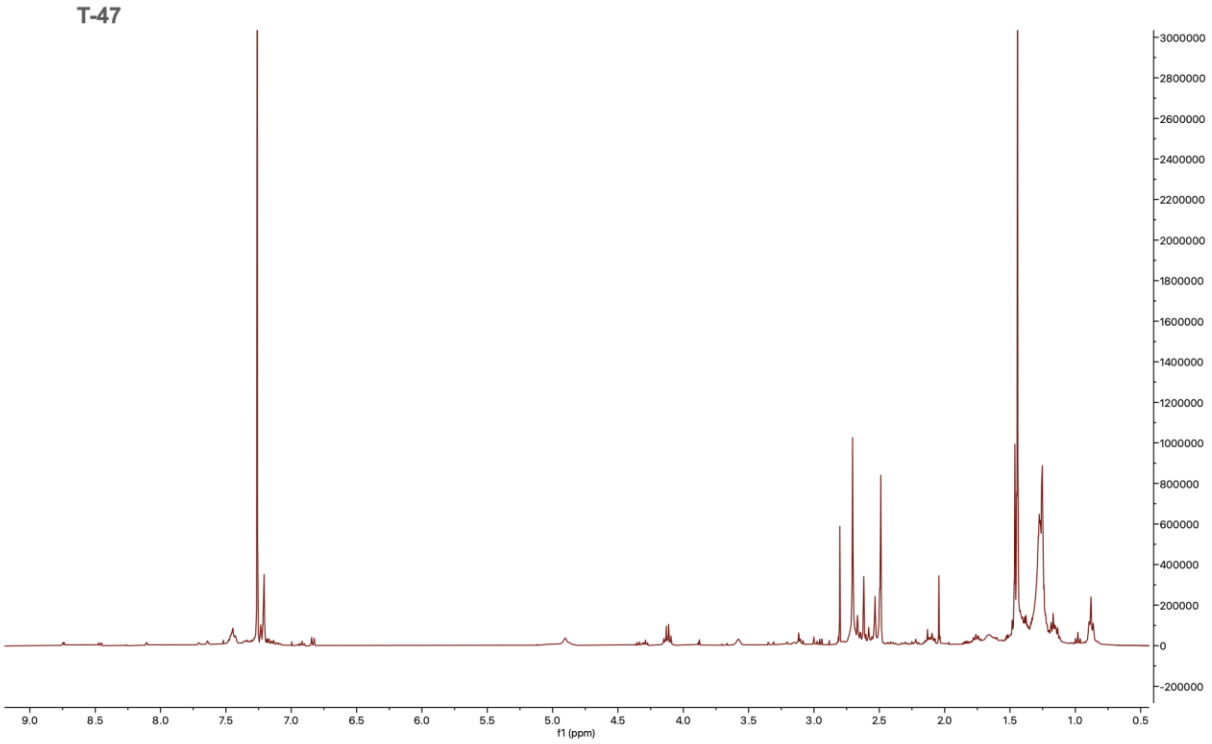
T-47
3000000
2800000
2600000
2400000
2200000
2000000
1800000
1600000
1400000
1200000
1000000
800000
600000
400000
200000
0
-200000
9.0
8.5
8.0
7.5
7.0
6.5
6.0
5.5
5.0
4.5
4.0
3.5
3.0
2.5
2.0
1.5
1.0
0.5
f1 (ppm)

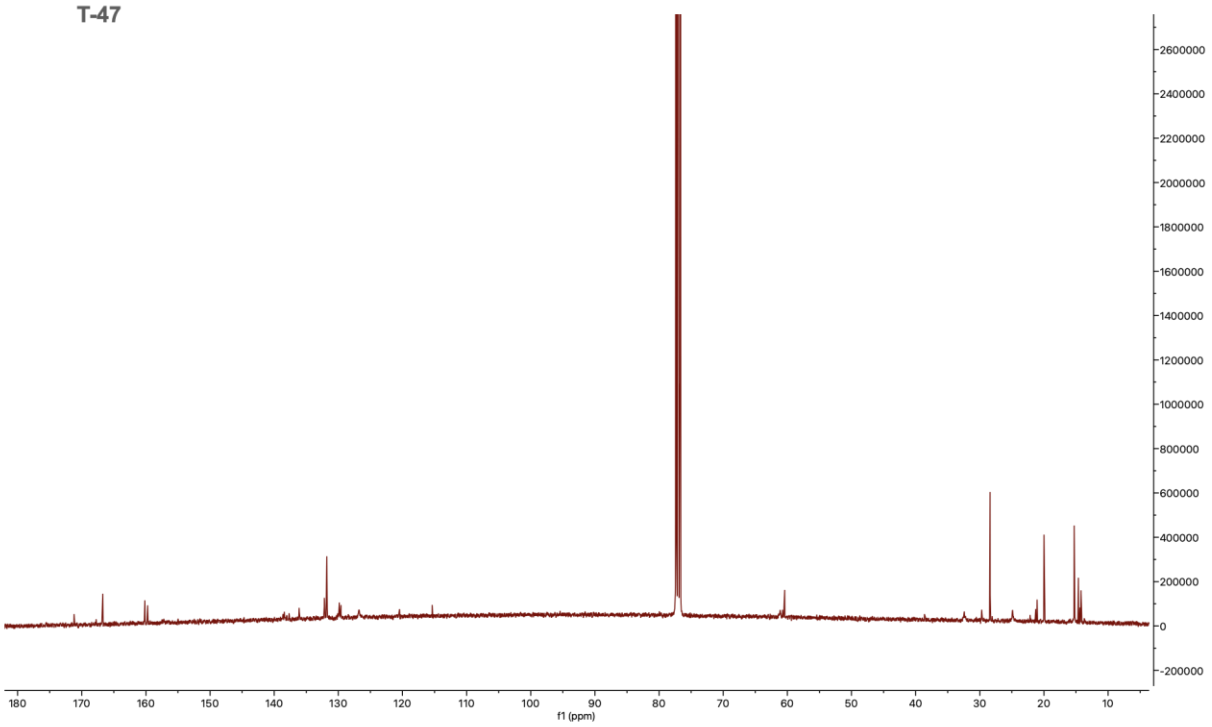
T-47
2600000
2400000
2200000
2000000
1800000
1600000
1400000
1200000
1000000
800000
600000
400000
200000
0
-200000
180
170
160
150
140
130
120
110
100
90
80
70
60
50
40
30
20
10
f1 (ppm)

T-20

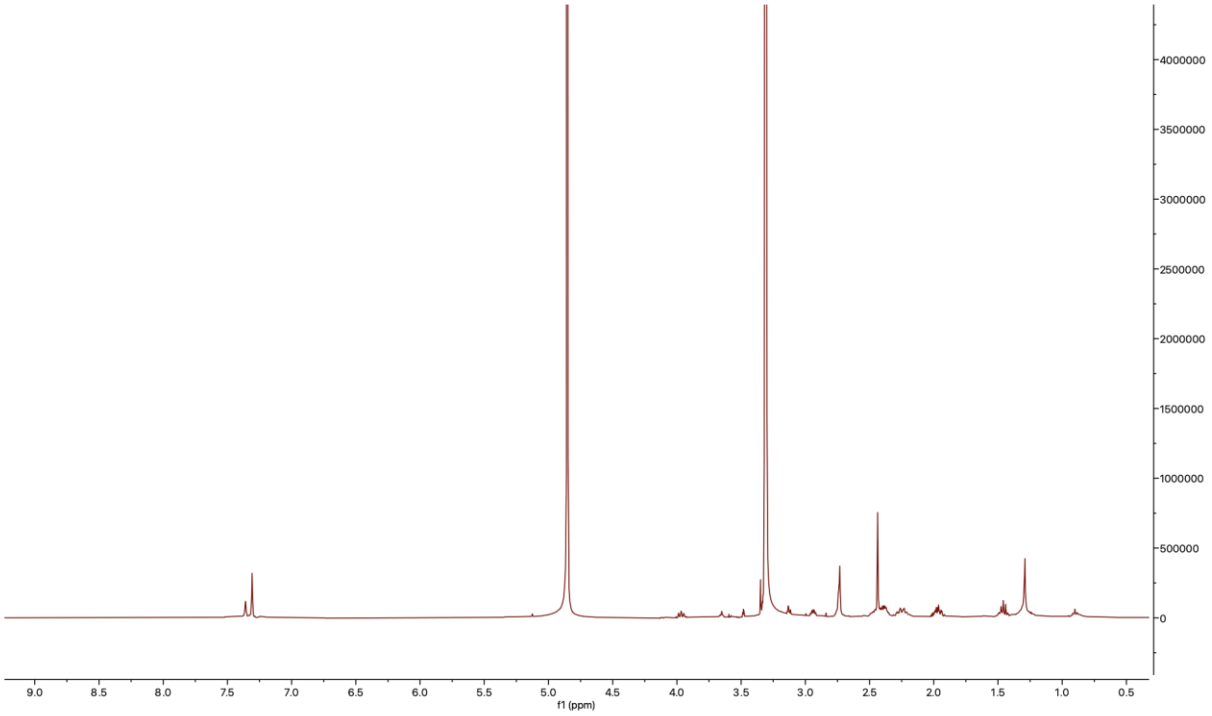
4000000
3500000
3000000
2500000
2000000
1500000
1000000
500000
0
9.0
8.5
8.0
7.5
7.0
6.5
6.0
5.5
5.0
4.5
4.0
3.5
3.0
2.5
2.0
1.5
1.0
0.5
f1 (ppm)

ST-1

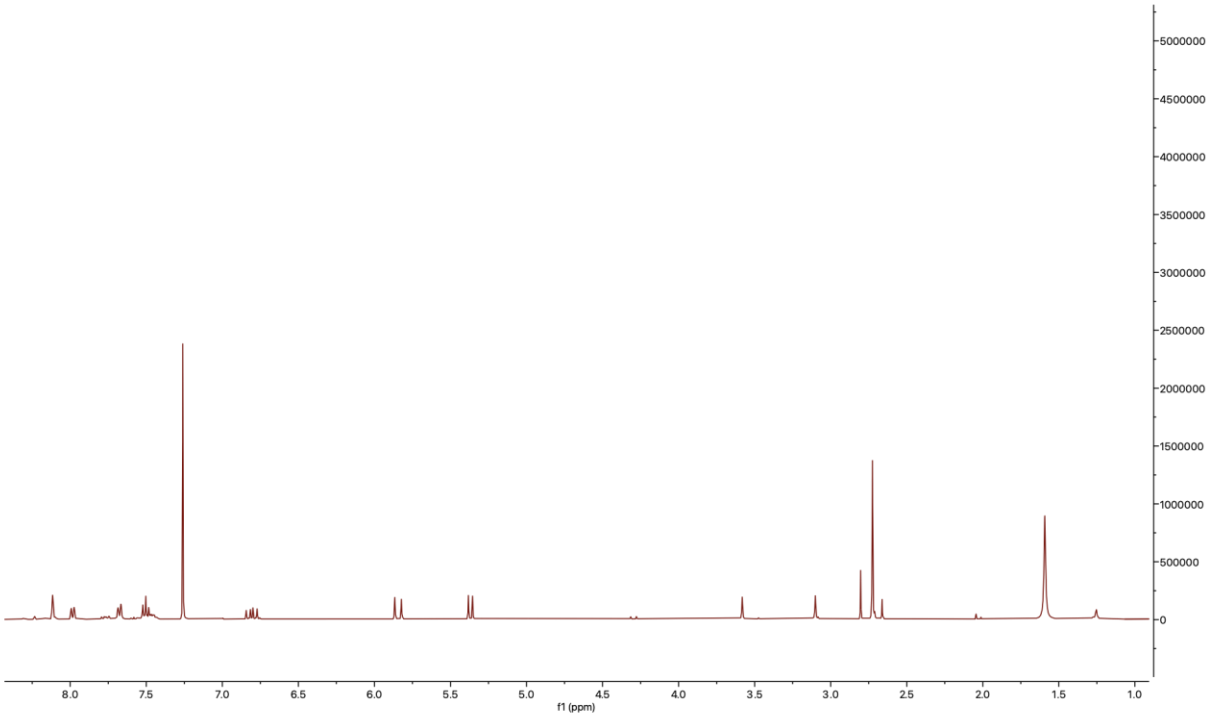
5000000
4500000
4000000
3500000
3000000
2500000
2000000
1500000
1000000
500000
0
8.0
7.5
7.0
6.5
6.0
5.5
5.0
4.5
4.0
3.5
3.0
2.5
2.0
1.5
1.0
f1 (ppm)

ST-1

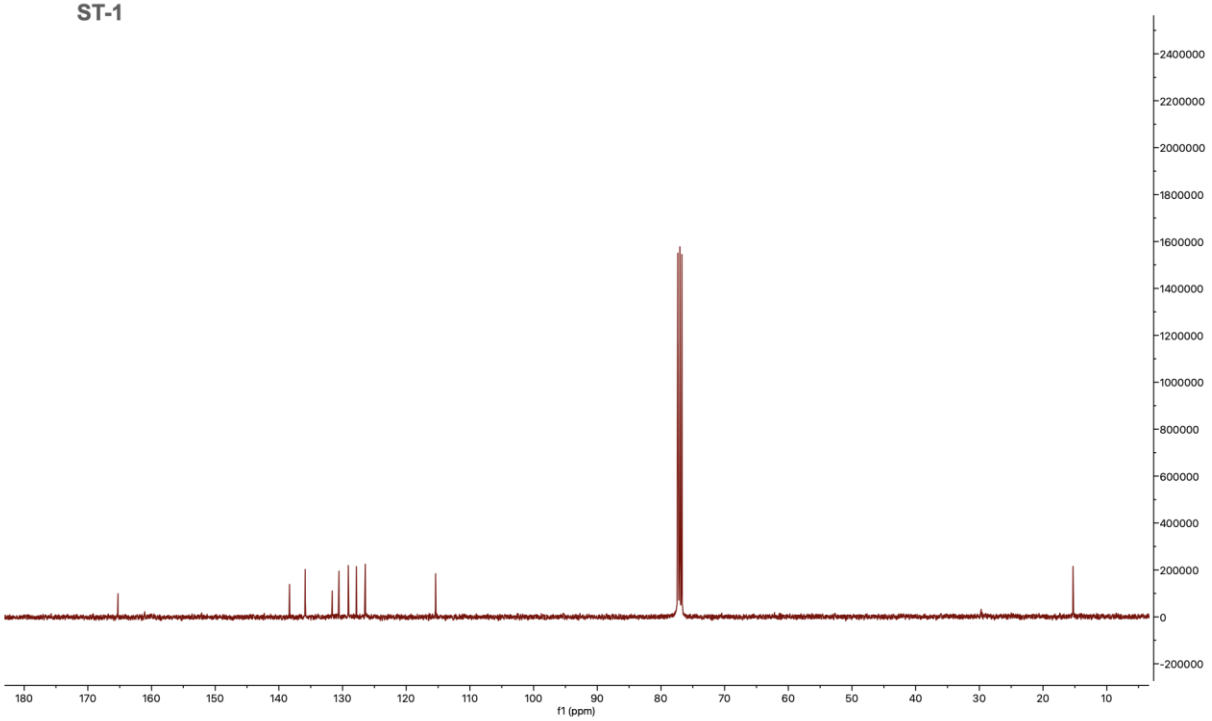
2400000
2200000
2000000
1800000
1600000
1400000
1200000
1000000
800000
600000
400000
200000
0
-200000
180
170
160
150
140
130
120
110
100
90
80
70
60
50
40
30
20
10
f1 (ppm)

ST-2

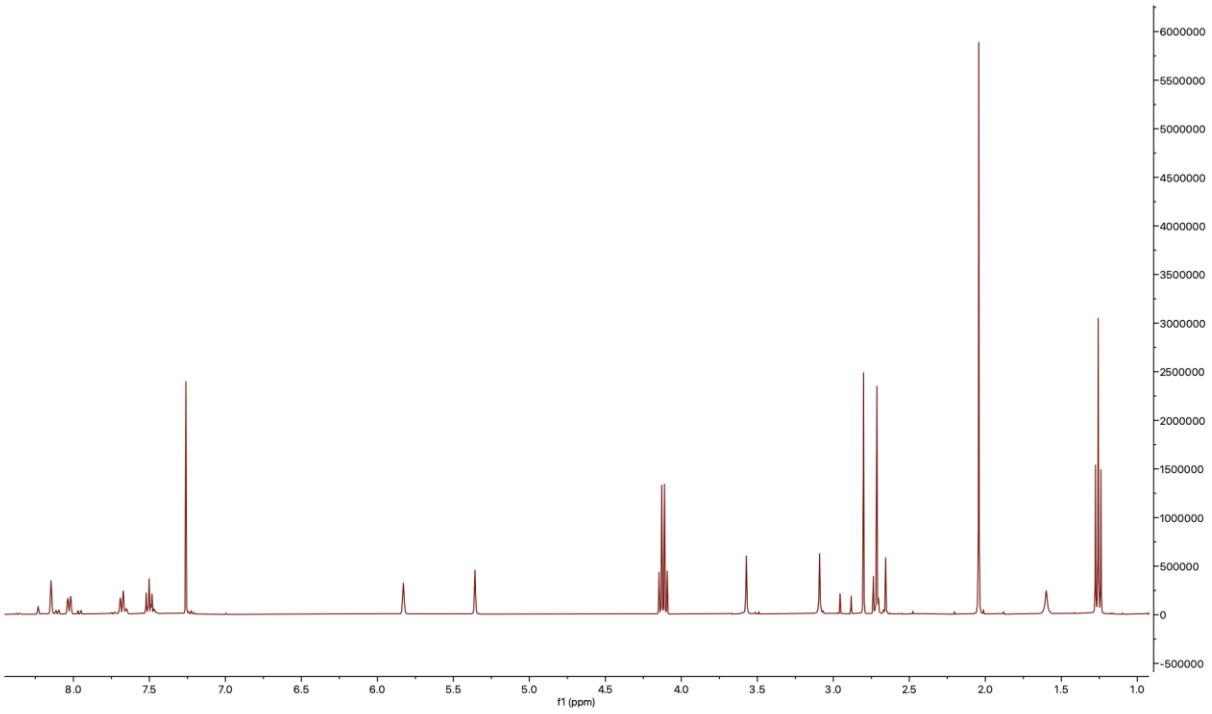
6000000
5500000
5000000
4500000
4000000
3500000
3000000
2500000
2000000
1500000
1000000
500000
0
-500000
8.0
7.5
7.0
6.5
6.0
5.5
5.0
4.5
4.0
3.5
3.0
2.5
2.0
1.5
1.0
f1 (ppm)

ST-3

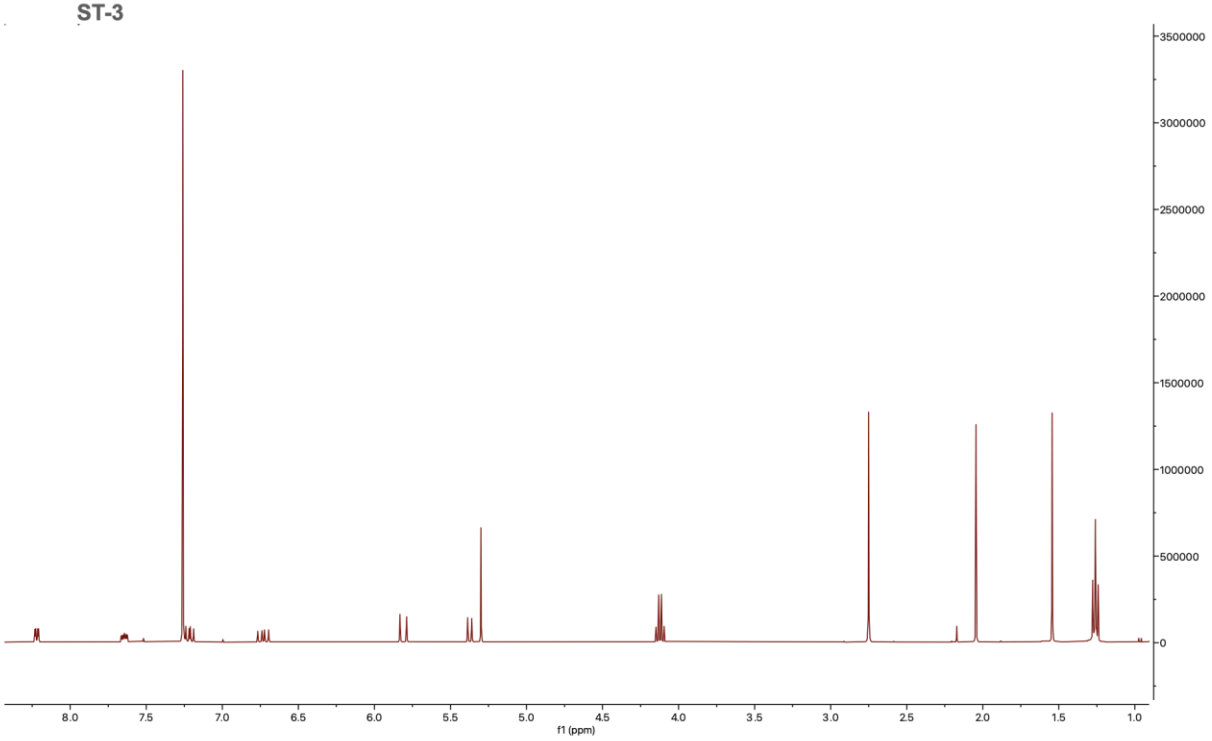
3500000
3000000
2500000
2000000
1500000
1000000
500000
0
8.0
7.5
7.0
6.5
6.0
5.5
5.0
4.5
4.0
3.5
3.0
2.5
2.0
1.5
1.0
f1 (ppm)

ST-3

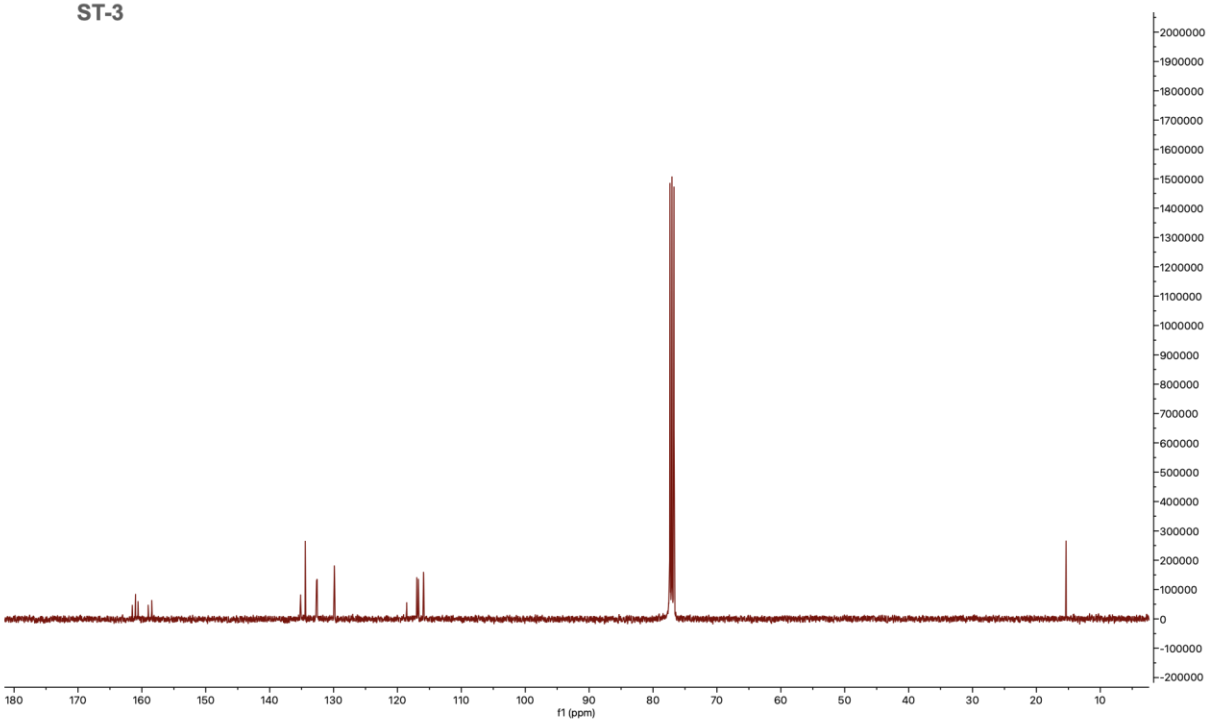
2000000
1900000
1800000
1700000
1600000
1500000
1400000
1300000
1200000
1100000
1000000
900000
800000
700000
600000
500000
400000
300000
200000
100000
0
-100000
-200000
180
170
160
150
140
130
120
110
100
90
80
70
60
50
40
30
20
10
f1 (ppm)

ST-4

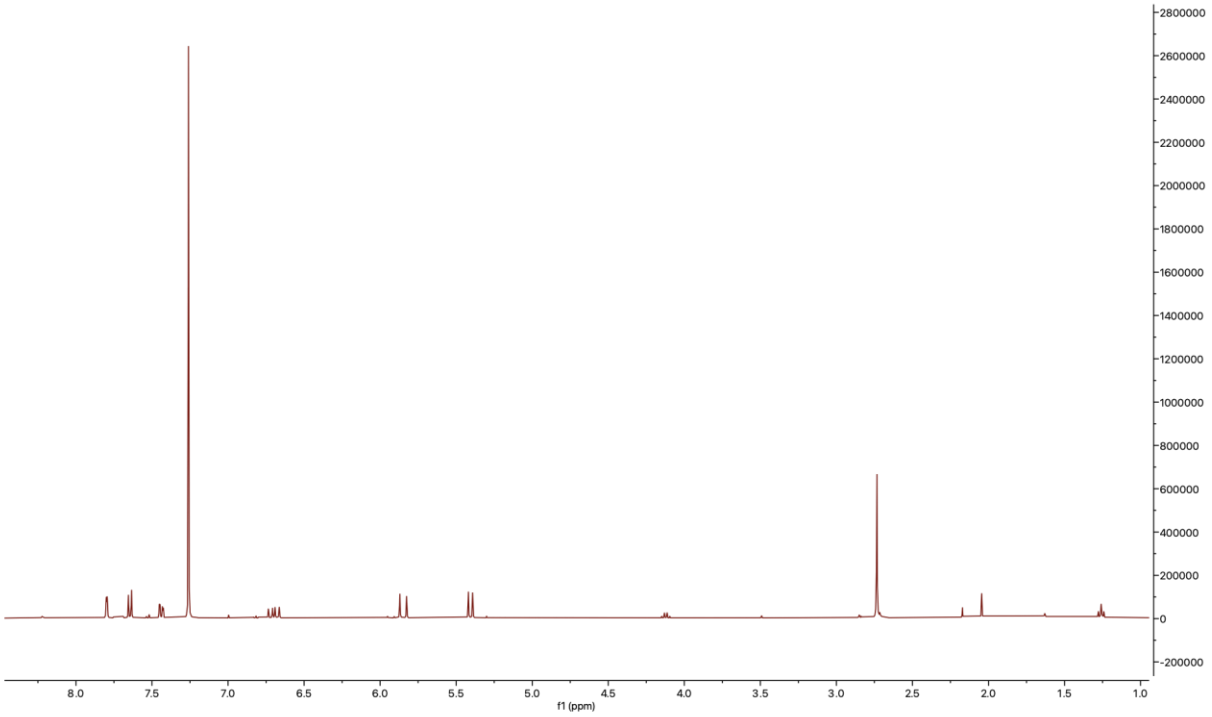
2800000
2600000
2400000
2200000
2000000
1800000
1600000
1400000
1200000
1000000
800000
600000
400000
200000
0
-200000
8.0
7.5
7.0
6.5
6.0
5.5
5.0
4.5
4.0
3.5
3.0
2.5
2.0
1.5
1.0
f1 (ppm)

ST-4

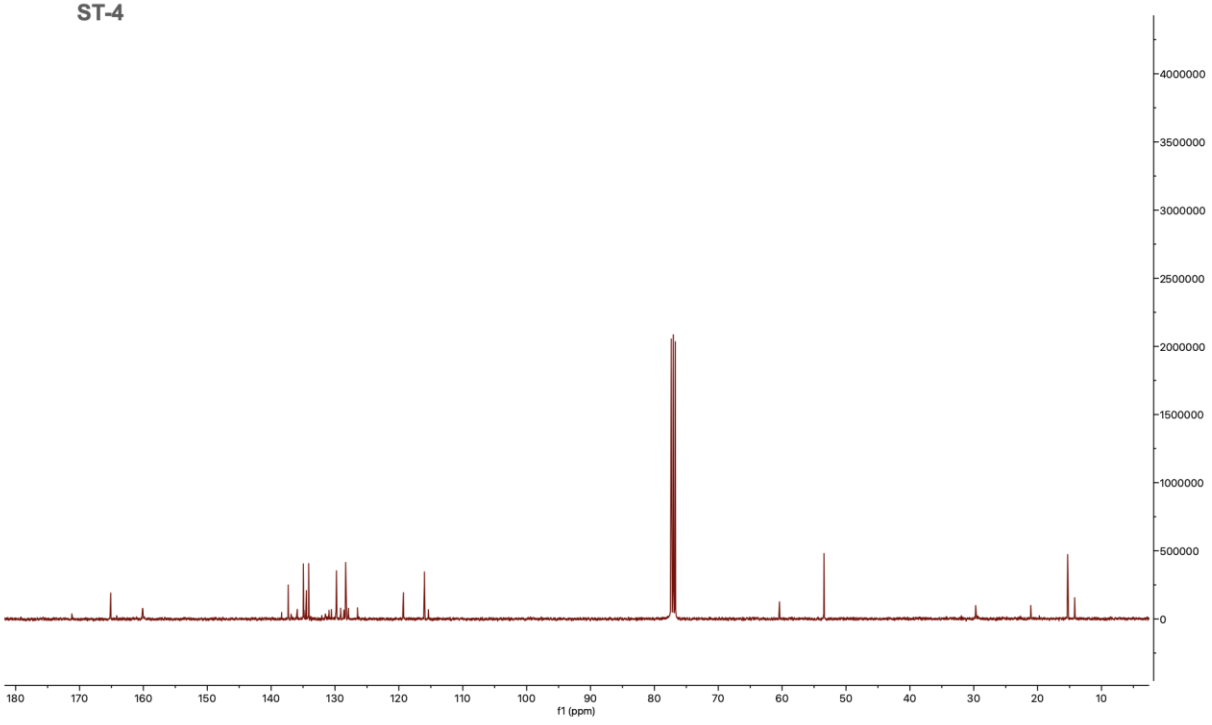
4000000
3500000
3000000
2500000
2000000
1500000
1000000
500000
0
180
170
160
150
140
130
120
110
100
90
80
70
60
50
40
30
20
10
f1 (ppm)

ST-5

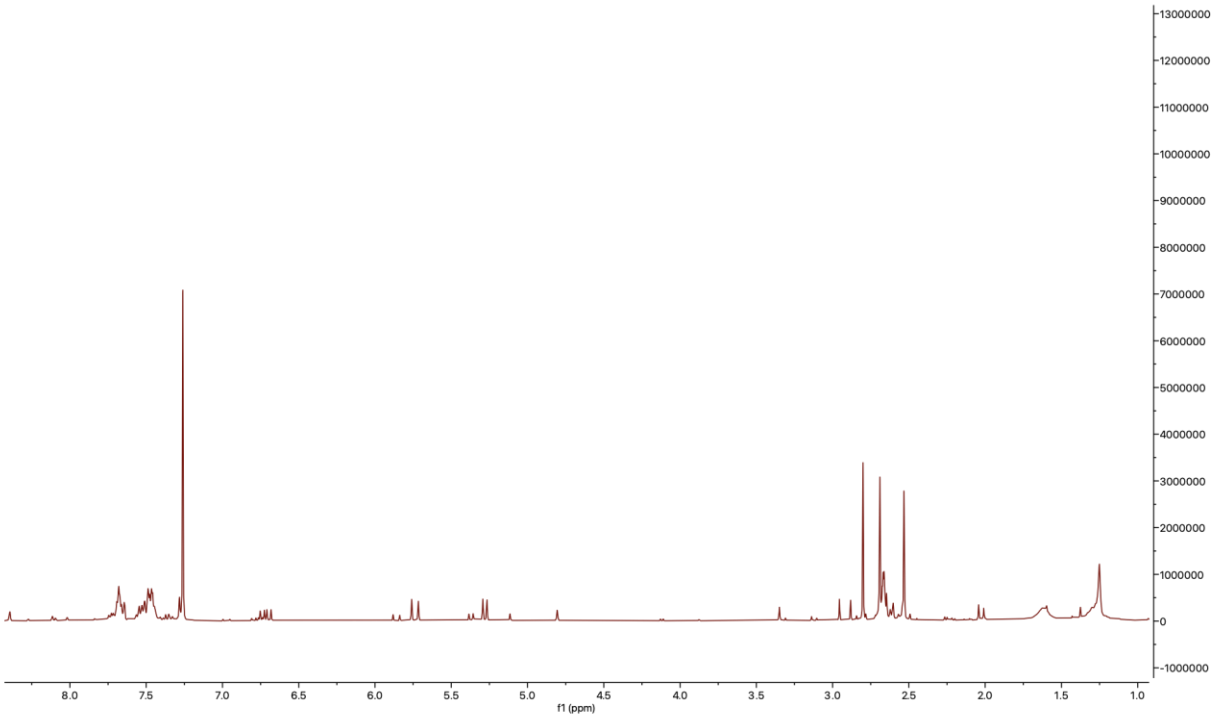
13000000
12000000
11000000
10000000
9000000
8000000
7000000
6000000
5000000
4000000
3000000
2000000
1000000
0
-1000000
8.0
7.5
7.0
6.5
6.0
5.5
5.0
4.5
4.0
3.5
3.0
2.5
2.0
1.5
1.0
f1 (ppm)